A Modelling Study of the Impact of Photolysis on Indoor Air Quality

Zixu Wang

PhD

University of York

Department of Environment and Geography

April 2021

Abstract

Most human exposure to air pollutants happen indoors, where people spend most of their time (~90%). In the ambient atmosphere, photolysis plays a major role in initiating chemical reactions. However, indoor photolysis is less well studied. Consequently, the role that photolysis plays in indoor chemical processing, particularly in the formation of harmful species, is unclear. The major aim of this thesis was, therefore, to improve the representation of indoor lighting and attenuated sunlight in the Indoor Detailed Chemical Model (INDCM). The improved model was then used to investigate the impacts of glass type, indoor artificial light, cloudiness, time of year and latitude on indoor photolysis rates and hence indoor air chemistry.

The results show that variations in glass composition produce the highest deviations (~71%) in predicted concentrations of key indoor species (ozone, nitrous acid, nitric oxide, hydroxyl radicals, hydroperoxy radicals, organic peroxy radicals, peroxyacetyl nitrates and organic nitrates), followed by cloud level (~53%) and proximity to artificial light source (~53%), when compared to baseline conditions. These impacts were greatest for predicted hydroxyl radical concentrations, which deviated by an average of ~142% from the baseline scenario depending on the conditions studied.

Enhanced radical concentrations were found during two cleaning case studies (automated and traditional techniques), with predicted hydroxyl radical concentrations up to 1.3×10^7 and 1.5×10^6 molecule/cm^3 respectively. Furthermore, radical concentrations were found to be highest under stronger lighting conditions, persisting for several hours after the cleaning events.

This study provides a valuable contribution to the understanding of the impacts of photolysis on indoor air chemistry. Indoor artificial lights, such as LED, together with low cut-off wavelength glasses, will likely reduce the effects of photolysis indoors, but more research is needed on the health effects of different indoor air mixtures to confirm this recommendation.

List of contents

List of Tables

Chapter 5

Chapter 6

Chapter 7

List of Figures

Chapter 1

Chapter 2

Chapter 3

Chapter 4

Chapter 5

Chapter 6

Chapter 7

Chapter 8

Acknowledgements

First and foremost, I would like to express my sincere thanks to my supervisor, Prof. Nicola Carslaw, for her constant help and support. She provides indispensable support throughout all aspects of this research project. She has both challenged and enriched my ideas. I would particularly like to express my gratitude for the doors she has opened and her continuous support in the progression of my academic career. Her encouragement, motivation, patience and great guidance were extremely helpful to complete my doctorate programme.

I wish to thank my family and friends. Particularly, I would like to thank to my wife, MinJie, and my parents, KeJun and XuHua, for their constant love and support during all the time. Without their help and encouragement, I would never achieve what I already did in my life.

I would like to show my gratitude to my Progression Meeting members, Prof. Alistair Bruce Alleyne Boxall and Dr Sylvia Toet, for their support and useful advice that they provided during my doctorate programme.

Declaration

I declare that this thesis is a presentation of original work and I am the sole author. This work has not previously been presented for an award at this, or any other, University. All sources are acknowledged as References.

The work of Chapter 7 has been published in the scientific journal Indoor Air (2020), for which I was the principal author, and the scientific journal Environmental Science & Technology (2020), for which I carried out the modelling studies, in support of the experimental work carried out by colleagues in Canada.

To cite:

1. Wang ZX, Kowal SF, Carslaw N and Kahan TF. (2020). Photolysis-driven indoor air chemistry following cleaning of hospital wards. Indoor Air. 30:1241-1255.

2. Zhou S, Liu ZL, Wang ZX, Young CJ, VandenBoer TC, Guo BB, Zhang JS, Carslaw N and Kahan TF. (2020). Hydrogen peroxide emission and fate indoors during non-bleach cleaning: a chamber and modelling study. Environ. Sci. Technol. 54(24):15643-15651.

Chapter 1: Introduction

1.1. Why study indoor air quality?

In recent years, much attention has been focused on outdoor air pollution and it is well established that some outdoor air pollutants, such as ozone (O_3) and particulate matter, particularly the finer fraction, ($PM_{2.5}$), have adverse health effects (e.g. Domingo and Rovira 2020; Kim et al., 2020). Diesel exhaust was classified as a carcinogen by the International Agency for Research on Cancer, part of the World Health Organisation in 2012 (IARC, 2012). Furthermore, human exposure to particulate matter has been estimated to cause 29,000 deaths every year in the UK (Public Health England, 2013). Consequently, the concentrations of key outdoor atmospheric pollutants are strictly limited by regulation in many parts of the world. However, WHO air quality guidelines are still exceeded in numerous locations worldwide and ambient air pollution causes approximately 4.2 million deaths every year (WHO, 2016). Figure 1.1 shows the number of deaths by ambient air pollution around the world in 2012 (WHO 2016). As shown in this figure, the number of deaths were particularly high (≥150,000) in some Asian countries (e.g. China).

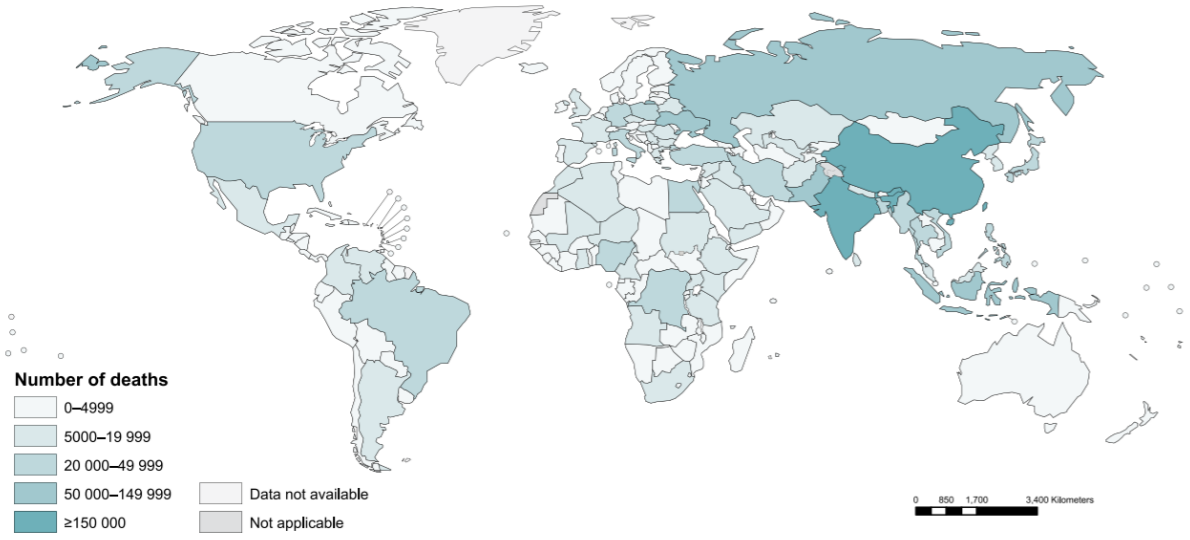

Figure 1.1: Number of deaths by ambient air pollution all over the world in 2012 (WHO 2016).

Despite the focus on outdoor air pollution, people in developed countries spend most of their time (~90%) indoors (Weschler and Shields, 1999). Consequently, the indoor environment is

where people receive most of their exposure to air pollutants, whether those pollutants are generated indoors or outdoors. Indoor air pollutants can be generated by human activities, including cooking (nitrogen oxides (NO_X), particulate matter (PM), carbon monoxide (CO)), cleaning (volatile organic compounds (VOCs), nitryl chloride ($ClNO_2$), molecular chlorine (Cl_2), hypochlorous acid (HOCl)) and smoking (VOCs, NO_X, PM, CO) (Steinemann et al., 2011; Petry et al., 2014; Nazaroff and Weschler, 2004). Meanwhile, consumer products, including toiletries, cleaning products and paints, building materials and furniture can also emit pollutants (Wolkoff et al., 2000; Nazaroff and Weschler 2004; Kruza et al., 2017). Finally, air pollutants from the outdoor environment can move into the indoor environment, through infiltration and ventilation. Therefore, a complex mixture of chemicals will occur in indoor environments, some of which exist at higher concentrations than outdoors.

As well as emissions and ingress of pollutants indoors, the various chemical species can undergo a series of physical and chemical transformations to form secondary products (Han et al., 2010; Schripp et al., 2014), particularly organic species such as formaldehyde (HCHO) (Mendez et al., 2016). Two key indoor oxidants are O_3 (Weschler, 2000) from both outdoors (Blondeau et al., 2005) and generated indoors by printers and air cleaners (Destaillats et al., 2008) and the hydroxyl radical (OH) produced by the photolysis of HONO (Gomez Alvarez et al., 2013), or ozonolysis reactions (Nazaroff and Weschler, 2004). In addition, the use of bleach can lead to the production of HOCl which is also a source of OH (Wong et al., 2017).

Public awareness of poor indoor air quality in working or living areas has grown over recent years. Although adverse health effects such as sick building syndrome have been reported (Sun et al., 2019), it is still unclear what exactly causes these adverse health impacts. It has been reported that the products of VOC degradation may cause some of the reported symptoms instead of the primary emissions (Weschler and Wells, 2004; Weschler, 2004; Nazaroff and Weschler, 2004; Buchanan et al., 2008). According to Mendell (2007), strong associations were found between allergy or respiratory health in children or infants and particleboard (contain formaldehyde-emitting material), plastic materials (contain phthalates-emitting material), recent painting activities, textile wallpaper, new furniture and cleaning activities. Bentayeb et al. (2013) reported strong associations between indoor air pollution and long and short-term respiratory diseases, including lung cancer, asthma, phlegm, cough, breathlessness and wheezing in people aged over 65 years.

There is some evidence in the literature about which compounds might be causing health effects. For example, sensory irritants are produced by the products of the ozone-limonene reaction (Nazaroff and Weschler, 2004; Wolkoff et al., 2005; Hansen et al., 2016). There is also evidence that domestic cleaners have high rates of asthma (Quirce and Barranco, 2010). In particular, using sprays more frequently, particularly air-freshener, furniture and glass-cleaners sprays, was associated with a rise (30-50%) in the risk of incident asthma. According to Jones (1999), many adverse impacts of health can be caused by indoor formaldehyde, including pulmonary effects and irritation of the lower airways when the indoor concentration is between 5 and 30 ppm; irritation of the upper airway when the concentration is between 0.1 and 25 ppm; eye irritation when the concentration is between 0.01 and 2 ppm; neurophysiologic effects when the concentration is between 0.05 and 1.5 ppm and even death when the concentration exceeds 100 ppm. Particles, particularly particles that are small enough to penetrate into the lung, are of great concern in terms of damage to health (e.g. Pope et al., 1995). Finally, cultural artefacts and electronic equipment can also be damaged by indoor particles (Weschler and Shields, 1999).

In summary, human activities, use of consumer products indoors and the ingress of outdoor pollutants can lead to the presence of air pollutants in the indoor environment. Meanwhile, physical and chemical transformations of these indoor chemical species can lead to the formation of secondary products. As discussed above, previous studies have shown that some of these indoor air pollutants are linked to adverse health effects. Therefore, it is important to focus on indoor air quality, particularly given people spend most of their time indoors.

1.2. Why is photolysis important?

Photolysis is the process by which a chemical bond is dissociated by energy from photons. Higher energy is needed to dissociate stronger chemicals bonds while weaker bonds can be dissociated by lower energy. The efficiency of photolysis of an atmospheric species will depend on its bond strength, the wavelength of light to which it is subjected and the intensity of that light. A measure of the efficiency of these processes for individual molecules is found through the photolysis rate coefficient, j (in units of s^{-1}). These are calculated using the following equation E1:

$$j = \int_{700\text{nm}}^{300\text{nm}} \varphi(\lambda) * \sigma(\lambda) * F(\lambda) * d\lambda \quad \text{E1}$$

Where φ(λ) is the primary quantum yield (dimensionless) for the photolysis of an individual molecule averaged over the wavelength interval dλ (in the example shown for E1, a typical surface level wavelength range of 300-700 nm is shown). The quantum yield represents the fraction of molecules that undergo photolysis at each wavelength. σ(λ) (units nm^2/molecule) is the absorption cross section of a molecule and is again considered over a particular wavelength interval dλ. It measures the ability of a molecule to absorb light at a particular wavelength. F(λ) is the irradiance (units of quanta/nm^2/s), describing the intensity of light available to the molecules for absorption. The irradiance depends on many factors, such as time of day and year, location, cloud conditions and the total amount of particles and O_3 in the air between the sun and the location of interest (Finlayson-Pitts and Pitts, 2000).

Figure 1.2 shows the electromagnetic spectrum with the absorption of some key atmospheric gases (O_3, HCHO, hydrogen peroxide (H_2O_2), nitrogen dioxide (NO_2), nitrous acid (HONO) and chlorine dioxide (OClO)) in the atmosphere on it. As shown in Figure 1.2, OClO can absorb over a large range of wavelengths compared to O_3, HCHO, H_2O_2, NO_2 and HONO.

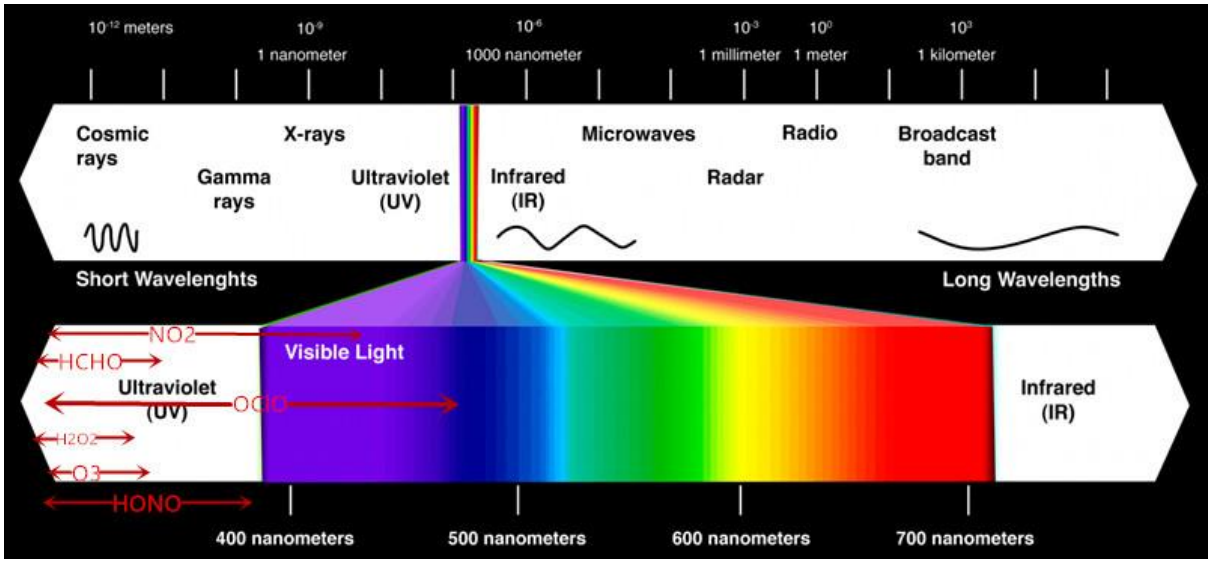

Figure 1.2: Electromagnetic spectrum with the absorption of key gases (O_3, HCHO, H_2O_2, NO_2, OClO and HONO) in the atmosphere (adapted from Mukesh 2015).

Photochemistry drives the composition of the outdoor atmosphere. Radicals, such as OH and hydroperoxy (HO_2), which are produced from the photolysis of trace gases (e.g. O_3 and

HCHO respectively), control the oxidizing capacity of the troposphere. In the atmosphere, OH reacts with trace gases (e.g. VOC) rapidly in order to form more radicals and a range of secondary species, some of which are harmful to health (e.g. PM: Lippmann et al., 2003; Englert, 2004; Valavanidis et al., 2008). It is therefore important to understand the impacts of photochemical production of different species, so we can mitigate against the formation of harmful products such as PM.

Photolysis of many atmospheric gases will directly or indirectly produce radicals (e.g. OH, HO_2 and Cl), which control the oxidizing capacity in the atmosphere. The next section therefore summarises these processes.

1.3. Photolysis of major atmospheric gases

1.3.1. Ozone (O_3)

O_3 plays an important role on the chemistry in the troposphere due to its highly reactive characteristics: it can absorb ultraviolet and infrared light (Finlayson-Pitts and Pitts-Jr, 2000). It is photolysed in one of two ways:

$O_3 + h\nu \rightarrow O_2 + O(^1D)$ $\lambda < 349$ nm R1a

$\rightarrow O_2 + O(^3P)$ $\lambda < 700$ nm R1b

$O(^1D)$ and $O(^3P)$ are atomic oxygen atoms, which are very reactive. The O (^1D) atoms can then react further with H_2O and N_2O to form OH radicals (Figure 1.3) and NO respectively (Matsumi et al., 2002), R2-3:

$O\ (^1D) + H_2O \rightarrow 2OH$ R2

$O\ (^1D) + N_2O \rightarrow 2NO$ R3

These OH radicals can then react with numerous trace gases (e.g. VOC) in order to form more radicals and a range of secondary species in the atmosphere (Figure 1.3). The O (^3P) produced in R1b reacts immediately with O_2 to reform O_3 (Matsumi and Kawasaki 2003), R4:

$O\ (^3P) + O_2 + M \rightarrow O_3 + M$ R4

1.3.2. Nitrogen dioxide (NO_2)

The photolysis of NO_2 can produce O (^3P) through R5, which then reacts with O_2 to produce O_3 in the atmosphere through R4.

$NO_2 + h\nu \rightarrow NO + O\ (^3P)$ $\lambda<424$ nm R5

This reaction plays an important role in the atmosphere as the most important source of tropospheric O_3.

1.3.3. Nitrous acid (HONO) and Nitric acid (HNO_3)

Both HONO and HNO_3 are important photochemical reactants in the atmosphere due to the direct production of OH (Figure 1.3).

$HONO + h\nu \rightarrow OH + NO$ $\lambda < 395$ nm R6

$HNO_3 + h\nu \rightarrow OH + NO_2$ $\lambda < 350$ nm R7

Photolysis of HONO is an important source of OH radicals in the polluted urban atmosphere, particularly when sunlight reaches its highest intensity (e.g. Calvert et al., 1994). It can also contribute to OH formation early in the morning before ozone photolysis, as it requires lower energy light than ozone to dissociate and form radicals. This difference in absorption characteristics is also important for indoors as shown later in section 4.4. Compared to HONO, the photolysis rate for HNO_3 is very slow.

1.3.4. The nitrate radical (NO_3) and dinitrogen pentoxide (N_2O_5)

In the atmosphere, NO_3 is an important oxidant for the chemistry at night-time (Finlayson-Pitts and Pitts-Jr, 2000). Photolysis of N_2O_5 produces NO_3 directly (R9), whilst the reaction of NO_3 with NO_2 can reform N_2O_5 (R10), linking these two species together.

$NO_3 + h\nu \rightarrow NO_2 + O(^3P)$ $\lambda < 690$ nm R8a

$\rightarrow NO + O_2$ $\lambda < 690$ nm R8b

$N_2O_5 + h\nu \rightarrow NO_3 + NO_2\ (NO + O)$ $\lambda < 398$ nm R9

$NO_3 + NO_2 + M \leftrightarrow N_2O_5 + M$ R10

1.3.5. Organic nitrates and peroxyacetyl nitrates

Photolysis of organic nitrates such as ethyl nitrate ($C_2H_5ONO_2$) can produce NO_2 and HONO as shown through pathways R11. For $C_2H_5ONO_2$, R11a is the favoured path (50.8%) followed by R11c (29.3%) and then R11b (19.9%) (Rebbert 1999, Finlayson-Pitts and Pitts-Jr, 2000).

$C_2H_5ONO_2 + h\nu \rightarrow C_2H_5O + NO_2$ $\lambda < 330$ nm R11a

$\rightarrow CH_3CHO + HONO$ $\lambda < 330$ nm R11b

$\rightarrow C_2H_5ONO + O$ $\lambda < 330$ nm R11c

Photolysis of peroxyacetyl nitrate species such as $CH_3C(O)OONO_2$ (PAN) can produce NO_2 and NO_3, but R12b is the most important pathway (~83%). PAN is recognized as an important reservoir for nitrogen oxides (Singh and Hanst, 1981) and is also confirmed to be a strong eye irritant (e.g. Stephens et al., 1961). It is stable under low temperatures but can be decomposed to produce NO_2 at higher temperatures (Finlayson-Pitts and Pitts-Jr, 2000).

$CH_3C(O)OONO_2 + h\nu \rightarrow CH_3C(O)O + NO_3$ $\lambda < 350$ nm R12a

$\rightarrow CH_3C(O)OO + NO_2$ $\lambda < 350$ nm R12b

$\rightarrow CH_3C(O) + O_2 + NO_2$ $\lambda < 350$ nm R12c

1.3.6. Hydrogen peroxide (H_2O_2), organic hydroperoxides (CH_3OOH) and organic hydroxymethyl hydroperoxide ($HOCH_2OOH$)

During photolysis of these chemicals, OH is the major product produced. Some of these reactions also produce oxy radicals (RO) which can then react with O_2, thermally decompose or isomerise (depending on the parent VOC) to typically produce HO_2.

$H_2O_2 + h\nu \rightarrow 2OH$ $\lambda < 350$ nm R13

$CH_3OOH + h\nu \rightarrow CH_3O + OH$ $\lambda < 365$ nm R14

$HOCH_2OOH + h\nu \rightarrow HOCH_2O + OH$ $\lambda < 365$ nm R15

The OH radicals can then react with trace gases (Figure 1.3).

1.3.7. Aldehydes and Ketones

Formaldehyde photolysis forms a formyl radical (HCO) and an H atom (R16a), with both products reacting almost exclusively with molecular oxygen to form HO_2 (R17 and R18). Formaldehyde can also photolyse to form carbon monoxide (CO) and hydrogen gas (H_2) (R16b). This reaction pathway does not lead to radical formation. For normal conditions, R16b dominates HCHO photolysis at wavelengths below 270 nm and over 327 nm while R16a dominates at wavelengths between 270 and 327 nm.

$HCHO + h\nu \rightarrow H + HCO$ $\lambda < 356$ nm R16a

$\rightarrow H_2 + CO$ $\lambda < 356$ nm R16b

$HCO + O_2 \rightarrow CO + HO_2$ R17

$H + O_2 \rightarrow HO_2$ R18

For CH_3CHO, R19a dominates in the wavelength range between 265 and 330 nm. Again, HCO and H produced from CH_3CHO photolysis will react with molecular oxygen to form HO_2 (R17 and R18). The CH_3 radical produced in R19a can react with O_2 to produce CH_3O_2 which can then react rapidly with OH (Assaf et al., 2017).

$CH_3CHO + h\nu \rightarrow CH_3 + HCO$ $\lambda < 330$ nm R19a

$\rightarrow CH_3CO + H$ $\lambda < 320$ nm R19b

Ketones such as acetone shown in R20 (CH_3COCH_3) can also be an important source of free radicals (Finlayson-Pitts and Pitts-Jr, 2000). For CH_3COCH_3, R20a is more important when $\lambda<315$ nm while R20b is more important between 315 and 327 nm (Blitz et al., 2004).

$CH_3COCH_3 + h\nu \rightarrow CH_3CO + CH_3$ $\lambda < 327$ nm R20a

$\rightarrow 2CH_3 + CO$ $\lambda < 327$ nm R20b

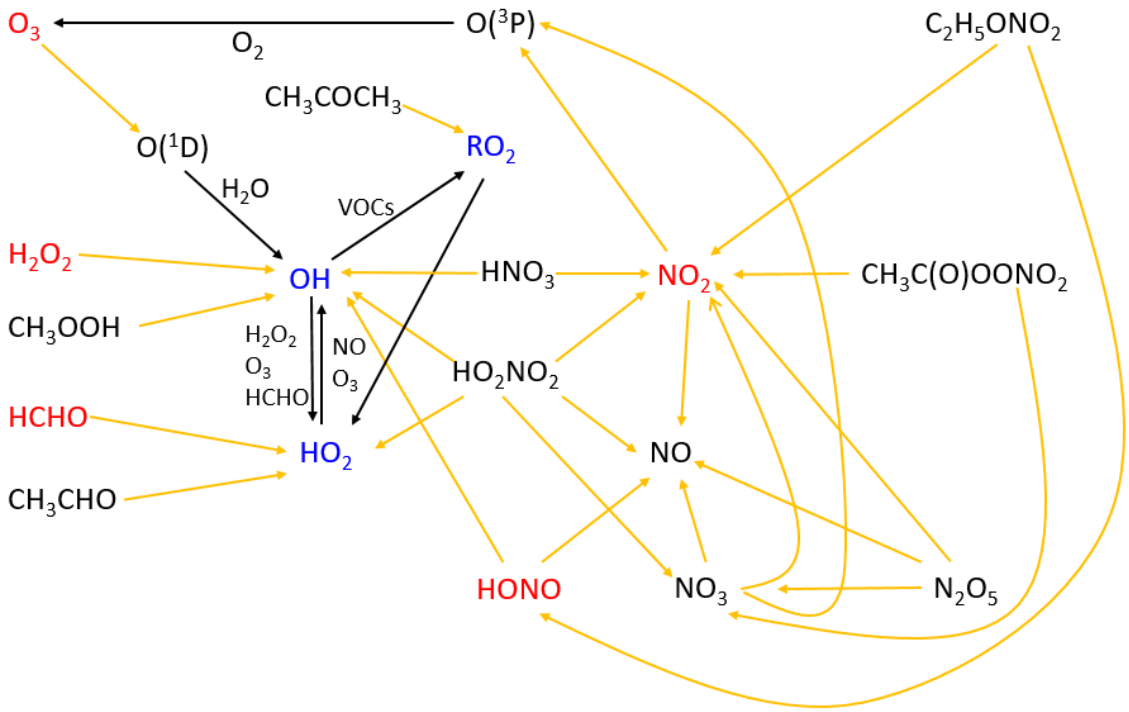

Figure 1.3: Summary of the photochemistry of important atmospheric species. Photolysis routes are marked in yellow. The radicals studied in this thesis are marked in blue, whilst other key indoor species investigated in this thesis are marked in red.

1.3.8. Summary

In summary, photolysis of important atmospheric species can directly (including HNO_3, HONO, HO_2NO_2, H_2O_2, CH_3OOH) or indirectly (including O_3, NO_2, NO_3, $C_2H_5ONO_2$, HCHO, CH_3CHO, CH_3COCH_3) produce radicals. The ongoing chemistry can then often lead to the formation of harmful secondary species, such as OH reactions with VOCs to produce more radicals and harmful secondary species, including PM (e.g. Lippmann et al., 2003; Englert, 2004; Valavanidis et al., 2008).

1.4. Indoor photolysis

The importance of photolysis for outdoor air chemistry is well established, but the role of indoor photolysis is less well studied and hence quantified. Indoor photolysis has not been traditionally recognized as an important source of oxidants in indoor environments, as indoor lights do not generally emit photons within the low wavelength range between 290 and 330 nm which is responsible for initiating the vast majority of outdoor photolysis processes. Also,

the amount of light passing indoors through windows was thought to be too low to affect indoor chemistry.

Indoor light includes artificial lighting indoors and attenuated sunlight that can move into indoor environments through windows and skylights. The contribution of artificial light to overall photolysis indoors depends on the location of the light within the room, the geometry of the room and the type of light (Kowal et al., 2017). The amount of light that can penetrate indoors is influenced by many factors, including the type of window, meteorological conditions (e.g. cloudiness), time of year and day and the building orientation and location. In turn, the properties of different glasses, such as transmittance and cut-off wavelengths, may be influenced by many factors, such as the solar angle (Rubin et al., 1998), the applied coatings (Bloquet et al., 2018; Gomez Alvarez et al., 2013) and the structure of window (Asdrubali and Baldinelli, 2009).

Just as for outdoors, the most efficient photolysis occurs where high values of absorption tendency overlap with high values of emission intensity. In Figure 1.4, the left-hand y-axis shows the product of the absorption cross-sections and quantum yields for different gases commonly found indoors. The higher values indicate more efficient absorption. The right-hand y-axis shows the spectral emissions of different indoor light sources (fluorescent lamps and attenuated sunlight), with the higher values on this axis indicating that more photons are emitted by that light source.

Figure 1.4 shows that OClO will be photolysed at greater rates than the other species over almost the entire 290-410 nm wavelength range. Meanwhile, the strongest absorption of light for O_3 and H_2O_2 happens at lower wavelengths, but there is still some absorption overlap with the fluorescent bulbs and sunlight above 350 nm. For HCHO, its absorption bands only really overlap with bare fluorescent bulb transmission, which suggests indoor photolysis may not be that important for this species (see Chapter 6). Therefore, all of these chemical species can be photolysed in the indoor environment under some conditions. So indoor photolysis is worth researching as it can directly or indirectly produce radicals which can then lead to the formation of harmful secondary species indoors as explained above.

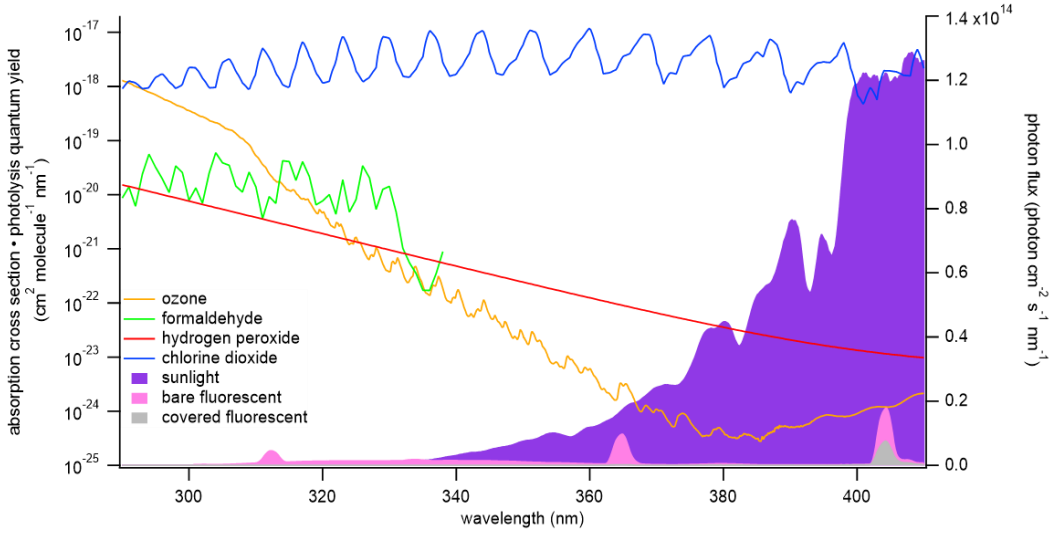

Figure 1.4: The product of photolysis quantum yields and absorption cross sections for O_3, HCHO, H_2O_2 and OClO in the actinic region (left y axis), and measured photon fluxes 1m away from fluorescent lights and a sunlit window in an office (right y axis). Source: Kowal et al. (2017).

In the absence of measurements of photolysis rates indoors, our early understanding of indoor photolysis was based on model results (Nazaroff and Cass 1986; Carslaw 2007; Wong et al., 2017) as discussed in Chapter 2. These studies suggested that although photolysis is indeed diminished indoors (e.g.by glass in windows and coverings on light sources), it still occurs, particularly for reactions that occur at longer wavelengths. Therefore, there could be notable impacts on indoor air chemistry.

1.5 Aims of the dissertation

The aims of this thesis are therefore to:

- Improve the representation of artificial indoor lighting in an existing detailed chemical model (the INDCM).
- Improve the treatment of attenuated sunlight in the same model.
- Use the improved model to investigate how building-related factors (indoor artificial lights and window glass composition) affect indoor photolysis rates and hence indoor air chemistry.
- Use the improved model to investigate how external factors (cloudiness, latitude and season) affect indoor photolysis rates and hence indoor air chemistry.

- Use the new model to explore the impact of different cleaning activities on indoor air chemistry under different indoor lighting conditions.

1.6 Structure of the thesis

The thesis is now structured as follows:

Chapter 2: This chapter presents a literature review of models that have been used previously to study indoor air, focusing on those with relevance for indoor photolysis. There is also a review of the relevant measurements for studying indoor photolysis.

Chapter 3: This chapter introduces the Indoor Chemical Model (INDCM) and the methodology used in this thesis in detail.

Chapter 4: This chapter describes the improvements made to the representation of artificial indoor lighting and the treatment of attenuated sunlight in the INDCM. The improved model is then used to investigate the impacts of building-related factors (indoor artificial lights and window glass composition) on indoor photolysis rates and hence indoor air chemistry. Seven different indoor artificial lights together with three different glass types with very different cut-off wavelengths are selected for the study. Concentrations of key indoor species and the rates of key reactions for different lighting conditions are reported.

Chapter 5: This chapter uses the improved INDCM to investigate the impacts of external factors (cloudiness, latitude and season) on indoor photolysis rates and hence indoor air chemistry. Three different cloudiness levels, twelve days (one from each month) and eight different locations on the planet are selected for investigation. Again, concentrations of indoor key species and predicted concentrations of radicals are studied in order to find out the impacts of different controlling factors on indoor air chemistry.

Chapter 6: This chapter compares the impacts of all of the controlling factors on indoor photolysis rates explored in chapters 4 and 5, and ranks them in order of importance, as well as identifying which predicted indoor species concentrations are most sensitive to changes in these different model inputs.

Chapter 7: This chapter includes two case studies describing the impacts of indoor photolysis on radical production following two very different ways of indoor cleaning (automated and traditional cleaning techniques). The first case study focuses on No-touch devices (NTDs), which are a relatively recent innovation for automated cleaning, and the

second case study investigates indoor air chemistry following the use of a household non-bleach cleaning fluid for surface cleaning. For both cleaning activities, different lighting conditions were explored.

Chapter 8: This chapter summarises the overall findings of this thesis together with wider implications and recommendations for further study.

Chapter 2. Literature Review

2.1. Introduction

It has been several decades since the first indoor air chemistry model was proposed. Models for indoor air chemistry have become more and more complex since then, aiming to better represent the real indoor environment. This chapter first describes the development of some of the most important indoor air chemistry models, which have investigated aspects of indoor air chemistry relevant to this work. It then moves on to review modelling studies that have focused on aspects of indoor photochemistry and finishes with a review of indoor photolysis measurements of relevance to this dissertation.

2.2. Indoor air models

2.2.1. Simple chemical models

Nazaroff and Cass (1986) first used a mathematical model to predict the concentrations of some key chemical species in a simulated museum. This model considered photolytic and chemical reactions, direct emissions, heterogeneous removal, filtration and ventilation (Nazaroff and Cass, 1986). In the model, the concentration of each pollutant was calculated by summing contributions from all sources, including formation from chemical reactions, indoor direct emissions, introduction through the ventilation system from outdoors via infiltration (which is air directly infiltrated from outdoor environment) and transport between the individual rooms, and then subtracting losses, such as removal through chemical reactions and surface processes. E2 describes the rate of change of the concentration of each chemical species in the model (Nazaroff and Cass, 1986).

$$\frac{dC}{dt} = S - LC \qquad E2$$

Where S is the sum of all sources, including production by chemical reaction, transport from other places (e.g. outdoors) and direct emission. L is the sum of all sinks, such as removal by transport, surface loss and loss by chemical reactions. C is the concentration of a pollutant (molecule/cm^3).

The simulated museum gallery had a surface area of 3060 m^2 and a volume of 2530 m^3. The mechanical ventilation system exchanged and supplied air for the rooms at rates between 0.3-2.0 h^{-1}, which was adopted from measured data in the museum (Nazaroff and Cass, 1986).

Meanwhile, photolysis from both indoor artificial lights and attenuated sunlight were considered in this work. This method is explained in further detail in Chapter 3.

Indoor background concentrations of NO, NO_2 and O_3 were measured in the museum. Moreover, hourly averaged outdoor concentrations of individual or groups of species used in the model (e.g. NO, NO_2, O_3, HONO, H_2O_2, HCHO, nitro compounds (RNO_2), alkenes, aromatics, olefins, higher aldehydes and ethylene) were measured either in this study or in previous studies in California (Nazaroff and Cass, 1986). Irreversible surface deposition was also added into the model for some species, including HCHO, NO, NO_2 and O_3 using deposition velocities from previous studies, although surface reactions had not been well studied at the time.

The model was used to compare with measured concentrations of NO, NO_2, NO_3, O_3, HONO, H_2O_2, HCHO and HNO_3 and was in relatively good agreement for NO_2 and O_3 (6% and 3% difference respectively on average), while NO was under predicted (15% difference on average) (Nazaroff and Cass, 1986). Their work emphasised the important role of photochemical reactions in the indoor environment and created a new way to study indoor air chemistry. However, there were still many limitations in their study, including the lack of representation of detailed indoor surface processes. Nazaroff and Cass (1986) suggested that further study on the kinetics of mass transport and surface-reaction was necessary, especially on indoor heterogeneous chemistry, the rate of chemical reactions, surface interactions and the process of deposition, in order to have a better understand of indoor air chemistry.

A more recent study used a simple mass balance model to focus on indoor production of the hydroxyl radical (OH), which extended the use of indoor air chemistry models (Weschler and Shields 1996). The OH radical had received little attention in previous studies, although it was recognised as a photolysis product in Nazaroff and Cass (1986). OH radicals are formed through the reactions between ozone and alkenes/monoterpenes in the atmosphere (Atkinson et al., 1992; Paulson and Seinfeld; 1992; Paulson et al., 1992). However, the potential impacts of these reactions indoors were examined in detail by Weschler and Shields (1996).

Weschler and Shields (1996) included the reactions of 13 VOCs selected for being common in the indoor environment (1,3-butadiene, ethane, camphene, propene, styrene, iso-butene, isoprene, cis-2-butene, trans-2-butene, α-pinene, 2-methyl-2-butene, α-terpinene and d-limonene) with ozone in the indoor environment to produce OH radicals. OH radicals were then assumed to be removed by 39 reactions with the 13 VOCs (and inorganic gases)

following a chain of oxidation reactions (Weschler and Shields 1996). In addition, this one-compartment mass balance model included not only indoor concentrations of VOCs, NH_3, SO_2, O_3, CO and NO_2 and outdoor chemical concentrations, but also assumed a surface to volume ratio of 2.8 m^{-1}, the deposition velocity of indoor OH at 0.0007 m/s and air exchange rate (AER) of 1 h^{-1}.

The indoor ozone concentration was set to 20 ppb (as a typical indoor concentration), the concentrations of CO and NOx were measured and indoor concentrations of VOCs and their rates of reactions were based on previous literature (Brown et al., 1994). The OH formation yield for each VOC and the individual rate constants were obtained from the literature and together with the indoor VOC concentrations, used to calculate OH production rates (Weschler and Shields 1996). E3 was used to calculate indoor concentrations of the OH radical.

$$\frac{\mathrm{d}[OH_{indr}]}{\mathrm{dt}} = E_x[OH_{otdr}] + \sum y_i k_{O_{3i}}[O_3][VOC_i] - E_x[OH_{indr}] - k_d\left(\frac{A}{V}\right)[OH_{indr}] - \sum k_{OH_i}[OH_{indr}][VOC_i] \quad \text{E3}$$

Where $[OH_{indr}]$ and $[OH_{otdr}]$ are concentrations of indoor and outdoor OH radicals in ppb. E_x is the air exchange rate (s^{-1}). y_i is the OH formation yield for the reaction of ozone-alkene while k_{O3} is its reaction rate constant in $ppb^{-1}\ s^{-1}$. $[O_3]$ and $[VOC_i]$ are indoor concentrations of O_3 and VOC in ppb respectively. k_d is the indoor deposition velocity of OH in m s^{-1}. A/V is the indoor surface to volume ratio in m^{-1}. k_{OHi} is the rate constant for the reaction between OH and each individual VOC species ($ppb^{-1}\ s^{-1}$).

The results from their model showed the predicted indoor concentration of OH was 1.7×10^5 molecule/cm^3 which was lower than the typical concentration of OH at noon in the outdoor environment (5.0×10^6 molecules/cm^3), but almost four times larger than its outdoor concentration at night time (Weschler and Shields 1996). Moreover, when comparing the impacts on OH formation of the VOCs included in the model, the reaction between O_3 and d-limonene had the greatest contribution to OH production (OH production rate 2.6×10^{-4} ppb/s, ~56% of indoor OH production), followed by α-terpinene (1.2×10^{-4} ppb/s, 26%), 2-methyl-2-butene (4.2×10^{-5} ppb/s, 9%) and α-pinene (1.6×10^{-5} ppb/s, 3.4%). The reactions between O_3 and VOCs were also found to have higher OH production rates than the reaction of HO_2 with NO, photolysis of O_3 (λ<320 nm), H_2O_2 (λ<360 nm) and HONO (λ<400 nm) and transport from the outdoor environment (Weschler and Shields, 1996). Meanwhile, the

OH loss rate for the reaction between OH and d-limonene with calculated to be 12.3 s^{-1}, followed by those for NO_2 (9.0 s^{-1}), C_2H_5OH (7.9 s^{-1}), HCHO (7.2 s^{-1}), CO (5.9 s^{-1}) and C_5H_8 (5.0 s^{-1}), which were found to play the most important role in the removal of OH radicals (Weschler and Shields 1996). The need for further improvement in the representation of indoor air chemistry in indoor air models was highlighted (Weschler and Shields 1996).

2.2.2. Moderately complex chemical models

A much more complex indoor air quality model is the Indoor Chemistry and Exposure Model (ICEM), which was developed and used to study indoor concentrations of OH radicals by Sarwar et al. (2002). An updated version of the SAPRC-99 mechanism (Carter 2000, 2003) was used in the ICEM together with improved representation of indoor formation and removal of OH (Sarwar et al., 2002). In addition, the formation yields for OH radicals from alkene reactions were updated based on Paulson et al. (1999). The ICEM considered indoor deposition and homogeneous chemistry assuming a single well-mixed environment for the indoor setting. Moreover, it included indoor emissions, chemical reactions and air exchange reactions. The deposition velocities, air exchange rate and indoor and outdoor pollutant concentrations were obtained from the previous literature. Sarwar et al. (2002) highlighted that although the use of cleaning agents and smoking could influence indoor VOC concentrations, they just assumed average concentrations of VOCs to simulate background concentrations of radicals.

The ICEM model contained 51 species including 46 VOCs. Half of the indoor light was assumed to come from artificial lights while half came from sunlight, while the surface area was ~610 m^2, the volume of the building was 500 m^3, the indoor temperature was 297 k, relative humidity was 50% and the air exchange rate was 0.5 h^{-1} (Sarwar et al., 2002).

Figure 2.1 shows the list of reactions included in the ICEM, which produce and remove OH radicals. The results showed that the predicted OH concentration under the background conditions was 1.2×10^5 molecule/cm^3. As for Weschler and Shields (1996), the predicted concentration was lower than ambient levels of OH radicals during the summer time (5-10 $\times$ 10^6 molecule/cm^3), but similar or higher than typical levels of OH radicals outdoors during the night-time (~5×10^4 molecule/cm^3) (Sarwar et al., 2002). Moreover, according to Sarwar et al. (2002), the predicted OH concentrations were within 0.3-12% of the predicted concentrations by Weschler and Shields (1996) for similar background conditions.

No.	Reactions that produce $OH^{\bullet}$	No.	Reactions that consume $OH^{\bullet}$
3	$NO + HO_2^{\bullet} = OH^{\bullet} +$	23	$NO + OH^{\bullet} =$
4	$O_3 + HO_2^{\bullet} = OH^{\bullet} +$	24	$O_3 + OH^{\bullet} =$
5	$NO_3^{\bullet} + HO_2^{\bullet} = 0.8\ OH^{\bullet} +$	25	$NO_3^{\bullet} + OH^{\bullet} =$
6	Ethene $+ O_3 = 0.18\ OH^{\bullet} +$	26	Ethene $+ OH^{\bullet} =$
7	Isoprene $+ O_3 = 0.25\ OH^{\bullet} +$	27	Isoprene $+ OH^{\bullet} =$
8	Propene $+ O_3 = 0.35\ OH^{\bullet} +$	28	Propene $+ OH^{\bullet} =$
9	Isobutene $+ O_3 = 0.72\ OH^{\bullet} +$	29	Isobutene $+ OH^{\bullet} =$
10	*cis*-2-Butene $+ O_3 = 0.37\ OH^{\bullet} +$	30	*cis*-2-Butene $+ OH^{\bullet} =$
11	*trans*-2-Butene $+ O_3 = 0.64\ OH^{\bullet} +$	31	*trans*-2-Butene $+ OH^{\bullet} =$
12	2-Methyl 2-butene $+ O_3 = 1.0\ OH^{\bullet} +$	32	2-Methyl 2-butene $+ OH^{\bullet} =$
13	1,3-Butadiene $+ O_3 = 0.13\ OH^{\bullet} +$	33	1,3-Butadiene $+ OH^{\bullet} =$
14	3-Carene $+ O_3 = 1.0\ OH^{\bullet} +$	34	3-Carene $+ OH^{\bullet} =$
15	d-Limonene $+ O_3 = 0.86\ OH^{\bullet} + 0.04$ AMCYCHEX $+ 0.04$ IPOH $+ 0.19$ HCHO	35	d-Limonene $+ OH^{\bullet} = 0.2$ AMCYCHEX $+ 0.29$ IPOH $+$
		36	AMCYCHEX $+ OH^{\bullet} =$
		37	IPOH $+ OH^{\bullet} =$
16	Styrene $+ O_3 = 0.07\ OH^{\bullet} +$	38	Styrene $+ OH^{\bullet} =$
17	Criegee biradical $1 = 0.8\ OH^{\bullet} + 0.3$ PINALD	39	α-Pinene $+ OH^{\bullet} = 0.34$ PINALD $+$
18	Criegee biradical $2 = 0.8\ OH^{\bullet} +$	40	PINALD $+ OH^{\bullet} =$
19	Methacrolein $+ O_3 = 0.20\ OH^{\bullet} +$	41	Methacrolein $+ OH^{\bullet} =$
20	Methyl vinyl ketone $+ O_3 = 0.16\ OH^{\bullet} +$	42	Methyl vinyl ketone $+ OH^{\bullet} =$
21	Lumped isoprene product species $+ O_3 = 0.285\ OH^{\bullet}$	43	Lumped isoprene product $+ OH^{\bullet} =$
22	Reactive aromatic fragmentation products $+ O_3 = 0.5\ OH^{\bullet} +$	44	Reactive aromatic fragmentation products $+ OH^{\bullet} =$
		45	HONO $+ OH^{\bullet} =$
		46	$NO_2 + OH^{\bullet} =$
		47	$HNO_3 + OH^{\bullet} =$
		48	$CO + OH^{\bullet} =$
		49	$HO_2NO_2 + OH^{\bullet} =$
		50	$H_2O_2 + OH^{\bullet} =$
		51	$HO_2^{\bullet} + OH^{\bullet} =$
		52	$SO_2 + OH^{\bullet} =$

Figure 2.1: The list of reactions producing and removing OH radicals in ICEM (Sarwar et al., 2002).

Concentrations of indoor OH radicals were found to increase non-linearly with the increase in emission rates of indoor alkenes, outdoor O_3 levels and air exchange rates. OH concentrations increased slightly and peaked at an outdoor NO concentration of 12 ppb and then decreased as outdoor NO concentrations increased further (Sarwar et al., 2002). A sensitivity study showed that the predicted OH concentrations increased by only 20% when the indoor light intensity was doubled, and by 66% when indoor temperature rose from 290 to 315 K (note that is a large range in indoor temperatures). The deposition rate of hydroxyl radicals (0.0006 ppt/min) and transportation of outdoor OH indoors (at 0.02 ppt/min) had little influence on predicted indoor OH concentrations, compared to the ~10 ppt/min consumption rate through OH-alkene reactions and ~10 ppt/min production rate through O_3-alkene reactions.

Again, the reactions of O_3 with VOCs were found to dominate indoor production of OH radicals, especially the reactions of O_3 with d-limonene (production rate 6.4 ppt/min) which constituted 40% of the total production. On the contrary, the reactions with d-limonene and isoprene were proved to be the main sinks of indoor OH radicals with consumption rates of

2.6 and 1.3 ppt/min respectively. Nevertheless, the highest indoor OH concentration occurred when both the products and substrates were in high concentrations at the same time, suggesting that significant and rapid chemical processing was occurring.

Sarwar et al. (2002) also found a wide range of secondary chemicals were produced by the reaction of O_3 with limonene, which indicated that OH radicals may have negative impacts on air quality in the indoor environment. For instance, oxidised products, such as pinonaldehyde and 3-isopropenyl-6-oxoheptanal (IPOH), which have multifunctional groups (-COOH, -OH and =O) can be produced by the reaction of OH with terpenes. According to Nazaroff and Weschler (2004), these products can have negative health impacts, including occupational asthma and eye and skin irritation. In addition, fine particles can also be formed through secondary reactions (Wallace, 1996), leading to the recommendation for further research on the production of secondary pollutants through the reactions between VOCs and OH radicals (Sarwar et al., 2002).

A time-averaged model by Waring and Wells (2015) investigated the impacts of predicted concentrations of NO_3, OH and O_3 on the gas-phase conversion rates of VOCs in typical residences. This work was based on a Monte Carlo framework in which inputs were varied probabilistically. The reactions shown in Figure 2.3 were used in their model to predict concentrations of stabilized Criegee intermediates (SCI), N_2O_5, HONO, NO_2, NO NO_3, OH and O_3. The reactions between SCI and NO_2 to produce NO_3, photolysis of HONO to produce OH radicals and previously mentioned sources of indoor oxidants were also included in this model. Compared to other explicit models which are suitable for investigating detailed investigation of the chemistry (e.g. Sarwar et al., 2002, 2004; Carslaw, 2007, Carslaw et al., 2012; Carslaw, 2013), this time-averaged model was not explicit and the kinetics were simplified in the model. In addition, air exchange in the model was considered as a combination of natural ventilation and infiltration with an assumption of a single well-mixed environment.

No.	Reaction
1	$O_3 + \text{alkene}_i \rightarrow \text{intermediates} \rightarrow OH + SCI + \text{products}$
2	$OH + VOC_i \rightarrow \text{products}$
3	$O_3 + NO \rightarrow NO_2 + O_2$
4	$O_3 + NO_2 \rightarrow NO_3 + O_2$
5	$OH + NO + M \rightarrow HONO + M$
6	$OH + NO_2 + M \rightarrow HONO_2 + M$
7	$OH + NO_3 \rightarrow HO_2 + NO_2$
8	$OH + OH \rightarrow H_2O + O$
9	$OH + O_3 \rightarrow HO_2 + O_2$
10	$NO_3 + VOC_i \rightarrow \text{products}$
11	$NO_3 + NO \rightarrow 2NO_2$
12	$NO_3 + NO_2 \rightarrow N_2O_5$
13	$N_2O_5 \rightarrow NO_3 + NO_2$
14	$2NO_2(g) + H_2O(aq) \rightarrow HONO(aq) + H^+ + NO_3^-$
15	$NO_2(g) + HONO(aq) \rightarrow H^+ + NO_3^- + NO$
16	$HONO(aq) \leftrightarrow HONO(g)$
17	$HONO + h\nu \rightarrow OH + NO$
18	$OH + HONO \rightarrow H_2O + NO_2$
19	$SCI + NO_2 \rightarrow NO_3 + \text{products}$
20	$SCI + H_2O \rightarrow \text{products}$

Figure 2.2: List of reactions and their rates constants in the time-averaged model (Waring and Wells 2015).

According to Waring and Wells (2015), the time-averaged equations in their model were solved in four different sets based on the Monte Carlo analysis, with each set run 10,000 times. All four sets included variable concentrations of outdoor NO_x and O_3, and stable indoor background VOCs. The second set included additional variable concentrations of indoor limonene while the third set included additional variable emissions of HONO and NO_x in the indoor environment. The fourth set included both additional variable emissions of HONO and NO_x in the indoor environment and variable concentrations of limonene. Median residential VOC concentrations and reaction rate coefficients were obtained from the literature and used to determine total VOC oxidation rates by NO_3, OH and O_3. The total VOC oxidation rates declined with an increase in O_3 deposition or NO concentrations, but increased with AER, the HONO photolysis rate and concentrations of indoor limonene and outdoor NO_2 and O_3.

Photolysis of HONO was an important source of indoor OH radicals as well as ozone-alkene reactions under some conditions. In addition, VOC oxidation rates were found to be dominated by OH when outdoor NO_x was high (~116 ppb) and outdoor O_3 was low (~4 ppb) and by both OH and O_3 when outdoor NO_x was low (~0.3 ppb) and outdoor O_3 was high (~142 ppb). Many secondary products, including SOA, carboxylic acids, carbonyls and alcohols, were produced following the oxidation reactions. Waring and Wells (2015) recommended further research on terpenes other than limonene, in order to better improve and validate the predictions.

2.2.3. Near-explicit chemical models

Carslaw (2007) constructed a detailed chemical box model to study indoor air chemistry. The reactions of inorganic species and VOCs which drive the air chemistry in indoor environments were included in the near-explicit chemical mechanism in this model. The basis of the INdoor air Detailed Chemical box Model (INDCM) is a comprehensive chemical mechanism (the Master Chemical Mechanism, MCM v3.1) (Jenkin et al., 1997, 2003; Saunders et al., 2003). Compared to previous indoor air models, no simplifications (the use of surrogate species and lumping) were used in the mechanism of this model, which allowed further detailed research on air chemistry in the indoor environment. Approximately 5,000 species and 20,000 reactions (describing gas-phase chemistry, surface reactions, deposition, emissions and exchange with outdoors) were represented in this comprehensive mechanism. The INDCM assumes a single well-mixed environment.

Carslaw (2007) researched a typical urban residence in the UK assuming a 2.0 h^{-1} air exchange rate, a temperature of 293 K, 50% relative humidity and 3.0 m^{-1} surface to volume ratio. Meanwhile, irreversible surface deposition (many of the values of surface deposition were adopted from Sarwar et al. (2002)) were also included in this model. Both indoor artificial lighting and attenuated sunlight were considered for photolysis based on the method described by Nazaroff and Cass (1986).

The results showed a factor of ~10-20 lower predicted indoor OH concentrations (up to 4.0×10^5 molecule/cm^3) than outdoors, but these were still sufficient to have important impacts on indoor air chemistry (Carslaw 2007). Through investigating the formation, propagation and termination routes of radicals (OH, HO_2 and RO_2), the results demonstrated that reactions of O_3 with terpenes dominated the production of OH and RO_2 radicals. The results also

indicated that the transformation between OH and HO_2 was driven by the reaction of OH with alcohols and that the reactions of OH with monoterpenes dominated the cycling between OH and RO_2 (Carslaw 2007). Figure 2.2 shows the main chemical processes between radicals in indoor air.

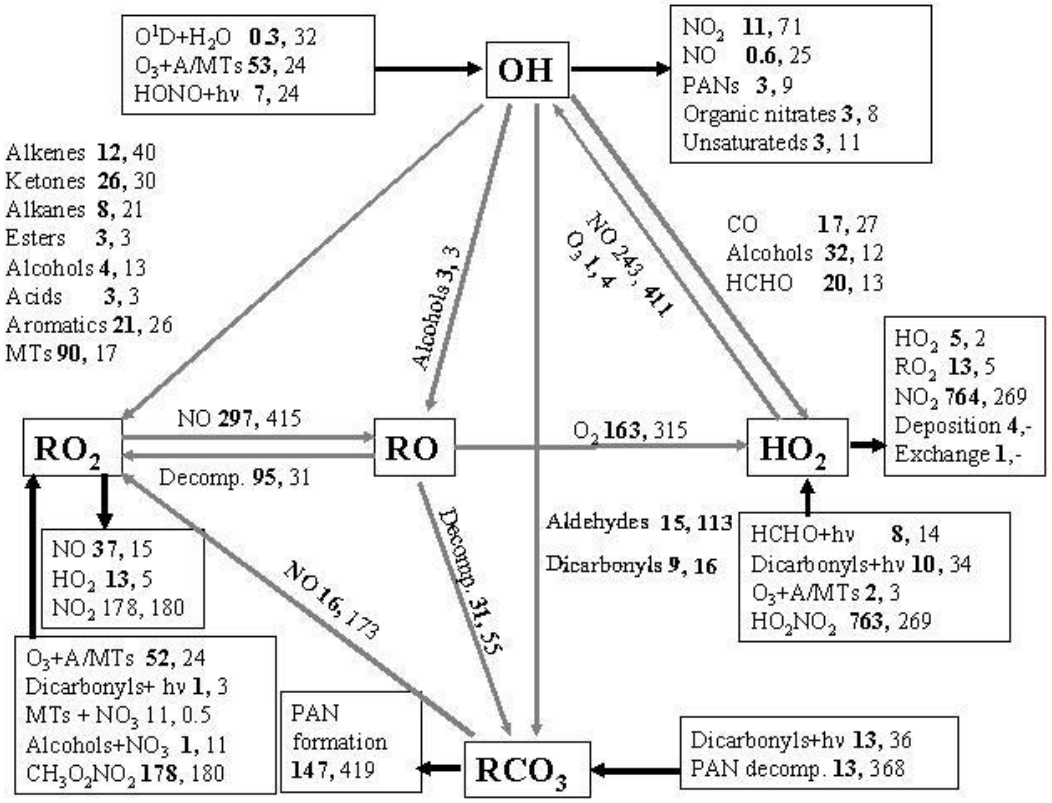

Figure 2.3: indoor chemical processes (initiation, termination and propagation) between different radicals. The numbers in bold show indoor reaction rates while normal type numbers indicate outdoor reactions rates (in units of 10^5 molecule/cm^3/s). Black arrows pointing in and out of the boxes of radicals indicate initiation and termination routes, respectively, while grey arrows indicate propagation routes (Carslaw 2007).

A sensitivity test indicated that indoor photolysis and air exchange rates were the most important factors which determined the indoor concentration of OH radicals. Moreover, Carslaw (2007) showed that nitrated species could be found in relatively high concentrations indoors. The results indicated that 72% of the total organic nitrates (e.g. RNO_3) and 30% of the PAN species (e.g. RCO_3NO_2) were likely to participate in the formation of secondary organic aerosols. Therefore, Carslaw (2007) recommended further detailed study was needed

on indoor photolysis rates, and the oxidation reactions of secondary products, nitrate species and radicals.

Following these recommendations, Carslaw et al. (2012) improved the INDCM model to include gas to particle formation from the degradation of limonene. This allowed the investigation of the formation of secondary organic aerosol (SOA) during cleaning activities. In the absence of cleaning activities, the indoor SOA concentration was estimated to be approximately 1 $\mu g/m^3$ in a typical suburban residence in the UK. PAN species and organic nitrates dominated the composition of SOA (in total ~85%), with smaller contributions from carbonyl and peroxide species. SOA concentrations reached 20 $\mu g/m^3$ during simulated cleaning, with the composition dominated by peroxides (~73%), followed by organic nitrates (18 %) and PANs (3%). Carslaw et al. (2012) found that the outdoor O_3 concentration, indoor VOC concentrations, the parameterisation of gas-to-particle partitioning and the assumed deposition rates most strongly influenced the predicted SOA concentration and composition. Carslaw et al. (2012) also emphasized the importance of investigating the composition of SOA under realistic conditions, and also recommended further study on the deposition rates of gases onto different indoor surfaces, in order to reduce the model uncertainties.

Carslaw (2013) used the detailed chemical model (INDCM) to further investigate the species formed and the major reaction pathways during and after high concentration cleaning activities using a limonene-based cleaning product. Multi-functional carbonyl species, including 4-acetyl-1-methyl-1-cyclohexene (limona ketone) and limonaldehyde, were found to be the main gas-phase products while peroxide species dominated the particle-phase products. It was also found that the competition between OH radicals and O_3 determined the exact formation of SOA. Compared to published human reference values (Wolkoff et al. 2013), the modelled concentrations of three limonene-oxidation products (3-isopropenyl-6-oxo-heptanal (IPOH), 4-acetyl-1-methylcyclohexene (4-AMCH) and 4-oxopentanal (4-OPA)) were lower than the reference values, suggesting that their concentrations following cleaning were unlikely to be a cause for concern (Carslaw 2013). Nevertheless, many terpenes are typically present in cleaning products as well as limonene, which could further enhance the production of secondary pollutants, including PANs, glyoxal, 4-OPA or formaldehyde. Carslaw (2013) therefore recommended further research on indoor carbonyl species in particular, to better improve and validate the models.

Carslaw et al. (2015) used the INDCM to compare O_3 and particulate matter ($PM_{2.5}$) concentrations during a typical summertime period and during an intense summertime heatwave in offices in three European cities (Helsinki, Milan and Athens) and also the impacts of outdoor vegetation on indoor air quality. The results indicated that concentrations of indoor average O_3 were enhanced by 17, 4, and 7 ppb in Milan, Helsinki and Athens respectively due to the intense heatwave compared to typical conditions. Meanwhile, the heatwave also caused an increase of 6.7, 0.4 and 0.5 $\mu g/m^3$ in indoor $PM_{2.5}$ concentrations in Milan, Helsinki and Athens respectively.

Carslaw et al. (2017) measured OH and HO_2 concentrations in a computer classroom under three conditions (without any activities; desk cleaning with products containing limonene; operation of an air cleaning device). The potential consequences on indoor air chemistry by measured levels of OH and HO_2 were predicted by the INDCM. The model results showed good agreement with the measured data and also indicated that aromatic species degradation products (e.g. ~100 ppt glyoxal and ~160 ppt methylglyoxal) were the main reaction products during the operation of the air cleaning device, while terpene oxidation products (e.g. ~100 ppt limonaketone, ~100 ppt limonaldehyde and ~800 ppt heptanal) dominated the composition of products during the desk cleaning (Carslaw et al., 2017).

A new indoor air quality model (INCA-Indoor) was developed and used to simulate indoor concentrations of oxidants and VOCs following the consideration of indoor air processes, including surface interactions (uptake, deposition, sorption), ventilation and emission (Mendez et al., 2015). INCA-Indoor was based on the INteraction with Chemistry and Aerosols (INCA) model, which was a box model developed for the outdoor environment (Hauglustaine et al., 2004; Folberth et al., 2006). The chemical mechanism in this model was simplified and developed from the mechanism of SAPRC-07 (including 1400 oxidation reactions of 640 VOCs) as described by Carter (2010). Some parameters in the model like emission rates and deposition velocities were taken from previous literature while surface to volume ratio, the volume of the room and AER were assumed to be 3.0 m^{-1}, 250 m^3 and 2.0 h^{-1} respectively. Concentrations of pollutants were assumed to be spatially homogenous due to the lack of fluid mechanics in the model. Three regimes were considered for VOCs which were surface, the boundary layer close to the surface and the bulk air. Gases were able to transport from boundary layer to the bulk air and also to uptake to the surface through the boundary layer from the bulk air. Desorption of VOCs could happen due to an assumption that reversible adsorption on the surface occurred.

According to Mendez et al. (2015), the model was used to simulate indoor cleaning and cooking under different conditions (e.g. ventilation rate, photolysis) and the results indicated that 88-99% of HCHO came from building materials. Moreover, deposition processes and ventilation determined the loss of HCHO and contributed to 24.5% and 74.5% respectively with an AER of 2 h^{-1} and 73.3% and 25.5% respectively with an AER of 0.2 h^{-1}. In addition, an increase in OH concentrations (587% increase compared to background concentration of 4.7×10^5 molecule/cm^3) lead to chemical production of HCHO (up to 6.5 ppb/h; surface emission was the main source (88-99%) of HCHO under background conditions) and acetaldehyde (CH_3CHO) (~9 ppb/h compared to background chemical production of 1.5 ppb/h). The results also showed that indoor OH concentrations strongly depended on the concentration of HONO. Moreover, this work also found transport from outdoors to indoors of species like VOCs, NOx and O_3 became more efficient when the ventilation rate was high, which in turn, could accelerate the formation of OH from HO_2 radicals, given increased concentrations of NO and hence a faster rate of reaction between HO_2 and NO.

Mendez et al. (2015) also showed that the production of secondary species became more efficient when the ventilation rate was low (e.g. 0.2 h^{-1}) due to extended reaction times. Compared to the model results presented by Carslaw (2007) from the INDCM, the INCA-Indoor model results had OH and HO_2 concentrations that were overestimated by 34% and 38% respectively, NO and NO_2 were underestimated by 35% and 63% respectively and predicted O_3 concentrations were similar (~ 4% difference). However, according to Schoemaecker et al. (2014), the development of the INCA-model was specifically intended to study indoor air quality in low energy buildings and may not be suitable for use in predicting concentrations of indoor pollutants under all conditions. For instance, the predicted concentrations of alkenes and HONO by this model were lower than measured data (Alvarez et al., 2013).

2.3. Previous modelling studies of indoor photolysis

Nazaroff and Cass (1986) were the first to recognise the importance of indoor photolysis, using the general mathematical model described in 2.2.1. Outdoor photon fluxes were measured in order to calculate the attenuated photolysis rates inside a museum, while quantum yield and absorption cross section data were used to calculate photolysis rates by indoor lighting (Nazaroff and Cass 1986). The indoor light was modelled based on two

components, including ultraviolet (300-400 nm) and visible (400-760 nm) light, and this paper also considered variables (temporal, spatial and spectral distribution of the ambient lighting) which may influence photolysis rates (Nazaroff and Cass, 1986). The results from their measurements showed that only 0.15% of UV and 0.7% of visible sunlight was transmitted through the museum skylights indoors (Nazaroff and Cass, 1986). These measured data were then added into their model. The results indicated that under conditions of increased lighting in indoor environments (50% of visible sunlight transmitted under the condition of glass-walled building), the increased photolysis rates directly enhanced the homogeneous chemical reactions which caused greater concentrations of reactive species (Nazaroff and Cass, 1986).

Carslaw (2007) investigated the indoor air chemistry of a typical urban residence in the UK by using a detailed chemical box model and showed that light intensity levels were a key determinant of model uncertainty when simulating OH concentrations. The concentration of OH was up to 4×10^5 molecule/cm^3 in the residence which was sufficient for OH to react with trace gases to form more oxidized species (Carslaw 2007). However, the OH concentration increased by 281% when the UV and visible light fluxes were increased to 27.5% and 75% of outdoor light fluxes from 3% and 10% respectively.

Wong et al. (2017) used the INDCM to predict concentrations of radicals, chlorine monoxide (ClO) and chlorine (Cl_2) under different lighting conditions during and after a floor cleaning event with products containing bleach. The measured concentrations of both particles and chlorinated gases were increased by the activities of floor cleaning. The INDCM model showed that the uptake of hypochlorous acid (HOCl) onto the floor had an important impact on the indoor chemistry. The model also indicated that photolysis of HOCl and Cl_2 could produce high concentrations of Cl and OH radicals indoors depending on the assumed lighting conditions (Figure 2.4). Concentrations of indoor OH radicals could reach 2.0×10^6 molecule/cm^3 when it was assumed that 3% of outdoor UV and 10% of outdoor visible light were coupled with indoor lighting. These concentrations are much higher than typical OH levels indoors and even greater or similar to typical outdoor levels (Wong et al., 2017).

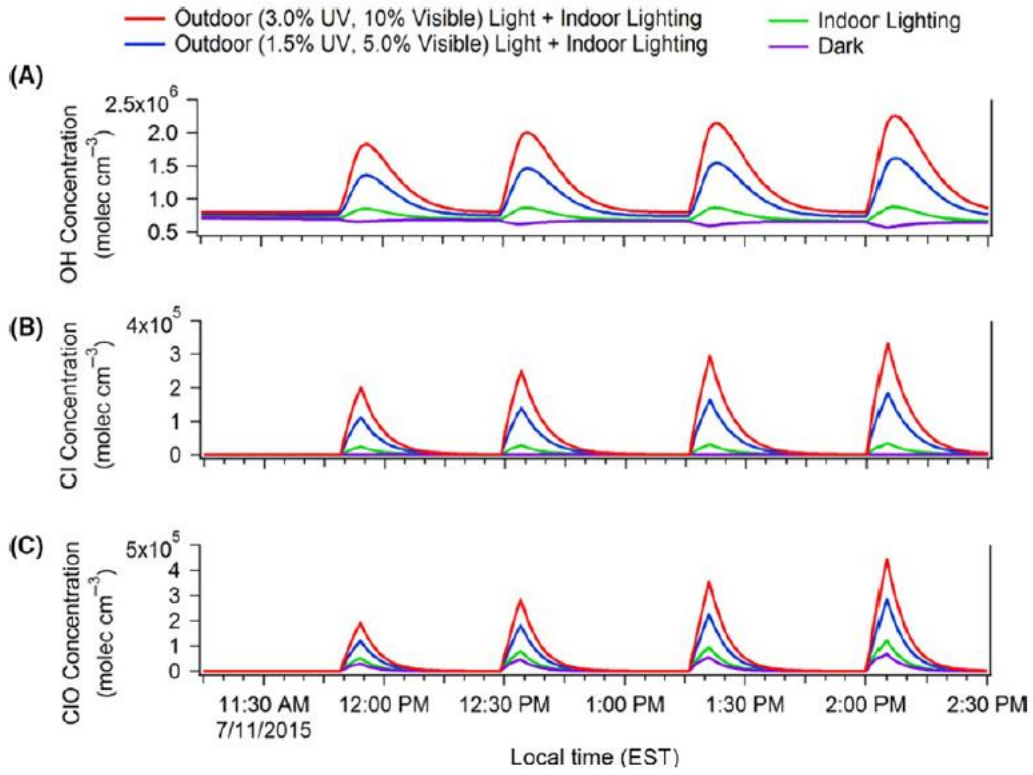

Figure 2.4: Predicted OH, Cl and ClO radicals under different lighting conditions (Source: Wong et al., 2017). Red line: attenuated sunlight (3% UV, 10% Visible) + indoor artificial light; Blue line: attenuated sunlight (1.5% UV, 5% Visible) + indoor artificial light; Green line; indoor artificial light only; Purple line: no light.

The OH and Cl radicals produced in this way can both react with trace gases (e.g. VOC) in order to form more radicals and a range of secondary species (e.g. PM) in the indoor environment (Figure 1.3). The paper showed therefore, that indoor photolysis could initiate gas-phase oxidation in addition to the liquid-phase oxidation caused by the bleach on the laboratory floor.

A recent paper used a computational fluid dynamics (CFD) model framework to study the formation of OH from HONO photolysis (Won et al., 2019). HONO was produced from the combustion of gas in a simulated ventilated room (30 m^3) with an indoor temperature of 26˚C and AER=1 h^{-1}. Five lighting conditions were considered (sunlight, florescent tube, compact florescent light (CFL), incandescent and halogen). A range of OH concentrations of 6.2 to 7.0 $\times 10^5$ molecule/cm^3 was predicted in the sunlight zone (part of the room that was in sunlight), whilst approximately one order of magnitude lower OH radical concentrations were predicted outside the sunlight zone. Therefore, their results showed that the OH concentrations showed

a high spatial dependence (Won et al., 2019). Moreover, their results also showed that different indoor artificial lights produced different spatial distributions of OH, and that concentrations of OH (up to ~5.0 × 10^5 molecule/cm^3 when adjacent to CFL, Figure 2.5) decreased with distance from the light sources (Won et al., 2019).

The average concentration of OH predicted with the fluorescent tube was greater than that for CFL, even though the maximum concentration was predicted for CFL. This was due to differences in the lighting geometry (Figure 2.5). The predicted concentrations of OH adjacent to CFL lighting were approximately five times greater than that adjacent to incandescent light as the photon fluxes were about five times greater with CFL (Won et al., 2019). Also, concentrations of OH were approximately two times greater for incandescent compared to halogen lighting, owing to a narrower radiation angle for the halogen light. Therefore, this paper showed that indoor photolysis played an important role on indoor air species concentrations, whilst of intensity and spatial distribution differences for different lighting, produced different impacts on indoor air chemistry.

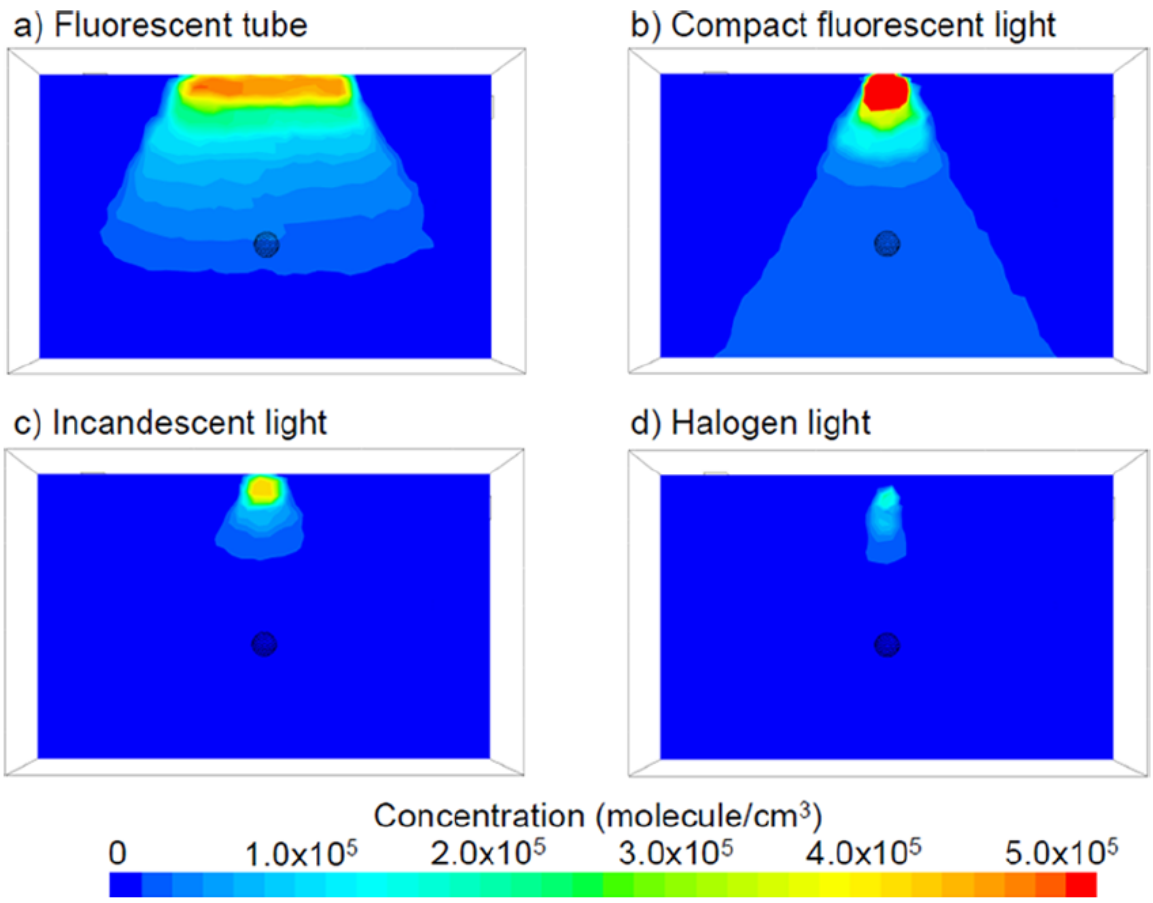

Figure 2.5: Spatial distributions of OH concentrations under fluorescent tube (a), compact fluorescent light (b), incandescent light (c) and halogen light (d). Source: Won et al. (2019).

2.4. Past measurements relevant for indoor photolysis

Gomez-Alvarez et al. (2013) measured up to 1.8×10^6 molecule/cm^3 of OH in a school classroom in Marseille, similar to outdoor urban OH concentrations. There were two large windows (dimension of 2.5 m × 1.2 m) in the classroom they studied, which had a total volume of 170 m^3. The instrument used in this study to measure the concentration of OH radicals was installed in a location exposed to direct sunlight in the late afternoon (Gomez Alvarez et al., 2013). In this study, the source of OH was the photolysis of HONO (Gomez Alvarez et al., 2013) and was the first experimental study to show that indoor photolysis could produce high concentrations of radicals indoors and also affect indoor air chemistry.

According to Gandolfo et al. (2016), this paper used both measurement (by a Metcon 2π spectral radiometer) and model (by the architectural model) to study actinic fluxes and photolysis frequencies of NO_3, NO_2 and HONO during summer and winter. The results showed that measured actinic fluxes were nearly same during the period of summer and winter. Meanwhile, indoor actinic fluxes could reach maximum 30% and 50% of outdoor values in summer and winter, owing to sunlight is attenuated in indoor environment (Gandolfo et al., 2016). In addition, measured photolysis rate coefficients of HONO in their study (maximum 1.72×10^{-4} and 1.44×10^{-4} s^{-1} in summer and winter respectively) showed good agreement with measured data in Gomez-Alvarez et al (2013) (1-1.5 $\times 10^{-4}$ s^{-1}). Moreover, maximum measured photolysis rate coefficients of NO_3 to NO were 9.22×10^{-3} and 1.07×10^{-2} s^{-1}, whilst NO_3 to NO_2 were 7.48×10^{-3} and 8.37×10^{-2} s^{-1} in summer and winter respectively (Gandolfo et al. 2016). However, no previous study measured indoor NO_3 after it was first detected by Platt et al. (1980) (Gligorovski and Weschler 2013). Furthermore, measured photolysis rate coefficients of NO_2 in their study (maximum 1.4×10^{-3} and 1.2×10^{-3} s^{-1} in summer and winter respectively) were approximately a factor of 8 smaller than its maximum value in outdoor environment (Kraus 1998). However, the measured photolysis rate coefficients of NO_2 were greater than values measured by Gomez-Alvarez et al (2013) (6-8 $\times 10^{-4}$ s^{-1}), owing to the measurement was carried out around noon (Gandolfo et al. 2016).

Bartolomei et al (2015) used chamber experiments which included a burning candle to produce HONO to measure concentrations of OH radical under different indoor lighting conditions (light from a solar simulator passed into the chamber through different filters of window glass). Concentrations of measured OH radicals from photolysis of HONO were between 5.7×10^6 and 1.6×10^7 molecule/cm^3 with the highest concentration under the condition with no glass window filter, which allowed more light to pass into the chamber (Bartolomei et al., 2015).

Blocquet et al. (2018) used both modelling and experimental tools to research the spatial and spectral distribution and intensity of indoor sunlight which passed from outdoors through windows. The type of glass was the primary factor which influenced the amount of transmitted light and the cut-off wavelength for that light. The window transmittances of two different types of window, including a Low Emissivity window (LE) and a Low Emissivity High Performance window (LEHP), were measured in different rooms on different levels of a building. The windows at ground level in the building (LO) both had a film on them, whilst the LEHP window also had an additional coating. The film effectively cuts the transmittance of UV radiation (below 380 nm) and decreases the amount of light passing into the room (Figure 2.6).

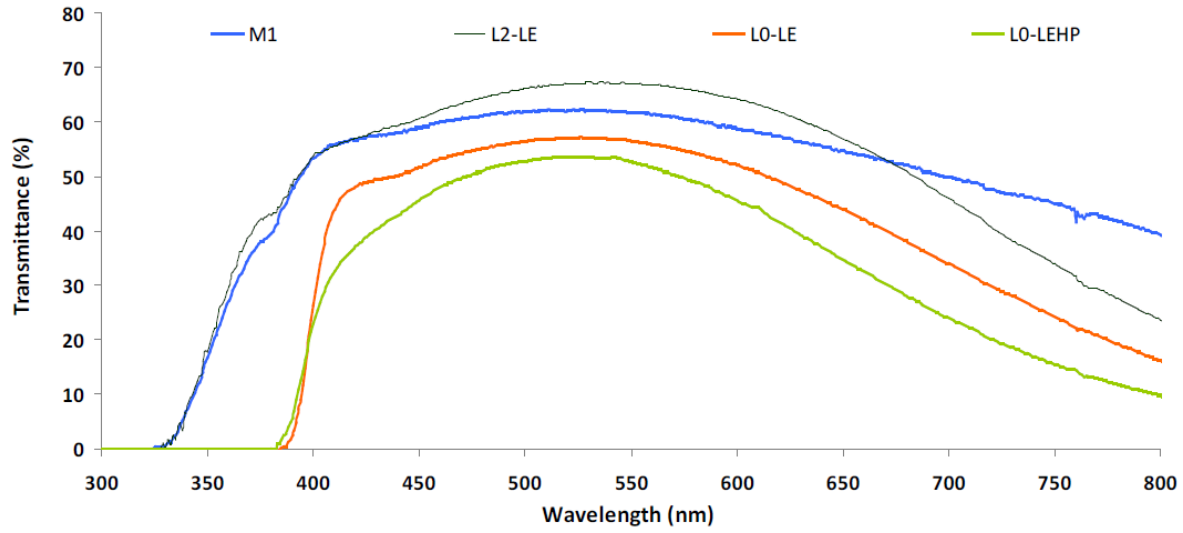

Figure 2.6: Transmittances of different windows. M1: double glazed, Saint Gobain Planilux outer glass 4 mm + argon 22 mm + Planitherm Ultra N coating: noble metal layer deposited by magnetron sputtering under vacuum + inner glass 6 mm. L0-LEHP: low emissivity high performance window, Saint Gobain 44.2 Cool lite SKN154/14 argon /33.2 with film. L0-LE: low emissivity window, Saint Gobain 44.2 Planistar /16 argon/44.2, with film. L2-LE: Saint Gobain 4 Planistar/16 argon/4. Source: Blocquet et al. (2018).

The coating applied on the LEHP window decreased the amount of light passing into the room compared to the LE window by approximately 10% (Blocquet et al., 2018). It is therefore very hard to generalise how different glasses will affect the transmission of indoor light. Based on different conditions, 0.15 % to 30 % of UV light (300-400 nm) and 0.7 % to 80 % of visible light (400-750 nm) from outdoor light can be observed indoors (Blocquet et al., 2018). Therefore, the impacts of different types of window (e.g. different window materials and with or without film) on indoor photolysis rates vary widely, as different species absorb light at different wavelengths with differing efficiencies.

Figure 2.7 shows the evolution of irradiance over the course of a day of indoor measurements: the irradiance changed by more than a factor of ten and the impact of clouds can also be seen (10:00, 12:00, and 15:00), compared to clear sky conditions (Blocquet et al., 2018).

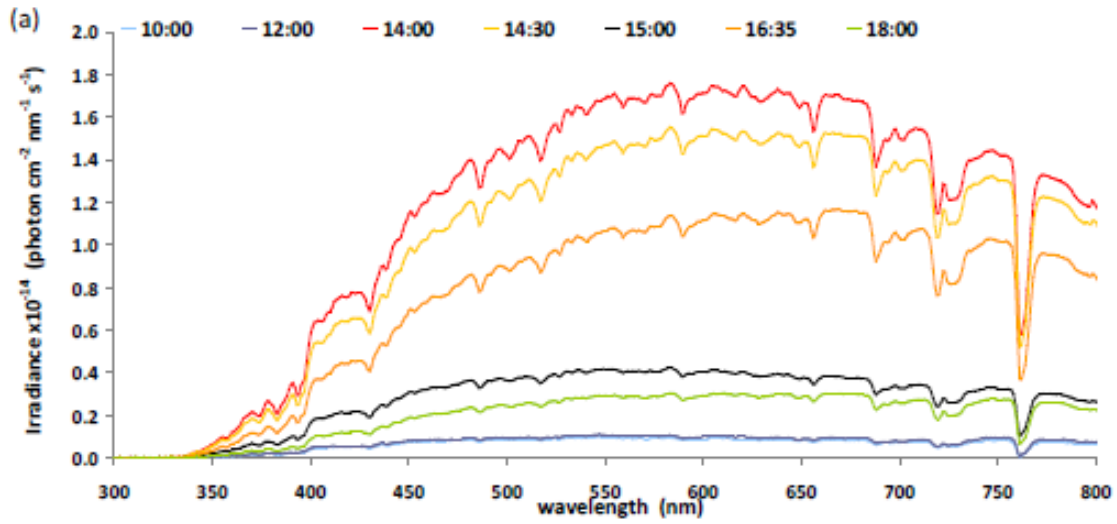

Figure 2.7: Irradiance measured by LICOR (a calibrated spectroradiometer LICOR-LI 1800, spectral range: 300-850 nm, resolution: 1 nm) at different hours of the day April 24th 2014. Source: Blocquet et al. (2018).

The light intensity also varies spatially within a room. For instance, Blocquet et al. (2018) showed that the transmitted solar irradiance strongly decreased with the distance from the windows (Figure 2.8).

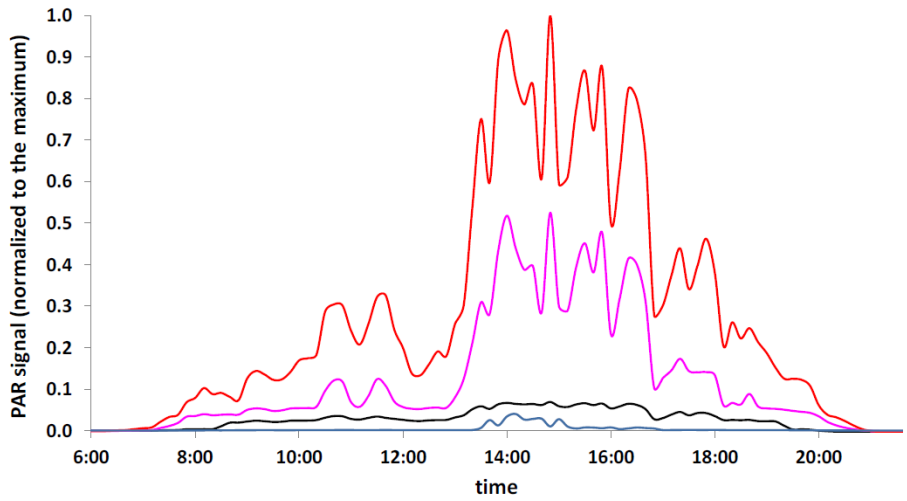

Figure 2.8: Normalized irradiance measured by several PAR (photosynthetically active radiation) sensors at different locations: red line: outdoors (3.2 m from the window); pink line: 0.3 m from the window (indoor); black line: 4.4 m from the window (middle of the room); blue line: 6.7 m from the window (back of the room). Normalized to the maximum. Source: Blocquet et al. (2018).

Kowal et al. (2017) measured the intensity and wavelength dependence of several different light sources (halogen; incandescent; compact fluorescent lamps (CFL); covered or uncovered fluorescent tubes (CFT/UFT); LED; and attenuated sunlight). There were large variations (Figure 2.9): LED lighting had no emission observed below 400 nm, the intensities of incandescent and halogen bulbs increased with wavelength and are low at short (around 300 nm) wavelengths, whilst compact fluorescent lamp intensity fluctuates and corresponds to the emission line of mercury (Kowal et al., 2017), as shown in Figure 2.9b. These peaks at the lower wavelengths (e.g. around 310 nm) explain why fluorescent tubes photolyse ozone reasonably effectively when compared to the other lamps.

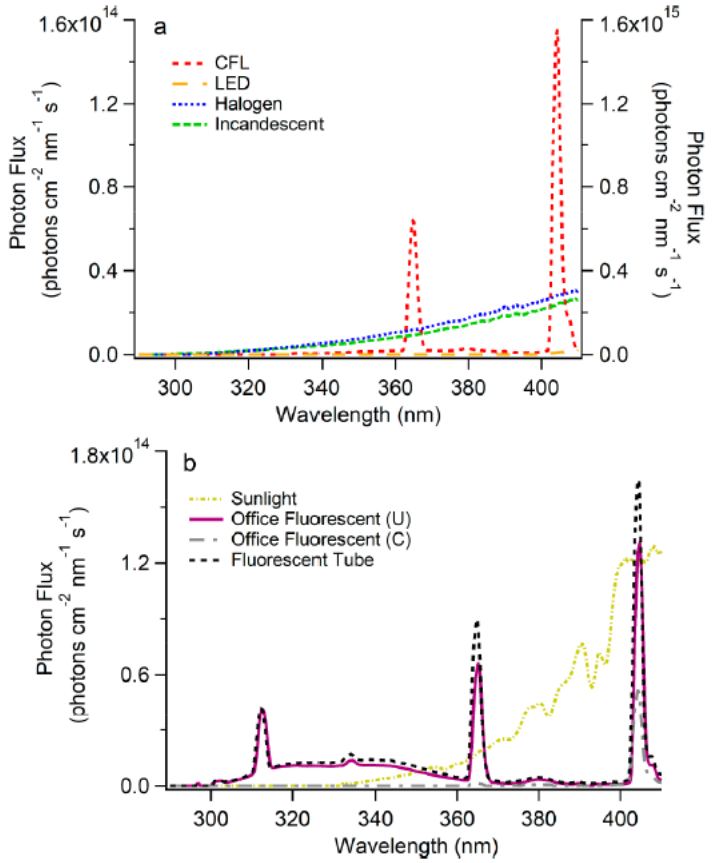

Figure 2.9: a: wavelength resolved photon fluxes for the compact bulbs. b: photon fluxes from a fluorescent tube and from fluorescent lights in two offices. Source: Kowal et al., 2017.

Kowal et al (2017) used their photon flux measurements to calculate photolysis rates and hence production rates of HO_x from photolysis of CH_3CHO (R14), HCHO (R16), O_3 (R1), H_2O_2 (R13) and HONO (R6). These rates vary quite considerably depending on the light source (Table 2.1). Photolysis of HONO produces the greatest production rates of OH for all light sources and especially when exposed to a compact fluorescent light. LED lights have no emission below 400 nm so lead to very low radical production rates. For OH production from ozone photolysis, the uncovered office fluorescent tube and the general fluorescent tube (FT) led to the highest production rates.

Table 2.1: Predicted Indoor OH Production Rates from H_2O_2, O_3, and HONO Photolysis, and HO_2 Production Rates from HCHO and CH_3CHO Photolysis (adjacent to light sources). Source: Kowal et al., 2017.

	production rate (molecules cm^{-3} s^{-1})				
	OH			HO_2	
light source	H_2O_2	O_3	HONO	HCHO	CH_3CHO
LED	9.90×10^2	7.44	none	none	none
halogen	1.18×10^4	4.82×10^4	1.05×10^7	7.34×10^5	2.11×10^4
incandescent	1.25×10^4	1.86×10^5	8.52×10^6	9.14×10^5	4.57×10^4
CFL	2.44×10^4	7.40×10^3	4.42×10^7	1.49×10^5	1.03×10^3
fluorescent tube	6.38×10^4	9.05×10^5	1.20×10^7	5.86×10^6	3.54×10^5
office fluorescent (C)[a]	3.50×10^2	9.00×10^1	1.19×10^5	none	none
office fluorescent (U)[a]	5.73×10^4	8.82×10^5	9.51×10^6	5.62×10^6	3.35×10^5
sunlight[b]	7.38×10^3	2.34×10^3	1.70×10^7	6.22×10^3	none

[a]"C" and "U" refer to covered and uncovered fluorescent tubes, respectively. [b]Values assume direct sunlight.

HONO and HCHO were both photolysed by uncovered fluorescent lights to form OH (photolysis rates between 10^6 and 10^7 molecules/cm^3/s) and HO_2 (photolysis rates around 10^6 molecules/cm^3/s) respectively (Kowal et al., 2017), whilst photolysis of CH_3CHO was relatively unimportant (Table 2.1). In addition, this paper also confirmed an important indoor source of O_3 is from photolysis of NO_2 while photolysis of NO_3 (in indoor environment) is not that important as VOCs rapidly react with any formed NO_3 (Kowal et al., 2017).

Kowal et al. (2017) also investigated the dependence of distance from the light source on the measured photon flux and hence photolysis rates for different gases. Photon fluxes from CFL and fluorescent tube strongly depend on the distance from the illumination sources, decreasing sharply between 0 and 0.5 m from the source (Figure 2.10). However, the photon flux from sunlight at the window (90%) was similar to 2.4 m from the window (Figure 2.10b). The results indicated that photon fluxes from sunlight did not strongly depend on the distance from the window (Kowal et al., 2017).

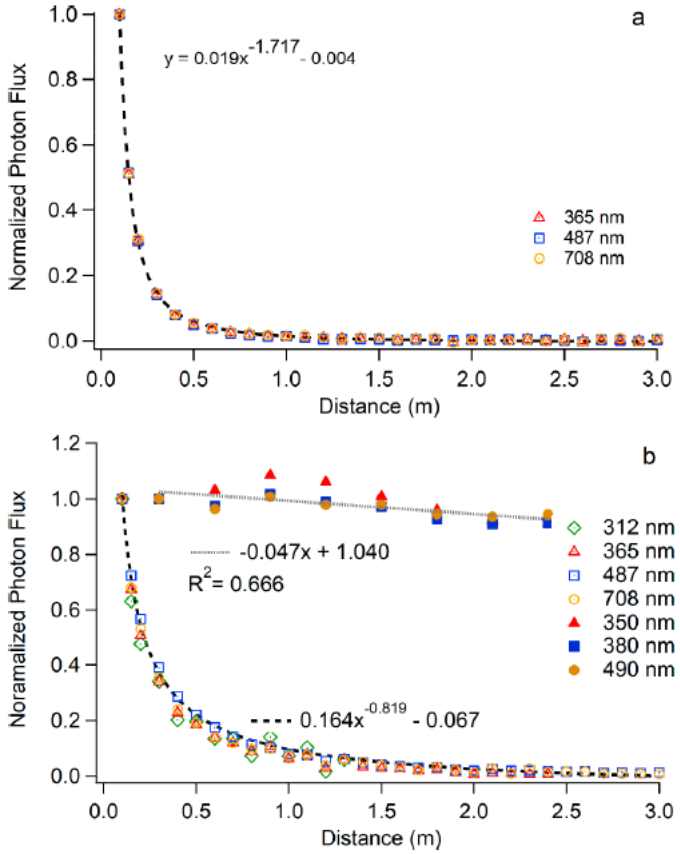

Figure 2.10: Distance dependence of photon flux emitted from different lights. a: CFL fluxes at several wavelengths normalized to the flux near the lamp. b: fluorescent tube (open symbols) fluxes at several wavelengths normalized to the flux near the lamp and photon fluxes from sunlight (solid symbols) entering a room through a window. Source: Kowal et al., 2017.

2.5. Summary

The importance of modelled studies is increasingly recognised as the challenges of making real measurements (e.g. noise, temporal and spatial coverage technical limitations of instrumentation, human activities) mean that real measurements do not provide all of the detailed information required. Data from the measurements can help the development and improvement of models, which can then provide more accurate predictions.

Previous studies have started to consider the importance of indoor photolysis and made huge developments on the treatment of indoor photolysis in the models, including:

- The development of equations to treat indoor photolysis by both attenuated sunlight and indoor artificial lights (Nazaroff and Cass, 1986).
- The contribution of photolysis of O_3 to indoor OH production (Weschler and Shields 1996).

- The discovery that indoor photolysis was one of the most important factors to determine levels of indoor OH radicals (Carslaw 2007).
- Photolysis of HOCl and Cl_2 were found to produce high concentrations of Cl and OH radicals indoors especially under high attenuated factors for sunlight + indoor lighting (Wong et al., 2017).
- Photolysis of HONO was found to be an important source of indoor OH radicals (Waring and Wells 2015; Gomez-Alvarez et al., 2013).

However, there are still many limitations, including the fact that there has been no distinction between different artificial lights in models, and that these models assume that transmission of light is constant through large wavelength regions (e.g. 300-400 nm and 400-750 nm).

This review has also demonstrated that the photolysis of many trace gases (e.g. O_3 and HCHO) will produce radicals (e.g. OH and HO_2 respectively) in the indoor environment. Some of the radicals (e.g. OH) can react with trace gases (e.g. VOC) rapidly in order to form more radicals and a range of secondary species, some of which are harmful to health (e.g. PM). In order to better understand the impact of indoor photolysis, factors which may influence the intensity of attenuated sunlight and artificial lights indoors need to be considered, including the type of window (material, film and coating conditions), the meteorological conditions and the building orientation and location which can directly influence the amount of attenuated sunlight. There also needs to be a consideration of the different artificial lighting sources, the distance from the illumination sources and so on. This thesis therefore aims to explore how best to represent such processes in models, to minimise uncertainties in predicted radical concentrations indoors and the subsequent chemical processing.

Chapter 3: Methods

3.1. Introduction

Indoor air quality models can be used to quantify the concentrations of indoor air pollutants in the absence of comprehensive, labour-intensive and time-consuming measurements in the indoor environment. The basis of the INdoor air Detailed Chemical box Model (INDCM) is a comprehensive chemical mechanism (the Master Chemical Mechanism, MCM v3.2, http://mcm.leeds.ac.uk/MCM/), which was developed by Carslaw (2007) and improved by Carslaw et al. (2012). This model has been developed and used in this study to investigate the impact of photolysis on indoor air chemistry and particularly how that affects the formation of radicals, such as hydroxyl, hydroperoxy and organic peroxy radicals (OH, HO_2, and RO_2 respectively).

The following sections describe the experimental framework of the INDCM, before the photolysis code was developed for this thesis. In turn, the chapter discusses the software used, the Master Chemical Mechanism which forms the basis of the chemical reaction set, exchange with outdoors, deposition onto surfaces, indoor emissions and photolysis. The model developments carried out as part of this dissertation are discussed and evaluated in chapter 4 and the improved model then used to gain insight into indoor chemistry in Chapters 4, 5 and 6.

3.2. Integrating software

The INDCM model runs using Facsimile for Windows (F4W) software (produced by MCPA Software Ltd.). This software is user-friendly and was developed to model chemical kinetics and transport. Chemical species are defined as a parameter, a variable, or assigned a constant value. For those declared as variables, F4W will solve an ordinary differential equation to calculate their concentration for each time step. The user needs to list each chemical reaction using a specified format. The rate coefficient is shown at the beginning of each equation line, prefixed by a '%' sign. Following a colon, the reactions are then listed with an equals sign before the products and then each line finishing with a semi-colon. Figure 3.1 shows a screenshot of some example chemical reactions in this format.

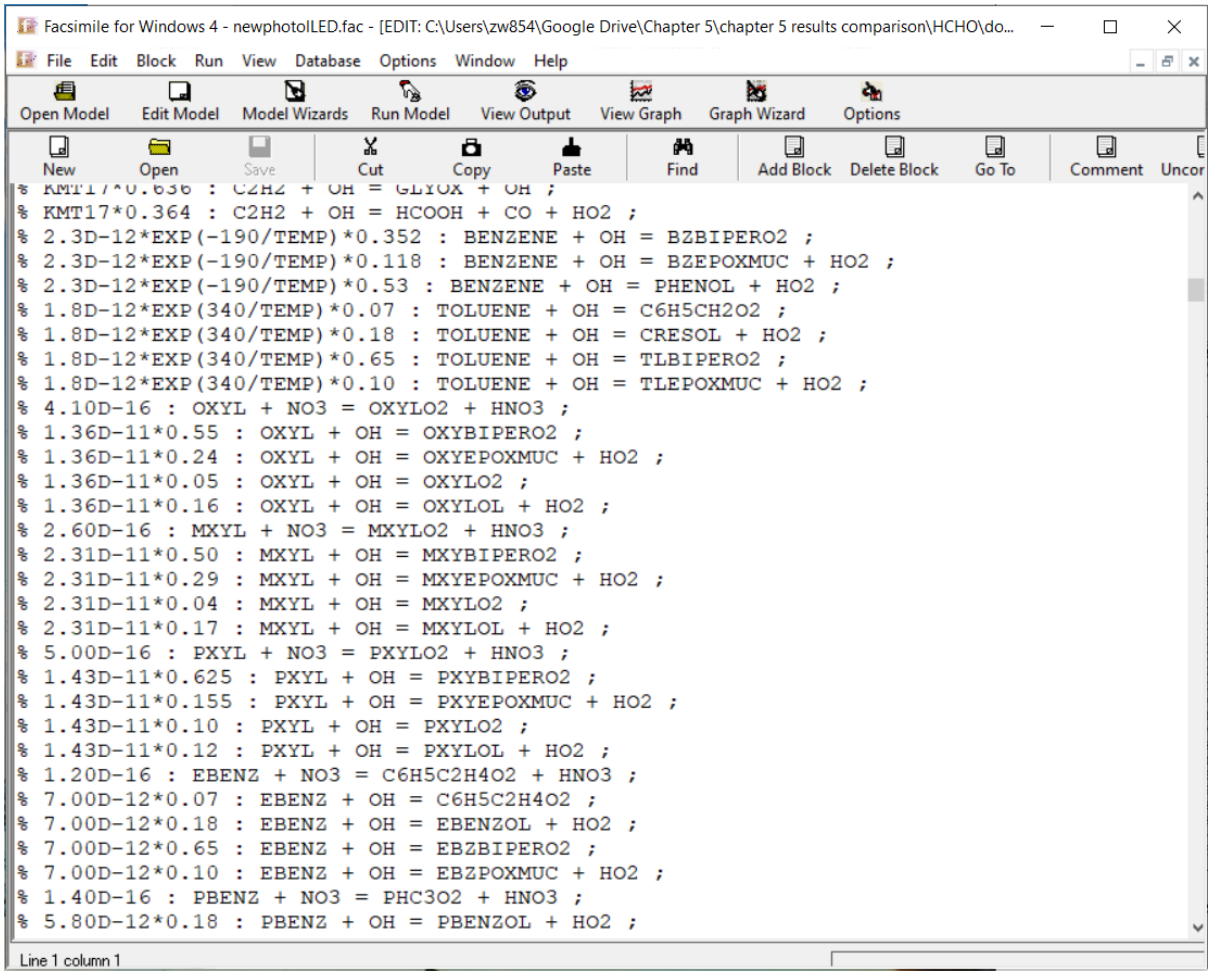

Figure 3.1: Screenshot of the box model INDCM to illustrate F4W format for representation of reactions.

3.3 The Master Chemical Mechanism

3.3.1. Chemical reactions

The chemical mechanism used in the model is called the Master Chemical Mechanism and includes around 20,000 reactions and 5,000 species, representing the near-explicit degradation of ~ 143 VOCs (including limonene) in the gas-phase (Jenkin et al., 1997; Jenkin et al., 2003; Saunders et al., 2003; Bloss et al., 2005). The MCM is compiled following a defined protocol, which uses the latest kinetic and product data where available, or structure activity relationships in their absence (Jenkin et al., 1997).

The first step (process of initiation) in the oxidation chain is that the chemical degradation of each VOC is initiated by reaction with OH, NO_3 and O_3, and photolysis where relevant (Figure 3.2). The process of initiation is quite complex and can generate many products. For instance, Figure 3.2 shows that radicals are generated immediately through the first oxidation

step, including RO (oxy), RO_2 (peroxy), and RRCOO (Criegee) radicals (propagation steps), which can each undergo a number of further reactions until the final oxidation products of CO_2 and H_2O are formed (termination steps) (Saunders et al., 2003).

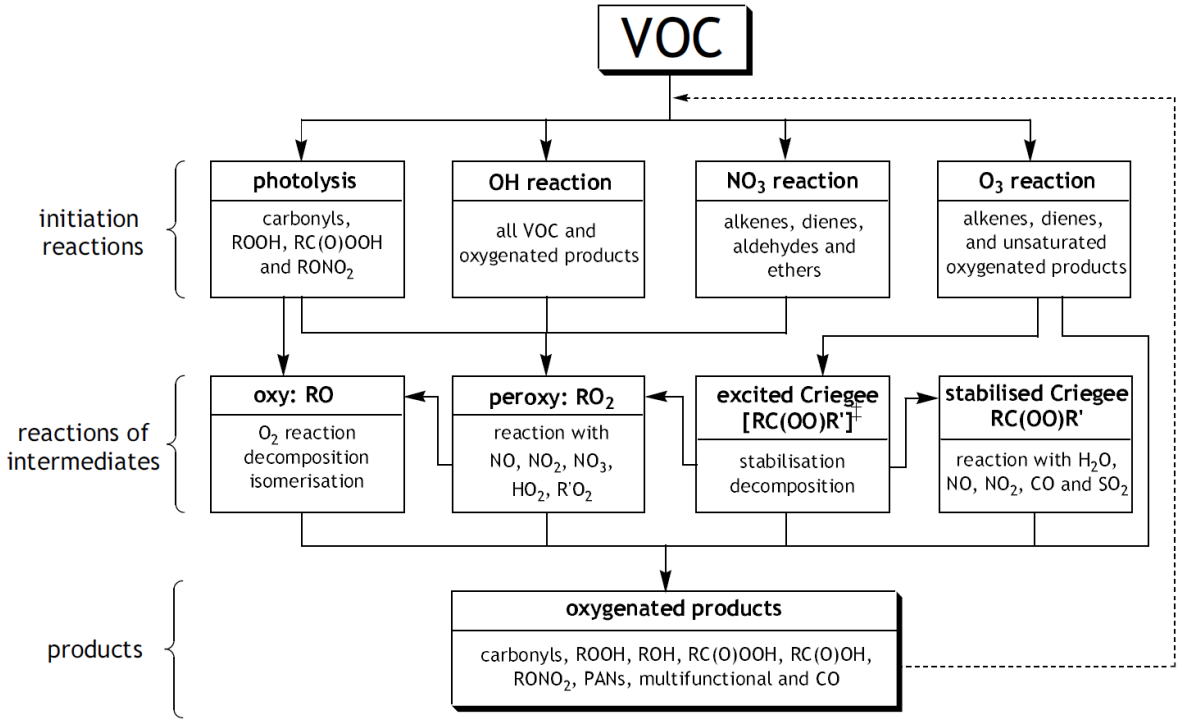

Figure 3.2: Flow chart indicating the degradation process of VOCs in the MCM. Source: Saunders et al., 2003.

Peroxy radicals (RO_2) can be formed through the reactions of the hydroxyl radical (OH) with all VOC species. All of the alkanes, alkenes, alkynes and aromatics can react with OH to produce RO_2, which themselves can undergo a number of further reactions (Jenkin et al., 1997; Atkinson and Arey, 2003; Saunders et al., 2003). The pathways will depend on the structure and size of the parent VOC. Reactions R21-R24 show examples of the OH radical reaction with alkanes (R21), alkenes (R22), alkynes (R23) and aromatics (R24) respectively. Note that $BZBIPERO_2$ is an MCM name (MCM nd) not a chemical structure.

$$C_2H_6 + OH\ (+O_2) \rightarrow C_2H_5O_2 + H_2O \qquad R21$$

$$C_2H_4 + OH\ (+O_2) \rightarrow HOCH_2CH_2O_2 \qquad R22$$

$$C_2H_2 + OH\ (+O_2) \rightarrow HCOOH + CO + HO_2 \qquad R23$$

$$C_6H_6 + OH\ (+O_2) \rightarrow BZBIPERO_2 \qquad R24$$

As shown in R21, ethane will lose an H atom when it reacts with OH. The added O_2 then reacts with the $C_2H_5^-$ radical to form $C_2H_5O_2$. Degradation of alkenes, alkynes and aromatics can be exemplified by the oxidation of ethene (R22), ethyne (R23) and benzene (R24) respectively. They all undergo addition of OH to the double bond/ triple bond/aromatic ring and then form a peroxy radical following addition of O_2

Furthermore, many of the reactions of VOC species with NO_3 are similar to OH but with the formation of nitrated products, as shown in R25 and R26 for acetaldehyde, whilst R27 and R28 are analogous to reactions R22 and R24 respectively. However, NO_3 does not react with alkanes.

$CH_3CHO + OH\ (+O_2) \rightarrow CH_3CO_3 + H_2O$ R25

$CH_3CHO + NO_3\ (+O_2) \rightarrow CH_3CO_3 + HNO_3$ R26

$C_4H_8 + NO_3 \rightarrow CH_2(ONO_2)CHC_2H_5$ R27

$C_6H_5OH + NO_3 \rightarrow C_6H_5O + HNO_3$ R28

Aldehyde species will lose an H atom from their carbon chain when they react with NO_3 as shown in reaction R26 to form HNO_3 while the addition of O_2 leads to the formation of RCO_3 radicals. NO_3 reacts with alkenes through the addition to the double bond (e.g. R27). Aromatic species will lose an H atom from their carbon chain when they react with NO_3 (e.g. R28).

In addition, many of the reactions of VOC species with Cl radicals are similar to OH but tend to react more quickly (e.g. R29, the rate coefficient of R29 is ~20 faster than the equivalent for OH).

$CH_4 + Cl\ (+O_2) \rightarrow CH_3O_2 + HCl$ R29

In the chemical mechanism, large quantities of RO_2 radicals are formed as a result of the oxidation of VOCs by NO_3, OH and Cl radicals as shown in the reactions above, where each VOC can typically lead to the formation of 3-4 peroxy radicals. Furthermore, RO_2 radicals can potentially react with all other RO_2 species through 2-3 different pathways each, and it is computationally and chemically complex to describe each of these reactions explicitly in the mechanism. For this reason, an 'RO_2 pool' is used in the MCM in order to simplify reactions of RO_2 radicals (Jenkin et al., 1997). The pool is the sum of the concentrations of all peroxy

radicals excluding HO_2, and each individual RO_2 can then react with the pool instead of reacting with every other individual RO_2 explicitly.

According to Jenkin et al. (1997), peroxy radicals can undergo a number of reactions. As well as reacting with the RO_2 pool, they can react with NO, NO_2, NO_3 and HO_2 as shown in R30-34.

$C_2H_5O_2 + RO_2 \rightarrow C_2H_5O$ R30a

$\rightarrow C_2H_5OH$ R30b

$\rightarrow CH_3CHO$ R30c

$C_2H_5O_2 + NO \rightarrow C_2H_5O + NO_2$ R31a

$\rightarrow C_2H_5NO_3$ R31b

$C_2H_5O_2 + NO_3 \rightarrow C_2H_5O + NO_2 + O_2$ R32

$C_2H_5O_2 + HO_2 \rightarrow C_2H_5OOH$ R33

$C_2H_5O_2 + NO_2 \rightarrow C_2H_5O_2NO_2$ R34

RO radicals can then react with O_2, thermally decompose or isomerise which is determined by the nature of the parent VOC. HO_2 can typically be produced by such reactions (e.g. R35) and then the reaction of NO with HO_2 leads to the formation of OH (R36). R35 shows the fate of a relatively simple RO radical (C_2H_5O).

$C_2H_5O + O_2 \rightarrow CH_3CHO + HO_2$ R35

$HO_2 + NO \rightarrow NO_2 + OH$ R36

According to Atkinson (1997), ozone can react with unsaturated species with double bonds to form an ozonide (Figure 3.3). Ozonides decompose very quickly, and stabilized and excited Criegee biradicals (RRCOO) and a carbonyl compound are then formed (Murray, 1968; Criegee, 1975). The stabilized RRCOO will mainly react with water under most outdoor and indoor conditions, but also with CO, SO_2, NO, NO_2. In the indoor environment, Criegee biradicals have an important role as they are an important source of OH radicals, particularly in the absence of the traditional outdoor source via photolysis of ozone (Shallcross et al., 2014). Some previous studies found rapid reaction rates between Criegee intermediates and NO_2, SO_2 and halogenated carbonyls (Taatjes et al., 2008; Taatjes et al., 2012; Taatjes et al., 2013). Moreover, reactions involving Criegee intermediates are also found to accelerate SO_2

removal and NO_3 formation indoors which could lead to indoor formation of aerosols and potential direct impacts on human health (Shallcross et al., 2014).

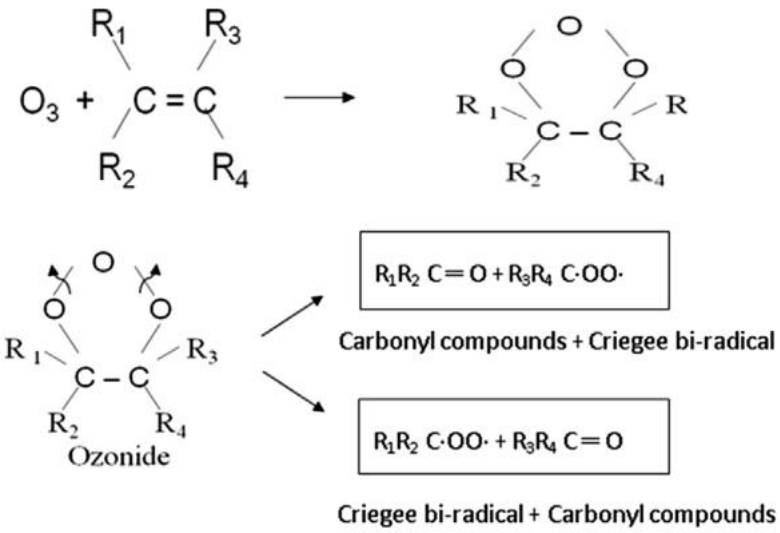

Figure 3.3: Reaction of ozone with an alkene to form a Criegee biradical species and a carbonyl compound. Source: Cheng et al. (2015).

Photolysis of some VOC species (aldehydes, ketones, peroxides, organic nitrates) can also lead a variety of products, including the formation of oxy and peroxy radicals as discussed in detail in the introduction. For the purpose of simplification, the photolysis rates for the larger VOC species in MCM are generalised according to their structure. For instance, the photolysis rate for HCHO to produce HO_2 is treated as a single reaction in MCM. However, the photolysis rates for all other aldehyde species are assumed to be the same.

A comprehensive inorganic scheme is also contained within the MCM, which includes CO, NO_x and O_3, and their key reactions with radical species (Table 3.1).

Table 3.1: Some key inorganic reactions in the MCM (MCM nd).

No.	Reactions
1	$OH + O_3 \rightarrow HO_2 + O_2$
2	$OH + H_2 \rightarrow H_2O + H$
3	$OH + CO \rightarrow H + CO_2$
4	$OH + CO + M \rightarrow HOCO + M$
5	$OH + H_2O_2 \rightarrow H_2O + HO_2$

6	$OH + NO + M \rightarrow HONO + M$
7	$OH + NO_2 + M \rightarrow HONO_2 + M$
8	$OH + NO_3 \rightarrow HO_2 + NO_2$
9	$OH + HO_2NO_2 \rightarrow H_2O + O_2 + NO_2$
10	$OH + HO_2NO_2 \rightarrow H_2O_2 + NO_3$
11	$OH + HO_2NO_2 \rightarrow HO_2 + HNO_3$
12	$OH + HONO \rightarrow H_2O + NO_2$
13	$OH + HNO_3 \rightarrow H_2O + NO_3$
14	$OH + SO_2 + M \rightarrow HOSO_2 + M$
15	$HO_2 + O_3 \rightarrow OH + 2O_2$
16	$HO_2 + NO \rightarrow NO_2 + OH$
17	$HO_2 + NO + M \rightarrow HNO_3 + M$
18	$HO_2 + NO_2 + M \rightarrow HO_2NO_2 + M$
19	$HO_2 + NO_3 \rightarrow O_2 + HNO_3$
20	$HO_2 + NO_3 \rightarrow OH + NO_2 + O_2$

The original MCM has now been improved through various supplements/updates to the original (v1, v2, v3, v3.1, v3.2), as described by Jenkin et al. (1997, 2003), Saunders et al., (2003) and Bloss et al. (2005). Jenkin et al., (2003) used new information to define improved representation of aromatic VOC degradation (including 18 aromatic compounds) in the mechanism protocol. Saunders et al. (2003) improved the representation of the degradation of 107 non-aromatic compounds in the scheme. Bloss et al. (2005), carried out further improvements in the representation of the oxidation of aromatic hydrocarbons in the mechanism. Moreover, based on Volkamer et al. (2001, 2002), updated information on the branching ratios for the various oxidation routes of aromatics under relatively low NOx conditions were adjusted in the mechanism (Bloss et al., 2005). Jenkin et al. (2012, 2015) added new schemes for α-pinene, isoprene and β-caryophyllene which were considered the most structurally complex species to be included in the scheme. Throughout the work presented in this thesis, version 3.2 has been used.

Some of the species which have important impacts on indoor air chemistry are not included in the MCM, such as many of the monoterpenes, as the MCM was constructed for researching outdoor air chemistry (Jenkin et al., 1997). α- and β-pinene and limonene are the

only monoterpenes contained in the mechanism. New schemes have been developed as required and these are discussed in the next 3 chapters as relevant.

3.3.2. Generic rate parameters

Generic rate coefficients for the vast majority of reactions involving RO_2, are calculated using structure activity relationships in the chemical mechanism due to the absence of kinetic data. Table 3.2 shows the values of these rate coefficients used in the MCM

Table 3.2: Simple rate coefficients in MCM (MCM nd).

Generic	Rate coefficients (cm^3/molecule/s)
KRO_2NO	$2.70 \times 10^{-12} \times e^{(360/T)}$
KRO_2HO_2	$2.91 \times 10^{-13} \times e^{(1300/T)}$
$KAPHO_2$	$5.20 \times 10^{-13} \times e^{(980/T)}$
KAPNO	2.30×10^{-12}
KRO_2NO_3	$2.29 \times 10^{-13} \times e^{(980/T)}$
KNO_3AL	$1.40 \times 10^{-12} \times e^{(-1860/T)}$
KROPRIM	$2.50 \times 10^{-14} \times e^{(-300/T)}$
KROSEC	$2.50 \times 10^{-14} \times e^{(-300/T)}$
KCH_3O_2	$1.03 \times 10^{-13} \times e^{(365/T)}$
$K298CH_3O_2$	3.50×10^{-13}

*T = temperature

3.4. Exchange with outdoor air

The air exchange rate (AER or air changes per hour) measures the replacement of air in an indoor environment each hour (unit: h^{-1}) due to leakage through the building fabric or via the ventilation system (Dimitroulopoulou et al., 2001). Indoor-outdoor exchange will impact indoor species concentrations. If the main source of an indoor species is indoors, ventilation with outdoors will decrease the indoor concentration. On the other hand, if the main source is outdoors, increasing ventilation rates will increase indoor concentrations. Many factors can impact on AER, such as the building characteristics (e.g. age, building materials, leakiness)

and the behaviour of residents (e.g. period and degree of opening windows). Based on Dimitroulopoulou et al. (2001), the use of a cooker hood can increase the AER in the kitchen compared to bedrooms and living rooms.

According to Persily (2006), measurements of some tracer gases, including CO_2, can be used to determine the average AER in naturally ventilated spaces. This is done through mass balance analysis which calculates the reduction of indoor CO_2 concentration during a specific period assuming there are no additional indoor sources of CO_2 (Coley and Beisteiner, 2002; Roulet and Foradini, 2002; Gao et al., 2008; Cui et al., 2015; Mendez et al., 2015). There are also other tracers that can be used e.g. nitrous oxide (N_2O) (Gao et al., 2008).

According to Weschler (2000), the AER can be as low as 0.2 h^{-1} in an energy-efficient and tightly constructed typical residential building, while it can reach 2.0 h^{-1} in a loosely constructed building, and can even exceed 5.0 h^{-1} in some cases. A statistical study which investigated the AER of 2844 households in the US found an average value of 0.76 h^{-1} (Murray and Burmaster, 1995). Another study which focused on approximately 470 dwellings in the UK found a similar mean value of the AER (mean: ~0.7 h^{-1}, range: 0.2-1.5 h^{-1}) (Dimitroulopoulou et al., 2006). Values of the AER were commonly larger than 0.5 h^{-1} in Mediterranean countries, including Greece and Portugal, but lower than 0.5 h^{-1} in Nordic countries (Dimitroulopoulou, 2012). Moreover, a higher frequency of opening windows in summer causes a greater air exchange rate than in the other seasons (Weschler, 2000).

3.5. Outdoor concentrations

The lifetimes of longer-lived species are sufficient that they can be transported between indoors and outdoors. Therefore, it is necessary to set the outdoor concentrations of these to appropriate values in the model. Outdoor concentrations of HNO_3 and H_2O_2 are assumed to be constant at 2 ppb outdoors (Carslaw 2007). Photolysis drives the formation of CH_3O_2, HO_2, and OH outdoors and their concentrations show a strong diurnal variation in the outdoor environment. Maximum outdoor concentrations of CH_3O_2, HO_2, and OH at solar noon were assumed to be 2.5×10^7, 21×10^8 and 2.5×10^7 molecule/cm^3 respectively, broadly in line with the conditions measured in urban field campaigns (Platt et al., 2002; Emmerson et al., 2005). Furthermore, the outdoor concentration of HONO is low during the daytime due to its fast photolysis rate and it tends to accumulate during night-time. The outdoor concentration of HONO in the model is therefore assumed to follow a diurnal profile with approximately 20

ppt at noon and 300 ppt at night, consistent with previous measurements in the urban atmosphere (Alicke et al., 2003).

One-year of data from an urban background site in London (Eltham in Greenwich) was used to calculated typical outdoor profiles of NO_2, O_3 and NO. The outdoor concentrations of NO and NO_2 which are mainly influenced by traffic, reach maximum concentrations during morning (NO: ~12 ppb; NO_2: ~17 ppb) and evening (NO: not distinct during evening rush hour; NO_2: ~20 ppb) rush hours respectively while the O_3 concentration reaches a maximum value (~35ppb) in the early afternoon (Carslaw 2007). Moreover, the outdoor concentrations of VOCs were based on the measured data from Sarwar et al. (2002).

3.6. Deposition to surfaces

According to Raunemaa et al. (1989), the deposition velocity is an important component needed to describe the process of deposition onto surfaces. The deposition velocity is used in E4 to calculate the deposition rate onto indoor surfaces:

$$K = V_d \left(\frac{A}{V}\right) \qquad \text{E4}$$

Where K is the loss rate of a pollutant to deposition (h^{-1}), V_d is its deposition velocity (m/h), and (A /V) is the surface to volume ratio where A is the indoor surface area (m^2) and V is the volume of indoor air (m^3). V_d is effectively a mass transfer coefficient which describes the reactivity of surfaces in the indoor environment (Wang and Morrison, 2006).

A new approach was described in Carslaw et al. (2012) for calculating relevant indoor deposition velocities, due to a lack of measured data indoors. Zhang et al. (2002) researched 15 different outdoor surfaces at different times of the year and provided deposition velocities of 31 different species onto these surfaces. The deposition velocities of 25 of these species that appeared in the INDCM, were then averaged for different outdoor surfaces (including urban, interrupted woodlands, shrubs, grass and mixed broadleaf and needleleaf trees) during the summer by Carslaw et al. (2012) to give a typical outdoor deposition velocity for suburban surfaces outdoors.

For ozone and nitrogen dioxide, indoor deposition velocities on different surfaces such as wood and linoleum were reported by Grontoft and Raychaudhuri (2004) to give values of 0.0345 and 0.0261 cm/s for O_3 and NO_2 respectively (Carslaw et al., 2012). These two values

are 17.6 and 21.7 times lower than the calculated suburban values for O_3 and NO_2 respectively as described in the previous paragraph. Therefore, the suburban deposition velocities were all divided by 20 to get 'typical' indoor deposition velocities for use in the model (Table 3.3).

Table 3.3: Averaged deposition velocities of 25 species measured by Zhang et al. (2002) and adapted for indoor use by Carslaw et al. (2012).

Species	Deposition velocity (cm/s)	
	Suburban	Indoor
Sulphur dioxide	0.584	0.0292
Sulphuric acid	0.763	0.0382
Nitrogen dioxide	0.566	0.0261
Ozone	0.607	0.0345
Hydrogen peroxide	0.909	0.0455
Organic peroxides	0.585	0.0292
Nitric acid	3.518	0.1759
Nitrous acid	1.290	0.0645
Peroxynitric acid	2.256	0.1128
Peroxyacetyl nitrate (PAN)	0.395	0.0197
PPN, APAN, MPAN	0.363	0.0182
Formaldehyde	0.700	0.0350
Acetaldehyde	0.247	0.0123
C_3, C_4-C_5, C_6-C_8 and aromatic aldehydes	0.205	0.0103
Methyl vinyl ketone	0.320	0.0160
Methacrolein	0.218	0.0109
Methyl Glyoxal	0.306	0.0153
Methanol	0.614	0.0307
Ethanol	0.528	0.0264
Cresol	0.262	0.0131
C_3 alcohols	0.325	0.0162
Formic acid	0.877	0.0438

Ethanoic acid	0.718	0.0359
Isoprene organic nitrates	0.292	0.0146
Other organic nitrates	0.328	0.0164

For simplification, the same deposition velocity is assumed for all higher aldehydes (longer chain than C_8) with a value of 0.0103 cm/s. Meanwhile, the deposition velocity for all long chain acids and alcohols (longer chain than acetic acid and C_3 alcohols respectively) are assumed to be 0.0359 and 0.0162 cm/s respectively.

3.7. Photolysis

The INDCM includes terms that represent both indoor and attenuated outdoor lighting (e.g. see Carslaw, 2007). In the original model, there was no differentiation between indoor light sources, and constant transmission of light was assumed between 300-400 nm (UV) and 400-760 nm (visible) according to the method developed by Nazaroff and Cass (1986).

The photolysis coefficient (j) for each species *i*, was calculated using E5-7:

$$j_i = h_{uv} I_{uv} + h_{vis} I_{vis} \quad \text{E5}$$

Where:

$$h_{uv} = (100nm)^{-1} \int_{300nm}^{400nm} \sigma \varphi d\lambda \quad \text{E6}$$

$$h_{vis} = (360nm)^{-1} \int_{400nm}^{760nm} \sigma \varphi d\lambda \quad \text{E7}$$

I_{uv} and I_{vis} represent the spherically integrated photon fluxes (photons/cm^2/s) in the UV and visible bands, respectively. The values of I_{uv} = 2.3 x 10^{13} and I_{vis} = 7.0 x 10^{14} photons/cm^2/s given by Nazaroff and Cass (1986) were used, whilst h_{uv} and h_{vis} were determined using E6 and E7, where σ is the absorption cross-section of the molecule in question, (in units of cm^2), φ the quantum yield (dimensionless) and dλ the relevant wavelength interval (in nanometres). The values of cross-sections and quantum yield of the photolysis values were obtained from the IUPAC (IUPAC nd) and MCM (MCM nd) websites.

Outdoor photolysis rates were treated as described by Carslaw (2007). A 2-stream scattering model was used to calculate the photolysis rates outdoors (Hough, 1988). This scattering model calculates the specific rates of photolysis through the consideration of all factors which affect how the light from the sun reaches the surface of the Earth, including time of day and year, latitude and longitude (Jenkin et al., 1997). The scattering model assumes a typical mid-latitude value for the ozone column and clear skies (e.g. no clouds).

These rates are then attenuated to be representative for the indoor environment, as sunlight is attenuated as it passes through windows. A study in a museum (Nazaroff and Cass, 1986) found that only 0.15% of UV and 0.7% of visible sunlight was transmitted through skylights indoors, whilst for two laboratories in Greece with large windows (Drakou et al., 1998), 25-30% of UV and 70-80% of visible light penetrated indoors. At the time of the Carslaw (2007) paper, one previous study measured photolysis coefficients for indoor and outdoor NO_2 and found that indoor photolysis coefficient of NO_2 were only 10% of outdoor values (Fiadzomor 2002). Therefore, transmission of visible light was assumed as 10% in the model. Furthermore, transmission of UV light was assumed as 3% as it was assumed that transmitted UV light is approximately 3 times less than transmitted visible light (Carslaw 2007). Improvement of this representation of photolysis in the INDCM is the key feature of this thesis and is described in more detail in subsequent chapters.

3.8. Running conditions

The box-model used in this work assumes a single well-mixed environment and E8 is used to calculate the indoor concentration of each model species (Carslaw et al., 2012):

$$\frac{dC_i}{dt} = -V_d(\frac{A}{V})C_i + \lambda_r f C_o - \lambda_r C_i + \frac{Q_i}{V_i} + \sum_{j=1}^{n} Rij \qquad \text{E8}$$

where C_i (C_o) is the indoor (outdoor) concentration of species *i* (molecule/cm^3), υ_d its deposition velocity (cm/s), A the surface area indoors, V the volume of air in the indoor environment (cm^3), λ_r the air change rate between indoors and outdoors (ACR, s^{-1}), f the building filtration factor, was assumed to be 1 (Dimitroulopoulou et al., 2001), Q_i the indoor emission rate for species *i* (molecule/cm^3/s) and R_{ij} the reaction rate between species *i* and *j* (cm^3/molecule/s).

Indoor emission rates of VOCs were used based on the values reported by Sarwar et al. (2002). A model run will usually take approximately 15 minutes. In order to make sure the

model has reached steady-state, the model is set to run for three days and only data from the third day is used for analysis. In the model, the location can be easily set through a change of latitude and longitude, while the time of year can be set through a change of the declination angle. Moreover, the temperature and relative humidity can also be easily set in the model as can the AER. Finally, the dimensions of the studied room/building can be set through a change in the A/V ratio (surface to volume ratio).

3.9. Summary

This chapter describes how the model used in this dissertation functions. The following four chapters describe how the model was developed and improved for use, focusing on the treatment of photolysis indoors.

Chapter 4: Building Factors affecting indoor photolysis rates

4.1. Abstract

Studying chemical processing indoors is vital to understand what causes pollutants to accumulate, particularly those harmful to health. Indoor photolysis is an often overlooked process in the indoor environment, but it can be important for some species. This chapter describes improvements to a detailed chemical model for indoors, in order to better investigate the impact of photolysis (driven by both indoor and outdoor light sources) on indoor air chemistry. The improved model is then used to investigate the concentrations of key indoor species and the impacts of different types of glass and indoor artificial lights on indoor air chemistry. The results show that the type of artificial light can impact the indoor air chemistry, with uncovered fluorescent tube (UFT) and fluorescent tube (FT) lighting having the largest effects (average OH concentration: 1.5×10^5 and 1.2×10^5 molecule/cm^3 respectively compared to baseline condition (no indoor photolysis) 9.9×10^4 molecule/cm^3). Meanwhile, the distance from the artificial lights also affects indoor air chemistry. There was up to a 76% difference in predicted indoor concentrations for key species, depending on whether photolysis rates were calculated to be adjacent or 1m away from artificial lights. The greatest impacts were on predicted OH (up to 72% difference) and HO_2 (up to 76% difference) concentrations, whilst those of HCHO (less than 1% difference) and NO_2 (less than 10% difference) were similar no matter the distance from the light source. Compared to indoor artificial lights, attenuated sunlight from outdoors has a greater impact on predicted indoor concentrations. The lowest peak OH concentration with a covered fluorescent tube (CFT) light and with a high transmission glass (9.1×10^5 molecule/cm^3) was much greater than the highest peak under UFT for an intermediate transmission glass (6.1×10^5 molecule/cm^3) and a low transmission glass (2.4×10^5 molecule/cm^3). Indoor photolysis rates are affected moderately by changes to the indoor lighting, but more so by the glass type in the windows, which in turn affects the ability for harmful products to form indoors.

4.2. Introduction

As described in Chapter 2, the amount of light that can penetrate indoors is influenced by many factors, including the type of window and its constituent glass, the meteorological

conditions outdoors, the time of day and year and the building orientation and location (Blocquet et al., 2018). These factors could then be expected to cause wide variations to indoor photolysis rates, as different species absorb light at different wavelengths with differing efficiencies (chapter 1).

Different artificial lights can transmit light over a range of wavelengths and have unique spectral characteristics. Table 4.1 shows the transmission wavelength range between 300 and 700 nm for 7 different indoor artificial lights (Kowal et al., 2017). Therefore, depending on the absorption characteristics of indoor air species, different indoor chemistry may be expected with different artificial lights. However, this topic has not been investigated in depth to date.

Table 4.1: Wavelength range over which 7 different light sources transmit (Kowal et al., 2017).

	UV/nm	VIS/nm
Halogen	308-400	400-700
Incandescent	300-400	400-700
Compact fluorescent lamp (CFL)	331-400	400-700
LED	/	400-700
Uncovered fluorescent tube (UFT)	301-400	400-700
Covered fluorescent tube (CFT)	363-400	400-700
New fluorescent tube (FT)	301-400	400-700

Blocquet et al. (2018) found that the type of glass and hence the cut-off wavelength was the primary factor which influenced the amount of transmitted light indoors. As explained in Chapter 2 (Figure 2.6), the film on the window can effectively decrease the amount of light passing into the indoor environment. Therefore, different types of window materials may have important impacts on indoor photolysis rates and hence indoor air chemistry. Again, the impacts of glass composition on the concentrations of key indoor species and especially on predicted concentrations of radicals (e.g. OH), have not been researched in depth to date.

The aim of this chapter is therefore to improve the model representation of photolysis processes in the INDCM, using recent research in this area (Kowal et al., 2017; Blocquet et al., 2018). The specific objectives are to:

- Improve the representation of artificial indoor lighting in an existing detailed chemical model (the INDCM)
- Improve the treatment of attenuated sunlight in the same model
- To use the modified model to explore the impact of this improved representation on:
    - Predicted indoor photolysis rates
    - Predicted concentrations of radicals and other key species indoors
    - Our understanding of indoor chemical processing

4.3. Method

4.3.1. Introduction

The model used in this study is the INDCM (INdoor air Detailed Chemical box Model), which has been described in Chapter 3 and in detail in previous studies (Carslaw, 2007; Carslaw et al., 2012). This section now describes the modifications that have been made to improve the treatment of photolysis in the INDCM model for use in this dissertation.

4.3.2. Representation of artificial lighting

4.3.2.1. New methodology

The chemical mechanism used in the INDCM considers the photolysis of 35 species/groups of species based on the Master Chemical Mechanism protocol (Jenkin et al., 1997; Saunders et al., 2003). Of these 35 photolysis processes, 27 species absorb light in the UV region only. However, NO_2, O_3, glyoxal (CHOCHO), methylglyoxal (CH_3COCHO), and biacetyl ($CH_3COCOCH_3$) absorb in the UV and visible wavelength regions. The nitrate radical only absorbs in the visible region. As described in Chapter 3, in previous work, the INDCM assumed flat transmission of light in the UV and visible wavelength ranges, while only one type of indoor lighting (incandescent) was assumed, based on Nazaroff and Cass (1986).

For the modifications made for this dissertation, the UV wavelength region was split into ten different 10 nm sub-regions (300-310 nm; 310-320 nm; 320-330 nm; 330-340 nm; 340-350 nm; 350-360 nm; 360-370 nm; 370-380 nm; 380-390 nm; 390-400 nm). According to Kowal et al. (2017), the photon flux intensities of halogen and incandescent lights show a steady

increase from 300 to 400 nm while two/three large fluctuations were found in the photon flux intensities for CFL, UFT, CFT and FT lighting. The only difference between FT and C(U)FT was the environment and age of the tube (so basically FT was a new fluorescent tube used only during the experiment, while CFT and UFT were used in the laboratory before the experiment). The CFL described in Kowal et al. (2017) was a bulb not a tube that fits in a regular fixture and is often used in houses. As well as the difference in shape between this bulb and the fluorescent tubes, the composition of the glass casing was different in that it attenuated light further into the UV. Note that for the visible wavelength range, we considered the 400-800 nm region as one wavelength region as before. This is because only 8 species absorb light in this region, and transmission is much flatter than in the 300-400 nm wavelength range (Figure 2.6) (Kowal et al., 2017).

For each of these UV sub-regions and the one visible wavelength region, the photolysis rate coefficient (j) was calculated for each species using a modified form of equation E9:

So j (300-800 nm) = $(h_{uv300-309} \times I_{uv300-309}) + (h_{uv310-319} \times I_{uv310-319}) + (h_{uv320-329} \times I_{uv320-329}) + (h_{uv330-339} \times I_{uv330-339}) + (h_{uv340-349} \times I_{uv340-349}) + (h_{uv350-359} \times I_{uv350-359}) + (h_{uv360-369} \times I_{uv360-369}) + (h_{uv370-379} \times I_{uv370-379}) + (h_{uv380-389} \times I_{uv380-389}) + (h_{uv390-399} \times I_{uv390-399}) + (h_{vis400-800} \times I_{vis400-800})$ E9

The values of h_{uv} and h_{vis} (σ x φ) for these calculations were taken from IUPAC (IUPAC, nd) or the MCM (Jenkin et al., 1997; Saunders et al., 2003) and I_{uv} and I_{vis} represent the measured spherically integrated photon flux (photons cm^{-2} s^{-1}) from Kowal et al. (2017) for each specific wavelength region and for the different indoor light sources. A summary of the absorbing wavelength range and the wavelength interval used for calculating the j values is shown in Table 4.2.

Table 4.2: Wavelength range and interval for absorption cross section and quantum yield data for each of the species/groups of species undergoing photolysis. Where more than one set of products is possible, the main product is shown in brackets. The absorption cross section and quantum yield data are taken from IUPAC (IUPAC, nd) or the MCM (Jenkin et al., 1997; Saunders et al., 2003). The *j* value labels are according to the convention used in the MCM.

J value	Species	Wavelengths range (nm)	Wavelength interval (nm)
J1	O_3 ($O(^1D)$)	300-349	1

J2	O_3 ($O(^3P)$)	300-349; 400-700	1
J3	H_2O_2	300-350	5
J4	NO_2	300-425	5
J5	NO_3 ($NO + O_2$)	586-640	1
J6	NO_3 ($NO_2 + O(^3P)$)	585-640	1
J7	HONO	300-399	1
J8	HNO_3	300-350	5
J11	HCHO (H+HCO)	300-355	1
J12	HCHO (H_2+CO)	300-360	1
J13	CH_3CHO	300-330	5
J14	C_2H_5CHO	300-330	5
J15	C_3H_7CHO (n-C_3H_7 + HCO)	300-364	1
J16	C_3H_7CHO (C_2H_4 + CH_2CHOH)	300-364	1
J17	i-C_3H_7CHO	300-330	5
J18	$CH_2C(CH_3)CHO$ (CH_2=CCH_3+HCO)	300-395	1
J19	$CH_2C(CH_3)CHO$ ($CH_2C(CH_3)CO$+H)	300-395	1
J21	$CH_3C(O)CH_3$	300-327	1
J22	$CH_3C(O)C_2H_5$ ($CH_3CO+C_2H_5$)	300-352	1
J23	$CH_3C(O)CH=CH_2$ ($CH_3CH=CH_2$ + CO)	300-395	1
J24	$CH_3C(O)CH=CH_2$ (CH_3CO + CH_2=CH)	300-395	1
J31	CHOCHO (CO + CO + H_2)	300-355	5
J32	CHOCHO (HCHO + CO)	300-415	5
J33	CHOCHO (HCO + HCO)	300-445	5
J34	CH_3COCHO	300-440	10
J35	$CH_3C(O)C(O)CH_3$	300-460	1
J41	CH_3OOH	300-365	5
J51	CH_3ONO_2	300-340	5
J52	$C_2H_5ONO_2$	300-340	5
J53	n-$C_3H_7ONO_2$	300-340	5
J54	$(CH_3)_2CHONO_2$	300-360	5

J55	$(CH_3)_3CONO_2$	300-330	5
J56	NOA ($CH_3C(O)CH_2(O.) + NO_2$)	300-340	5
J57	NOA ($CH_3CO + HCHO + NO_2$)	300-340	5

This method was used to calculate new photolysis coefficients for the 35 species and for 7 different indoor artificial lights (Table 4.3).

Table 4.3: Photolysis coefficients (in units of s^{-1}) for the 35 species and for 7 different indoor artificial lights (adjacent to the light sources).

J value	Species	Incand.	Halogen	LED	CFL	UFT	CFT	FT
J1	O_3 ($O(^1D)$)	1.8×10^{-6}	5.9×10^{-7}	0	4.8×10^{-8}	9.3×10^{-6}	3.2×10^{-11}	1.0×10^{-5}
J2	O_3 ($O(^3P)$)	2.1×10^{-4}	1.9×10^{-4}	2.2×10^{-4}	3.1×10^{-4}	6.8×10^{-5}	2.7×10^{-5}	8.3×10^{-5}
J3	H_2O_2	2.3×10^{-7}	2.0×10^{-7}	1.8×10^{-8}	1.8×10^{-7}	1.1×10^{-6}	4.2×10^{-9}	1.3×10^{-6}
J4	NO_2	5.4×10^{-4}	6.5×10^{-4}	2.5×10^{-5}	2.2×10^{-3}	3.8×10^{-4}	4.3×10^{-5}	5.0×10^{-4}
J5	NO_3 ($NO + O_2$)	1.8×10^{-2}	1.6×10^{-2}	2.8×10^{-2}	4.7×10^{-2}	8.4×10^{-3}	3.8×10^{-3}	1.0×10^{-2}
J6	NO_3 ($NO_2 + O(^3P)$)	6.8×10^{-2}	6.2×10^{-2}	9.9×10^{-2}	1.7×10^{-1}	3.3×10^{-2}	1.5×10^{-2}	4.0×10^{-2}
J7	HONO	7.1×10^{-5}	8.8×10^{-5}	0	3.2×10^{-4}	6.7×10^{-5}	1.0×10^{-6}	8.8×10^{-5}
J8	HNO_3	2.7×10^{-8}	1.4×10^{-8}	0	2.7×10^{-9}	1.7×10^{-7}	0	1.9×10^{-7}
J11	HCHO (H+HCO)	7.4×10^{-7}	6.0×10^{-7}	0	1.5×10^{-7}	5.2×10^{-6}	0	5.7×10^{-6}
J12	HCHO (H_2+CO)	1.1×10^{-6}	1.1×10^{-6}	0	1.1×10^{-6}	4.3×10^{-6}	0	5.0×10^{-6}
J13	CH_3CHO	2.1×10^{-7}	1.1×10^{-7}	0	1.9×10^{-9}	1.5×10^{-6}	0	1.7×10^{-6}
J14	C_2H_5CHO	5.5×10^{-7}	2.5×10^{-7}	0	3.6×10^{-9}	4.2×10^{-6}	0	4.5×10^{-6}
J15	C_3H_7CHO (n-C_3H_7 + HCO)	3.0×10^{-7}	2.3×10^{-7}	0	8.1×10^{-8}	2.0×10^{-6}	5.9×10^{-12}	2.2×10^{-6}
J16	C_3H_7CHO (C_2H_4 + CH_2CHOH)	1.4×10^{-7}	1.1×10^{-7}	0	3.9×10^{-8}	9.5×10^{-7}	2.8×10^{-12}	1.0×10^{-6}
J17	i-C_3H_7CHO	1.6×10^{-6}	1.2×10^{-6}	0	2.3×10^{-7}	1.1×10^{-5}	0	1.2×10^{-5}
J18	$CH_2C(CH_3)CHO$ ($CH_2=CCH_3$+HCO)	3.0×10^{-8}	3.6×10^{-8}	0	1.3×10^{-7}	7.5×10^{-8}	2.9×10^{-10}	9.0×10^{-8}
J19	$CH_2C(CH_3)CHO$ ($CH_2C(CH_3)CO$+H)	3.0×10^{-8}	3.6×10^{-8}	0	1.3×10^{-7}	7.5×10^{-8}	2.9×10^{-10}	9.0×10^{-8}
J21	$CH_3C(O)CH_3$	1.8×10^{-8}	5.6×10^{-9}	0	0	1.0×10^{-7}	0	1.1×10^{-7}
J22	$CH_3C(O)C_2H_5$ ($CH_3CO+C_2H_5$)	5.6×10^{-8}	3.0×10^{-8}	0	1.7×10^{-9}	4.0×10^{-7}	0	4.3×10^{-7}
J23	$CH_3C(O)CH=CH_2$ ($CH_3CH=CH_2$ + CO)	5.4×10^{-8}	5.2×10^{-8}	0	8.7×10^{-8}	2.6×10^{-7}	1.2×10^{-10}	2.9×10^{-7}

J24	$CH_3C(O)CH=CH_2$ ($CH_3CO + CH_2=CH$)	5.4×10^{-8}	5.2×10^{-8}	0	8.7×10^{-8}	2.6×10^{-7}	1.2×10^{-10}	2.9×10^{-7}
J31	CHOCHO (CO + CO + H_2)	1.9×10^{-7}	1.5×10^{-7}	0	8.2×10^{-8}	1.2×10^{-6}	0	1.3×10^{-6}
J32	CHOCHO (HCHO + CO)	9.3×10^{-7}	9.0×10^{-7}	6.9×10^{-9}	1.9×10^{-6}	4.3×10^{-6}	2.9×10^{-8}	4.8×10^{-6}
J33	CHOCHO (HCO + HCO)	3.8×10^{-6}	4.2×10^{-6}	1.6×10^{-6}	1.7×10^{-5}	7.0×10^{-6}	8.5×10^{-7}	8.2×10^{-6}
J34	CH_3COCHO	6.6×10^{-6}	7.1×10^{-6}	1.3×10^{-6}	3.0×10^{-5}	1.5×10^{-5}	1.2×10^{-6}	1.7×10^{-5}
J35	$CH_3C(O)C(O)CH_3$	2.7×10^{-5}	3.0×10^{-5}	3.8×10^{-5}	1.2×10^{-4}	2.5×10^{-5}	9.7×10^{-6}	2.9×10^{-5}
J41	CH_3OOH	1.6×10^{-7}	1.5×10^{-7}	0	3.7×10^{-7}	7.4×10^{-7}	5.6×10^{-10}	8.3×10^{-7}
J51	CH_3ONO_2	4.0×10^{-8}	2.1×10^{-8}	0	3.1×10^{-9}	2.7×10^{-7}	0	2.9×10^{-7}
J52	$C_2H_5ONO_2$	6.2×10^{-8}	3.4×10^{-8}	0	5.8×10^{-9}	4.1×10^{-7}	0	4.4×10^{-7}
J53	n-$C_3H_7ONO_2$	7.1×10^{-8}	4.4×10^{-8}	0	1.9×10^{-8}	4.4×10^{-7}	0	4.8×10^{-7}
J54	$(CH_3)_2CHONO_2$	9.8×10^{-8}	5.6×10^{-8}	0	1.5×10^{-8}	6.4×10^{-7}	3.6×10^{-12}	7.0×10^{-7}
J55	$(CH_3)_3CONO_2$	2.3×10^{-7}	1.4×10^{-7}	0	2.3×10^{-8}	1.6×10^{-6}	0	1.7×10^{-6}
J56	NOA ($CH_3C(O)CH_2$(O.) + NO_2)	8.9×10^{-7}	6.6×10^{-7}	0	2.4×10^{-7}	5.8×10^{-6}	0	6.3×10^{-6}
J57	NOA (CH_3CO + HCHO + NO_2)	8.9×10^{-7}	6.6×10^{-7}	0	2.4×10^{-7}	5.8×10^{-6}	0	6.3×10^{-6}

Eight of these photolysis coefficients were then compared with those for the same species computed independently by Kowal et al. (2017) and using the same photon flux intensities (Table 4.4). As shown in Table 4.4, the difference between calculated photolysis coefficients and results from Kowal et al. (2017) is in the range of 0.1-96.4% except for the photolysis coefficient for NO_2 for LED lights which was much larger (~500%). This must be due to the values used for the absorption cross section and/or quantum yields over 400 nm (as LED lights do not emit below 400 nm) in this work being different to those used in Kowal et al. (2017). Most of the differences were small in absolute terms, particularly for those light sources that transmitted further into the UV.

Table 4.4: Comparison between calculated photolysis coefficients (s^{-1}) (adjacent to the light sources) for this work and compared to Kowal et al. (2017) for Incandescent (Incand), Halogen, LED, Compact fluorescent lamps (CFL), covered and uncovered fluorescent tubes (CFT and UFT) and fluorescent tubes (FT). % difference = |Kowal - calculated| / Kowal × 100.

	Incand	Halogen	LED	CFL	UFT	CFT	FT
O_3 $O(^1D)$	1.8×10^{-6}	5.9×10^{-7}	0	4.8×10^{-8}	9.3×10^{-6}	3.2×10^{-11}	1.0×10^{-5}

Kowal O_3 $O(^1D)$	1.8×10^{-6}	4.7×10^{-7}	0	7.2×10^{-8}	8.6×10^{-6}	8.8×10^{-10}	8.9×10^{-6}
% difference	**0.6**	**25.3**	**0**	**33.6**	**7.8**	**96.4**	**15.3**
H_2O_2	2.3×10^{-7}	2.0×10^{-7}	1.8×10^{-8}	1.8×10^{-7}	1.1×10^{-6}	4.2×10^{-9}	1.3×10^{-6}
Kowal H_2O_2	2.3×10^{-7}	2.2×10^{-7}	1.8×10^{-8}	4.5×10^{-7}	1.1×10^{-6}	6.5×10^{-9}	1.2×10^{-6}
% difference	**2.6**	**8.4**	**1.1**	**60.5**	**5.7**	**35.2**	**6.7**
NO_2	5.4×10^{-4}	6.5×10^{-4}	2.5×10^{-5}	2.2×10^{-3}	3.8×10^{-4}	4.3×10^{-5}	5.0×10^{-4}
Kowal NO_2	4.7×10^{-4}	5.7×10^{-4}	4.1×10^{-6}	2.4×10^{-3}	3.8×10^{-4}	4.0×10^{-5}	5.0×10^{-4}
% difference	**14.6**	**13.6**	**509.7**	**7.9**	**1.1**	**7.3**	**0.1**
NO_3 ($NO + O_2$)	1.8×10^{-2}	1.6×10^{-2}	2.8×10^{-2}	4.7×10^{-2}	8.4×10^{-3}	3.8×10^{-3}	1.0×10^{-2}
Kowal NO_3 ($NO + O_2$)	1.8×10^{-2}	1.6×10^{-2}	2.9×10^{-2}	4.1×10^{-2}	7.3×10^{-3}	3.3×10^{-3}	9.0×10^{-3}
% difference	**2.4**	**1.8**	**4.2**	**14.8**	**14.0**	**13.6**	**13.7**
NO_3 ($NO_2 + O(^3P)$)	6.8×10^{-2}	6.2×10^{-2}	9.9×10^{-2}	1.7×10^{-1}	3.3×10^{-2}	1.5×10^{-2}	4.0×10^{-2}
Kowal NO_3($NO_2 + O(^3P)$)	8.8×10^{-2}	8.1×10^{-2}	1.4×10^{-1}	1.9×10^{-1}	3.7×10^{-2}	1.8×10^{-2}	4.6×10^{-2}
% difference	**22.6**	**22.8**	**27.0**	**10.7**	**12.1**	**13.5**	**12.8**
HONO	7.1×10^{-5}	8.8×10^{-5}	0	3.2×10^{-4}	6.7×10^{-5}	1.0×10^{-6}	8.8×10^{-5}
Kowal HONO	6.3×10^{-5}	7.8×10^{-5}	0	3.3×10^{-4}	7.1×10^{-5}	8.8×10^{-7}	8.9×10^{-5}
% difference	**12.0**	**11.8**	**0**	**3.8**	**5.0**	**16.0**	**2.0**
HCHO(H+HCO)	7.4×10^{-7}	6.0×10^{-7}	0	1.5×10^{-7}	5.2×10^{-6}	0	5.7×10^{-6}
Kowal HCHO(H+HCO)	8.5×10^{-7}	6.8×10^{-7}	0	1.4×10^{-7}	5.2×10^{-6}	0	5.5×10^{-6}
% difference	**12.7**	**12.6**	**0**	**4.8**	**0.1**	**0**	**4.1**
$CH_3CHO(CH_3 + HCO)$	2.1×10^{-7}	1.1×10^{-7}	0	1.9×10^{-9}	1.5×10^{-6}	0	1.7×10^{-6}
Kowal $CH_3CHO(CH_3 + HCO)$	1.7×10^{-7}	7.8×10^{-8}	0	3.8×10^{-9}	1.3×10^{-6}	0	1.3×10^{-6}
% difference	**25.2**	**39.6**	**0**	**51.9**	**23.2**	**0**	**25.2**

Table 4.4 shows that the photolysis coefficients for the same chemical species can be quite different under different indoor artificial lights. Photolysis coefficients calculated in this work for O_3, H_2O_2, HCHO and CH_3CHO are highest for UFT and FT lights, while the highest values for NO_2, NO_3 and HONO are for CFL lights.

Kowal et al. (2017) reported photolysis rate coefficients of H_2O_2, O_3, HONO, HCHO and CH_3CHO both adjacent to and 1m away from different light sources. This permitted the % of light at 1m relative to that adjacent to the indoor lights to be calculated (Table 4.5). The value

at 1m can be considered to be more representative for an integrated average for a room (Kowal et al., 2017).

Table 4.5: Percentage of light at 1m relative to that adjacent to 7 indoor artificial light sources (Kowal et al., 2017). '/' means the measured and then calculated photolysis rate constants (s^{-1}) of chemicals under LED and CFT are zero or close to zero under either or both distances based on Kowal et al. (2017).

	H_2O_2	O_3	HONO	HCHO	CH_3CHO
LED	2%	/	/	/	/
Halogen	2%	2%	2%	2%	2%
incandescent	2%	2%	2%	2%	2%
CFL	2%	2%	2%	2%	2%
FT	4%	4%	4%	4%	4%
CFT	15%	15%	15%	/	/
UFT	15%	15%	15%	15%	15%

These attenuation factors were then applied to the photolysis rates of all 35 species shown in Table 4.3 to calculate the values 1m away for the different lights. The transmission of light was assumed to be 2% and 15% of the adjacent value for all species for LED and CFT lights respectively at 1m. Table 4.6 compares the photolysis coefficients calculated in this way compared with those used in the previous version of the model (which was based on 1m distance from an incandescent light source). In general, the previous values are within the range of the new photolysis coefficients. The new photolysis coefficients were compared to the former values used in the model to assess which type of lighting the old values were most similar to. The percentage difference between each new photolysis coefficient and the old value was calculated for each light source, and then absolute values of these differences averaged for each lighting type (Table 4.6). Compared to other lights sources, the values of the photolysis rates in the previous version of the model are most similar to newly calculated values for incandescent and halogen lighting. However, it does show that the previous values were unsuitable for much of the lighting currently used indoors (e.g. UFT), which will lead to incorrect predictions of the indoor concentrations of chemicals.

Table 4.6: Percentage difference in calculated photolysis coefficients (s^{-1}) (1m away from the light sources) in the updated model by lighting type compared to the old version, together with photolysis coefficients in old version. % difference = (new values – old values) / old values × 100. The average difference for each type of light is shown in the lowest row of the table.

1m	Incandescent	Halogen	LED	CFL	UFT	CFT	FT	old
J1	-91	-97	-100	-100	237	-100	-1	4.1×10^{-7}
J2	180	142	185	299	571	165	117	1.5×10^{-6}
J3	-83	-85	-99	-86	547	-98	94	2.6×10^{-8}
J4	-17	0	-96	246	337	-50	54	1.3×10^{-5}
J5	416	345	673	1224	1656	688	472	7.1×10^{-5}
J6	131	111	235	470	726	283	171	5.9×10^{-4}
J7	-26	-9	-100	228	423	-92	82	$1.9\times10\text{-}^{6}$
J8	-90	-95	-100	-99	405	-100	46	5.1×10^{-9}
J11	-88	-91	-100	-98	519	-100	80	1.3×10^{-7}
J12	-77	-75	-100	-75	623	-100	122	9.0×10^{-8}
J13	-90	-95	-100	-100	461	-100	61	4.1×10^{-8}
J14	-94	-97	-100	-100	242	-100	-3	1.9×10^{-7}
J15	-88	-91	-100	-97	493	-100	72	5.0×10^{-8}
J16	-88	-91	-100	-97	494	-100	73	2.4×10^{-8}
J17	-69	-76	-100	-95	1552	-100	379	1.0×10^{-7}
J18	-99	-99	-100	-97	-89	-100	-96	1.0×10^{-7}
J19	-99	-99	-100	-97	-89	-100	-96	1.0×10^{-7}
J21	-96	-99	-100	-100	77	-100	-49	8.8×10^{-9}
J22	-96	-98	-100	-100	123	-100	-36	2.7×10^{-8}
J23	-85	-86	-100	-77	430	-100	59	7.4×10^{-9}
J24	-78	-79	-100	-65	696	-100	138	4.9×10^{-9}
J31	N/A	N/A	N/A	N/A	N/A	N/A	N/A	N/A
J32	N/A	N/A	N/A	N/A	N/A	N/A	N/A	N/A
J33	-99	-99	-100	-97	-92	-99	-98	1.3×10^{-5}
J34	-74	-71	-95	19	346	-65	36	5.0×10^{-7}
J35	-92	-91	-89	-65	-45	-79	-83	6.8×10^{-6}
J41	-82	-83	-100	-56	551	-100	95	1.7×10^{-8}
J51	-89	-94	-100	-99	444	-100	57	7.5×10^{-9}
J52	-89	-94	-100	-99	439	-100	56	1.1×10^{-8}
J53	-88	-93	-100	-97	445	-100	59	1.2×10^{-8}
J54	-89	-94	-100	-98	452	-100	60	1.7×10^{-8}
J55	-62	-76	-100	-96	1856	-100	465	1.2×10^{-8}
J56	47	9	-100	-61	7115	-100	1999	1.2×10^{-8}
J57	47	9	-100	-61	7115	-100	1999	1.2×10^{-8}
difference	89	84	117	141	873	115	215	/

*Percentage difference = -100 is where the new photolysis coefficients are zero.

* N/A - means not applicable.

4.3.2.2. The influence of this update on model output

This section aims to test the impact of the new values of the indoor photolysis coefficients on the model predicted concentrations of radicals and other species. The calculated photolysis rate coefficients were based on indoor artificial lights only at 1m from the light source. Figures 4.1-4.8 show the differences in model predicted concentrations of O_3, HONO, HCHO, OH, HO_2, RO_2, NO and NO_2 before and after the updates to the model under the different lighting conditions.

O_3, HONO, HCHO and NO_2 concentrations using the old representation are similar to the new method for the 7 different indoor artificial lights (Figures 4.1, 4.2, 4.3 and 4.8). The profiles of OH, HO_2 and RO_2 radicals exhibit higher concentrations for UFT lights, then FT lighting, followed by the old representation and then the other light sources (Figures 4.4-4.6) while the profiles of NO exhibit the opposite pattern (Figure 4.7). The new photolysis coefficients for O_3, HONO and HCHO are approximately 5.0 and 1.8 times higher than with the old representation for UFT and FT respectively (Table 4.6). Given photolysis reactions of O_3, HONO and HCHO are all radical sources (R1, R6 and R16), the profiles of OH, HO_2 and RO_2 concentrations exhibit higher concentrations for UFT and FT lighting than for the other indoor lights. The additional HO_2 formed from HCHO photolysis (R16-18) can react with NO, which leads to the lowest NO concentration for UFT lighting (Figure 4.7).

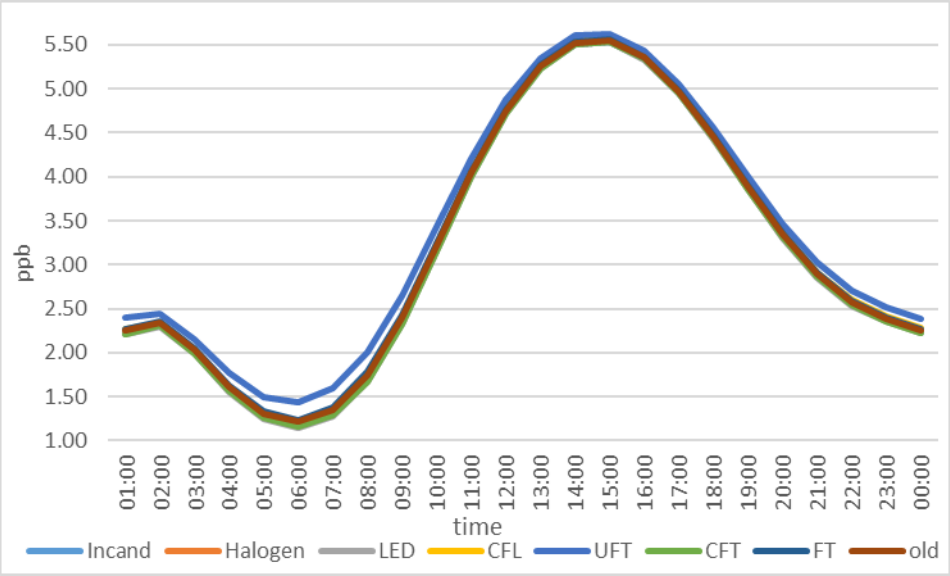

Figure 4.1: Concentrations of O_3 before (old) and after (Incandescent, Halogen, LED, CFL, UFT, CFT and FT) the model update. The profiles for Incandescent, Halogen, LED, CFL, UFT, CFT and FT closely track each other.

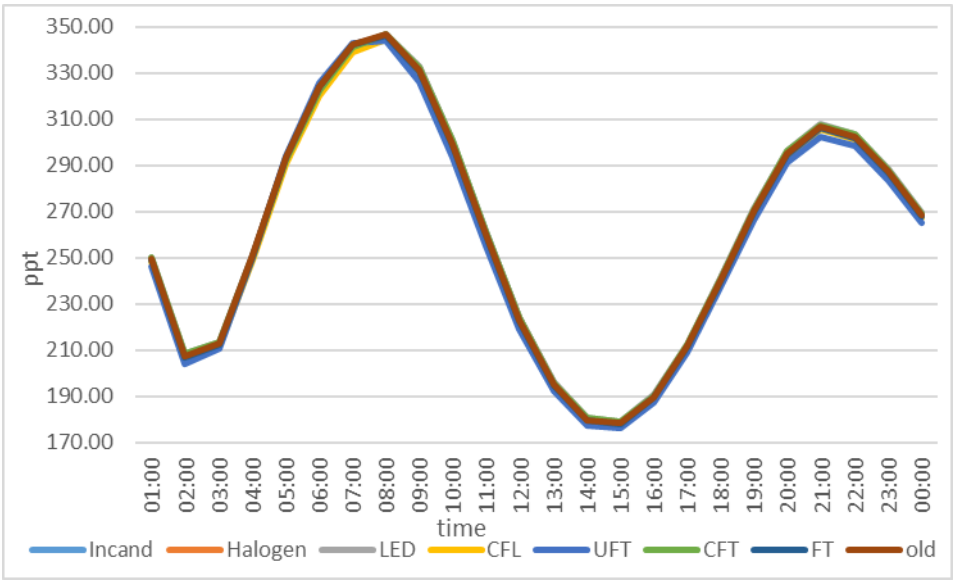

Figure 4.2: Concentrations of HONO before (old) and after (Incandescent, Halogen, LED, CFL, UFT, CFT and FT) the model update. The profiles for Incandescent, Halogen, LED, CFL, UFT, CFT and FT lighting closely track each other.

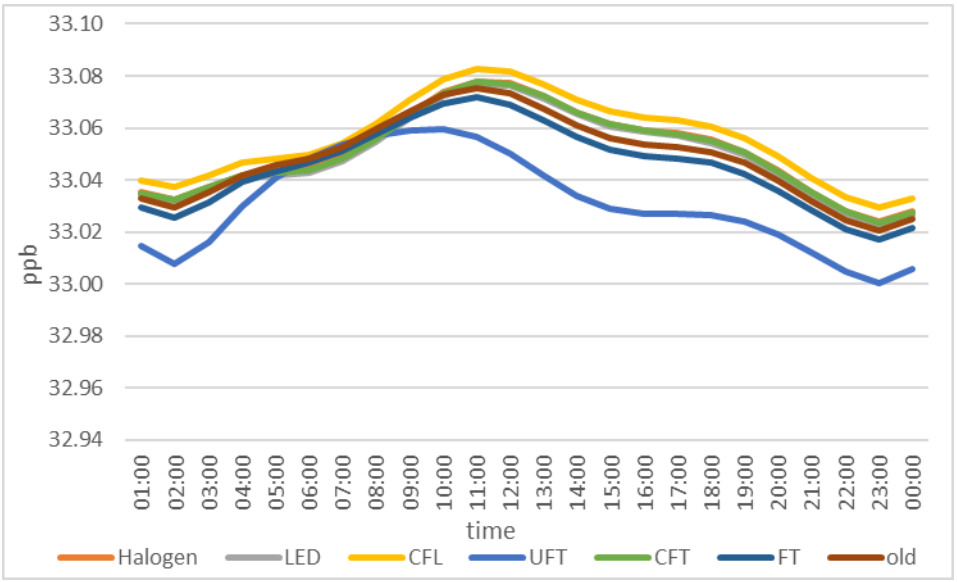

Figure 4.3: Concentrations of HCHO before (old) and after (Incandescent, Halogen, LED, CFL, UFT, CFT and FT) the model update.

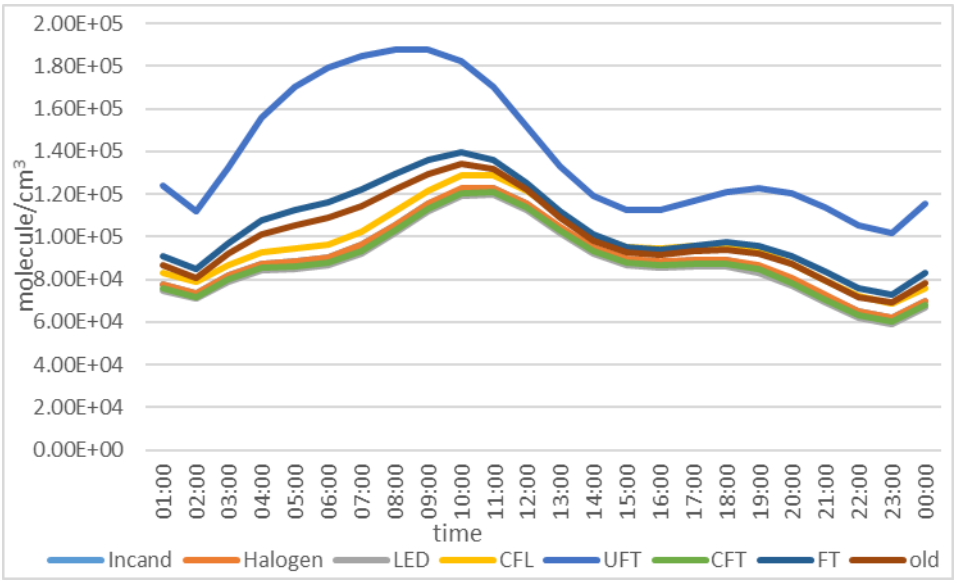

Figure 4.4: Concentrations of OH before (old) and after (Incandescent, Halogen, LED, CFL, UFT, CFT and FT) the model update.

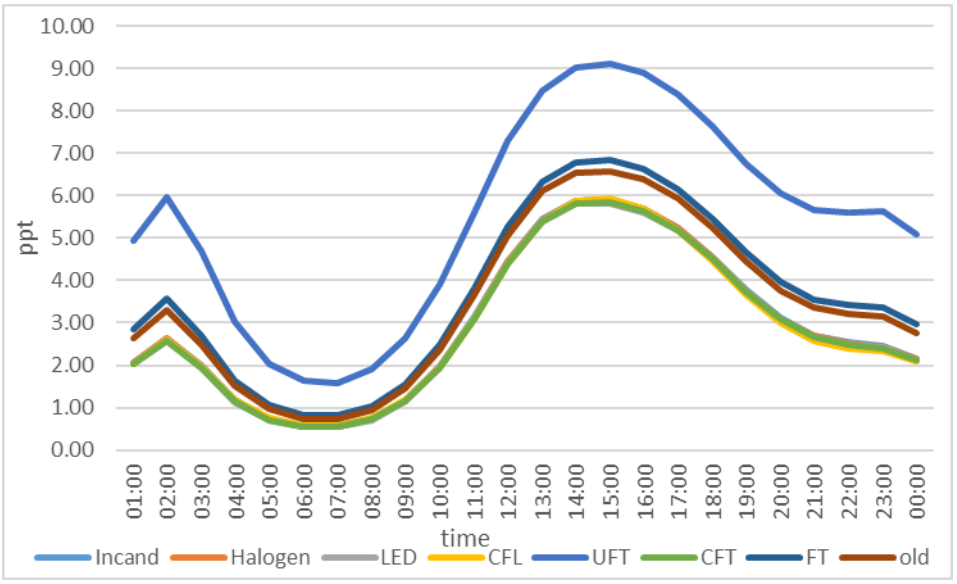

Figure 4.5: Concentrations of HO_2 before (old) and after (Incandescent, Halogen, LED, CFL, UFT, CFT and FT) the model update.

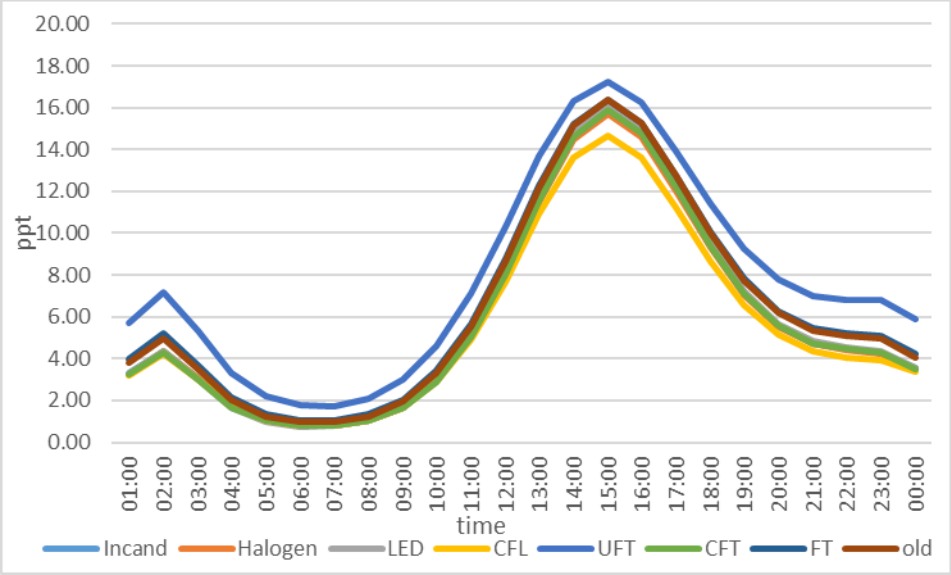

Figure 4.6: Concentrations of RO_2 before (old) and after (Incandescent, Halogen, LED, CFL, UFT, CFT and FT) the model update.

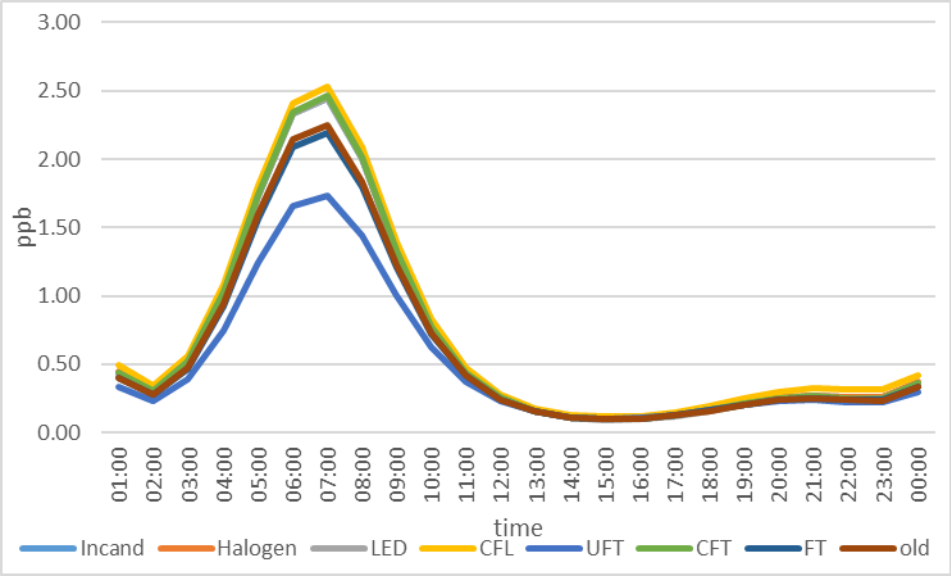

Figure 4.7: Concentrations of NO before (old) and after (Incandescent, Halogen, LED, CFL, UFT, CFT and FT) the model update.

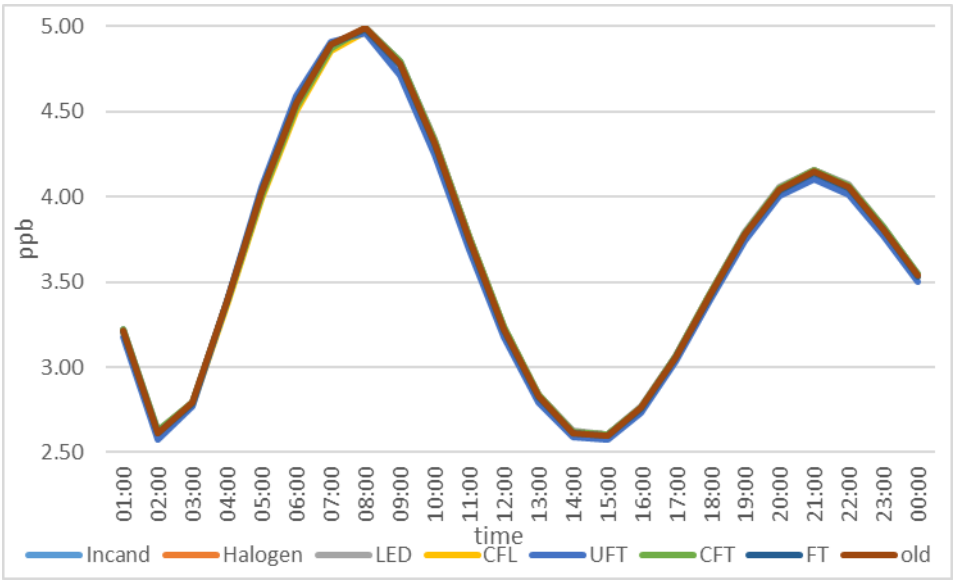

Figure 4.8: Concentrations of NO_2 before (old) and after (Incandescent, Halogen, LED, CFL, UFT, CFT and FT) the model update. All profiles closely track each other.

Table 4.7 shows the differences between the daily average concentrations of these key species for the 7 studied indoor artificial lights and the old representation. These differences are most important for the radical species as expected, with up to a 39.8% and 58.0% difference for OH and HO_2 respectively under UFT lighting compared to the old representation. For other species such as HCHO, the differences are minimal showing that there are other more important processes controlling their chemistry than lighting (which will be investigated in Chapter 6). Therefore, depending on the species of interest, making sure the indoor light source is properly represented can be important.

Table 4.7: Difference (%) between daily average concentrations of the key chemical species studied for 7 indoor artificial lights and the old model representation.

	O_3	HONO	HCHO	OH	HO_2	RO_2	NO	NO_2
Incand.	-0.9	0.1	0	-9.2	-15.1	-7.6	8.2	0.1
Halogen	-0.8	0.1	0	-9.0	-15.5	-8.2	8.9	0.1
LED	-1.4	0.3	0	-12.2	-16.5	-6.6	7.1	0.2
CFL	0.4	-0.4	0	-2.8	-16.4	-13.2	15.6	-0.3
UFT	4.5	-1.1	-0.1	39.8	58.0	21.8	-17.7	-0.8
CFT	-1.1	0.2	0	-11.0	-16.5	-7.7	8.3	0.1
FT	0.6	-0.1	0	4.6	5.3	1.5	-1.5	-0.1

4.3.3. Representation of attenuated outdoor sunlight

4.3.3.1. New methodology

As described earlier, the previous model assumed that 3% of UV and 10% of visible light from outdoors passed through the windows and ended up indoors. These values were first assumed by Carslaw (2007) which considered data available at the time, as discussed in detail in the previous chapter (Chapter 3). However, in reality, transmission of outdoor light indoors, will vary depending on the window material (glass) composition. Blocquet et al. (2018) measured the transmittance through 17 different window materials. For this work, three different glasses were selected that encompassed very different cut-off wavelengths, including 'Glass C Sacht Self-cleaning' (transmission from 315-800 nm, Glass C), 'Low Emissivity' (transmission from 330-800 nm, LE) and 'Low Emissivity With Film' (transmission from 380-800 nm, LEWF).

The value of the product of σ x φ for each available wavelength and for each photolysing species was calculated between 300-800 nm. The absorption cross section and quantum yield values were taken from the IUPAC (IUPAC, nd) or the MCM (Jenkin et al., 1997; Saunders et al., 2003) website. The wavelength intervals used for each species were based on the presented absorption cross section and quantum yield values on these two websites (Table 4.2). The sum of each of these contributions over each of the wavelength intervals was then calculated, so that the % contribution for each specific wavelength interval could be found. The measured transmission factor (% light transmitted through the glass) for each wavelength interval was then applied to each of these based on the information provided in Blocquet et al. (2018) to calculate a weighted transmission factor for each wavelength interval. Finally, the contributions from each individual wavelength over the entire 300-800 nm wavelength range were summed to provide a transmission factor for each photolysing species and for each window material.

For instance, for NO_2 photolysis with Glass C in the windows:

wavelength/nm	σ x φ (nm^2 $molecule^{-1}$; dimensionless)	% contribution for each specific wavelength	% transmission factor (Glass C) from Blocquet et al. (year)	Weighted transmission factor
300	1.3×10^{-19}	1.4	0	0
305	1.6×10^{-19}	1.7	0	0
310	1.9×10^{-19}	2.0	0	0

315	2.2×10^{-19}	2.4	0.8	0.02
320	2.5×10^{-19}	2.8	4.3	0.1
325	2.9×10^{-19}	3.1	7.7	0.2
330	3.2×10^{-19}	3.5	18.7	0.7
335	3.6×10^{-19}	3.9	26.6	1.0
340	4.0×10^{-19}	4.4	42.1	1.8
345	4.2×10^{-19}	4.5	53.1	2.4
350	4.6×10^{-19}	5.0	61.9	3.1
355	5.0×10^{-19}	5.4	66.0	3.6
360	5.1×10^{-19}	5.5	70.1	3.9
365	5.5×10^{-19}	6.0	73.9	4.4
370	5.6×10^{-19}	6.1	77.6	4.7
375	5.9×10^{-19}	6.4	77.6	5.0
380	5.9×10^{-19}	6.4	77.6	5.0
385	5.9×10^{-19}	6.5	79.7	5.1
390	6.2×10^{-19}	6.7	81.7	5.5
395	5.9×10^{-19}	6.4	81.7	5.3
400	5.6×10^{-19}	6.1	81.7	5.0
405	2.1×10^{-19}	2.3	81.7	1.9
410	9.2×10^{-20}	1.0	82.1	0.8
415	3.5×10^{-20}	0.4	82.4	0.3
420	1.1×10^{-20}	0.1	82.4	0.1
425	2.3×10^{-21}	0	82.4	0
Sum of (σ x φ) = 9.2×10^{-18}			Sum of weighted transmission factor/100 = 59.9%	

So in other words, the indoor j(NO_2) value is 59.9% of the calculated outdoor value for the glass C material.

Table 4.8 shows the transmission factors for all 35 species and for the three window glasses based on this method. Transmission factors range from 0 to 85% and are quite different from

the 3% transmission of UV and 10% of visible light assumed previously for all species. For some species such as NO_3, the new calculated transmission factors are large (Table 4.8), and this is due to very high measured transmission factors (e.g. ~70%-86% over 400 nm for Glass C) by Blocquet et al. (2018) in the selected wavelength ranges for these species. Meanwhile, O_3 photolysis to make $O(^1D)$ has transmission factors lower than 0.3% for all three glasses. The transmission factors show an obvious decrease as the cut-off wavelength increases for the different glasses as expected.

Table 4.8: Calculated transmission factors (%/100) for 35 species that undergo photolysis and for the three window glasses (see Blocquet et al., 2018).

		Glass C	Low Emissivity	Low Emissivity with film
J1	O_3 $O(^1D)$	0.003	0.0001	0
J2	O_3 $O(^3P)$	0.17	0.1	0.08
J3	H_2O_2	0.06	0.01	0
J4	NO_2	0.6	0.3	0.04
J5	NO_3 ($NO + O_2$)	0.85	0.63	0.51
J6	NO_3 ($NO_2 + O(_3P)$)	0.85	0.66	0.55
J7	HONO	0.58	0.24	0.001
J8	HNO_3 (OH)	0.01	0.0004	0
J11	HCHO (H+HCO)	0.03	0.001	0
J12	HCHO (H_2+CO)	0.15	0.02	0
J13	CH_3CHO (CH_3 + HCO)	0.003	0	0
J14	C_2H_5CHO	0.001	0	0
J15	C_3H_7CHO (n-C_3H_7 + HCO)	0.03	0.002	0
J16	C_3H_7CHO (C_2H_4 + CH_2CHOH)	0.03	0.002	0
J17	IPRCHO (n-C_4H_9 + HCO)	0.02	0	0
J18	MACR (CH_2=CCH_3+HCO	0.3	0.09	0.0001
J19	MACR ($CH_2C(CH_3)CO$+H	0.3	0.09	0.0001
J20	C_5HPALD1	0.3	0.09	0.0001
J21	$CH_3C(O)CH_3$	0.001	0	0

J22	MEK ($CH_3CO+C_2H_5$)	0.01	0.0002	0
J23	MVK ($CH_3CH=CH_2$ + CO)	0.09	0.02	0
J24	MVK (CH_3CO + $CH_2=CH$)	0.09	0.02	0
J31	GLYOX (CO + CO + H_2)	0.03	0.003	0
J32	GLYOX (HCHO + CO)	0.07	0.02	0.002
J33	GLYOX (HCO + HCO)	0.25	0.11	0.04
J34	MGLYOX	0.16	0.08	0.02
J35	BIACET	0.77	0.51	0.34
J41	CH_3OOH	0.08	0.02	0
J51	CH_3ONO_2	0.01	0.0001	0
J52	$C_2H_5ONO_2$	0.01	0.0002	0
J53	n-$C_3H_7ONO_2$	0.02	0.001	0
J54	i-$C_3H_7ONO_2$	0.01	0.001	0
J55	$TC_4H_9NO_3$	0.01	0	0
J56	NOA ($CH_3C(O)CH_2(O.)$ + NO_2)	0.02	0.001	0
J57	NOA (CH_3CO + HCHO + NO_2)	0.02	0.001	0

4.3.3.2. The influence of this update on model output

Indoor lighting was assumed to be off, so that photolysis rate coefficients were based only on transmission of outdoor sunlight. All other aspects of the model were as described in Section 4.3.4. Table 4.9 shows the % difference in average indoor concentrations of O_3, HONO, HCHO, OH, HO_2, RO_2, NO and NO_2 for the three glasses (Glass C, LE and LEWF) compared to the old representation. Among the three studied glasses, daily average concentrations of the old representation are most similar to those in the new simulation for the LEWF glass. Relative to the old representation, daily average concentrations of O_3, HCHO, OH and NO are higher for Glass C and LE, and the concentrations are slightly lower for HONO, RO_2, HO_2 and NO_2 (Table 4.9).

Table 4.9: Differences (%) between daily average concentrations of key chemical species for the 3 studied window materials and the old representation.

	O_3	HONO	HCHO	OH	HO_2	RO_2	NO	NO_2
Glass C	64.8	-19.8	0.5	418.0	15.6	-26.3	171.2	-8.8
LE	34.7	-11.3	0.4	208.3	-2.3	-32.9	117.9	-5.6
LEWF	5.5	-1.2	0.1	29.3	-3.7	-21.4	22.8	-1.3

Differences between the old and new predicted concentrations are important for all studied chemicals (apart from HCHO), with up to a 418% and 171.2% difference for OH and NO respectively under Glass C. Again, the differences are much smaller for HCHO showing that there are other more important processes controlling its chemistry than lighting. Therefore, depending on the species of interest, making sure the window material is properly represented in a model for indoor air chemistry is important. Figures 4.9-4.16 show the differences in predicted diurnal concentrations of these species before and after the changes to the treatment of attenuated light in the model.

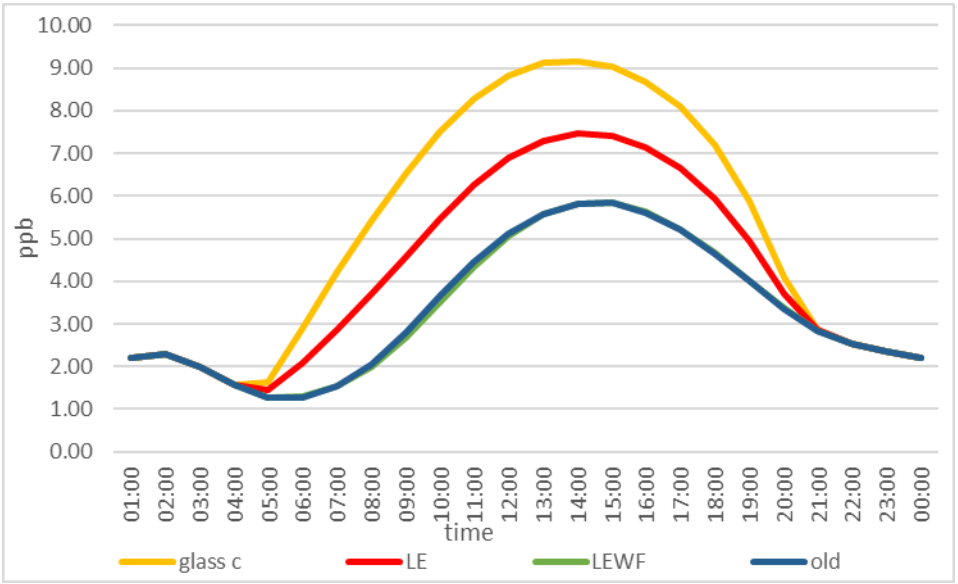

Figure 4.9: Concentrations of O_3 before (old) and after (Glass C Sacht Self-cleaning, Low Emissivity (LE) and Low Emissivity With Film (LEWF)) the model updates.

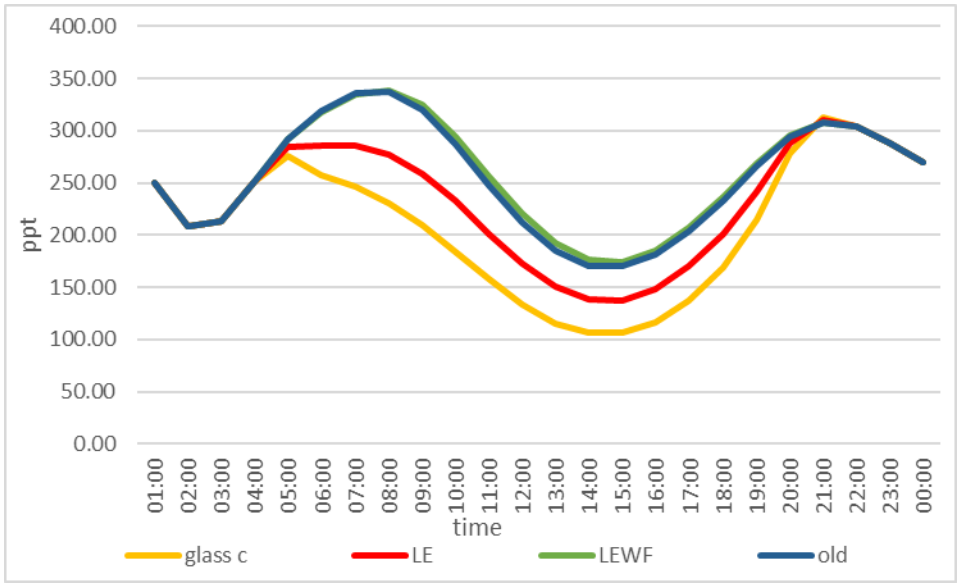

Figure 4.10: Concentrations of HONO before (old) and after (Glass C Sacht Self-cleaning, Low Emissivity (LE) and Low Emissivity With Film (LEWF)) the model updates.

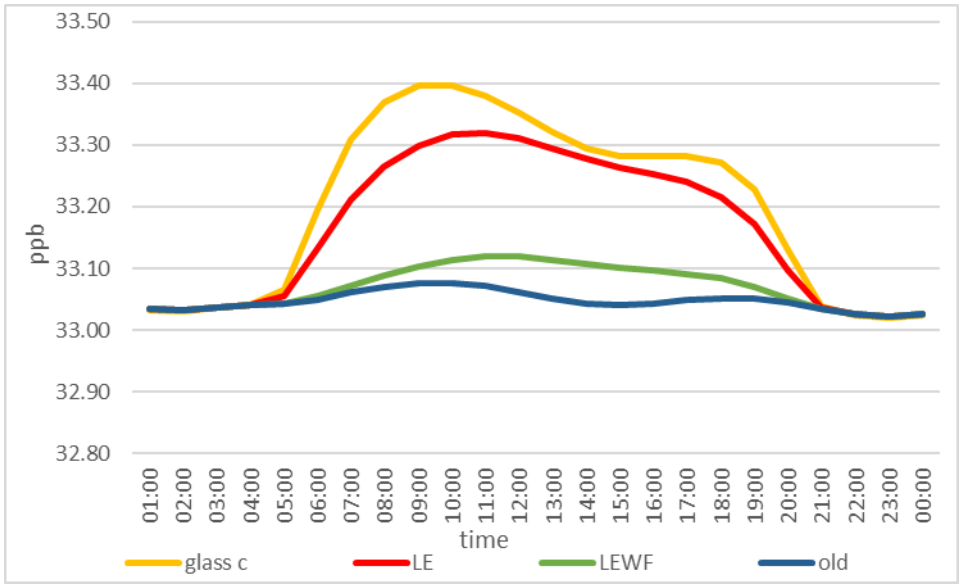

Figure 4.11: Concentrations of HCHO before (old) and after (Glass C Sacht Self-cleaning, Low Emissivity (LE) and Low Emissivity With Film (LEWF)) the model updates.

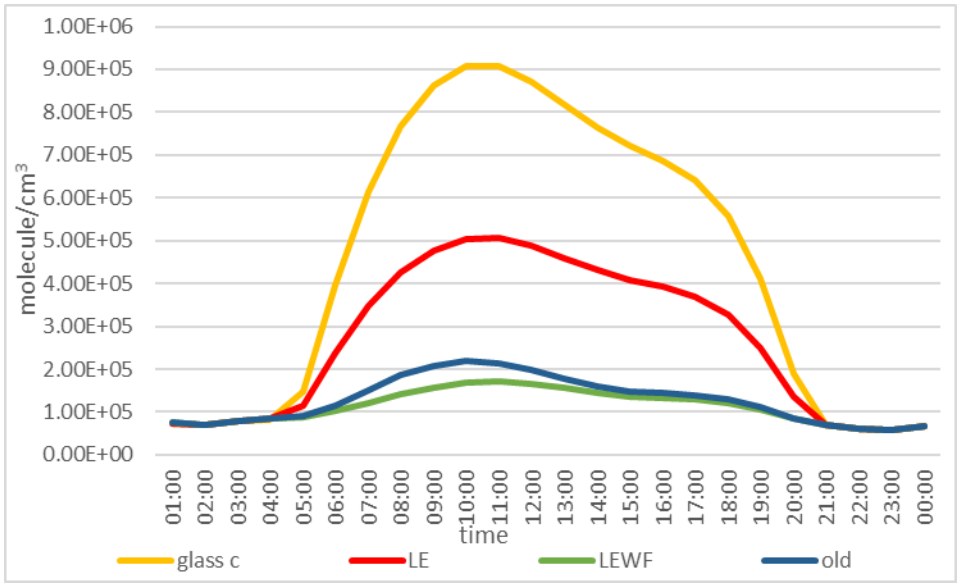

Figure 4.12: Concentrations of OH before (old) and after (Glass C Sacht Self-cleaning, Low Emissivity (LE) and Low Emissivity With Film (LEWF)) the model updates.

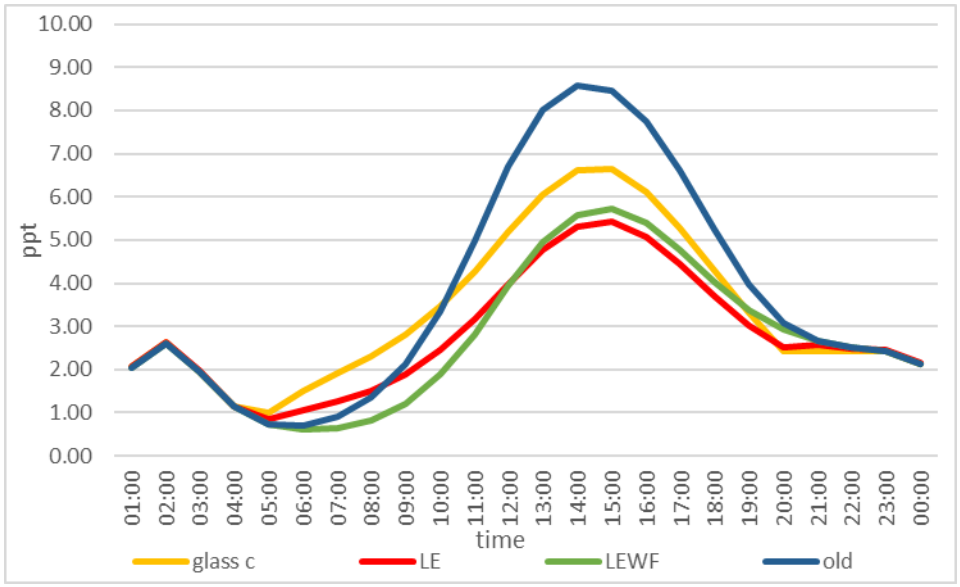

Figure 4.13: Concentrations of HO_2 before (old) and after (Glass C Sacht Self-cleaning, Low Emissivity (LE) and Low Emissivity With Film (LEWF)) the model updates.

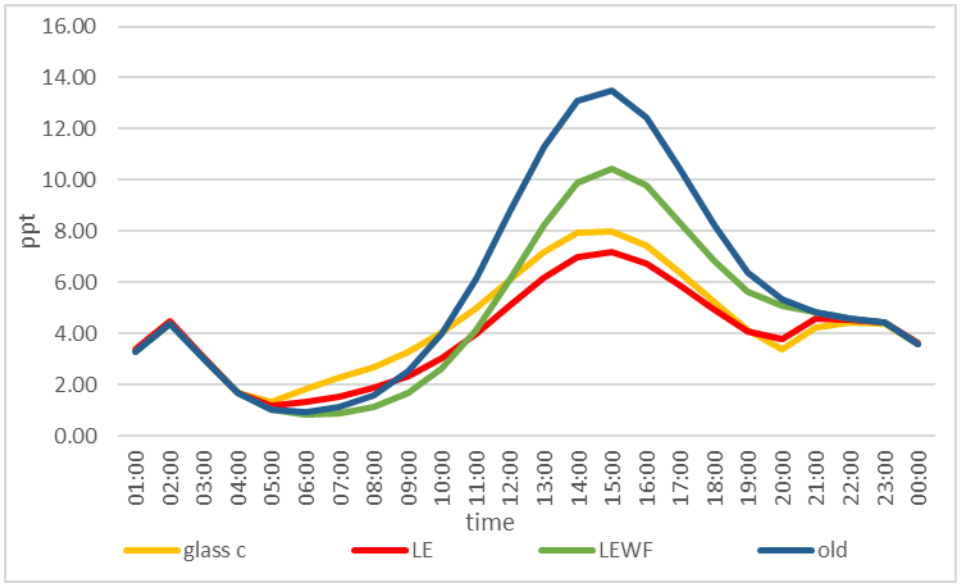

Figure 4.14: Concentrations of RO_2 before (old) and after (Glass C Sacht Self-cleaning, Low Emissivity (LE) and Low Emissivity With Film (LEWF)) the model updates.

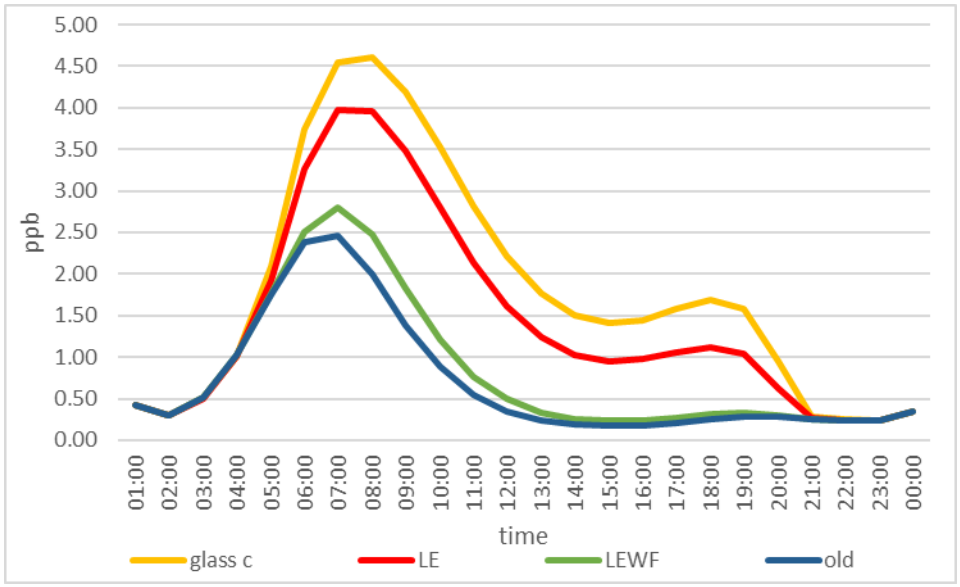

Figure 4.15: Concentrations of NO before (old) and after (Glass C Sacht Self-cleaning, Low Emissivity (LE) and Low Emissivity With Film (LEWF)) the model updates.

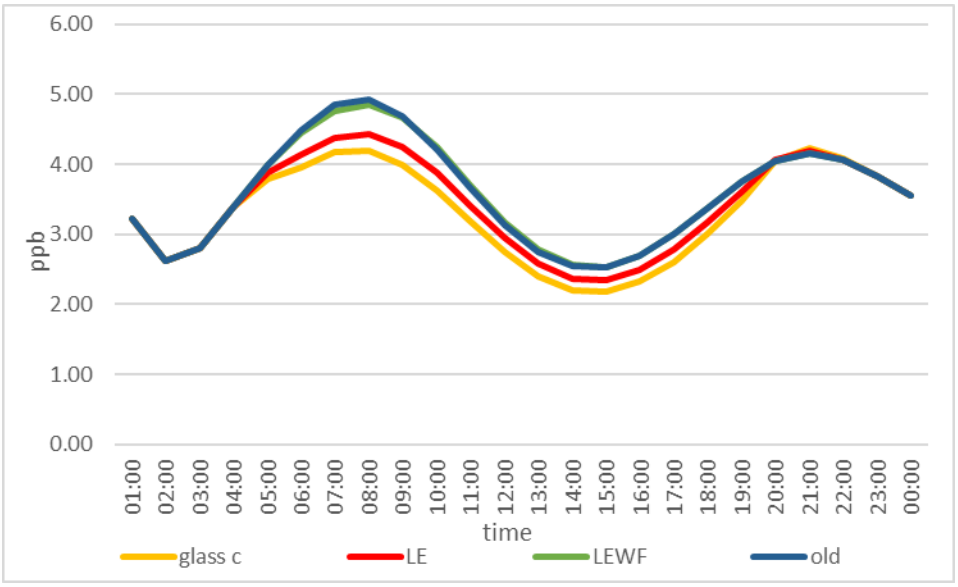

Figure 4.16: Concentrations of NO_2 before (old) and after (Glass C Sacht Self-cleaning, Low Emissivity (LE) and Low Emissivity With Film (LEWF)) the model updates.

Much more light comes through glass C and the LE glass than LEWF, which leads to more photolysis of HONO and NO_2 and hence lower HONO and NO_2 concentrations for LE and Glass C (Figures 4.10 and 4.16). Photolysis of HONO produces OH radicals, so the highest OH concentration is for Glass C, then LE, followed by the old parameterisation and LEWF, which are broadly similar (Figure 4.12). Furthermore, O atoms can be produced by the photolysis of NO_2 (R5) where the O atoms produced can recombine with O_2 to produce O_3 (R4). This process leads to greater concentrations of O_3 for Glass C and LE (Figure 4.9) compared to the old representation. This shows that NO_2 photolysis to produce O_3 indoors, outweighs loss of ozone through its own photolysis. Photolysis of NO_2 also produces NO, the concentration of the latter increasing as the glass lets more light in. The profiles of HCHO for different glasses show a similar distribution to that for O_3 (Figure 4.11), though concentrations are very similar for each glass.

HO_2 and RO_2 are produced by the reaction of OH with VOCs (Figure 1.3). The reactions of NO with HO_2 and RO_2 cause a reduction in their concentrations, which produces the highest peak peroxy radical concentrations for the old parameterisation followed by LEWF and then LE (Figures 4.13 and 4.14). These results show that the previous assumption that 3% of UV and 10% of visible light from outdoors passed through the windows was not accurate for all glass types and can have a profound effect on predicted radical concentrations.

4.3.4. Baseline condition for this thesis

A baseline condition was defined in order to compare the impacts of changes to the model and various sensitivity factors that affected the output in the following chapters. For this baseline scenario, the location was set to York, UK and the date was set to June 21st. Important parameters were set as follows: temperature was 300 K; relative humidity was 45% and AER was 0.76 h^{-1}. The outdoor concentrations of NO, NO_2 and O_3 in the model varied diurnally based on background UK suburban concentrations from Carslaw (2007). The average concentrations were 6.2, 15.0 and 22.9 ppb respectively. Predicted indoor concentrations of NO, NO_2, O_3 and OH from the baseline scenario were 0.7 ppb, 3.6 ppb, 4.0 ppb and 9.9×10^4 molecule/cm^3 respectively.

4.3.5. Model simulations

The new parameterisations were tested in a range of model simulations that incorporated different combinations of the three glass types and the 7 artificial lights. The impacts of two distances from the light sources (adjacent and 1m away) were also tested. All other aspects of the model were as described in Section 4.3.4.

4.4. Results and discussion

4.4.1. Impacts of different indoor artificial lights on indoor air chemistry

Figures 4.17-4.24 show little variation in the predicted concentrations of O_3, HONO, HCHO, OH, HO_2, RO_2, NO and NO_2 for the different indoor artificial lights (1m from the light sources), with the same glass type (Glass C). The average concentrations of key indoor species between 06:00-18:00 h (daylight hours) are calculated and summarised in Table 4.10.

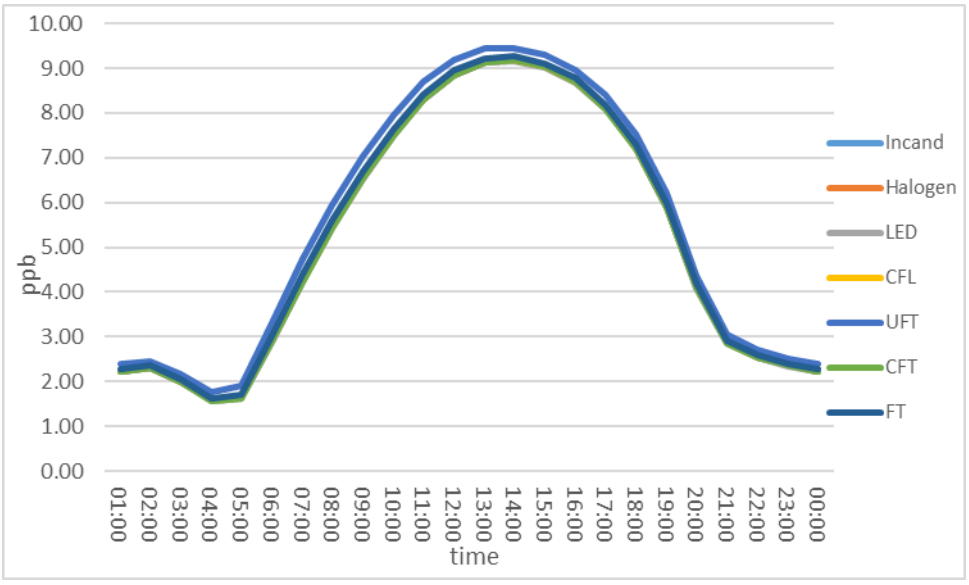

Figure 4.17: Concentrations of O_3 under different artificial lights (Incandescent, Halogen, LED, CFL, UFT, CFT and FT) and with Glass C.

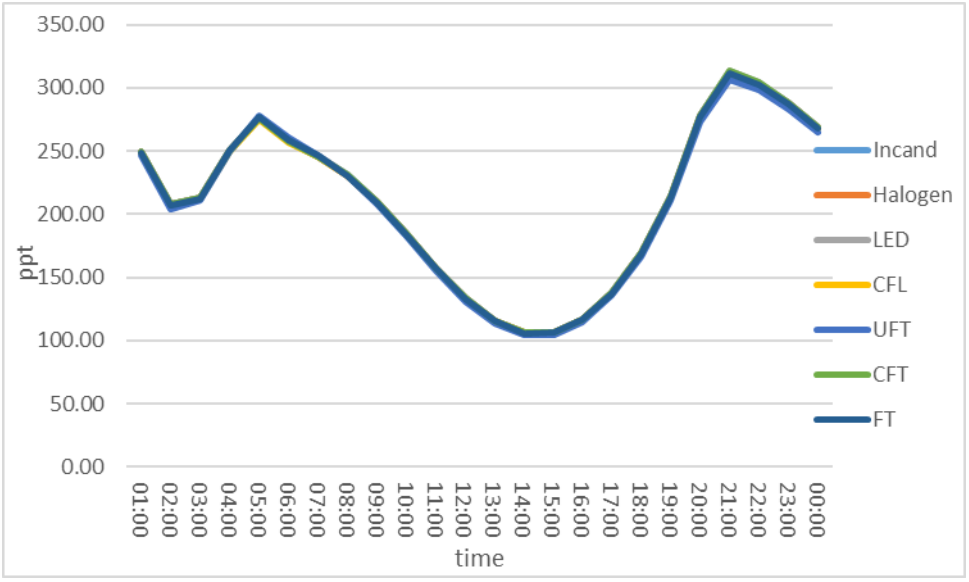

Figure 4.18: Concentrations of HONO under different artificial lights (Incandescent, Halogen, LED, CFL, UFT, CFT and FT) and with Glass C.

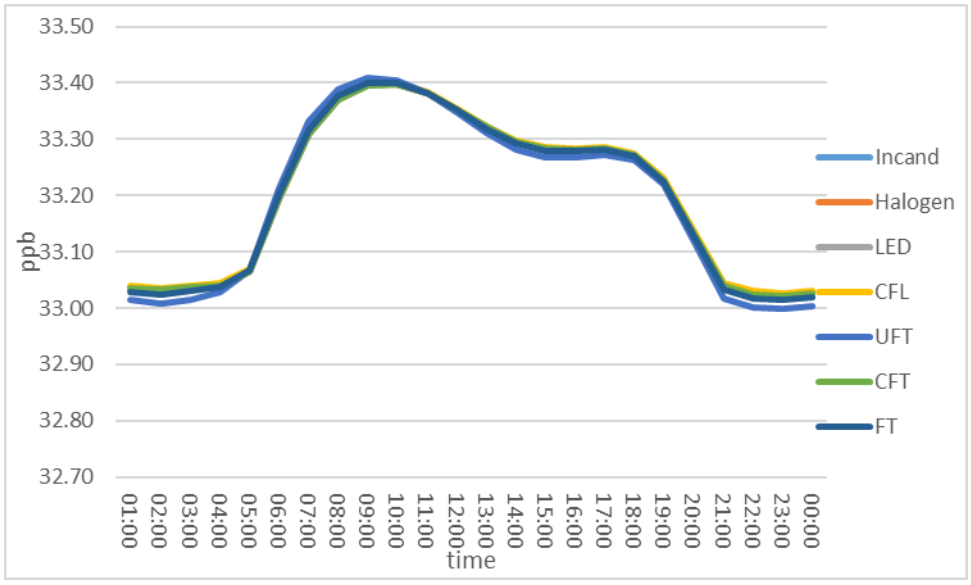

Figure 4.19: Concentrations of HCHO under different artificial lights (Incandescent, Halogen, LED, CFL, UFT, CFT and FT) and with Glass C.

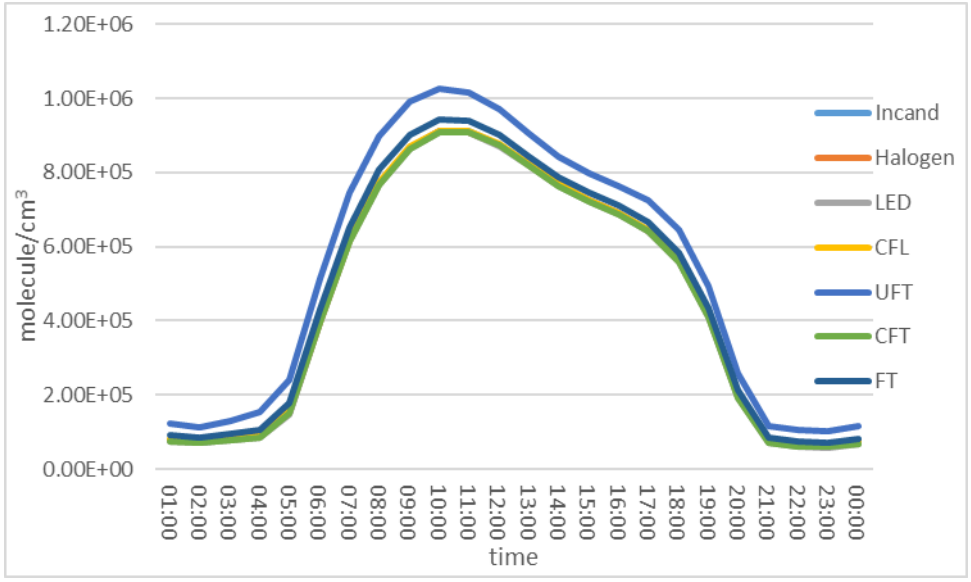

Figure 4.20: Concentrations of OH under different artificial lights (Incandescent, Halogen, LED, CFL, UFT, CFT and FT) and with Glass C.

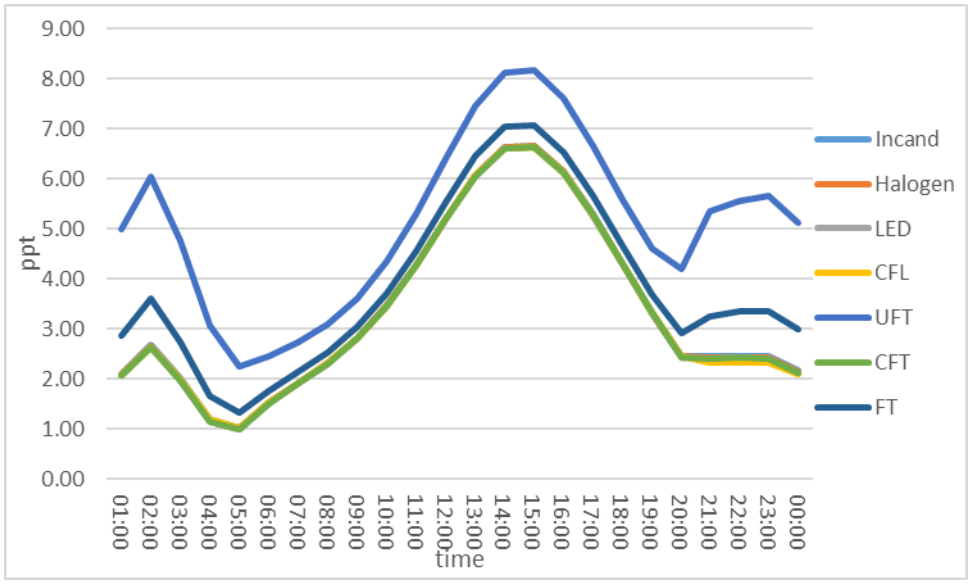

Figure 4.21: Concentrations of HO_2 under different artificial lights (Incandescent, Halogen, LED, CFL, UFT, CFT and FT) and with Glass C.

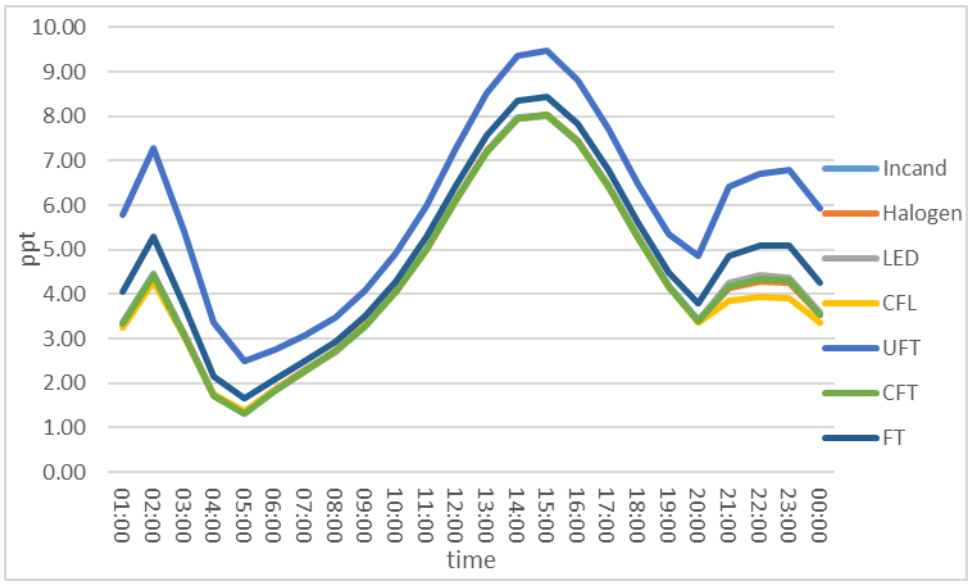

Figure 4.22: Concentrations of RO_2 under different artificial lights (Incandescent, Halogen, LED, CFL, UFT, CFT and FT) and with Glass C.

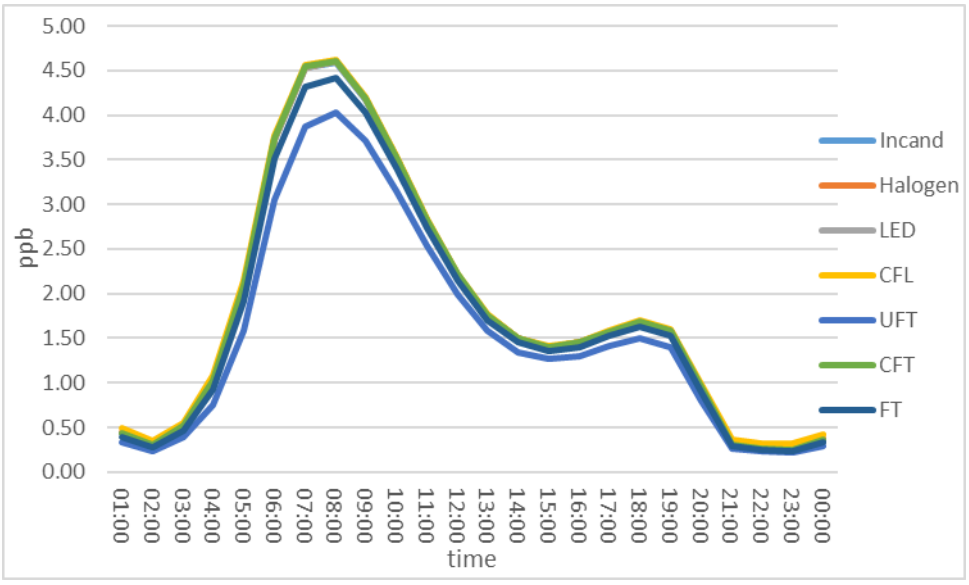

Figure 4.23: Concentrations of NO under different artificial lights (Incandescent, Halogen, LED, CFL, UFT, CFT and FT) and with Glass C.

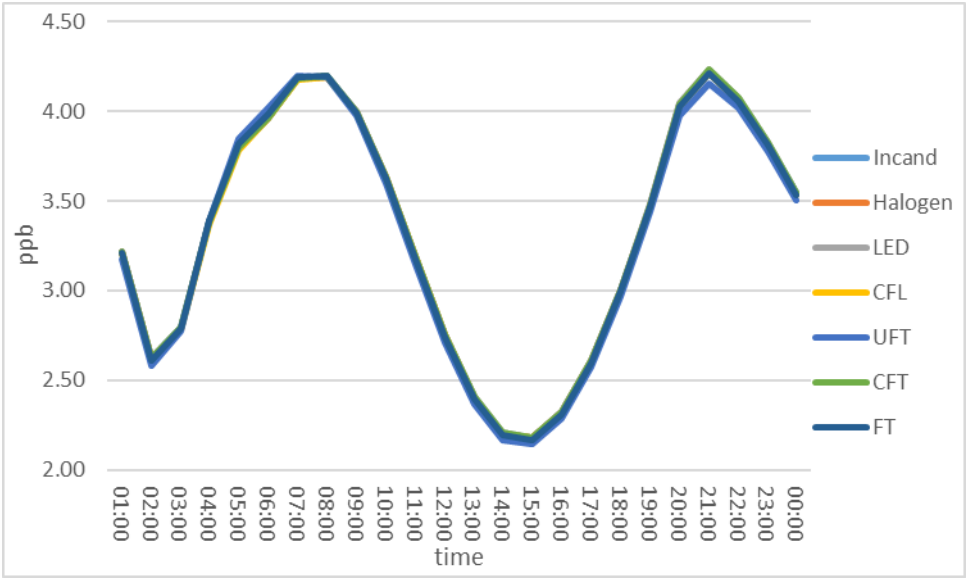

Figure 4.24: Concentrations of NO_2 under different artificial lights (Incandescent, Halogen, LED, CFL, UFT, CFT and FT) and with Glass C.

Table 4.10: Average concentrations of studied chemicals for different indoor artificial lights for the same glass type (Glass C) over the model simulation between 06:00-18:00 h. O_3, HCHO, NO and NO_2 in unit of ppb; HONO, HO_2 and RO_2 in unit of ppt; OH in unit of 10^5 molecule/cm^3.

	O_3	HONO	HCHO	OH	HO_2	RO_2	NO	NO_2
Incandescent	4.02	250.13	33.06	1.03	3.74	8.13	0.67	3.61
Halogen	4.03	250.05	33.06	1.03	3.72	8.09	0.67	3.61
LED	4.01	250.54	33.06	1.00	3.68	8.25	0.66	3.61
CFL	4.06	248.86	33.07	1.09	3.71	7.64	0.71	3.60

UFT	4.20	246.64	33.04	1.48	6.21	9.81	0.51	3.57
CFT	4.02	250.38	33.06	1.01	3.68	8.15	0.67	3.61
FT	4.07	249.32	33.06	1.15	4.43	8.68	0.61	3.60

As for the previous sections, the radical concentrations show the largest variations, although still small in absolute magnitude (see Table 4.10). Higher photolysis rates of HONO result in lower HONO concentrations for UFT (minimum: 104.2 ppt; average: 246.6 ppt) and FT (minimum: 105.7 ppt; average: 249.3 ppt) (Figure 4.18; Table 4.10), and also produce the highest OH concentrations for UFT (peak: 1.0×10^6 molecule/cm^3; average: 1.5×10^5 molecule/cm^3) and FT lighting (peak: 9.4×10^5 molecule/cm^3; average: 1.2×10^6 molecule/cm^3) (Figure 4.20; Table 4.10).

Photolysis of NO_2 produces O_3 as described in the previous section and production of O_3 from NO_2 photolysis is greater than its destruction via photolysis. A higher NO_2 photolysis rate coefficient therefore produces the largest concentrations of O_3 for UFT (peak: 9.5 ppb; average: 4.2 ppb) and FT (peak: 9.3 ppb; average: 4.1 ppb) (Figure 4.17; Table 4.10). The NO produced from both photolysis of HONO and NO_2 can react with HO_2 to produce OH and also suppresses RO_2 concentrations. These reactions lead to slightly lower peak NO concentrations for UFT (peak: 4.0 ppb; average: 0.5 ppb) and FT (peak: 4.4 ppb; average: 0.6 ppb) (Figure 4.23, Table 4.10) than the other lights. The OH radical can cycle to HO_2 (e.g. by the reaction with CO, O_3, H_2O_2) and also to RO_2 (through reaction with VOCs) which leads to similar profiles of HO_2 and RO_2 (Figure 4.21 and 4.22).

4.4.2. Impacts of glass type on indoor air chemistry

Figures 4.25-4.32 show the concentrations of O_3, HONO, HCHO, OH, HO_2, RO_2, NO and NO_2 for three different indoor lights (UFT, CFT and FT) and for three different glasses (Glass C, LE and LEWF), with the average values (between 06:00-18:00 h) for each of the species in each model run summarised in Table 4.11. These three indoor lights were selected as they provided a range of values for the indoor species concentrations (Table 4.10). However, as shown in these figures, the biggest difference is among different glasses. Glass C has the lowest wavelength cut-off so transmits most outdoor light, followed by LE and then LEWF. For O_3, the impact of different glasses is very clear (Figure 4.25). Similarly, for OH, the glass type has the largest impact on predicted concentrations when compared to indoor lighting. Its lowest peak value is under CFT (9.1×10^5 molecule/cm^3) for Glass C compared

to UFT (1.0×10^6 molecule/cm^3) and FT (9.4×10^5 molecule/cm^3). However, the lowest peak under Glass C is much greater than the highest peak under UFT, CFT and FT for the LE glass (UFT: 6.1×10^5 molecule/cm^3, CFT: 5.1×10^5 molecule/cm^3, FT: 5.4×10^5 molecule/cm^3), and the peaks of OH under LEWF are even lower (UFT: 2.4×10^5 molecule/cm^3, CFT: 1.7×10^5 molecule/cm^3, FT: 1.9×10^5 molecule/cm^3) (Figure 4.28). As shown in Table 4.11, the average concentrations of the indoor species also reflect these findings. The impacts of different window materials are therefore, much more important than the impacts of indoor artificial lights on indoor air quality.

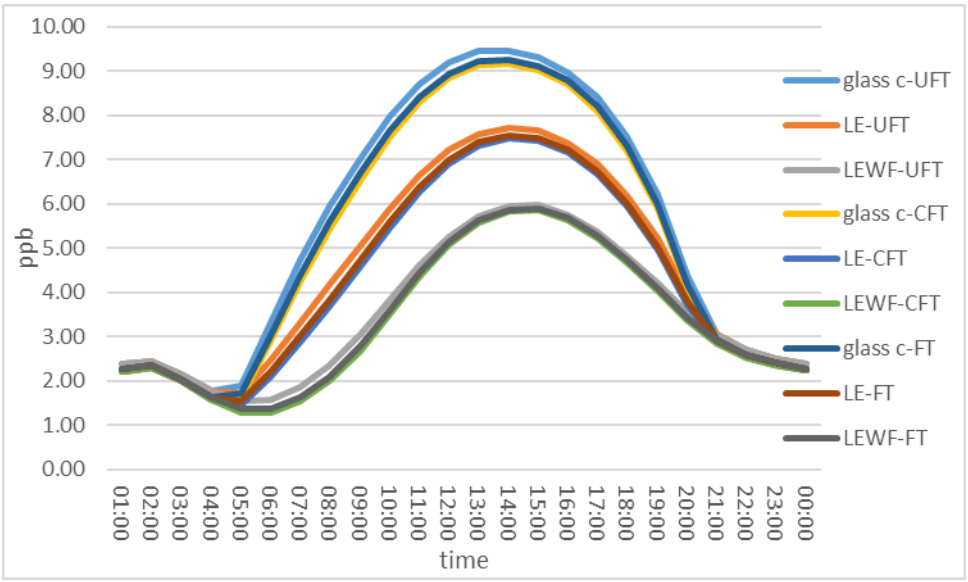

Figure 4.25: Concentrations of O_3 for UFT, CFT and FT and for Glass C, LE and LEWF.

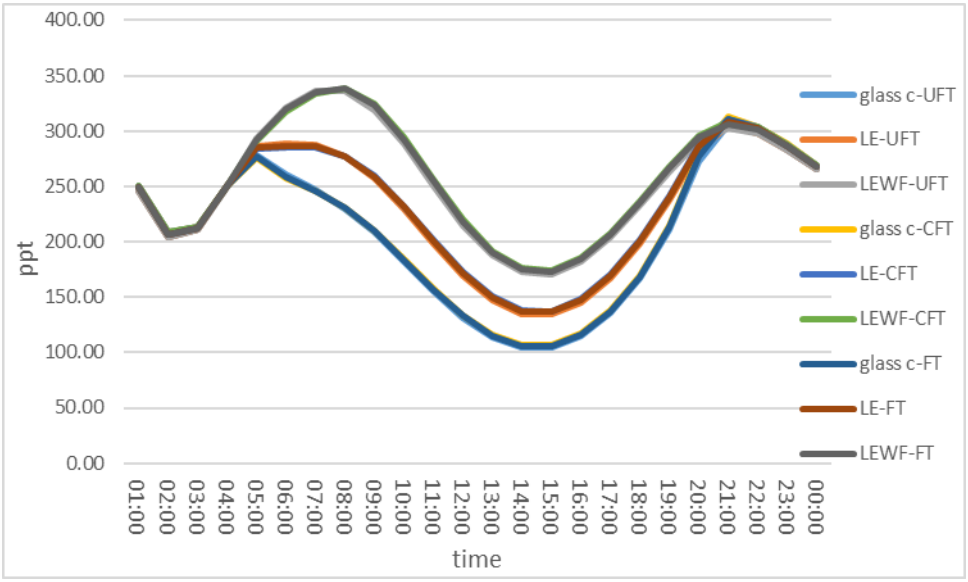

Figure 4.26: Concentrations of HONO for UFT, CFT and FT of Glass C, LE and LEWF.

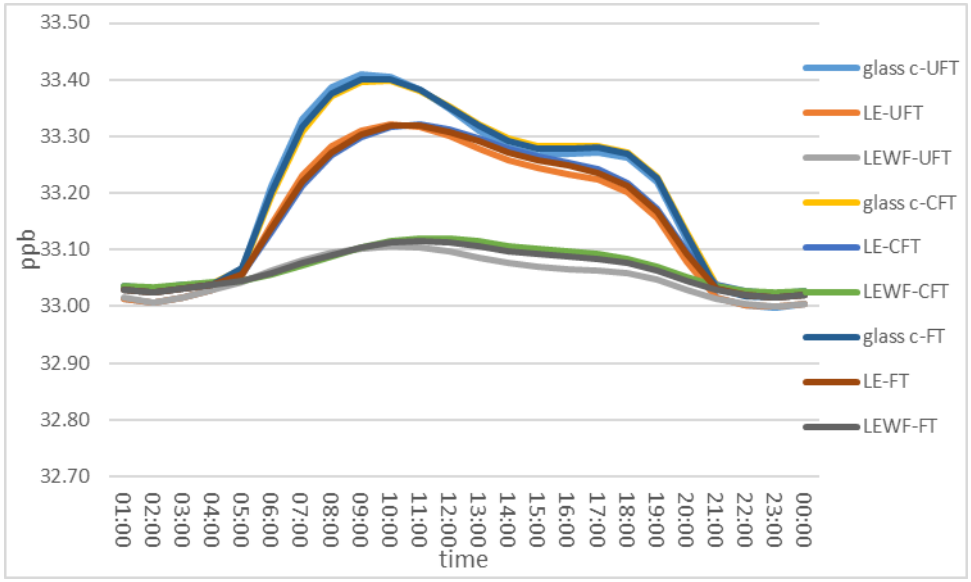

Figure 4.27: Concentrations of HCHO for UFT, CFT and FT of Glass C, LE and LEWF.

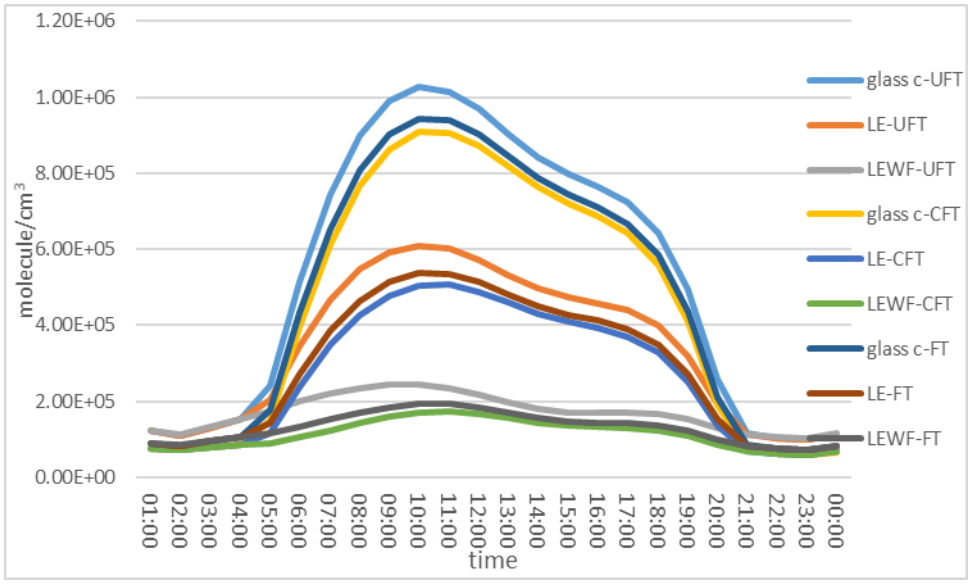

Figure 4.28: Concentrations of OH for UFT, CFT and FT of Glass C, LE and LEWF.

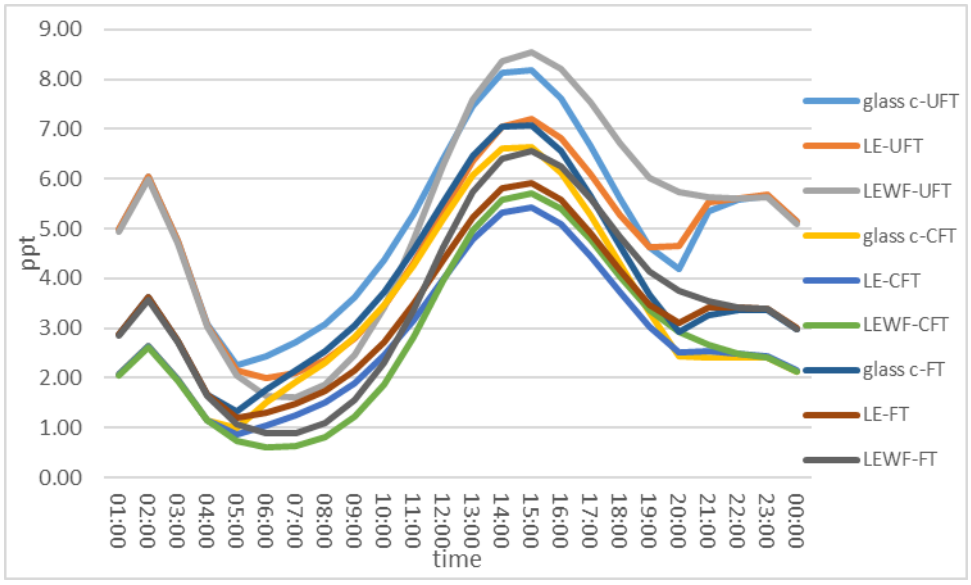

Figure 4.29: Concentrations of HO_2 for UFT of Glass C, LE and LEWF.

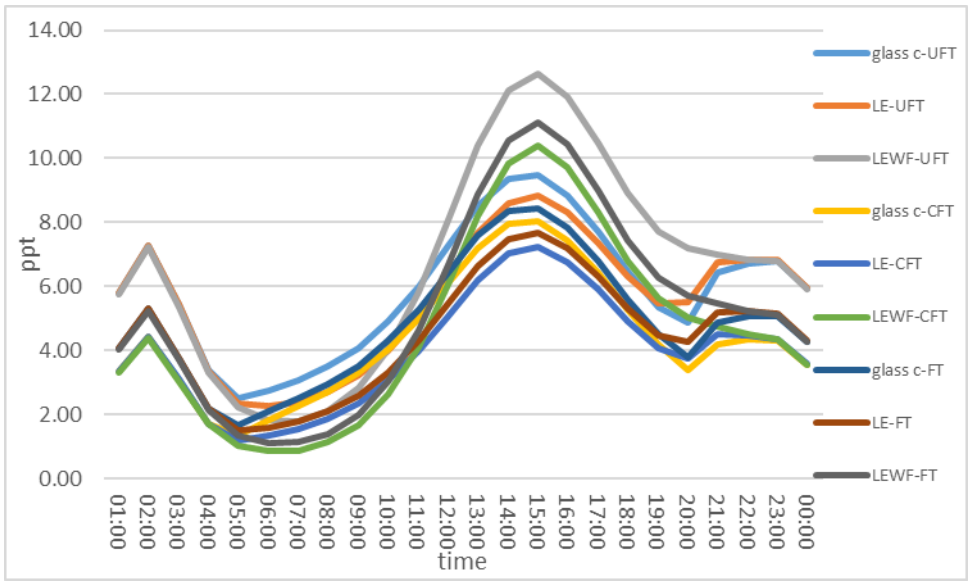

Figure 4.30: Concentrations of RO_2 for UFT of Glass C, LE and LEWF.

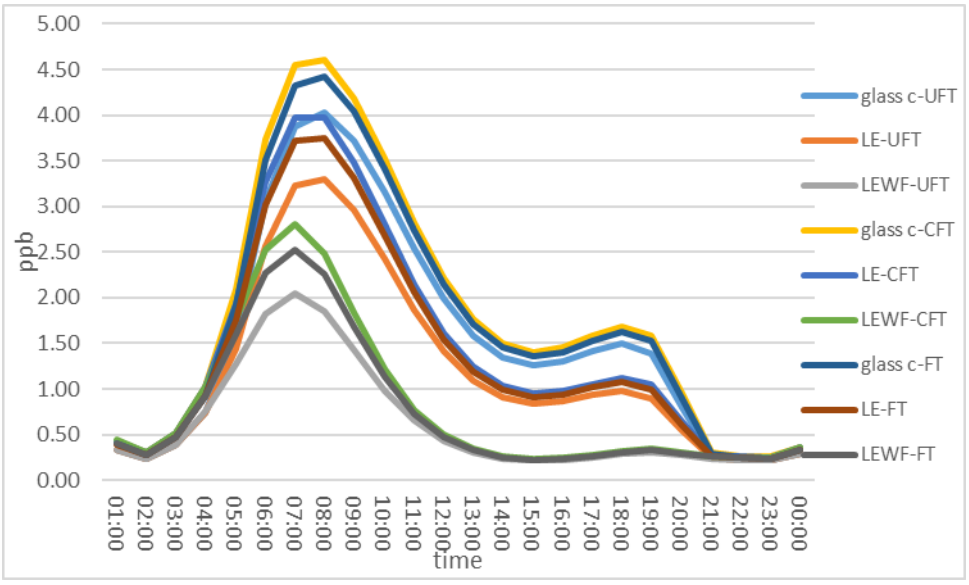

Figure 4.31: Concentrations of NO for UFT, CFT and FT of Glass C, LE and LEWF.

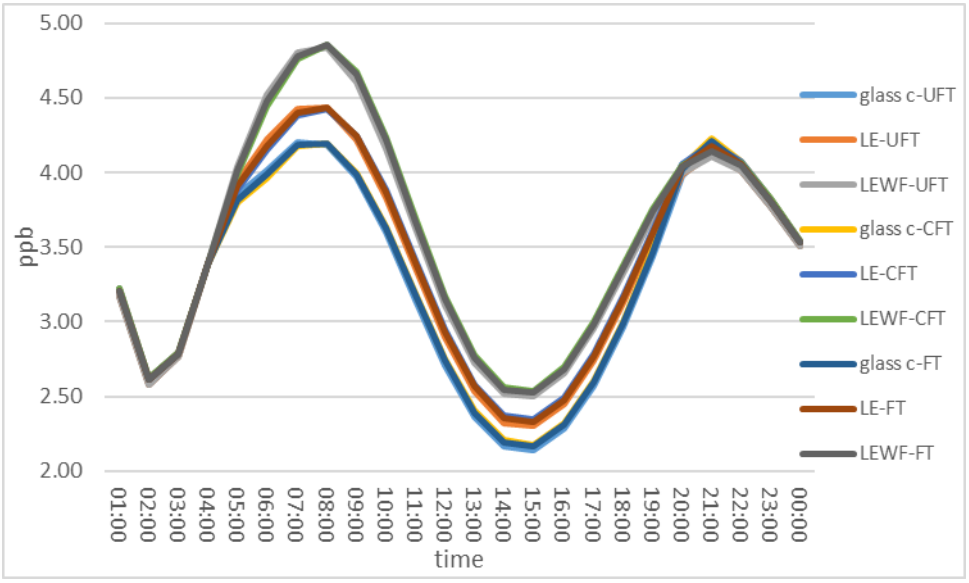

Figure 4.32: Concentrations of NO_2 for UFT, CFT and FT of Glass C, LE and LEWF.

The HO_2 and RO_2 concentrations respond quite differently to the OH concentrations (Figures 4.29 and 4.30). For RO_2, its peak concentrations (12.6, 10.4 and 11.1 ppt for UFT, CFT and FT respectively) are highest for LEWF (Figure 4.30), corresponding to the lowest peak concentrations of NO (2.1, 2.8 and 2.5 ppb for UFT, CFT and FT respectively) (Figure 4.31): higher NO concentrations suppress those of RO_2. Meanwhile, the average concentrations of RO_2 are highest for LEWF under the same artificial lights (Table 4.11). For HO_2, peak concentrations are highest under UFT for LEWF glass (8.5 ppt), followed by Glass C (8.2

ppt) and LE (7.2 ppt), whilst its peak concentrations under CFT and FT are highest for Glass C (6.6 and 7.1 ppt respectively), followed by LEWF (5.7 and 6.6 ppt respectively) and LE (5.4 and 5.9 ppt respectively). Average HO_2 concentrations show the highest values for Glass C, followed by LEWF and LE (Table 4.11). Although OH reactions can form these two peroxy radical species through various routes as mentioned above, the NO concentrations are also important. The NO concentrations (peak values) are very low under LEWF, approximately 2 and 1.6 times lower than the concentration under Glass C and LE respectively, so less NO is available to react with HO_2 and RO_2. So increased photolysis rates will increase OH and hence its ability to form HO_2 and RO_2, but more NO is also produced under the same conditions, which can then react with these latter two species. There are subtle differences in the balance between these processes which determine the predicted radical concentrations and explain why the profiles look less well ordered than for other species.

Table 4.11: Average concentrations of OH, HO_2, RO_2, O_3, HONO, HCHO, NO and NO_2 for UFT, CFT and FT of Glass C, LE and LEWF over the model simulation between 06:00-18:00 h. O_3, HCHO, NO and NO_2 in unit of ppb; HONO, HO_2 and RO_2 in unit of ppt; OH in unit of 10^5 molecule/cm^3.

	Glass C			LE			LEWF		
	UFT	CFT	FT	UFT	CFT	FT	UFT	CFT	FT
O_3	8.1	7.7	7.8	6.3	6.0	6.1	4.5	4.3	4.4
HONO	157.8	159.6	159.1	195.4	197.8	197.2	241.3	245.0	243.9
HCHO	33.3	33.3	33.3	33.3	33.3	33.3	33.1	33.1	33.1
OH	8.6	7.6	7.9	5.2	4.3	4.6	2.0	1.5	1.6
HO_2	5.8	4.6	4.9	4.9	3.6	4.0	5.6	3.5	4.1
RO_2	6.6	5.5	5.8	5.9	4.7	5.0	7.6	5.8	6.4
NO	2.3	2.6	2.5	1.7	2.0	1.9	0.7	0.9	0.9
NO_2	3.0	3.1	3.0	3.2	3.3	3.2	3.5	3.5	3.5

4.4.3 Impacts of indoor artificial lights at 1m versus adjacent.

Figures 4.33-4.40 show concentrations of O_3, HONO, HCHO, OH, HO_2, RO_2, NO and NO_2 under UFT, Incandescent and FT lighting, both 1m away from the light sources and also adjacent to the light sources.

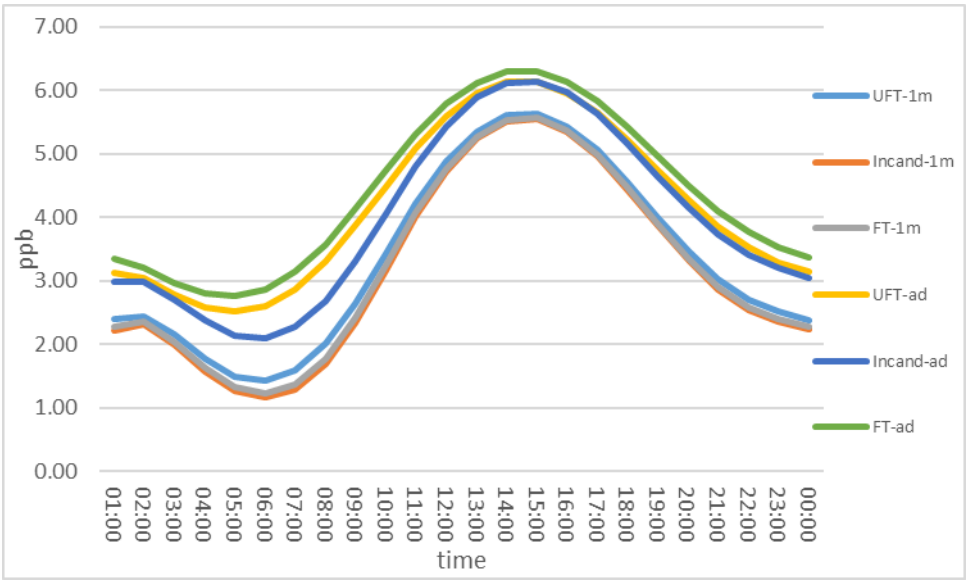

Figure 4.33: Differences in O_3 concentrations for UFT, Incandescent and FT lighting between 1m away from the light sources and adjacent to the light sources.

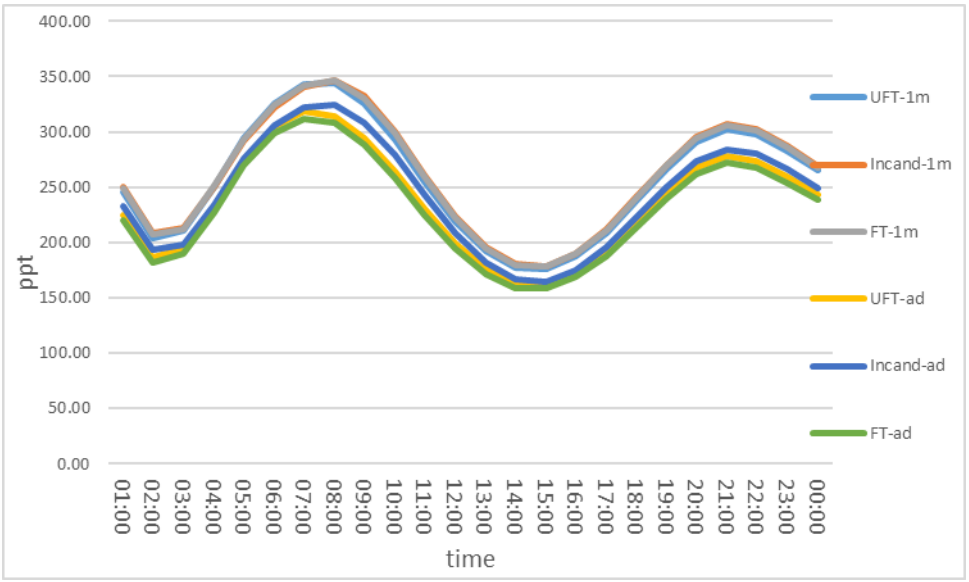

Figure 4.34: Differences in HONO concentrations for UFT, Incandescent and FT lighting between 1m away from the light sources and adjacent to the light sources.

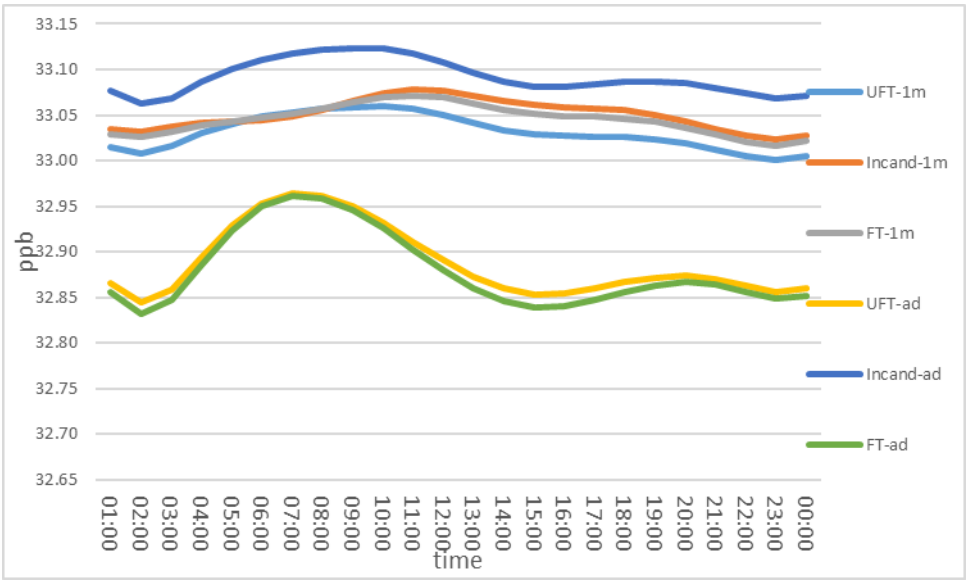

Figure 4.35: Differences in HCHO concentrations for UFT, Incandescent and FT lighting between 1m away from the light sources and adjacent to the light sources.

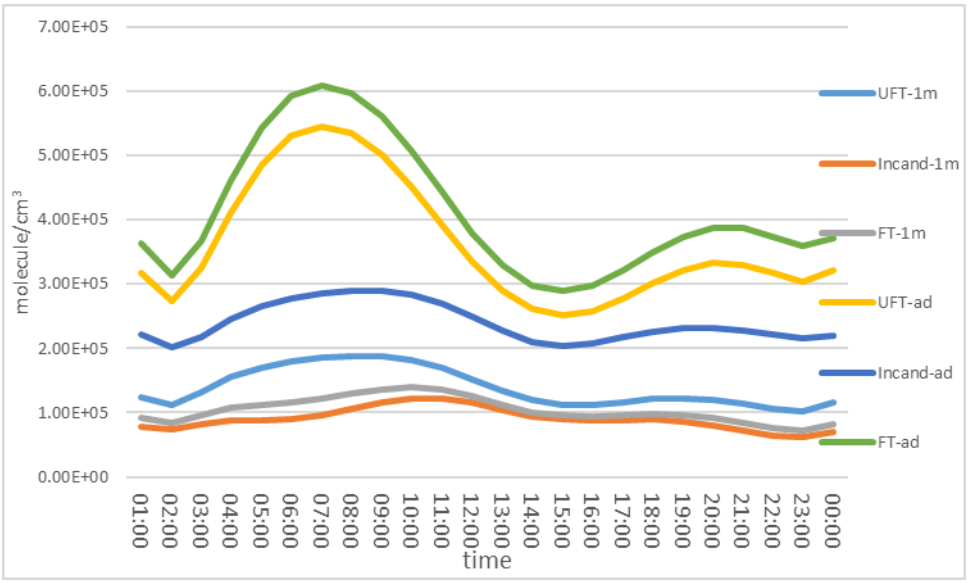

Figure 4.36: Differences in OH concentrations for UFT, Incandescent and FT lighting between 1m away from the light sources and adjacent to the light sources.

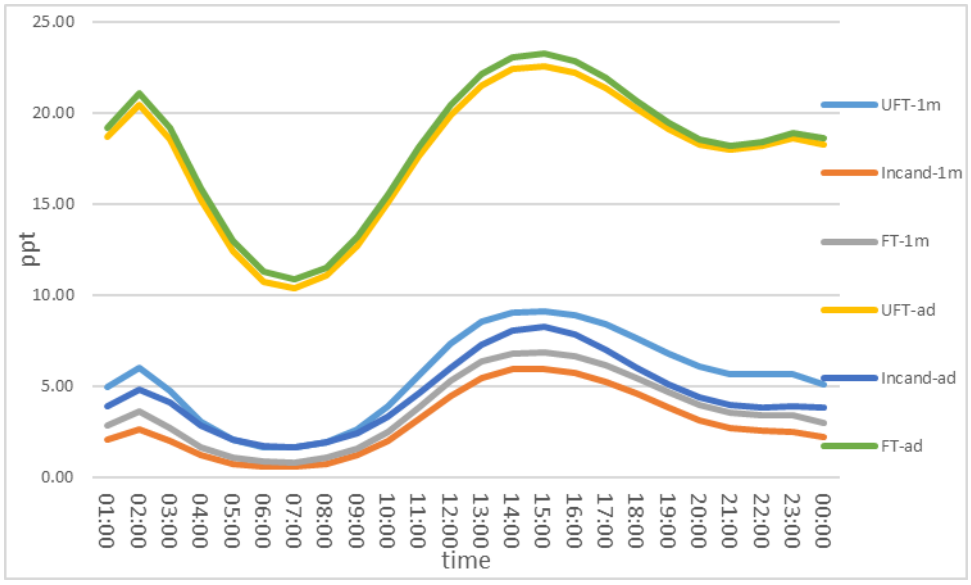

Figure 4.37: Differences in HO_2 concentrations for UFT, Incandescent and FT lighting between 1m away from the light sources and adjacent to the light sources.

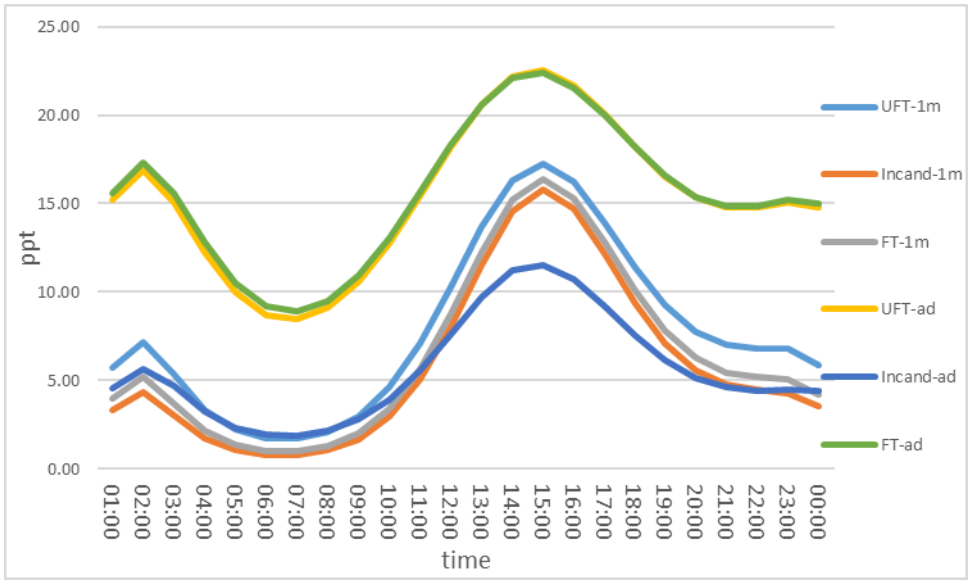

Figure 4.38: Differences in RO_2 concentrations for UFT, Incandescent and FT lighting between 1m away from the light sources and adjacent to the light sources.

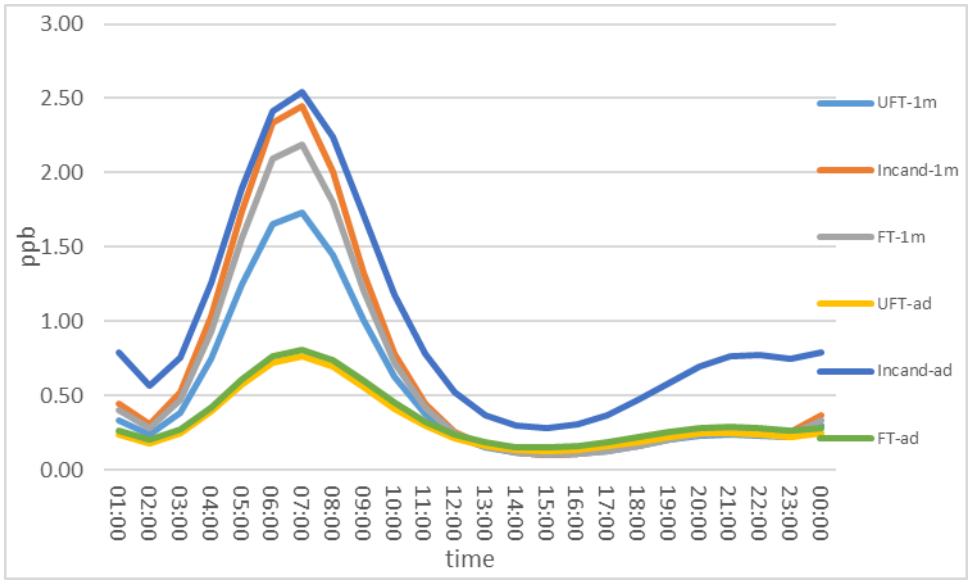

Figure 4.39: Differences in NO concentrations for UFT, Incandescent and FT lighting between 1m away from the light sources and adjacent to the light sources.

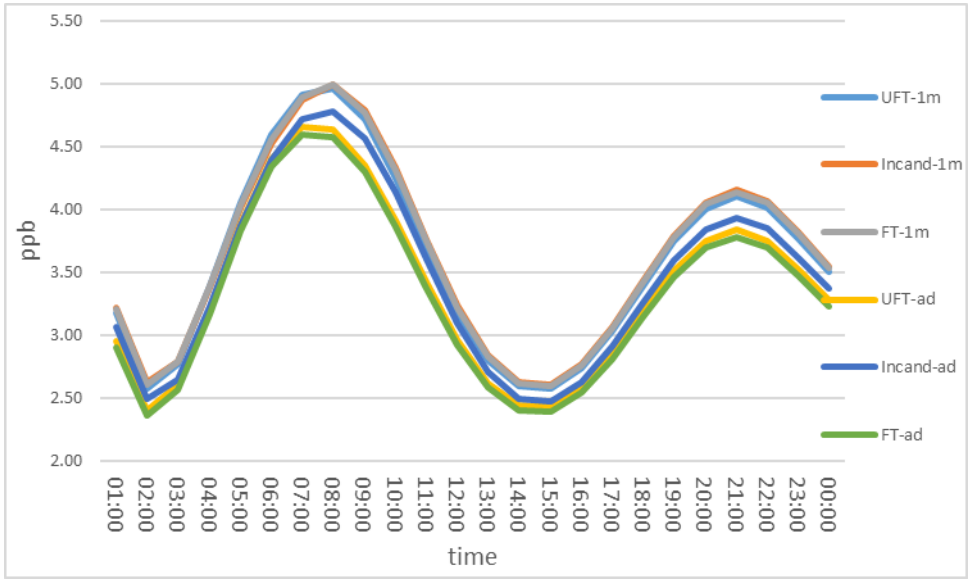

Figure 4.40: Differences in NO_2 concentrations for UFT, Incandescent and FT lighting between 1m away from the light sources and adjacent to the light sources.

Table 4.12 shows the average concentrations of studied chemicals at 1m and adjacent to UFT, Incandescent and FT lighting over the period between 06:00-18:00 h. Greater photolysis rate coefficients closer to the light sources lead to more photolysis of HONO (Figure 4.34) and NO_2 (Figure 4.40), which leads to lower average concentrations of these species adjacent to the light sources compared to 1m away (Table 4.12). Photolysis of NO_2 produces O_3 as described in the previous section and production of O_3 from NO_2 photolysis is greater than its

destruction via photolysis, leading to greater O_3 concentrations adjacent to the light sources compared to 1 m away (Figure 4.33; Table 4.12). The differences are small, however, showing that there are other more important processes controlling NO_2 chemistry than lighting (this issue will be investigated in Chapter 6). As shown in Figure 4.35, concentrations of HCHO adjacent to lights are greater than when the light is 1m away for incandescent, UFT and FT, although the differences are minimal (less than 0.1 ppb). This is because the chemistry that follows on from the increased concentration of OH radicals can produce RO_2, which goes on to form HCHO at a faster rate than it is photolysed.

Table 4.12: Average concentrations of OH, HO_2, RO_2, O_3, HONO, HCHO, NO and NO_2 at 1 m and adjacent to UFT, Incandescent and FT lightings over the model simulation between 06:00-18:00 h. % difference = (adjacent – 1m) / adjacent × 100. O_3, HCHO, NO and NO_2 in unit of ppb; HONO, HO_2 and RO_2 in unit of ppt; OH in unit of 10^5 molecule/cm^3.

	1m			adjacent			difference		
	UFT	Incand.	FT	UFT	Incand.	FT	UFT	Incand.	FT
O_3	4.2	4.0	4.1	5.0	4.8	5.2	16.3	16.0	22.1
HONO	246.6	250.1	249.3	225.3	232.6	220.4	-9.5	-7.5	-13.1
HCHO	33.0	33.1	33.1	32.9	33.1	32.9	-0.4	0.1	-0.5
OH	1.5	1.0	1.2	3.7	2.5	4.1	59.5	58.4	72.2
HO_2	6.2	3.7	4.4	18.1	5.3	18.6	65.6	30.1	76.2
RO_2	9.8	8.1	8.7	16.6	7.0	16.8	41.0	-16.4	48.2
NO	0.5	0.7	0.6	0.3	0.9	0.4	-60.2	27.4	-74.3
NO_2	3.6	3.6	3.6	3.3	3.4	3.3	-6.9	-4.7	-9.4

More photolysis of O_3, HONO, HCHO and NO_2 takes place as the distance to the light sources decreases, which leads to the production of more OH (Figure 4.36), HO_2 (Figure 4.37) and NO (Figure 4.39). The OH radicals produced in this way can cycle to HO_2 (e.g. by the reaction with CO, O_3, H_2O_2) and also to RO_2 (through reaction with VOCs). The NO produced from both photolysis of HONO and NO_2 can react with HO_2 to produce OH and also suppresses RO_2 concentrations. These reactions lead to slightly lower average NO concentrations when adjacent to light sources except for incandescent lights (Figure 4.39). According to Table 4.4, the photolysis rate coefficient of NO_2 adjacent to incandescent (5.4×10^{-4} s^{-1}) is greater than adjacent to UFT (3.8×10^{-4} s^{-1}) and FT (5.0×10^{-4} s^{-1}) (a similar distribution was found in Kowal et al. (2017), also reported in the same table). This produces more NO from NO_2 photolysis when adjacent to incandescent lights compared to adjacent to UFT and FT (Table 4.12). The highest average concentration of NO adjacent to incandescent

lights can react with RO_2 and HO_2 causing the reduction of their concentrations, which leads to the lowest average concentrations of RO_2 and HO_2 adjacent to incandescent lights (Table 4.12). For 1m away from the three studied artificial lights, the photolysis rate coefficient of NO_2 is lowest 1m away from incandescent (1.1×10^{-5} s^{-1}) compared to UFT (5.7×10^{-5} s^{-1}) and FT (2.0×10^{-5} s^{-1}) (Table 4.6), owing to greater attenuation of the light transmission from incandescent lights at 1m compared to the other two lights (Table 4.5). Low photolysis rate coefficients of O_3, HONO and HCHO 1m away from incandescent lights (Table 4.6) also lead to less production of HO_2 and RO_2 compared to 1m away from UFT and FT (Table 4.12). Therefore, less NO reacts with RO_2 and HO_2, so the average concentration of NO is higher 1m away from incandescent lights compared to UFT and FT (Table 4.12). So increased photolysis rates will lead to the production of more RO_2 and HO_2, but also lead to more NO formation which reacts with them. Therefore, the balance between these reactions for the different light sources will therefore determine the concentrations of predicted radicals.

As shown in Table 4.12, the average concentrations of O_3, OH and HO_2 increase by ~18%, ~63%, and ~57% respectively while HONO and NO_2 concentrations decrease ~10% and ~7% respectively as the distance to the light sources is reduced. Little change takes place for HCHO at the two different distances to the light sources, showing that photolysis is not a controlling factor on HCHO concentrations. As the distance to the light sources decreases, the average concentration of RO_2 and NO increase (~45%) and decrease (67%) respectively (except incandescent as explained above).

4.4.4. Spectral radiometer measurement

Photolysis values were measured indoors using a spectral radiometer. According to NCAS (2018), a direct measurement of solar actinic UV flux and determination of photolysis frequencies are provided by the spectral radiometer. The instrument consists of a 2-pi sr quartz diffuser coupled to an Ocean Optics spectrometer via a 10 m fibre optic cable. The spectrometer operates between 200 – 1000 nm and is calibrated over the wavelength region from 250 – 750 nm (< 1nm resolution). It utilises a Hamamatsu, back-thinned FFT-CCD detector with >90% quantum efficiency at 700 nm. It has an integration time between 8 ms to 15 minutes and fully automated data collection using Spectrasuite software (NCAS, 2018).

The measurements were made in a first floor office in the Environment building at the University of York for 10 days in January 2018 (Jan 20th – Jan 29th). The radiometer was placed on an office windowsill. For 9 of these days, the lights in the office were off, but lights were on for part of one day (Jan 27th). The results focus on 25th, which was the sunniest day.

Figures 4.41-4.45 show the profiles of J4 (NO_2), J5 (NO_3 to NO and O_2), J6 (NO_3 to NO_2 and $O^3(P)$), J7 (HONO) and J12 (HCHO to H_2 and CO) measured by the spectral radiometer and predicted by the model between 08:00-10:30 h when the sun was shining directly into the office. Although J1 ($O^1(D)$), J11 (HCHO to H and HCO) and J13 (CH_3CHO) were also measured, their very low values at this time of year meant that their values did not exceed the instrumental detection limit and so they have been excluded from this analysis. For the other measured photolysis rates, the measured data was then compared with model predicted results of the three studied glass types. Differences between the measured values and model predicted values were calculated by summing (measured data – model predicted values)^2 for each second for which measured data were available. The results show that the measured j values are most similar to the simulated LE glass results.

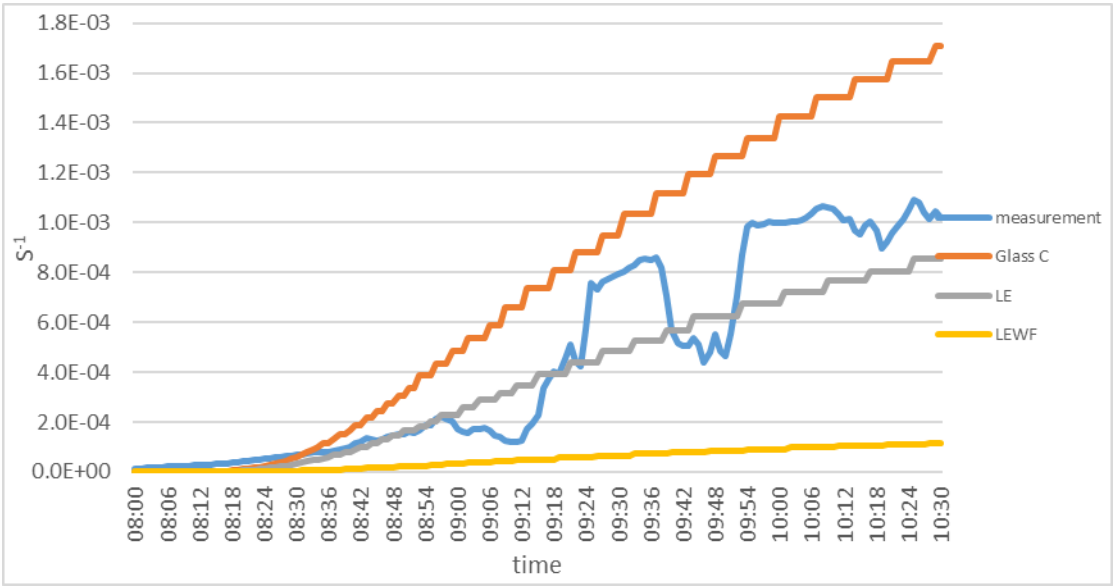

Figure 4.41: Profile of J4 (NO_2) measured by the spectral radiometer and from model results assuming Glass C, LE and LEWF. The location and time of year were set as the University of York and January 25th.

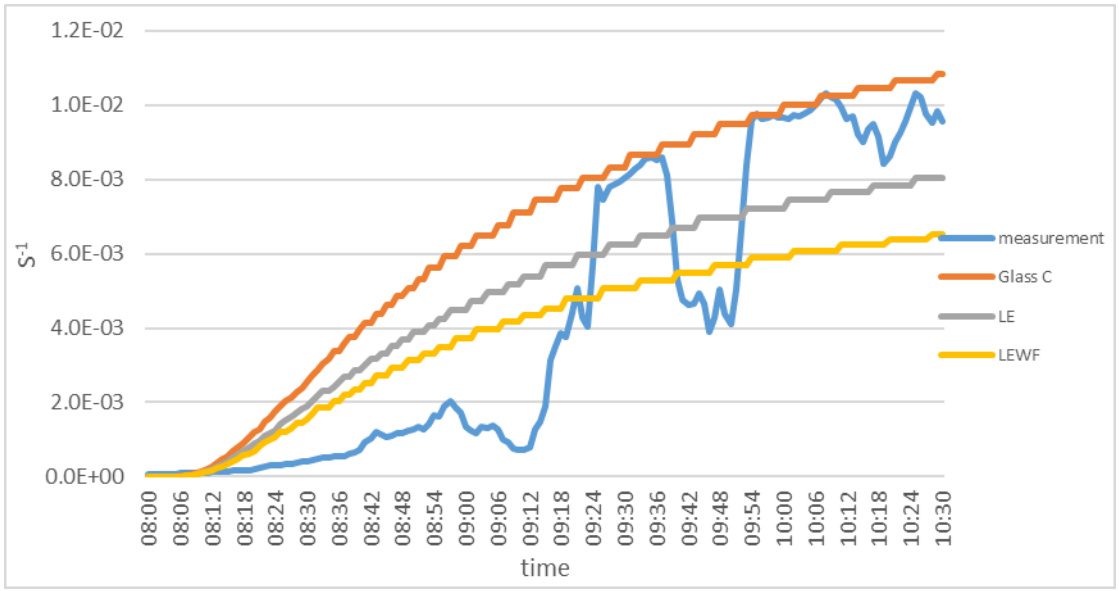

Figure 4.42: Profile of J5 (NO_3 to NO and O_2) measured by the spectral radiometer and from model results assuming Glass C, LE and LEWF. The location and time of year were set as the University of York and January 25th.

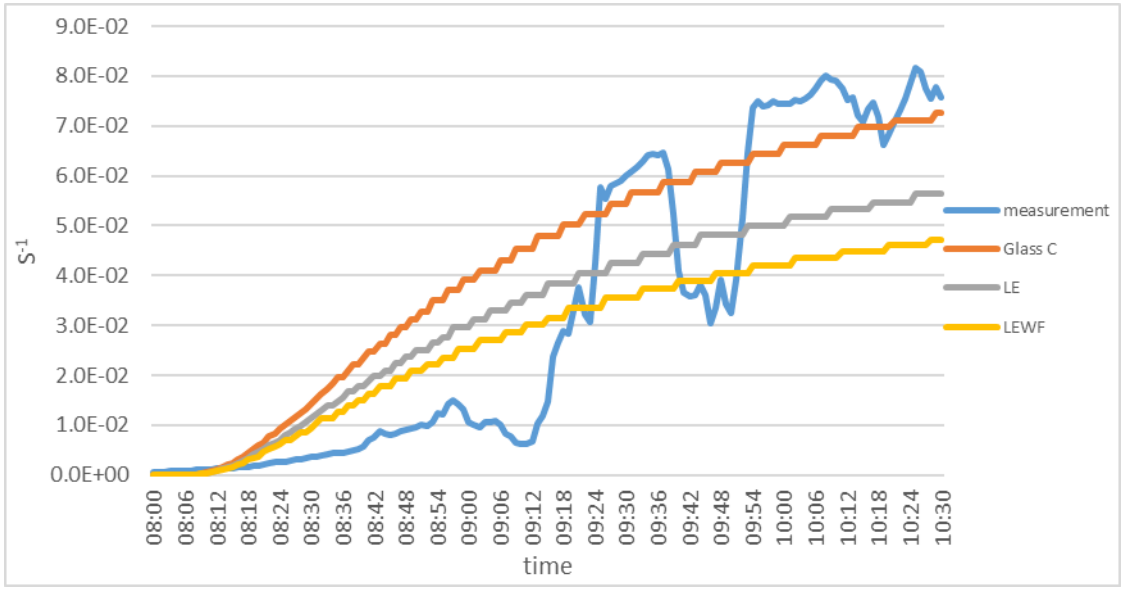

Figure 4.43: Profile of J6 (NO_3 to NO_2 and $O^3(P)$) measured by the spectral radiometer and from model results assuming Glass C, LE and LEWF. The location and time of year were set as the University of York and January 25th.

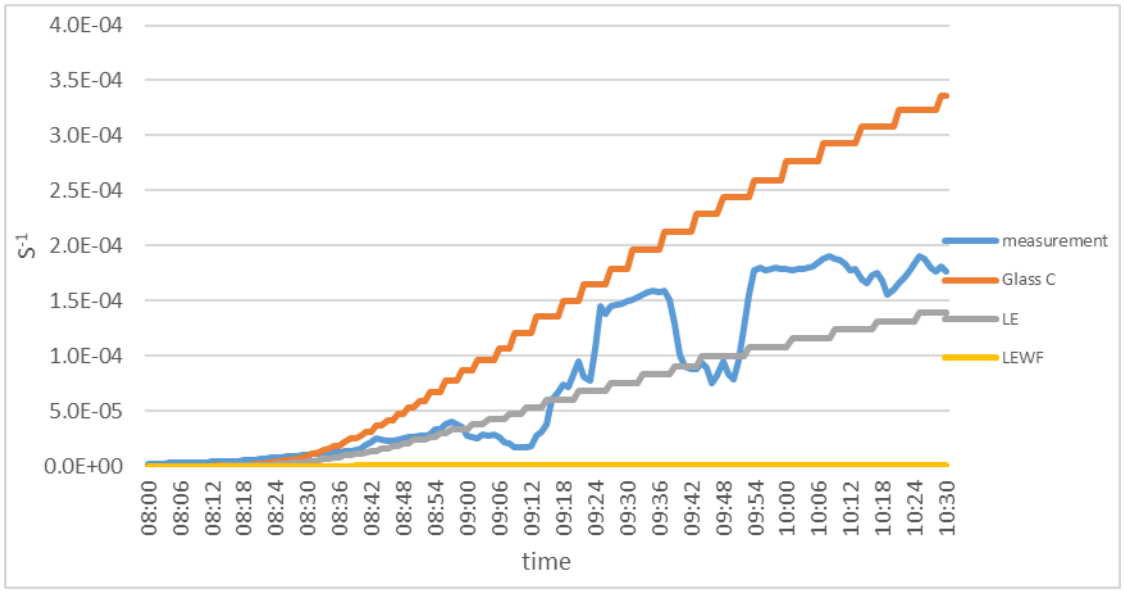

Figure 4.44: Profile of J7 (HONO) measured by the spectral radiometer and from model results assuming Glass C, LE and LEWF. The location and time of year were set as the University of York and January 25th.

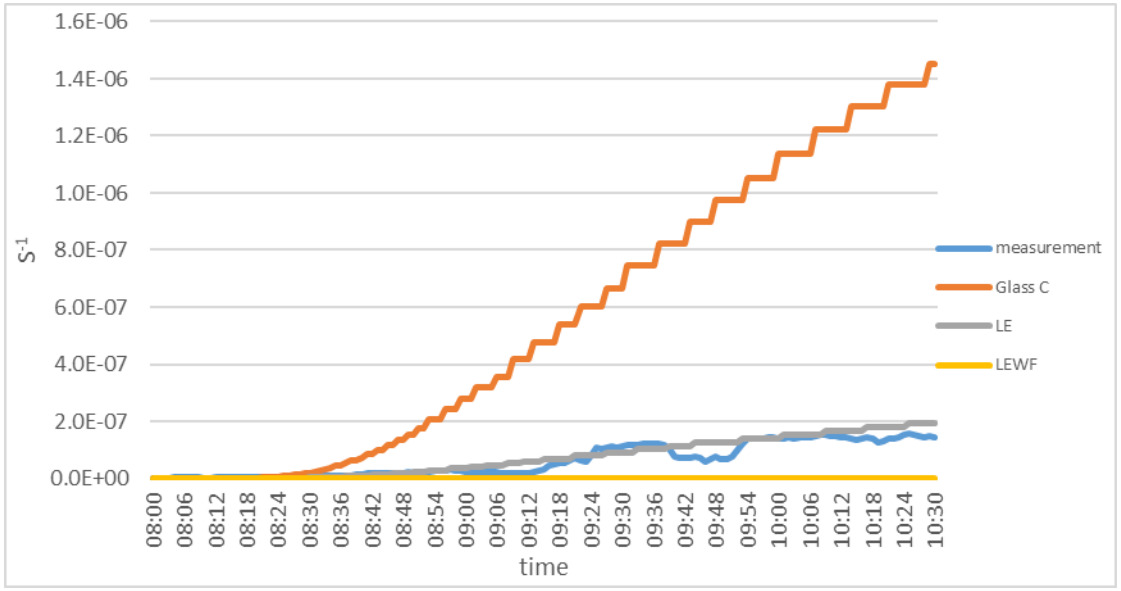

Figure 4.45: Profile of J12 (HCHO to H_2 and CO) measured by the spectral radiometer and from model results assuming Glass C, LE and LEWF. The location and time of year were set as the University of York and January 25th.

This small comparison between measured and modelled results shows that the new model formulation appears to give reasonable results. More measurements were planned at a time of year with more sunlight, but were unfortunately not possible owing to COVID-19 restrictions in the UK.

4.5. Conclusion

This chapter has summarised the methods for calculating improved indoor photolysis rates from a range of artificial indoor lighting and transmitted outdoor light based on recent measured data (Kowal et al., 2017; Blocquet et al., 2018). The results in this chapter show that:

- Different indoor artificial lights can have different impacts on indoor air chemistry. UFT and FT lights have the largest photolysis rates and hence the largest impacts, particularly on predicted radical concentrations.
- The transmission factors for sunlight through windows strongly depend on the wavelength cut-off of the glass.
- Attenuated light from outdoors tends to have a larger impact on indoor air chemistry than indoor lighting for the conditions studied.
- The distance from artificial indoor lights also affects the indoor air chemistry, with higher photolysis rates and more radical production expected closer to the light source.

Most species increase or decrease linearly with increasing light levels. However, some species such as RO_2 demonstrate more interesting behaviour. It is likely that different chemistry can occur in different parts of a room/building depending on light levels. More measurements determining how light from outdoors propagates around rooms and buildings would be valuable in this respect, as well as more measurements of indoor photolysis rates in general. This information could possibly be gained through use of a sensor network, where sensors measuring different chemical species and photon intensities could be placed in different places around a room/building under different lighting conditions (e.g. dark, attenuated sunlight only, indoor artificial lights only and so on) and at different times of day. The collected data can then be used in a model to simulate the radical concentrations and further understand the impacts.

Some of the indoor artificial lights had relatively few impacts on indoor air chemistry, including CFT and especially LED. Glass with a higher wavelength cut-off (e.g. LEWF) also had a smaller impact on indoor air chemistry. Combining low transmission lights and glass materials with a higher wavelength cut-off can effectively reduce the formation of radicals, hence reducing the formation of secondary pollutants (e.g. particulate matter) indoors. However, reducing indoor photolysis rates could have some further implications. For

example, reducing the photolysis rate of NO_2 can reduce the production rate of O_3, but more NO_2 will remain in the indoor environment. Both O_3 and NO_2 are found to have adverse health impacts on humans, including premature death hospital admission and respiratory function (Urman et al., 2014; Strickland et al., 2010; Malig et al., 2016; Nuvolone et al., 2018). For instance, according to WHO (2016), exposure guidelines for O_3 and NO_2 are:

- O_3: 100 µg/m^3 8-hour mean
- NO_2: 40 µg/m^3 annual mean; 200 µg/m^3 1-hour mean

However, health data only currently exist for a handful of indoor air pollutants and even then, it is often hard to compare the metrics as can be seen for O_3 and NO_2 above.

Consequently, it is hard to quantify health impacts under different indoor lighting conditions. Therefore, a future research goal would be a health-based assessment of the mixture of indoor air pollutants under different lighting conditions. Therefore, in the situation where there is more light indoors, and O_3 concentrations increase, whilst NO_2 concentrations decrease, we need to know if the increase in O_3 concentration is worse for health than the decrease in NO_2 concentration. Such an assessment would need to be for the whole pollutant mixture, given the connections between the different indoor species through chemical reactions.

Chapter 5: External Factors affecting indoor photolysis rates

5.1. Abstract

This chapter uses the improved INDCM to investigate the effects of cloudiness, latitude and time of year on indoor lighting and hence indoor air chemistry. Three different cloudiness levels were selected to study the impacts of clouds on the level of light transmitted through windows and hence indoor photolysis rates. In addition, twelve days, one from each month were used to study the impacts of different times of year on indoor air chemistry. Finally, the location on the planet affects indoor lighting levels, as a building's location (e.g. latitude) will affect how much solar radiation it receives. The results show that concentrations of most of the key indoor air species studied in this dissertation decrease (or increase for HONO and NO_2) as cloud level (CF) increases (e.g. average OH concentrations increase from 1.8×10^5 to 4.9×10^5 molecule/cm^3 from the most overcast to the sunniest conditions). Moreover, average concentrations of the key species are similar among twelve studied days over a year (e.g. average OH concentrations: ~6.7×10^5 molecule/cm^3, SD = 0.1 molecule/cm^3) at the lower latitudes (e.g. at the equator). At the higher latitudes (e.g. 65˚N), average concentrations of OH are highest in summer months (e.g. June, concentration: 7.3×10^5 molecule/cm^3), followed by autumn months (e.g. September, concentration: 4.2×10^5 molecule/cm^3). In addition, the average concentrations of O_3, HCHO, OH, HO_2 and NO decrease as the latitude increases (e.g. average OH concentrations range from 2.7×10^5 to 6.9×10^5 molecule/cm^3 with increase of latitude in March), whilst HONO and NO_2 concentrations increase with latitude for representative dates in spring, autumn and winter. For a representative date in summer, more sunlight across the hemisphere lead to similar average concentrations of key indoor species between the 0˚ and 65˚N latitudes (e.g. average OH concentrations: ~7.4×10^5 molecule/cm^3 on June, SD = 0.4 molecule/cm^3). The average concentrations of all the key indoor air species are highest at mid-latitudes (between 30˚N and 40˚N) in summer. There are more hours of sunlight at the pole compared to the equator in summer, but the sunlight is weaker. However, the best balance between the two happens at mid-latitudes, which lead to highest (or lowest for HONO and NO_2) average concentrations of chemicals. Therefore, cloudiness, latitude and season are all found to play important roles on resulting indoor air quality.

5.2. Introduction

Both latitude and season, can determine the amount of sunlight that reaches the Earth's surface. The declination angle of the sun is the angle between the Equator and the plane of the earth's orbit around the sun and it varies between +23.45˚ and -23.45˚. This variation then gives rise to the seasons (Figure 5.1). The summer solstice in the northern hemisphere corresponds to the maximum value of the declination angle and the minimum value of the declination angle corresponds with summer solstice in the southern hemisphere. An identical building, with the same indoor activities, could therefore have very different indoor concentrations depending on its location on the planet and the time of year.

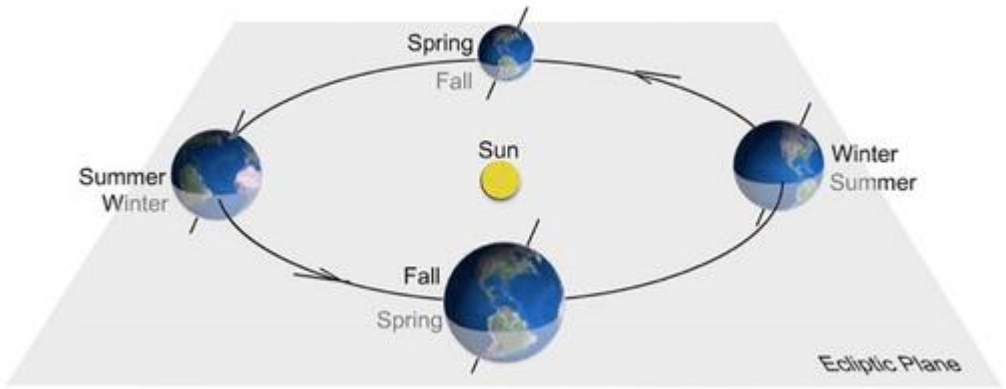

Figure 5.1: The declination angle of the Earth's axis from the Sun gives rise to the different seasons (source: De Paor et al., 2017).

For instance, Table 5.1 shows the times of sunrise and sunset for four cities located on or close to the prime meridian and for a representative date within the four seasons. As expected, although there is little variation between latitudes at the equinoxes, there is larger variation in the daylight hours with latitude in summer and winter. Daylight hours increase with latitude in summer and decrease in winter. Furthermore, differences in the total daylight hours for the four seasons are small at lower latitudes (e.g. only 38 minutes in Accra), but increase with latitude (e.g. up to 266 minutes in London, depending on the time of year).

Table 5.1: Four cities on or close to the prime meridian with their time of sunrise and sunset for the four seasons. All times are in local time.

City	Long.	Spring (Mar 21st)		Summer (Jun 21st)		Autumn (Sep 21st)		Winter (Dec 21st)	
Accra	6˚N	6:05 h	18:13 h	5:46 h	18:15 h	5:50 h	18:01 h	6:00 h	17:51 h
Ouagadougou	12˚N	6:09 h	18:17 h	5:42 h	18:33 h	5:55 h	18:02 h	6:22 h	17:46 h
Algiers	37˚N	6:49 h	19:00 h	5:29 h	20:10 h	6:35 h	18:45 h	7:56 h	17:35 h

London	52˚N	6:00 h	18:16 h	4:43 h	21:21 h	6:45 h	19:00 h	8:03 h	15:53 h

These differences in the amount of sunlight reaching the Earth's surface have impacts on the calculated photolysis rates. Figure 5.2 shows the peak indoor photolysis rate coefficients for attenuated outdoor sunlight for ozone (to form $O(^1D)$), nitrogen dioxide (to form NO and $O(^3P)$) and the nitrate radical (to form NO and O_2) in these four cities and for the four seasons. Again, there is relatively little variation in the peak photolysis rates at the equinoxes and greater variation in summer and winter. In spring, autumn and winter, Accra has the highest peak values, which decrease with increase in latitude. Meanwhile, Ouagadougou has the highest peak photolysis rate coefficients in summer. Therefore, both season and latitude are likely to play an important role in indoor photolysis rates.

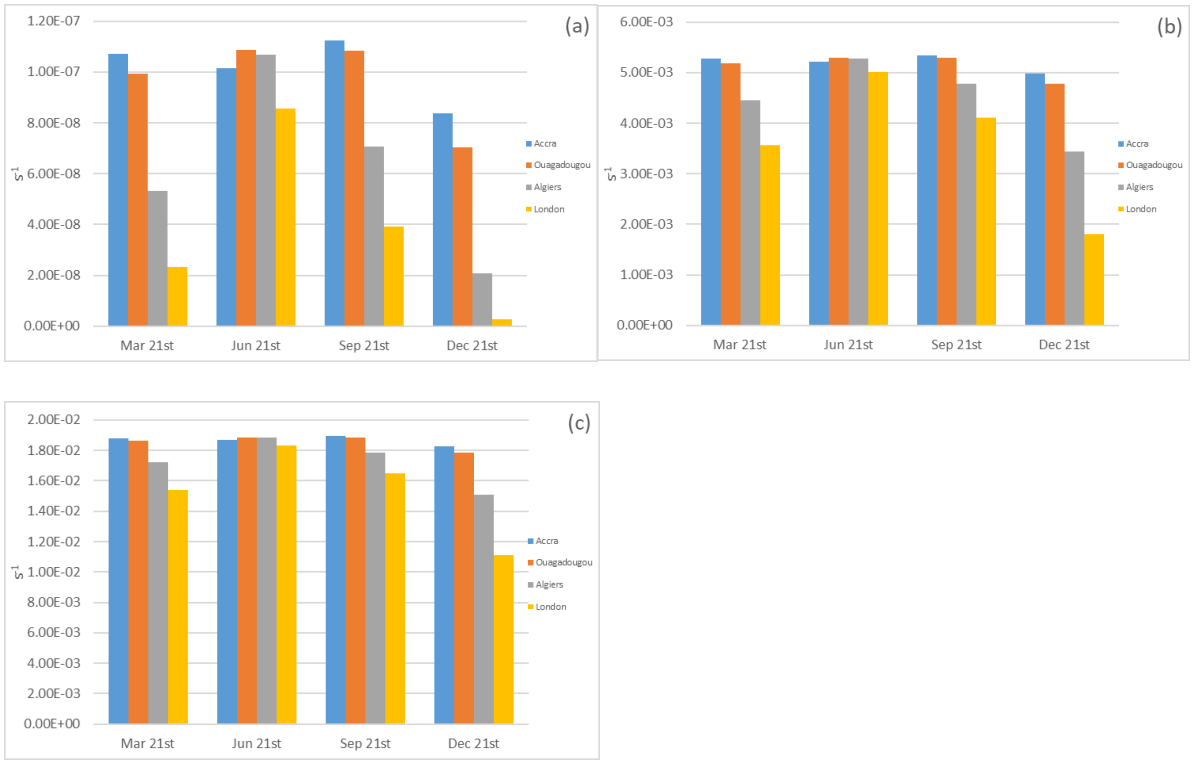

Figure 5.2: Peak indoor photolysis rate coefficients (s^{-1}) (indoor attenuated sunlight only) for: (a) J1 ($O_3 \rightarrow O(^1D)$) (b), J4 (NO_2) and (c) J5 ($NO_3 \rightarrow NO + O_2$) in the selected four cities and at four different times of year.

As well as season and latitude, another aspect that can affect the ability of light to propagate indoors is the level of cloudiness. Crawford et al. (2003) investigated the impacts of clouds on spectral actinic flux at the Earth's surface, and found that increased cloud fraction could enhance or decrease the surface actinic flux, depending on the cloud conditions. Figure 5.3

shows the actinic flux reported under 5 different cloud conditions between 320-420 nm (Crawford et al., 2003). The flux ratio shown in Figure 5.3 is the enhancement or reduction in actinic flux versus clear sky values. Crawford et al. (2003) found that the greatest enhancement (a factor of 1.2 compared to clear sky) happened with an unoccluded solar disk and slightly overcast conditions (situation 3 and 5, Figure 5.3), while the highest reduction (a factor of 0.2 compared to clear sky) took place with an occluded solar disk and more overcast conditions (situation 4, Figure 5.3).

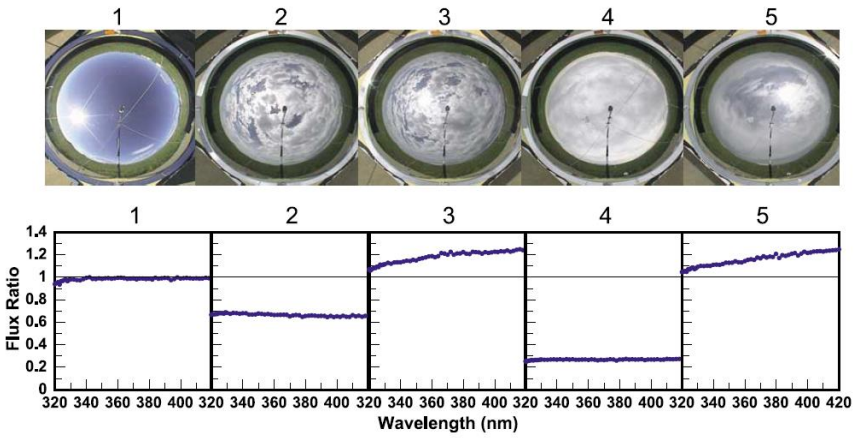

Figure 5.3: Variations in the actinic flux ratio under different cloud conditions (from Crawford et al., 2003).

The aim of this chapter is to investigate the impacts of cloudiness, latitude and time of year on indoor air chemistry. The specific objectives are to:

- Investigate how cloud conditions affect the concentrations of the key indoor species
- Investigate the impacts on indoor air chemistry as the latitude of a building changes
- Investigate the impact of different times of year on the predicted concentrations of key indoor species

5.3. Methodology

The INDCM was used in its updated form as described in Chapter 4. The model runs in local solar time, with the time of the year and the latitude determining the location of the sun in the sky for each model run. This chapter uses the updated model to study the impacts of cloud (by changing cloud conditions), latitude (by changing latitudes) and the time of year (by selecting different solar declination angles) on indoor air chemistry.

Based on Figure 5.3, a range of different cloud levels were used to test the impact on the model results: a maximum value of 1.2 (condition 3 and 5), 1 for clear sky conditions (condition 1) and 0.2 (condition 4) for very overcast conditions. In the original version of the model (Carslaw, 2007), clear sky conditions were assumed. These 'cloud factors' (CF) were then multiplied by the transmission values (calculated in Chapter 4). Indoor artificial lighting was assumed to be incandescent while window material was assumed to be LE because of their moderate impacts on indoor air chemistry as explained in Chapter 4. All other aspects of the model were as described in Section 4.3.4.

For the simulations investigating the impact of the time of year and variation in latitude on model results, indoor lighting was assumed to be off and the overall photolysis rate coefficients were based on attenuated sunlight only. The glass material was assumed to be Glass C, as described in chapter 4 and with a cloud factor of 1. The selected times of year were March 21st (declination angle: -7.15˚), June 21st (declination angle: 23.44 ˚; the longest day), September 21st (declination angle: 1.02 ˚) and December 21st (declination angle: -23.42 ˚; the shortest day). This chapter focuses on the northern hemisphere, but the results would be the same in both northern and southern hemispheres, just reversed for the time of year. The latitudes considered are the Equator (0˚), 10, 20˚, 30˚, 40˚, 50˚, 60˚ and 65˚, focusing on the main areas of land mass.

5.4. Results and discussion

5.4.1. Impacts of cloud conditions on indoor air chemistry

Figures 5.4-5.11 show the concentrations of O_3, HONO, HCHO, OH, HO_2, RO_2, NO and NO_2 for the glass material LE, for cloud factors of 1.2, 1 and 0.2, all with incandescent lighting. Table 5.2 summarises the average indoor concentrations for each of the key model species for each of the model runs between 06:00-18:00 h. The differences between different cloud factors are large. It can be seen that the concentrations of O_3 (Figure 5.4), HCHO (Figure 5.6), OH (Figure 5.7) and NO (Figure 5.10) increase as CF increases, while HONO (Figure 5.5) and NO_2 (Figure 5.11) concentrations decrease as CF increases (Table 5.2). The changes in RO_2 and HO_2 concentrations are again more complex in terms of their relationship with different cloud levels (Figures 5.8 and 5.9; Table 5.2). Again, this is due to the interplay between increased light leading to more OH radicals and hence more oxidation of VOCs to

produce peroxy (HO_2 and RO_2) radicals, versus more NO produced from photolysis that removes the same peroxy radicals as explained in Chapter 4.

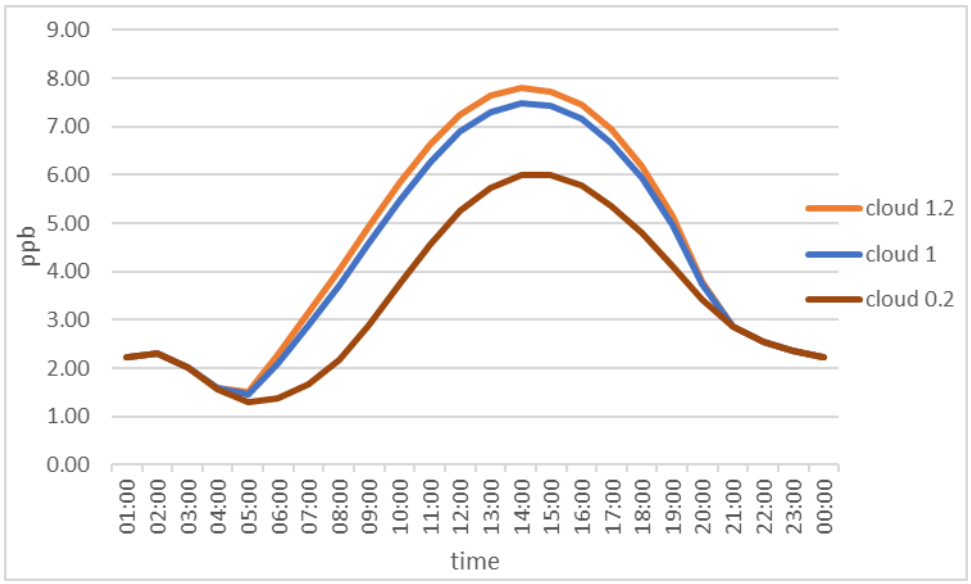

Figure 5.4: Concentrations of O_3 for cloud factor of 1.2, 1 and 0.2 for the LE glass and for incandescent lighting.

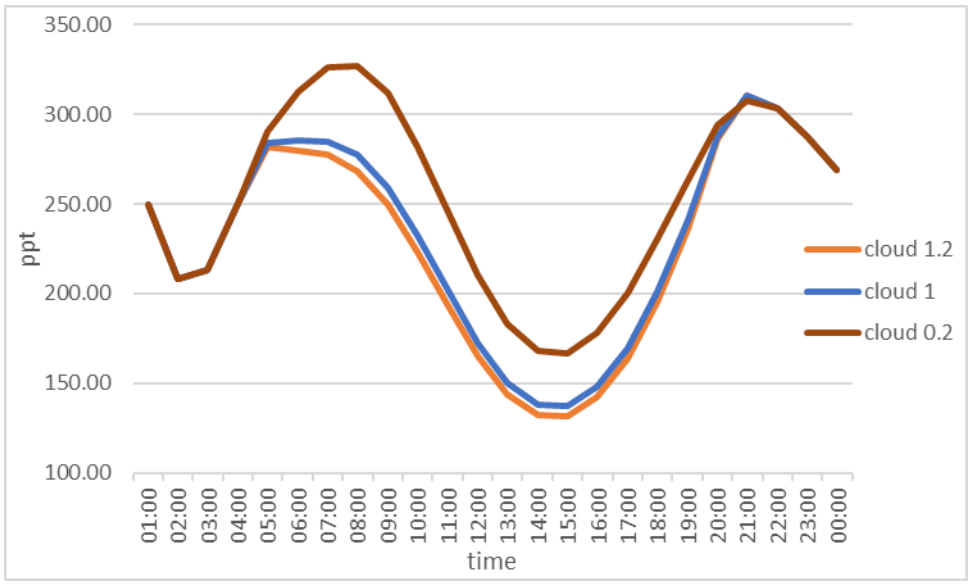

Figure 5.5: Concentrations of HONO for cloud factor of 1.2, 1 and 0.2 for the LE glass and for incandescent lighting.

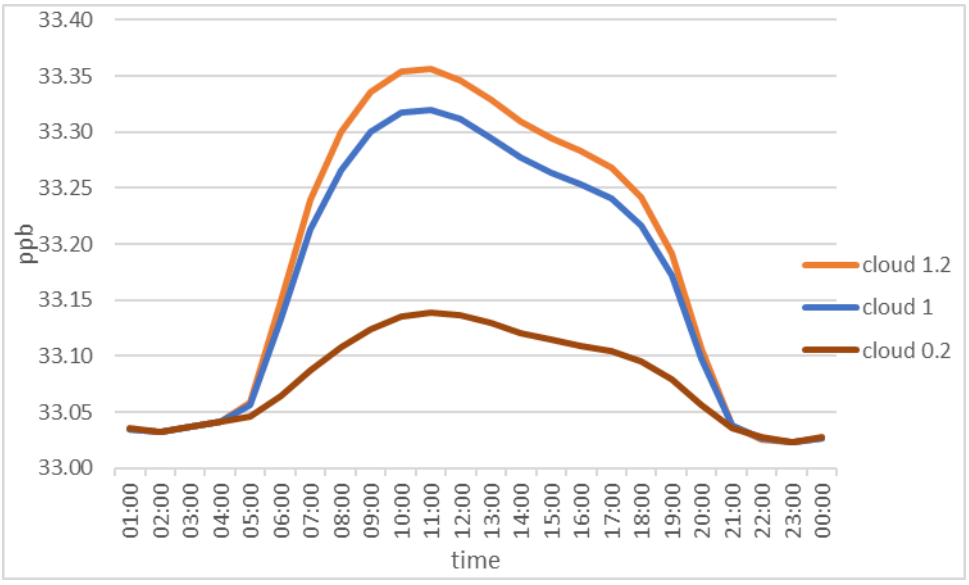

Figure 5.6: Concentrations of HCHO for cloud factor of 1.2, 1 and 0.2 for the LE glass and for incandescent lighting.

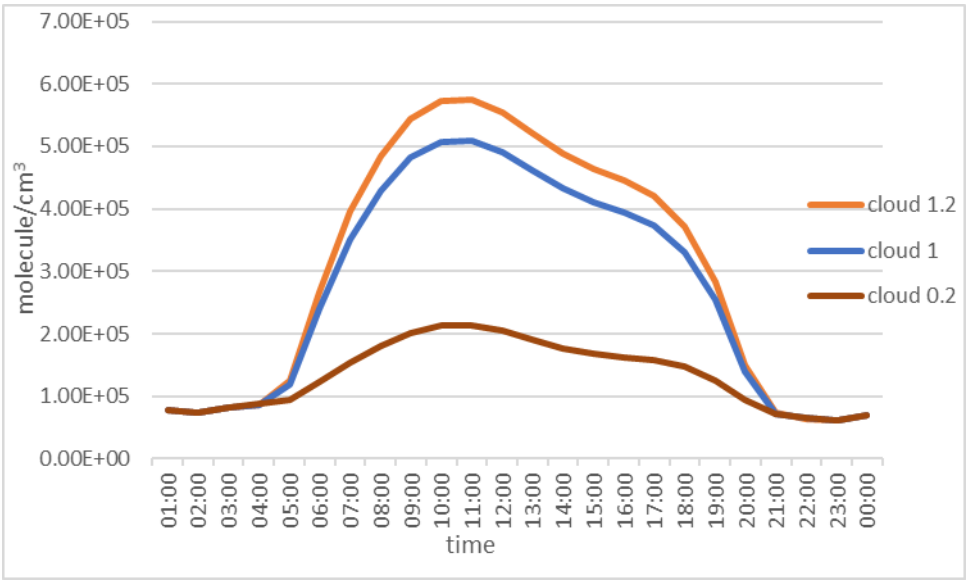

Figure 5.7: Concentrations of OH for cloud factor of 1.2, 1 and 0.2 for the LE glass and for incandescent lighting.

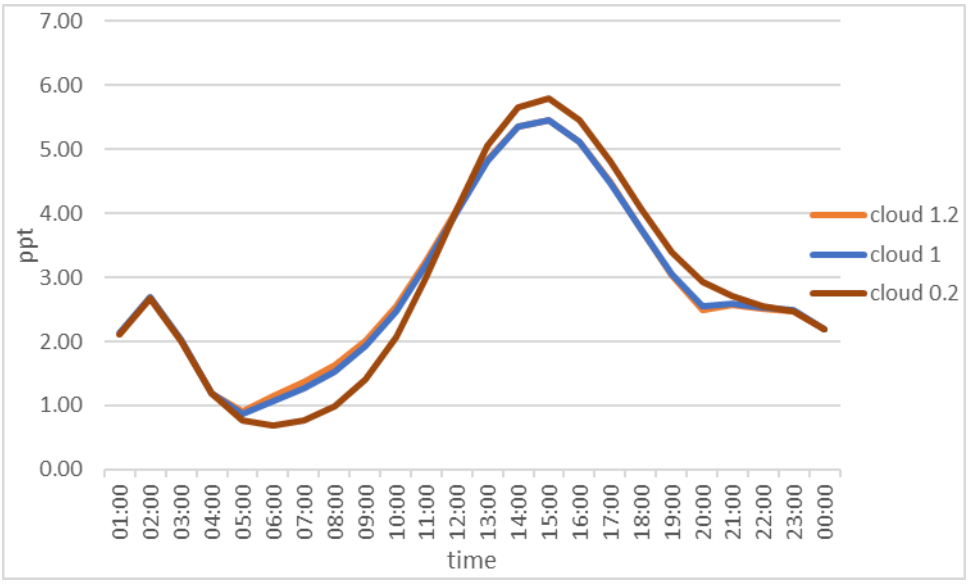

Figure 5.8: Concentrations of HO_2 for cloud factor of 1.2, 1 and 0.2 for the LE glass and for incandescent lighting.

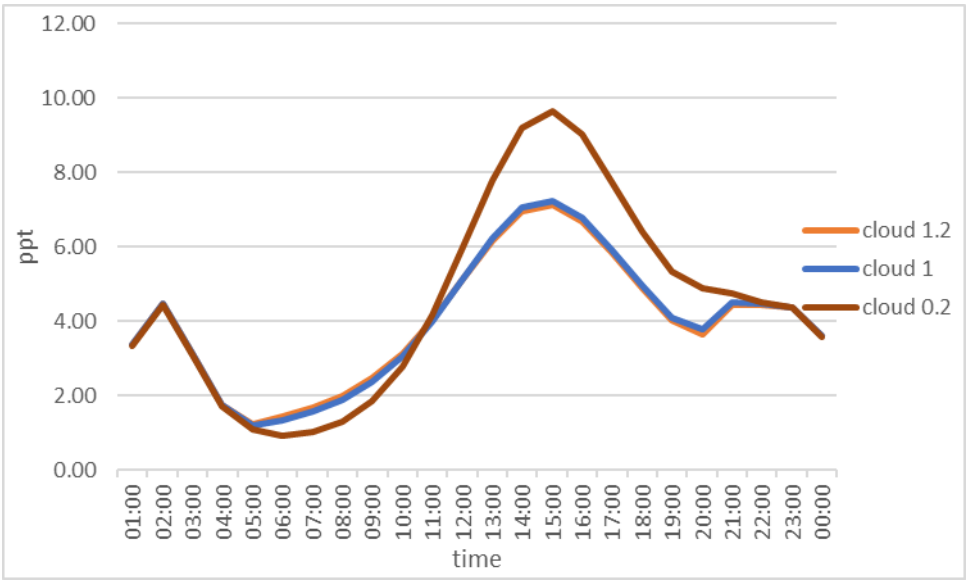

Figure 5.9: Concentrations of RO_2 for cloud factor of 1.2, 1 and 0.2 for the LE glass and for incandescent lighting.

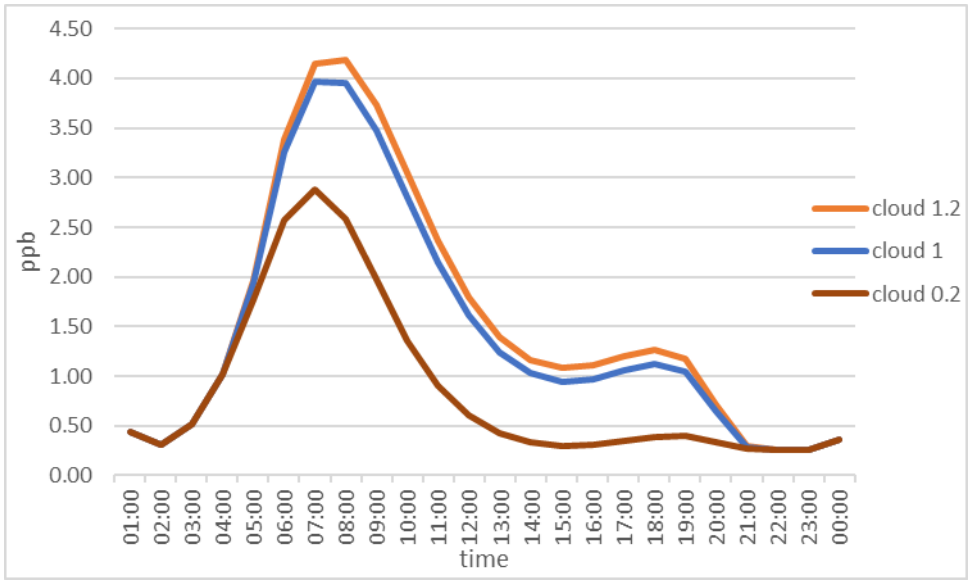

Figure 5.10: Concentrations of NO for cloud factor of 1.2, 1 and 0.2 for the LE glass and for incandescent lighting.

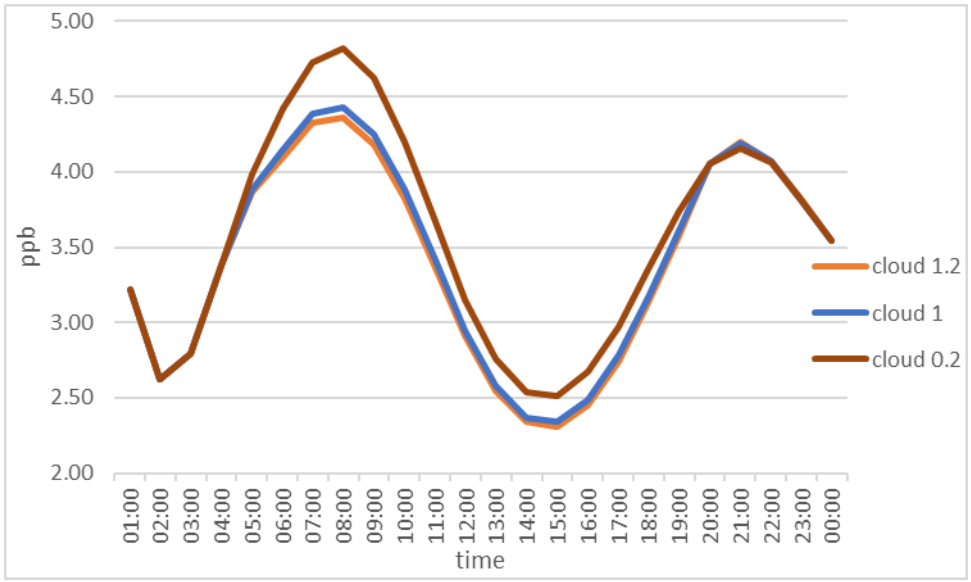

Figure 5.11: Concentrations of NO_2 for cloud factor of 1.2, 1 and 0.2 for the LE glass and for incandescent lighting.

***Table 5.2*:** Average concentrations of OH, HO_2, RO_2, O_3, HONO, HCHO, H_2O_2, NO and NO_2 for cloud 1.2, 1 and 0.2 for the LE glass and for incandescent lighting between 06:00-18:00h. O_3, HCHO, NO and NO_2 are in units of ppb; HONO, HO_2 and RO_2 in units of ppt; OH in units of 10^5 molecule/cm^3.

	O_3	HONO	HCHO	OH	HO_2	RO_2	NO	NO_2
cloud 1.2	6.3	190.6	33.3	4.9	3.7	4.7	2.2	3.2
cloud 1	6.0	197.7	33.3	4.3	3.6	4.7	2.0	3.3
cloud 0.2	4.5	235.8	33.1	1.8	3.6	5.6	1.0	3.5

In summary, these results show that assuming clear sky conditions may mean that predicted concentrations are over or underestimated, depending on the species. Such an omission would have potentially greater impacts in some locations compared to others. For instance, the annual average sunshine in the following cities are 3958 hours in Marsa Alam, Egypt (25˚N): 2771 hours in Athens, Greece (38˚N): and 1203 hours in Glasgow, United Kingdom (56˚N): (Met Office nd). Therefore, it is important to consider the impacts of cloudiness outdoors on indoor photolysis rates and hence species concentrations.

5.4.2. The impacts of different times of year on indoor air chemistry

Figures 5.12-5.19 show the concentrations of O_3, HONO, HCHO, OH, HO_2, RO_2, NO and NO_2 for the 21st of each month assuming no indoor lighting and for the Equator (0˚) and 65˚N latitudes. Table 5.3 shows the average concentrations of these species between 06:00-18:00 h. As shown in these figures, the differences in chemical concentrations during the year are very small at the Equator with very small standard deviations in the average concentrations for each month (SD=1.5 ppt for HONO while SD is close to zero for other chemicals; Table 5.3). The differences in concentrations become much greater at 65˚N for all of the studied indoor air species (Figures 5.12-5.19). Photolysis of O_3 and HONO produces OH, whilst that of HCHO produces HO_2 radicals (R1, R6, R16). Photolysis of NO_2 forms NO and O, the latter of which reacts with O_2 to produce O_3 (R4 and R5). Longer days in summer lead to more photolysis which can in turn produce higher concentrations of O_3 (Figure 5.12) and OH (Figure 5.15), than at other times of year. Meanwhile, HONO (Figure 5.13) and NO_2 (Figure 5.19) are photolysed more rapidly in summer, leading to lower concentrations than at the other times of year. The differences in HCHO (Figure 5.14) and NO_2 concentrations are very small at different times of year (Table 5.3). The NO produced from NO_2 photolysis can react with HO_2 and RO_2 which depletes their concentrations.

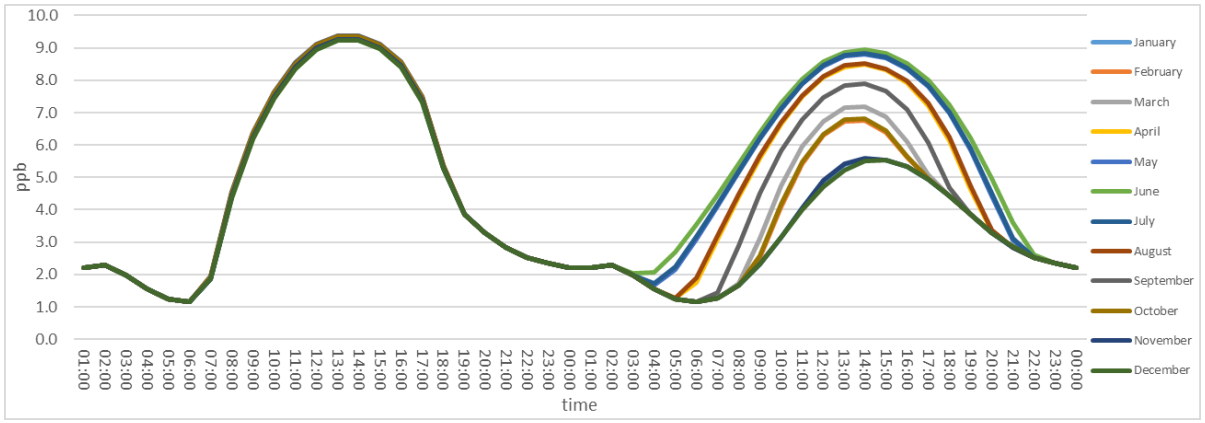

Figure 5.12: Indoor concentrations of O_3 at the Equator (0˚) on the left and at 65˚N on the right, for the 21st of each month and with no artificial lights indoors.

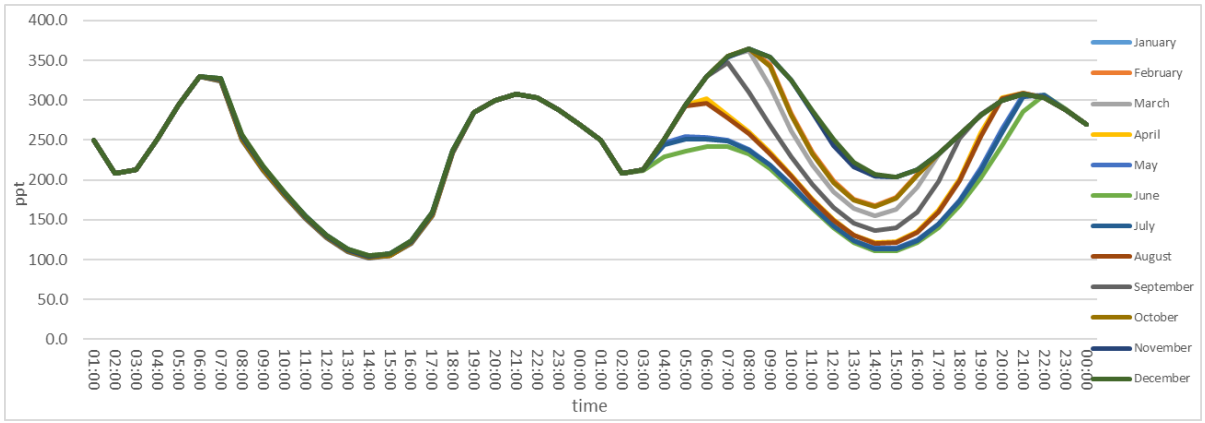

Figure 5.13: Indoor concentrations of HONO at the Equator (0˚) on the left and at 65˚N on the right, for the 21st of each month and with no artificial lights indoors.

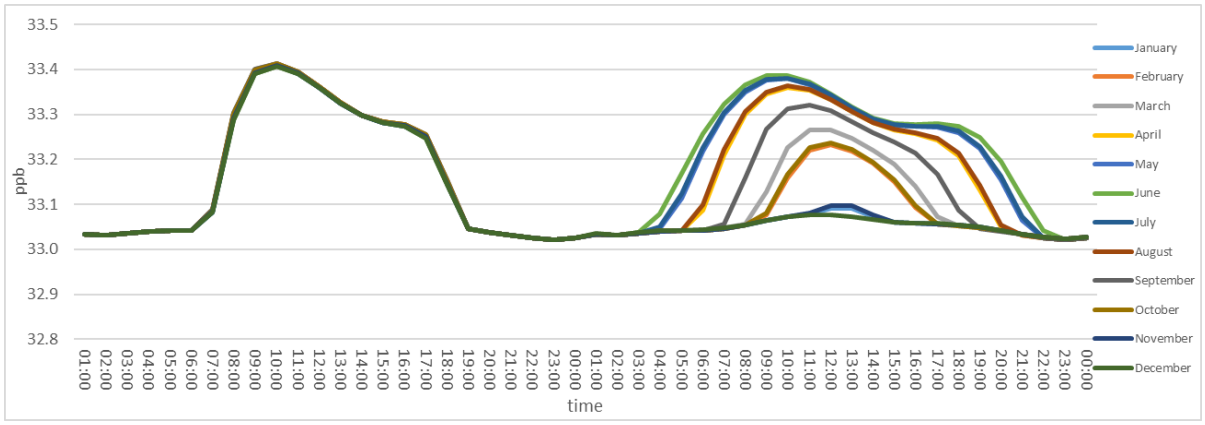

Figure 5.14: Indoor concentrations of HCHO at the Equator (0˚) on the left and at 65˚N on the right, for the 21st of each month and with no artificial lights indoors.

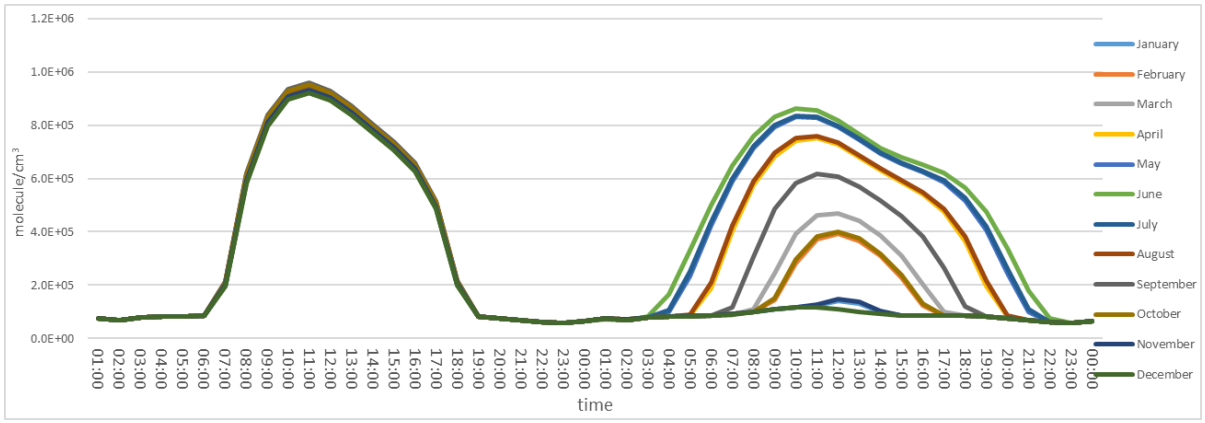

Figure 5.15: Indoor concentrations of OH at the Equator (0˚) on the left and at 65˚N on the right, for the 21st of each month and with no artificial lights indoors.

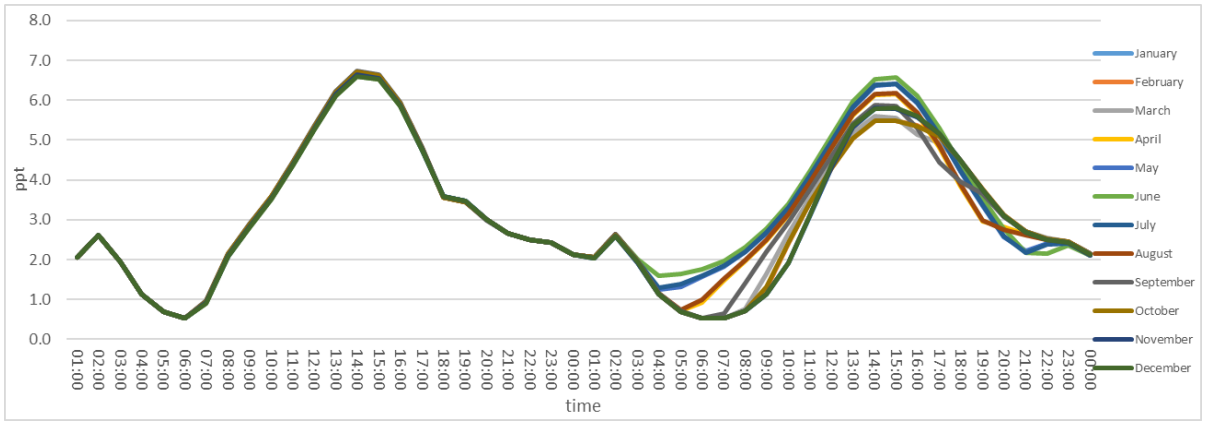

Figure 5.16: Indoor concentrations of HO_2 at the Equator (0˚) on the left and at 65˚N on the right, for the 21st of each month and with no artificial lights indoors.

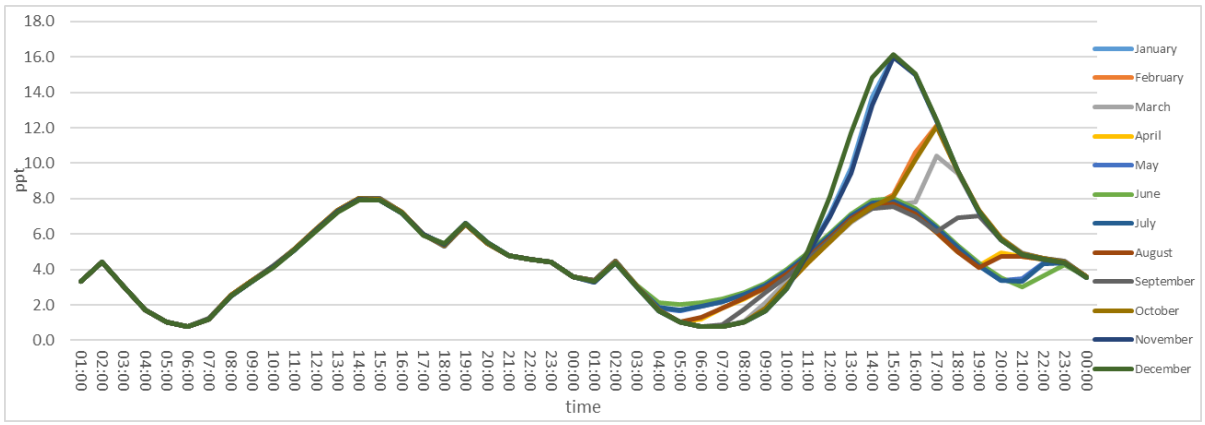

Figure 5.17: Indoor concentrations of RO_2 at the Equator (0˚) on the left and at 65˚N on the right, for the 21st of each month and with no artificial lights indoors.

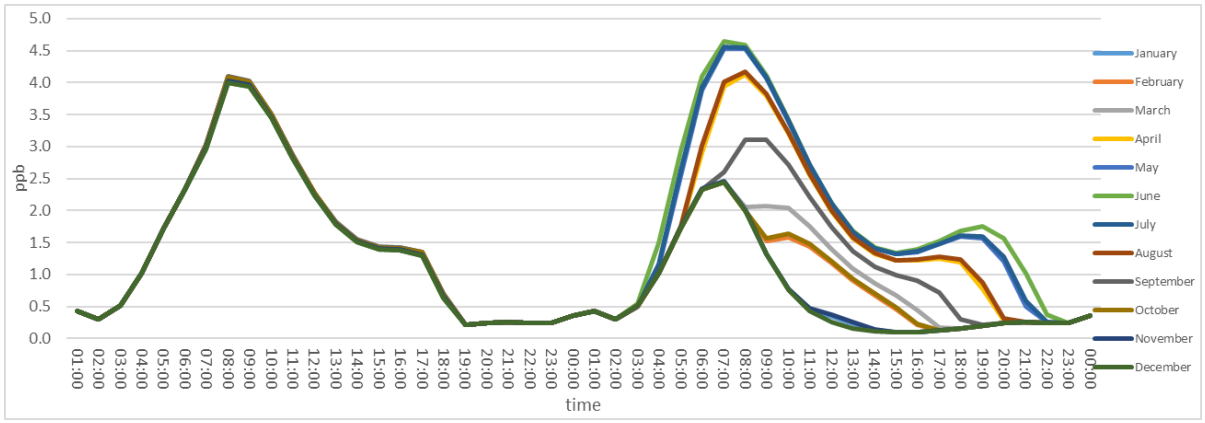

Figure 5.18: Indoor concentrations of NO at the Equator (0˚) on the left and at 65˚N on the right, for the 21st of each month and with no artificial lights indoors.

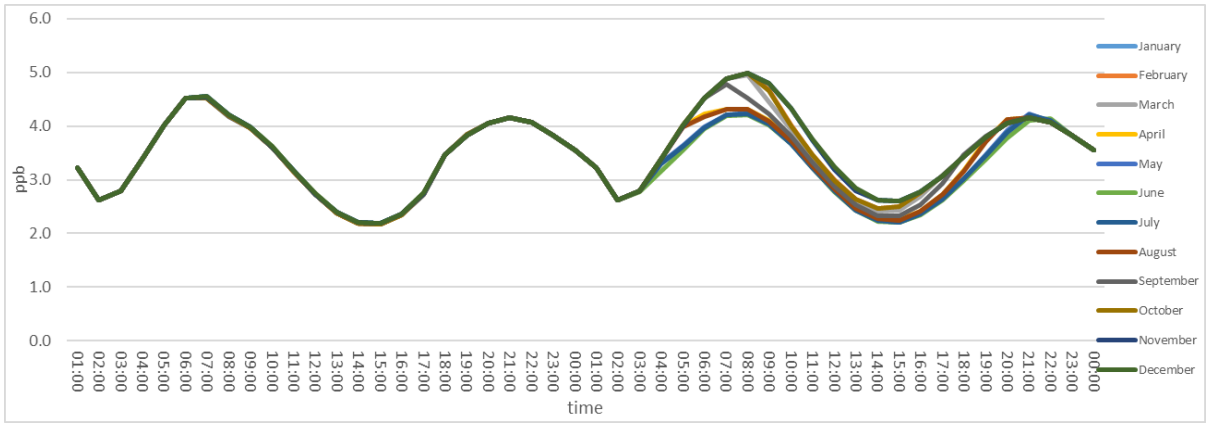

Figure 5.19: Indoor concentrations of NO_2 at the Equator (0˚) on the left and at 65˚N on the right, for the 21st of each month and with no artificial lights indoors.

As shown in Figure 5.18, profiles of NO between October and March 21st at 65˚N show lower peaks than between April and September 21st and then sharp decreases after the morning peak (especially in November, December and January as sunlight is less intense in winter as the sun is lower in the sky). This means less NO is produced by photolysis to react with HO_2 and RO_2 than for other times of year. Therefore, a higher peak of HO_2 is found between November 21st and January 21st (~5.8 ppt) than in February, March and October 21st (~5.5 ppt) (Figure 5.16). For the same reason, the highest RO_2 peaks are between November and January 21st at 65˚N (~16.2 ppt) followed by February, March and October 21st (~10.1 ppt) (Figure 5.17).

Concentrations of NO show a sharp increase and then peak at high values between April and September 21st, with the highest value of 4.6 ppb in June and July. Meanwhile, concentrations of NO increase slightly again at around 15:00 h at 65˚N between April and

August 21st. This is because RO_2 reaches its peak concentration at around 15:00 h and starts to decline afterwards at the same location and time of year, therefore, less RO_2 is available to react with NO leading to a reduced concentration during the period around summer with more sunlight. In addition, the small increase and then decrease of NO concentrations between April and August 21st is also linked to the small fluctuations in RO_2 concentrations during the same period, owing to the negative correlation observed between concentrations of RO_2 and NO (Figures 5.17 and 5.18).

Average concentrations of the key indoor air species in this dissertation show similar variations with the time of year as their diurnal profiles. The differences in chemical concentrations during the year are very small at the Equator, whilst the differences in concentrations become much greater at 65˚N for all of the studied indoor air species (Table 5.3). Highest (or lowest for HONO and NO_2) average concentrations happen in June, owing to the most intense sunlight being present in summer.

Table 5.3: Average concentrations of key chemicals at the Equator (0˚) and 65˚N and for 21st of each month under dark between 06:00-18:00 h. O_3, HCHO, NO and NO_2 in units of ppb; HONO, HO_2 and RO_2 in units of ppt; OH in units of 10^5 molecule/cm^3.

	O_3	HONO	HCHO	OH	HO_2	RO_2	NO	NO_2
0˚-January	7.2	175.8	33.3	6.7	4.4	5.4	2.3	3.1
0˚-February	7.3	173.7	33.3	6.8	4.4	5.4	2.3	3.1
0˚-March	7.3	173.2	33.3	6.9	4.4	5.4	2.3	3.1
0˚-April	7.3	173.8	33.3	6.8	4.4	5.4	2.3	3.1
0˚-May	7.2	175.8	33.3	6.7	4.4	5.4	2.3	3.1
0˚-June	7.1	176.9	33.3	6.6	4.4	5.3	2.3	3.1
0˚-July	7.2	176.0	33.3	6.7	4.4	5.4	2.3	3.1
0˚-August	7.2	174.0	33.3	6.8	4.4	5.4	2.3	3.1
0˚-September	7.3	172.9	33.3	6.9	4.4	5.4	2.3	3.1
0˚-October	7.3	173.7	33.3	6.8	4.4	5.4	2.3	3.1
0˚-November	7.2	175.7	33.3	6.7	4.4	5.4	2.3	3.1
0˚-December	7.1	176.9	33.3	6.6	4.4	5.3	2.3	3.1
65˚N-January	4.0	271.4	33.1	1.0	3.7	7.9	0.7	3.6
65˚N-February	4.7	250.0	33.1	2.1	3.6	6.0	1.1	3.5
65˚N-March	5.0	238.6	33.2	2.7	3.7	5.5	1.3	3.4
65˚N-April	6.8	181.9	33.3	6.0	4.2	5.1	2.3	3.2
65˚N-May	7.4	167.3	33.3	7.0	4.4	5.3	2.5	3.1
65˚N-June	7.5	163.0	33.3	7.3	4.5	5.4	2.6	3.1
65˚N-July	7.4	166.5	33.3	7.0	4.4	5.3	2.5	3.1
65˚N-August	6.9	180.2	33.3	6.1	4.2	5.1	2.3	3.2
65˚N-September	5.8	212.3	33.2	4.2	3.8	5.0	1.7	3.3

65˚N-October	4.7	248.8	33.1	2.2	3.6	5.9	1.1	3.5
65˚N-November	4.1	271.0	33.1	1.1	3.7	7.8	0.7	3.6
65˚N-December	4.0	272.5	33.1	1.0	3.7	8.2	0.7	3.6

5.4.3. The impacts of latitude on indoor air chemistry

Figures 5.20-5.27 show the concentrations of O_3, HONO, HCHO, OH, HO_2, RO_2, NO and NO_2 between 0˚ and 65˚N for March, June, September and December 21st for the case with no internal lighting. Table 5.4 shows the average concentrations of the key species for different latitudes and for four different times of year between 06:00-18:00 h. In spring (March 21st), autumn (September 21st) and winter (December 21st), the maximum (or minimum for HONO and NO_2) concentrations of O_3 (Figure 5.20), HONO (Figure 5.21), HCHO (Figure 5.22) and NO_2 (Figure 5.27) decrease (or increase) as the latitude increases. The average concentrations of these key chemicals between 06:00-18:00 h also show the same behaviour (Table 5.4), owing to more intense sunlight at the Equator.

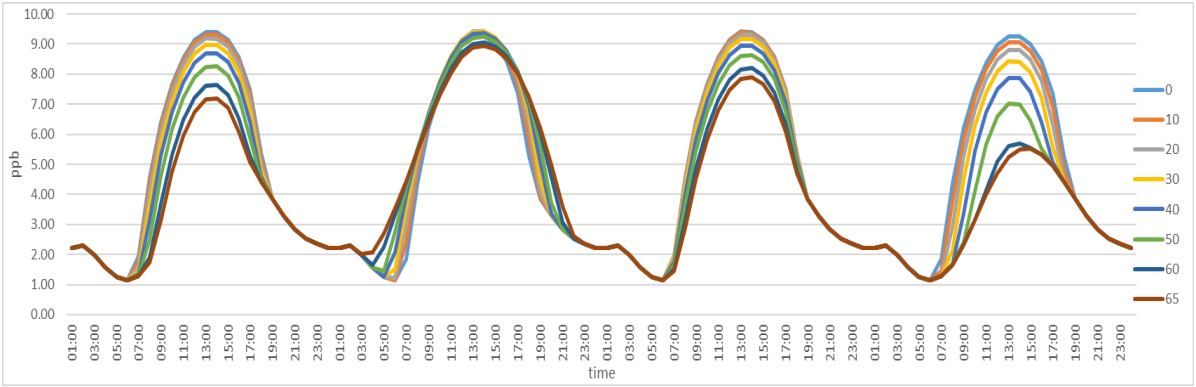

Figure 5.20: Concentrations of O_3 at equator (0˚), 10˚N, 20˚N, 30˚N, 40˚N, 50˚N, 60˚N and 65˚N with no internal lighting for from left to right, the 21st of March, June, September and December respectively.

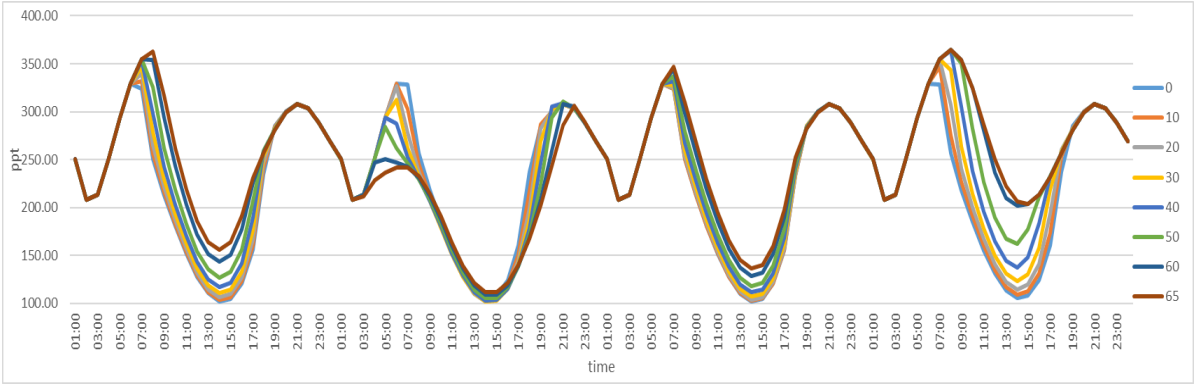

Figure 5.21: Concentrations of HONO at equator (0˚), 10˚N, 20˚N, 30˚N, 40˚N, 50˚N, 60˚N and 65˚N with no internal lighting for from left to right, the 21st of March, June, September and December respectively.

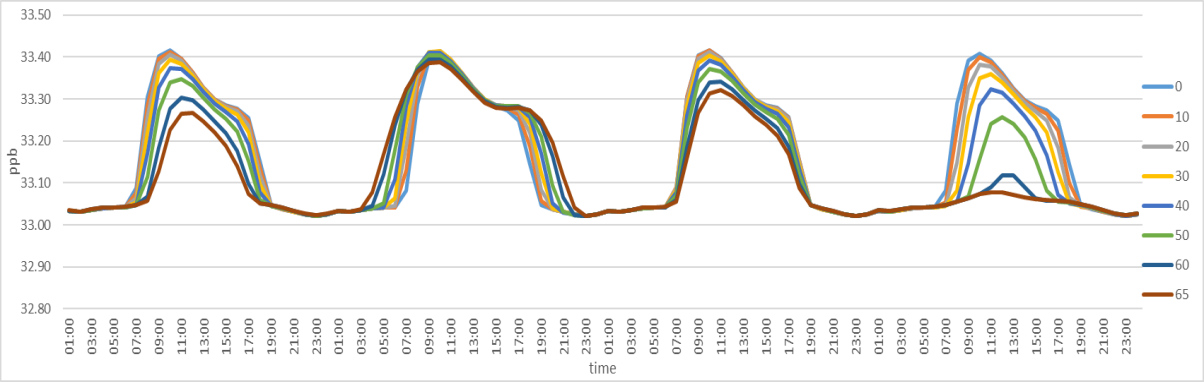

Figure 5.22: Concentrations of HCHO at equator (0˚), 10˚N, 20˚N, 30˚N, 40˚N, 50˚N, 60˚N and 65˚N with no internal lighting for from left to right, the 21st of March, June, September and December respectively.

The distribution of peak OH concentrations (Figure 5.23) is similar to those for O_3 and HCHO, with peak concentrations increasing with latitude in spring, autumn and winter. In addition, the peak concentrations of HO_2 (Figure 5.24) and NO (Figure 5.26) show similar behaviour to OH, O_3 and HCHO in spring and autumn. However, the profiles of HO_2 and NO look less well ordered than for other species in winter. At the higher latitudes (especially 60˚N and 65˚N) in winter, there is much less sunlight owing to shorter days, leading to less NO_2 photolysis. There is consequently a higher average concentration of NO_2 at high latitudes (e.g. 65˚N: 3.6 ppb) compared to other times of year, but also the lowest average concentration of NO (e.g. 65˚N: 0.7 ppb) (Table 5.4). Concentrations of NO peak at their lowest values in winter and then decrease sharply (Figure 5.26) at high latitudes, compared to locations close to the equator, whilst concentrations of NO at low latitudes (between 0˚ and 30˚N) increase and then peak at relatively greater values compared to higher latitudes owing to the much stronger sunlight. This is because daylight hours decrease markedly with the increase of latitude in winter (Table 5.1). So increased daylight hours together with greater intensity of sunlight, lead to higher photolysis rates at low latitudes, whilst less and weaker sunlight causes relative weaker photolysis at high latitudes. The mid latitudes (40˚N and 50˚N) have intermediate daylight hours and sunlight intensity, which leads NO concentrations to show an additional small increase after the morning peak at around 08:30 h This is due to the balance between NO_2 photolysis which produces NO and the reaction of

NO with HO_2 and RO_2 which reduces NO at mid-latitudes with an intermediate level of sunlight. Moreover, the peak concentrations of HO_2 decrease with latitude between 0˚ and 50˚N and then increase at 60˚N and 65˚N, as there is less NO to react with HO_2 at high latitudes (Table 5.4).

Concentrations of RO_2 are the reverse of those of NO. RO_2 concentration increases and then peaks at relatively higher values at high latitudes (60˚N and 65˚N) owing to low NO concentrations (Figure 5.25) at these latitudes. At the low and mid latitudes (between 0˚ and 50˚N), profiles of RO_2 show different levels of fluctuations between 15:00-19:00 h in winter. This is also related to the decrease of NO concentrations during this period as shown in Figure 5.26. In addition, RO_2 concentrations peak at a later time (e.g. ~17:00 h at 40 ˚N) in winter at the mid latitudes (between 30˚N and 50˚N), owing to an intermediate level of sunlight, which leads to an intermediate sized decrease of NO concentrations. The fluctuations in RO_2 concentrations in winter (less sunlight compared to other seasons) at the low and mid latitudes (more sunlight compared to high latitudes) as explained above is again due to the balance between the reactions of OH and VOCs which produce RO_2 and the reactions of RO_2 with NO which reduces RO_2 at different latitudes. In addition, the additional daylight at the Equator also causes broader profiles for most of the key indoor species compared to the other latitudes, and the concentration profiles become less broad with the increase in latitude in spring, autumn and winter.

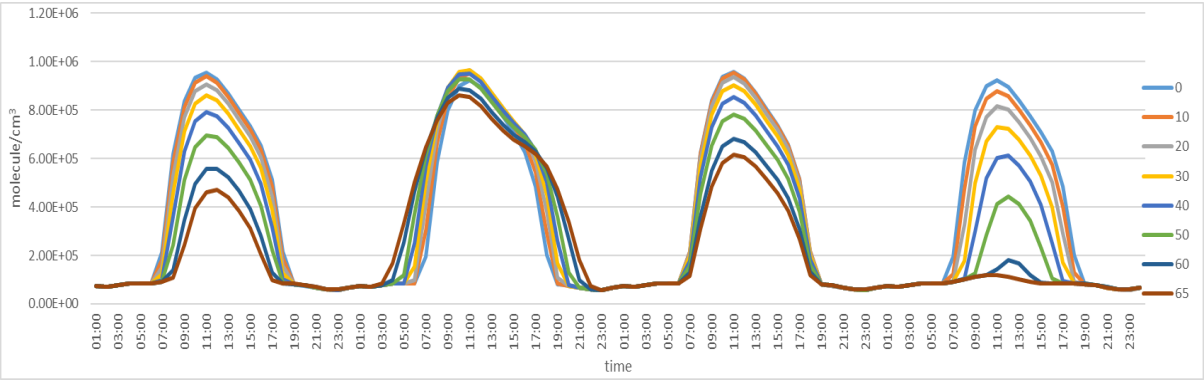

Figure 5.23: Concentrations of OH at equator (0˚), 10˚N, 20˚N, 30˚N, 40˚N, 50˚N, 60˚N and 65˚N with no internal lighting for from left to right, the 21st of March, June, September and December respectively.

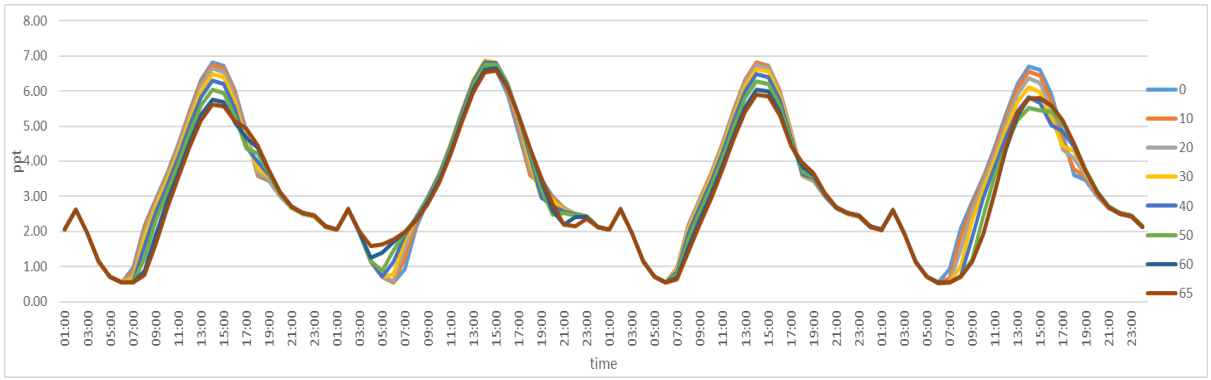

Figure 5.24: Concentrations of HO_2 at equator (0˚), 10˚N, 20˚N, 30˚N, 40˚N, 50˚N, 60˚N and 65˚N with no internal lighting for from left to right, the 21st of March, June, September and December respectively.

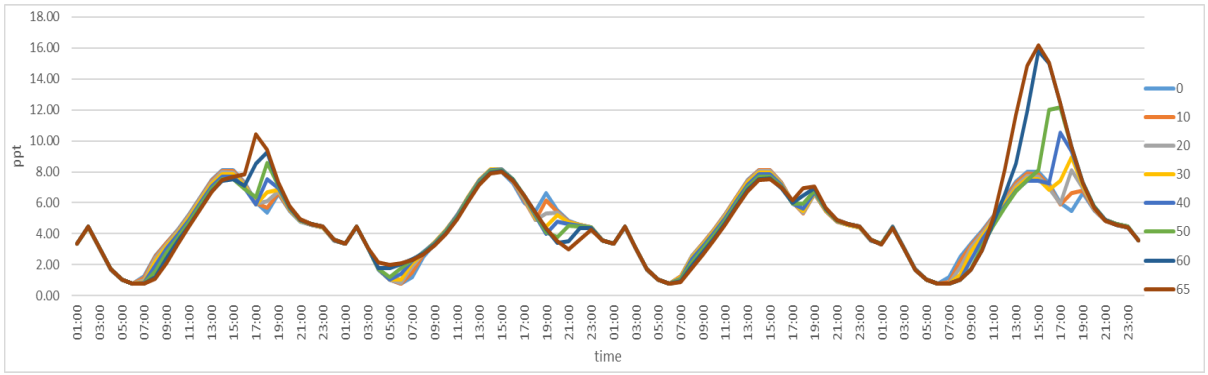

Figure 5.25: Concentrations of RO_2 at equator (0˚), 10˚N, 20˚N, 30˚N, 40˚N, 50˚N, 60˚N and 65˚N with no internal lighting for from left to right, the 21st of March, June, September and December respectively.

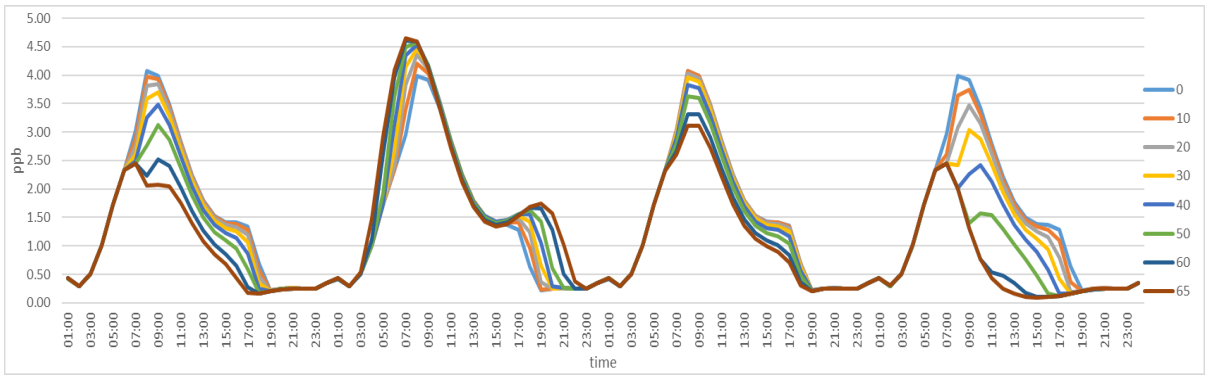

Figure 5.26: Concentrations of NO at equator (0˚), 10˚N, 20˚N, 30˚N, 40˚N, 50˚N, 60˚N and 65˚N with no internal lighting for from left to right, the 21st of March, June, September and December respectively.

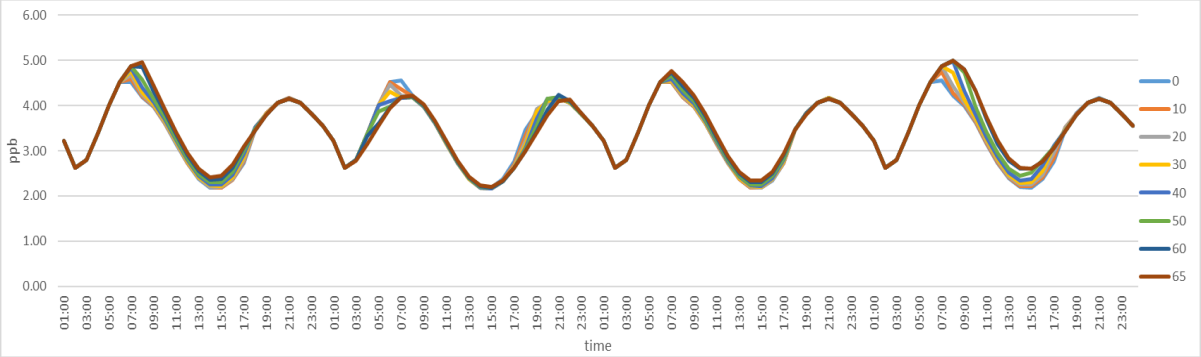

Figure 5.27: Concentrations of NO_2 at equator (0˚), 10˚N, 20˚N, 30˚N, 40˚N, 50˚N, 60˚N and 65˚N with no internal lighting for from left to right, the 21st of March, June, September and December respectively.

In summer, more sunlight reaches the Earth's surface over the entire hemisphere, leading to smaller differences in concentrations of key indoor species with latitude compared to the other seasons. In addition, the daylight hours during summer increase with latitude (Table 5.1). Because of the interplay between these two factors, the average concentrations of all the studied key indoor air species are highest (or lowest for HONO and NO_2) at mid-latitudes (between 30˚N and 40˚N). Although sunlight is not as intense as at the Equator, there are more daylight hours at these latitudes, such that overall photolysis processes peak at these latitudes.

Table 5.4: Average concentrations of key chemical species between 0˚ and 65˚N for different latitudes and for four seasons between 06:00-18:00 h. O_3, HCHO, NO and NO_2 in unit of ppb; HONO, HO_2 and RO_2 in unit of ppt; OH in unit of 10^5 molecule/cm^3.

		O_3	HONO	HCHO	OH	HO_2	RO_2	NO	NO_2
March 21st	0˚	7.3	173.2	33.3	6.9	4.4	5.4	2.3	3.1
	10˚N	7.2	176.5	33.3	6.7	4.4	5.4	2.3	3.1
	20˚N	7.0	181.3	33.3	6.3	4.3	5.3	2.2	3.2
	30˚N	6.7	188.0	33.3	5.9	4.2	5.3	2.1	3.2
	40˚N	6.4	197.1	33.3	5.3	4.1	5.2	2.0	3.2
	50˚N	6.0	209.7	33.2	4.4	3.9	5.2	1.8	3.3
	60˚N	5.4	227.3	33.2	3.4	3.7	5.4	1.5	3.4
	65˚N	5.0	238.6	33.2	2.7	3.7	5.5	1.3	3.4
June 21st	0˚	7.1	176.9	33.3	6.6	4.4	5.3	2.3	3.1
	10˚N	7.4	169.2	33.3	7.1	4.5	5.4	2.4	3.1
	20˚N	7.6	163.3	33.3	7.4	4.6	5.5	2.5	3.1
	30˚N	7.7	159.8	33.3	7.7	4.6	5.5	2.6	3.1
	40˚N	7.7	158.4	33.3	7.7	4.6	5.5	2.6	3.0
	50˚N	7.7	158.9	33.3	7.7	4.6	5.5	2.6	3.1

	60˚N	7.6	161.1	33.3	7.5	4.5	5.4	2.6	3.1
	65˚N	7.5	163.0	33.3	7.3	4.5	5.4	2.6	3.1
September 21st	0˚	7.3	172.9	33.3	6.9	4.4	5.4	2.3	3.1
	10˚N	7.3	173.2	33.3	6.9	4.4	5.4	2.3	3.1
	20˚N	7.2	175.1	33.3	6.7	4.4	5.4	2.3	3.1
	30˚N	7.1	178.6	33.3	6.5	4.3	5.3	2.3	3.1
	40˚N	6.8	184.1	33.3	6.1	4.2	5.2	2.2	3.2
	50˚N	6.5	192.2	33.3	5.5	4.1	5.1	2.1	3.2
	60˚N	6.1	204.2	33.2	4.7	3.9	5.1	1.9	3.3
	65˚N	5.8	212.3	33.2	4.2	3.8	5.0	1.7	3.3
December 21st	0˚	7.1	176.9	33.3	6.6	4.4	5.3	2.3	3.1
	10˚N	6.8	186.1	33.3	6.0	4.2	5.3	2.1	3.2
	20˚N	6.4	197.0	33.3	5.3	4.1	5.3	2.0	3.2
	30˚N	6.0	210.4	33.2	4.5	3.9	5.4	1.7	3.3
	40˚N	5.4	227.2	33.2	3.5	3.8	5.5	1.4	3.4
	50˚N	4.7	248.0	33.1	2.3	3.7	6.1	1.1	3.5
	60˚N	4.1	269.4	33.1	1.1	3.6	7.5	0.7	3.6
	65˚N	4.0	272.5	33.1	1.0	3.7	8.2	0.7	3.6

5.5. Conclusion

In summary, the results in this chapter found that cloudiness, time of year and latitude all had important impacts on indoor air chemistry. Specifically, they showed that:

1. Cloudiness has large impacts (e.g. 172% difference in the predicted average OH concentrations between CF=1.2 and 0.2), especially for an unoccluded sun with partly cloudy conditions, on indoor air chemistry.

2. Differences in average concentrations of key indoor species during the year are small at the lower latitudes (especially at the Equator). At the higher latitudes (e.g. 65˚N), more sunlight leads to highest average concentrations of O_3, OH, HO_2 and NO in summer, followed by spring and autumn and then winter. On the contrary, higher photolysis rates lead to lower concentrations of HONO (reduced by photolysis), RO_2 (reduced by the reaction with enhanced NO from NO_2 photolysis) and NO_2 (reduced by photolysis) compared to other seasons. Therefore, the time of year also impacts on indoor air chemistry.

3. Average concentrations of the key indoor air species decrease (or increase for HONO and NO_2) as the latitude increases in spring (March 21st), autumn (September 21st) and winter (December 21st). In summer, more sunlight across the entire hemisphere leads to smaller differences in concentrations of key indoor species and the average concentrations of all the studied key chemicals are highest (or lowest for HONO and NO_2) at mid-latitudes (between

30˚N and 40˚N), owing to the balance between level of sunlight and length of daylight as explained above.

All three factors (cloudiness, time of year and latitude) are found to play important roles on indoor air chemistry. Note that only three different scenarios of cloudiness were considered based on Crawford et al. (2003). For further study, it would be beneficial to have actinic flux measurements for a wider range of cloud cover and to account for how these vary with time of day and location on the planet. Also, it is worth linking different cloud levels with different latitudes as weather is not always same for different location. Such data could inform the model to better simulate the radical concentrations and understand the impacts.

Chapter 6: Identification of the most important factors affecting indoor photolysis rates

6.1. Abstract

This chapter compares the impacts of indoor artificial light and glass composition (based on chapter 4 results) and cloudiness, time of year and latitude (based on chapter 5 results), in order to find out the most important controls on indoor air chemistry with respect to indoor photolysis. The impacts of these selected controlling factors on the predicted concentrations of key indoor chemicals were compared with the baseline condition (dark indoors) and with each other. For all of the investigated controlling factors, glass type had the greatest impacts (~71%) on the concentrations of most of the key species (e.g. OH) followed by cloudiness and proximity of artificial light (~53%). Meanwhile, time of year and latitude also have important impacts on indoor concentrations of key species with average impacts of ~32% and 22% respectively. For all of the studied species, the greatest impacts are on predicted OH concentrations (with an average 142% deviation from the baseline) followed by total organic nitrates (TOTORGNO$_3$; with an average 113% deviation from the baseline) and then NO (with an average 56% deviation from the baseline). Meanwhile, there are smaller impacts on the predicted concentrations of the sum of all PAN-type species (TOTPAN; with an average 33% deviation from the baseline), HO$_2$ (with an average 28% deviation from the baseline) and O$_3$ (with an average 19% deviation from the baseline). Finally, predicted RO$_2$ concentrations are less sensitive to these factors (with an average 10% deviation from the baseline), as are HONO (with an average 7% deviation from the baseline), NO$_2$ (with an average 4% deviation from the baseline) and HCHO (close to zero in average). The predicted concentrations of NO$_2$ and HCHO are controlled by other factors, such as exchange rate, deposition rate and outdoor concentrations. The impacts of these findings for indoor air quality are discussed at the end of this chapter.

6.2. Aim

The aim of this short chapter is to bring together chapters 4 and 5 to:

- Quantify which of the controlling factors for indoor photolysis discussed in chapters 4 and 5 has the greatest overall impact on indoor air photolysis rates and hence the resulting chemistry.

- To understand the range of concentrations that is possible for each of the key species depending on the variation in lighting conditions
- To discuss the implications of these for our understanding of indoor air chemistry and to highlight key model uncertainties.

6.3. Methods

A set of model runs was selected to compare the impacts of variations in five factors that control indoor air photolysis rates with a specified baseline condition (dark indoors) and with each other. Table 6.1 shows the selected scenarios that have been compared. Three different latitudes are selected which represent the lowest (equator 0˚), mid (40˚N) and highest (65˚N) latitudes explored in chapter 5; the highest and lowest declination angles are selected which represent the longest and shortest day respectively; the highest and lowest cloud levels which are CF=1.2 and CF=0.2 are used to bound the impact of clouds; the window materials with the highest and lowest cut-off wavelengths which are Glass C and LEWF (chapter 4) are also used. For all of these scenarios, it was assumed indoor artificial lights were off.

In addition, model scenarios considering 7 different indoor artificial lights at two distances (1 m and adjacent to the light source, based on Chapter 4 were also selected, assuming it was dark outside. This produced 38 model runs, exploring the range of different controlling factors on the key species concentrations. These concentrations were averaged between 06:00-18:00 h and then compared against the background condition (no attenuated sunlight and no indoor artificial lights).

Table 6.1: The 39 selected scenarios with defined conditions.

number	List
1	0˚-summer-1.2-Glass C
2	0˚-summer-1.2-LEWF
3	0˚-summer-0.2-Glass C
4	0˚-summer-0.2-LEWF
5	0˚-winter-1.2-Glass C
6	0˚-winter-1.2-LEWF
7	0˚-winter-0.2-Glass C
8	0˚-winter-0.2-LEWF
9	40˚N-summer-1.2-Glass C
10	40˚N-summer-1.2-LEWF

11	40˚N-summer-0.2-Glass C
12	40˚N-summer-0.2-LEWF
13	40˚N-winter-1.2-Glass C
14	40˚N-winter-1.2-LEWF
15	40˚N-winter-0.2-Glass C
16	40˚N-winter-0.2-LEWF
17	65˚N-summer-1.2-Glass C
18	65˚N-summer-1.2-LEWF
19	65˚N-summer-0.2-Glass C
20	65˚N-summer-0.2-LEWF
21	65˚N-winter-1.2-Glass C
22	65˚N-winter-1.2-LEWF
23	65˚N-winter-0.2-Glass C
24	65˚N-winter-0.2-LEWF
25	Incand-1m
26	Halogen-1m
27	LED-1m
28	CFL-1m
29	UFT-1m
30	CFT-1m
31	FT-1m
32	Incand-adjacent
33	Halogen-adjacent
34	LED-adjacent
35	CFL-adjacent
36	UFT-adjacent
37	CFT-adjacent
38	FT-adjacent
39	Background (no indoor photolysis)

Unlike chapters 4 and 5, two important groups of secondary products produced through chemical reactions are also included in this analysis. These are the sum of peroxyacetyl nitrates (TOTPAN) and the sum of organic nitrates (TOTORGNO$_3$). The reactions of OH radicals with VOCs (such as alkanes and alkenes) produces RO$_2$ radicals which can then reacts with NO to mainly produce RO and NO$_2$ (~70%-90%). However, ~10-30% of these reactions (RO$_2$ with NO) can lead to the production of organic NO$_3$. An example is shown in R37 for a peroxy radical formed when α-pinene reacts with OH, (APINAO$_2$) reacts to form the respective organic nitrate, APINANO$_3$, which accounts for 23% of the overall reaction rate

$$APINAO_2 + NO \rightarrow APINANO_3 \qquad R37$$

These organic nitrate species (a total of 304 are included in the INDCM) are then summed in the model to give TOTORGNO$_3$.

When OH reacts with aldehydes, it is possible to form acetyl peroxy radicals with the formula, RCO$_3$. When NO$_2$ reacts with these radicals (e.g. peroxyacetyl radical (CH_3CO_3)), PAN can be produced (R38):

$$CH_3CO_3 + NO_2 \rightarrow PAN \qquad R38$$

Again, 234 are included in the INDCM in the model, so it is convenient to consider the sum of all of these species through TOTPAN.

Both of these groups of species are considered as indoor secondary pollutants, that form through indoor air chemistry. Previous studies have identified toxic impacts of PANs not only on animals and plants, but also on humans (Temple and Taylor, 1983; Vyskocil et al., 1998), such as skin cancer (Lovelock, 1977), changes in the DNA bases (Peak and Belser, 1969), mutagenicity (Shepson et al., 1986), phytotoxicity (Taylor, 1969) and eye irritation (Altshuller, 1983; Parrish et al., 2016). Organic nitrates were also found to have adverse health effects, including toxicity against endothelial progenitor cells (EPCs), rebound angina and endothelial and autonomic dysfunction (Gori and Daiber 2009). These two groups of species therefore act as a proxy for the potentially harmful species that can be formed through secondary chemistry indoors, so their concentrations can be explored under different lighting conditions.

6.4 Results

6.4.1 Comparison of different controlling factors on indoor photolysis rates.

Figures 6.1-6.10 show the average concentrations of O$_3$, HONO, HCHO, OH, HO$_2$, RO$_2$, TOTPAN and TOTORGNO$_3$ between 06:00-18:00 h for the selection of model runs described in Table 6.1. Table 6.2 shows the average concentrations of key chemical species between 06:00-18:00 h for the baseline scenario and the % difference in concentration between each scenario and the baseline. As shown in these figures and summarised in Table 6.2, all five factors have important impacts on indoor air chemistry.

Photolysis of O$_3$ causes a reduction in its concentration (R1) while photolysis of NO$_2$ forms NO and O (R5), the latter of which reacts with O$_2$ to produce O$_3$ (R4). As discussed in Chapters 4-5, the production of O$_3$ from NO$_2$ photolysis is more important than the reduction

in its concentration through its own photolysis. The concentrations of O_3 increase with increasing photolysis rates (Figure 6.1). The greatest deviations from the baseline (4 ppb) are for the following runs:

- Runs 1 and 5: the use of Glass C, CF=1.2 and for the longest and shortest day at the equator can cause a 90% increase in O_3 concentrations.
- Runs 9 and 17: the use of Glass C, CF=1.2 and for the longest day at 40˚N and 65˚N can cause 108% and 102% increase respectively in O_3 concentrations.
- For indoor artificial lights, different lights produce up to 5% (1m away from UFT, Run 29) and 54% (adjacent to CFL, Run 35) increases in the ozone concentration at distances of 1m and adjacent respectively relative to the baseline conditions (Table 6.2).

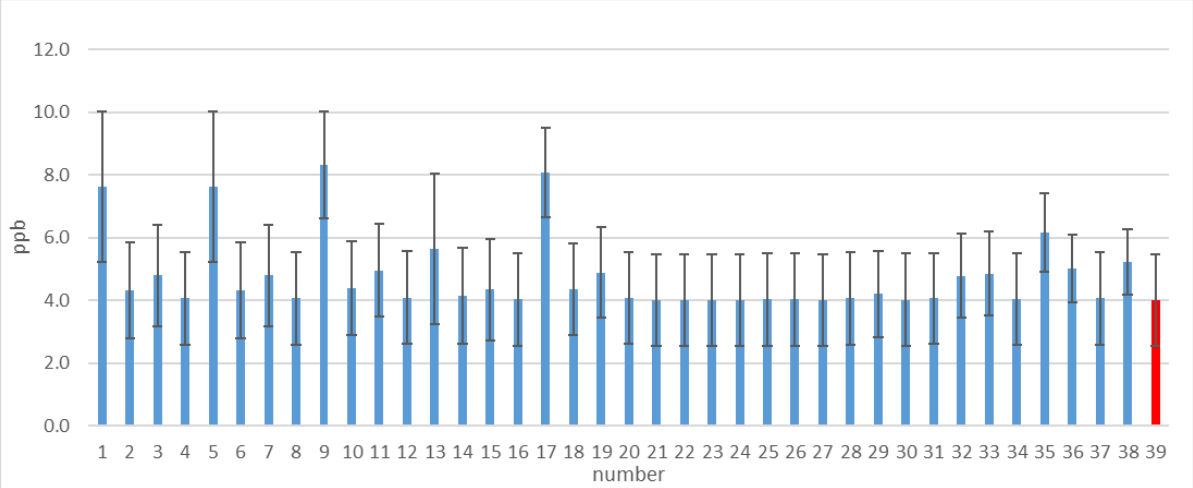

Figure 6.1: Average concentrations of O_3 with standard deviation between 06:00-18:00 h under different scenarios based on Table 6.1. The baseline scenario is marked in red.

Indoor photochemistry related to HONO is dominated by its photolysis. Photolysis of HONO (R6) reduces its concentration much more quickly than its production enhances it (e.g. the reaction of OH and NO to produce HONO). HONO concentrations therefore decrease with indoor photolysis compared to the baseline conditions for most selected scenarios, apart from winter and in high latitudes when daytime is very short and sunlight is less concentrated (Run14-16 and Run 21-24, Figure 6.2). The greatest deviations from the baseline concentration (253.8 ppt) are:

- Runs 1 and 5: the use of Glass C, CF=1.2 and for the longest and shortest day at the equator can cause a 34% decrease in HONO concentrations.
- Runs 9 and 17: the use of Glass C, CF=1.2 and for the longest day at 40˚N and 65˚N can cause 41% and 40% decrease respectively in HONO concentrations.
- The impacts of different indoor artificial lights on average HONO concentrations are relatively small compared to O_3. Different lights can cause up to 3% (1m away from UFT, Run 29) and 21% (adjacent to CFL, Run 35) decreases in HONO concentrations at the distances of 1m and adjacent respectively relative to the baseline conditions (Table 6.2).

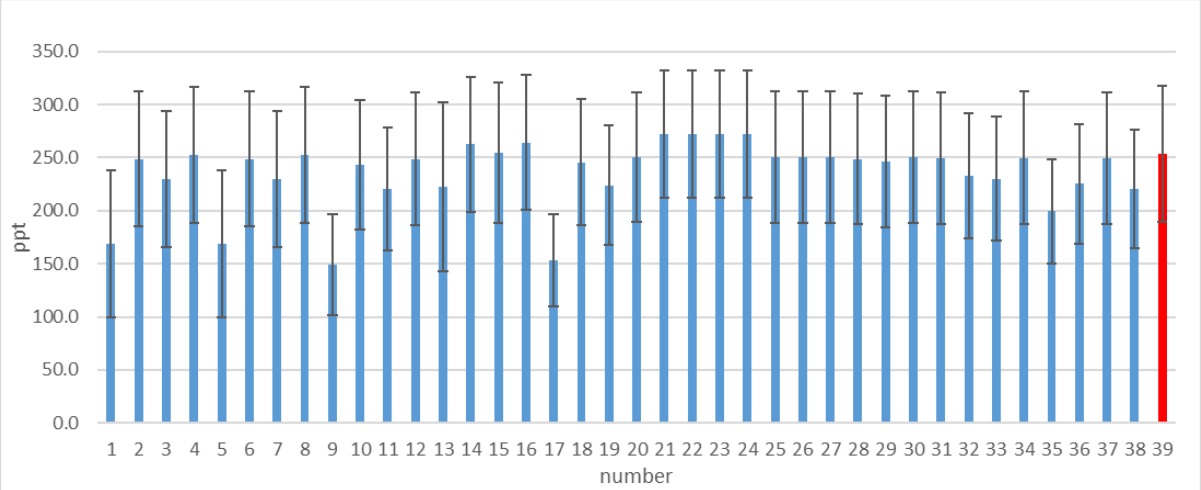

Figure 6.2: Average concentrations of HONO with standard deviation between 06:00-18:00 h under different scenarios based on Table 6.1. The baseline scenario is marked in red.

The impacts on NO_2 concentrations are similar to those for HONO, although the effects are smaller relative to those for HONO (Figure 6.3). The greatest deviations from the baseline concentration (3.6 ppb) are for the following runs:

- Runs 1 and 5: the use of Glass C, CF=1.2 and for the longest and shortest day at the equator can cause a 15% decrease in NO_2 concentrations.
- Runs 9 and 17: the use of Glass C, CF=1.2 and for the longest day at 40˚N and 65˚N can both cause ~17% decreases in NO_2 concentrations.
- For indoor artificial lights, different lights produce up to 1% (1m away from UFT, Run 29) and 11% (adjacent to CFL, Run 35) decreases in NO_2 concentrations at the

distances of 1m and adjacent respectively relative to the baseline conditions (Table 6.2).

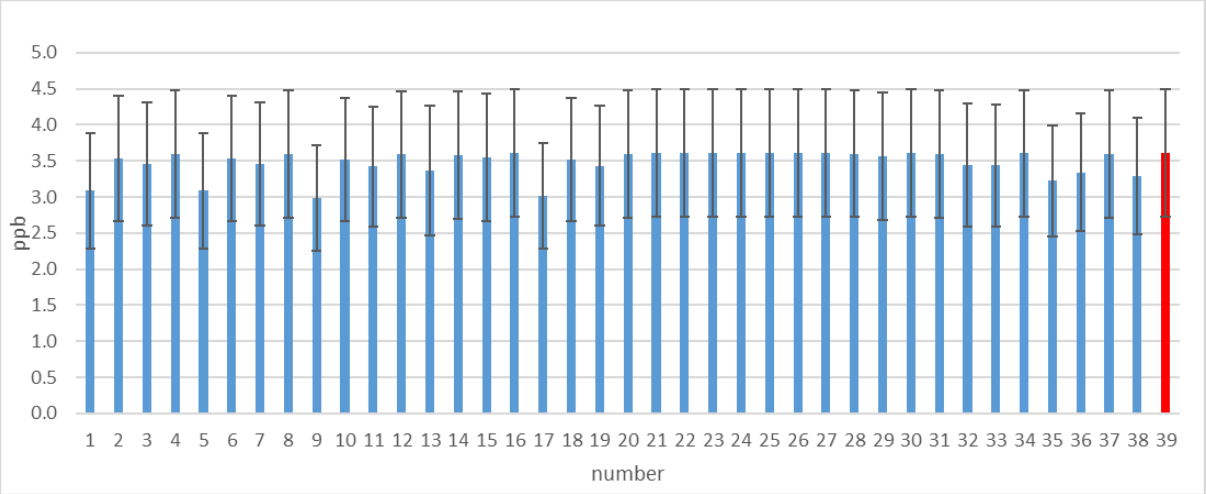

Figure 6.3: Average concentrations of NO_2 with standard deviation between 06:00-18:00 h under different scenarios based on Table 6.1. The baseline scenario is marked in red.

Photolysis of HCHO produces CHO and H which can react with O_2 to produce HO_2 radicals (R16-18). These reactions lead to the reduction of HCHO concentrations, although the differences between all selected scenarios and the baseline conditions are very small (<1%). The largest differences occur for Runs 1, 5, 9 and 17 (Figure 6.4). The concentration of HCHO indoors is clearly dominated by other factors, such as air exchange rate, deposition rate and so on. More sensitivity tests were carried out to further explore this point with the results shown in the next section.

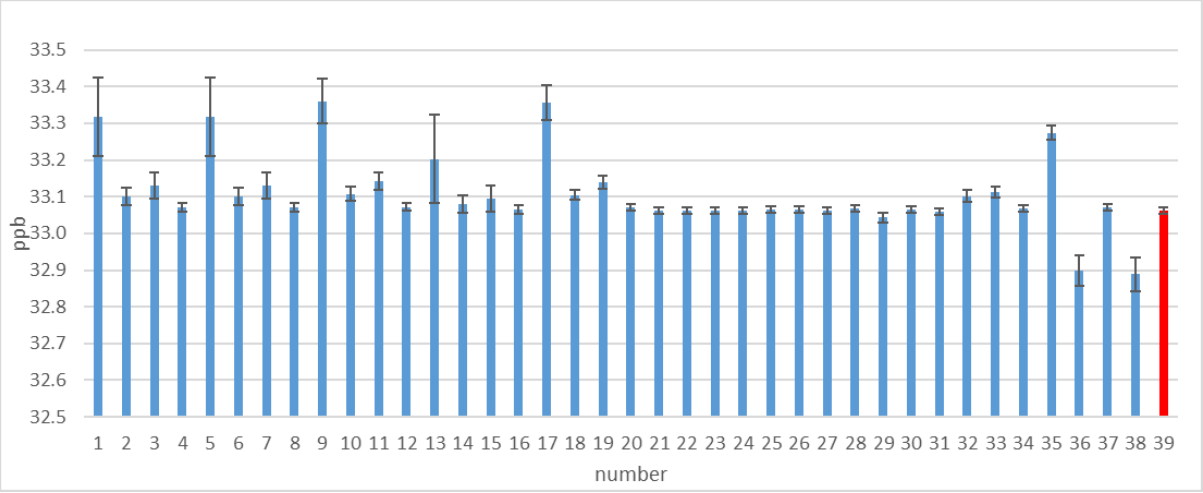

Figure 6.4: Average concentrations of HCHO with standard deviation between 06:00-18:00 h under different scenarios based on Table 6.1. The baseline scenario is marked in red.

Both photolysis of O_3 and HONO produce OH radicals, while OH can be reduced by reactions with VOCs, H_2O_2 and so on (Figure 1.3). Most of the selected scenarios have the highest impacts on average OH concentrations compared to the other species studied here (Figure 6.5). The greatest deviations from the baseline OH concentration (9.9×10^4 molecule/cm^3) are for the following runs:

- Runs 1 and 5: the use of Glass C, CF=1.2 and for the longest and shortest day at the equator can both cause a 657% increase in OH concentrations.
- Runs 9 and 17: the use of Glass C, CF=1.2 and for the longest day at 40˚N and 65˚N can cause 789% and 740% increases respectively in OH concentrations.
- For indoor artificial lights, different lights can cause up to 49% (1m away from UFT, Run 29) and 364% (adjacent to CFL, Run 35) increase in the OH concentrations at distances of 1m and adjacent respectively relative to the baseline conditions (Table 6.2).

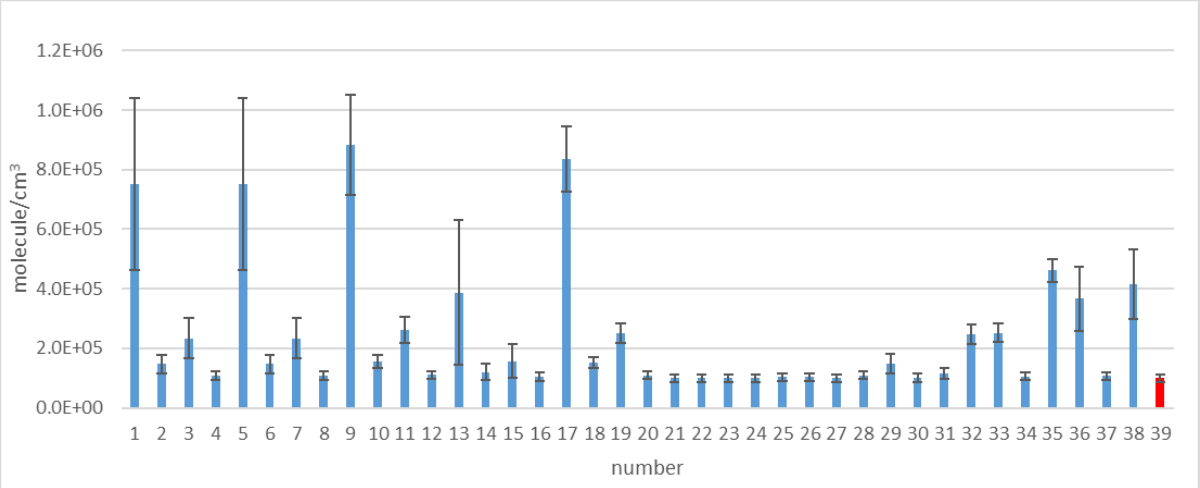

Figure 6.5: Average concentrations of OH with standard deviation between 06:00-18:00 h under different scenarios based on Table 6.1. The baseline scenario is marked in red.

The increase in TOTORGNO$_3$ for different scenarios mirrors the increase in OH radicals. Concentrations of TOTORGNO$_3$ are determined by the reactions of RO$_2$ with NO (e.g. R38). A higher photolysis rate leads to more NO (through NO$_2$ photolysis) and RO$_2$ can also be

enhanced by the reactions of OH with VOCs. This combination can lead to high concentrations of TOTORGNO$_3$. The greatest deviations from the baseline TOTORGNO$_3$ concentration (26.5 ppt) are for the following runs:

- Runs 1 and 5: the use of Glass C, CF=1.2 and for the longest and shortest day at the equator can cause a 515% increase in TOTORGNO$_3$ concentrations.
- Runs 9 and 17: the use of Glass C, CF=1.2 and for the longest day at 40˚N and 65˚N can cause 609% and 585% increases respectively in TOTORGNO$_3$ concentrations.
- For indoor artificial lights, different lights can cause up to 33% (1m away from UFT, Run 29) and 319% (adjacent to CFL, Run 35) increases in the TOTORGNO$_3$ concentrations at distances of 1m and adjacent respectively relative to the baseline conditions (Table 6.2).

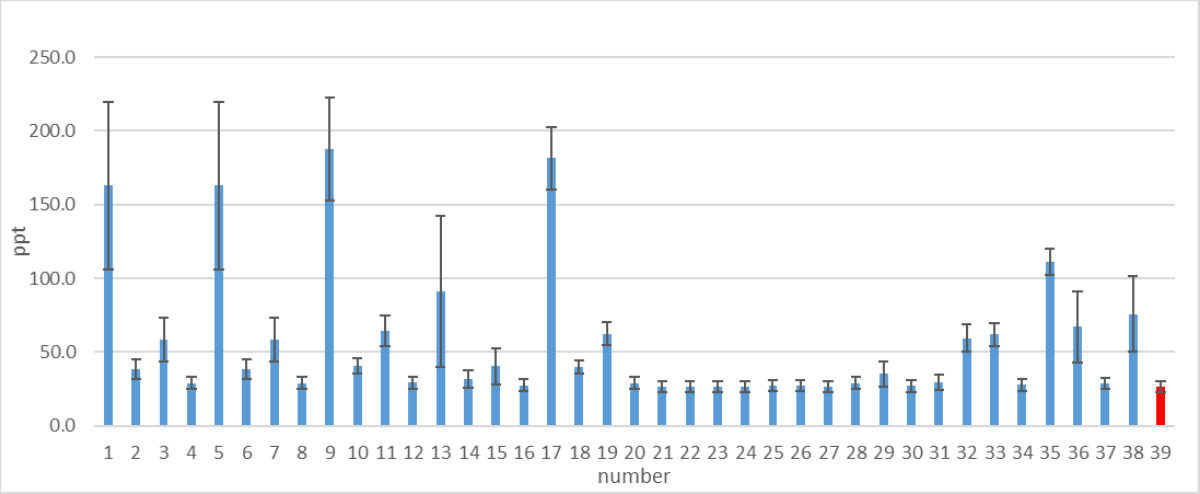

Figure 6.6: Average concentrations of total generated organic NO$_3$ (TOTORGNO$_3$) with standard deviation between 06:00-18:00 h under different scenarios based on Table 6.1. The baseline scenario is marked in red.

The impacts of different scenarios on the average concentrations of NO are large for some scenarios (Runs 1, 5, 9, 17 and 35), where photolysis rates of NO$_2$ are highest (and the largest decreases in the average concentrations of NO$_2$ happen) (Figure 6.7). The greatest deviations from the baseline NO concentration (0.7 ppb) are for the following runs:

- Runs 1 and 5: the use of Glass C, CF=1.2 and for the longest and shortest day at the equator can both cause a 271% increase in NO concentrations.

- Runs 9 and 17: the use of Glass C, CF=1.2 and for the longest day at 40˚N and 65˚N can cause 323% and 319% increase respectively in NO concentrations.
- For indoor artificial lights, different lights can cause up to 23% (1m away from UFT, Run 29) decrease and 217% (adjacent to CFL, Run 35) increase in the NO concentrations at distances of 1m and adjacent respectively relative to the baseline conditions (Table 6.2).

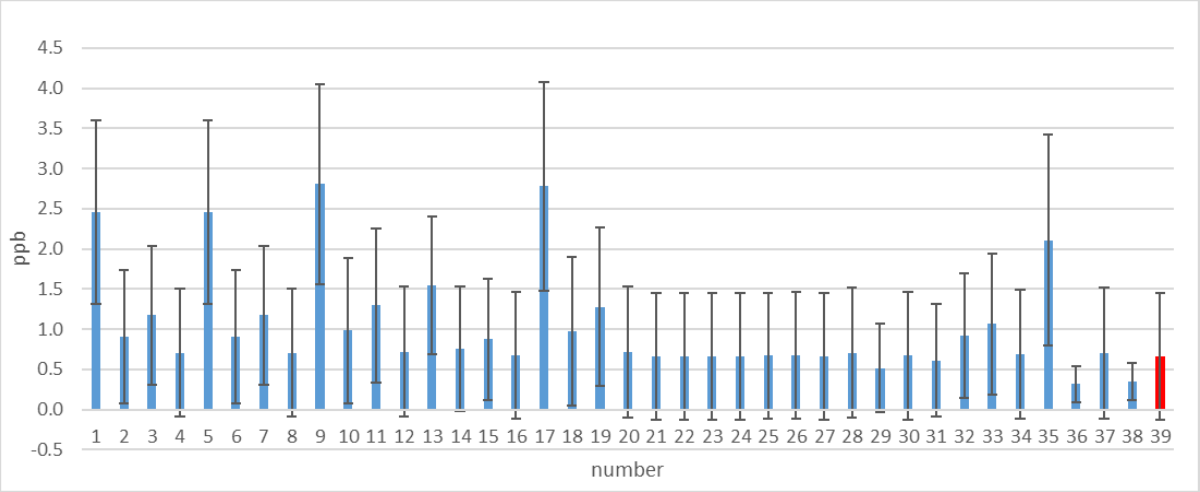

Figure 6.7: Average concentrations of NO with standard deviation between 06:00-18:00 h under different scenarios based on Table 6.1. The baseline scenario is marked in red.

Photolysis of HCHO produces HO_2 radicals (R16-18). Moreover, the OH produced by photolysis (e.g. O_3 and HONO) can then cycle to HO_2 (e.g. through the reaction of OH with HCHO, Figure 1.3) and RO_2 (e.g. by the reaction of OH with VOCs) radicals. Both HO_2 and RO_2 can react with NO which leads to reduced concentrations (Figure 1.3). For HO_2 radicals, the greatest deviations from the baseline concentration (3.7 ppt) are for the following runs:

- Runs 1 and 5: the use of Glass C, CF=1.2 and for the longest and shortest day at the equator can both cause a 23% increase in HO_2 concentrations.
- Run 9 and 17: the use of Glass C, CF=1.2 and for the longest day at 40˚N and 65˚N can cause 31% and 27% increase respectively in HO_2 concentrations.
- Some of the indoor artificial lights have much greater impacts on HO_2 concentrations compared to other controlling factors. 1m away from UFT (Run 29) can lead to a 69% increase in HO_2 concentrations. The greatest deviations from the baseline happen adjacent to UFT (Run 36) and FT (Run 38) lights, leading to 392% and 406%

increases in HO_2 concentrations respectively relative to the baseline conditions (Table 6.2). This is because of these runs coinciding with the lowest average NO concentrations (Figure 6.7)

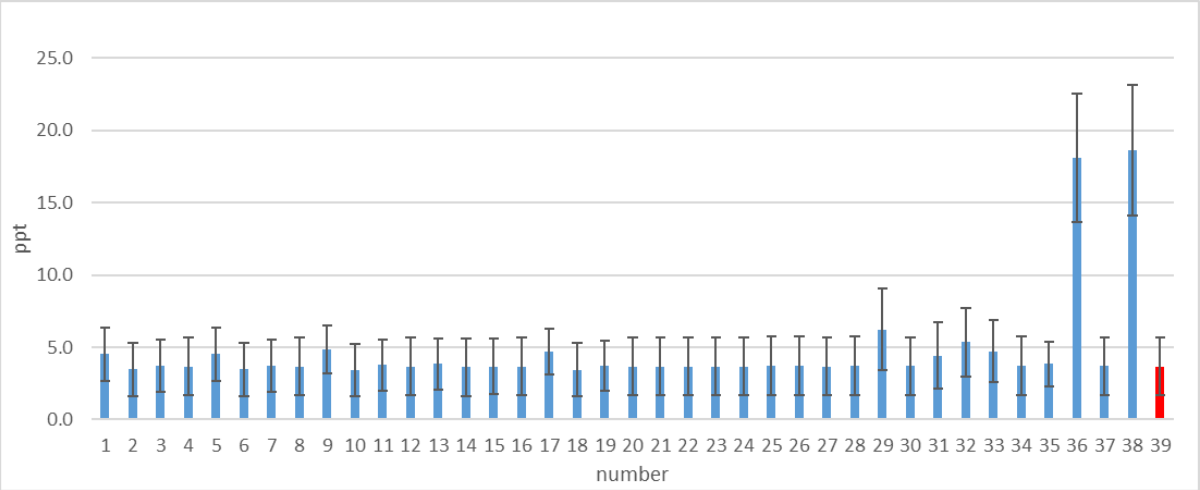

Figure 6.8: Average concentrations of HO_2 with standard deviation between 06:00-18:00 h under different scenarios based on Table 6.1. The baseline scenario is marked in red.

For RO_2 radicals, the greatest deviations from the baseline concentration (8.2 ppt) are for the following runs:

- Adjacent to UFT (Run 36) and FT (Run 38) can lead to 102% and 103% increases in RO_2 concentrations respectively relative to the baseline conditions, owing to the lowest average NO concentrations for these two scenarios (Figure 6.7).
- Adjacent to CFL (Run 35) can cause a 41% decrease in RO_2 concentrations, linked to a large increase in NO concentrations.
- The use of Glass C in some scenarios (e.g. Runs 1, 3, 5, 7, 11) can also have important impacts on RO_2 concentrations, causing an ~35% decrease.

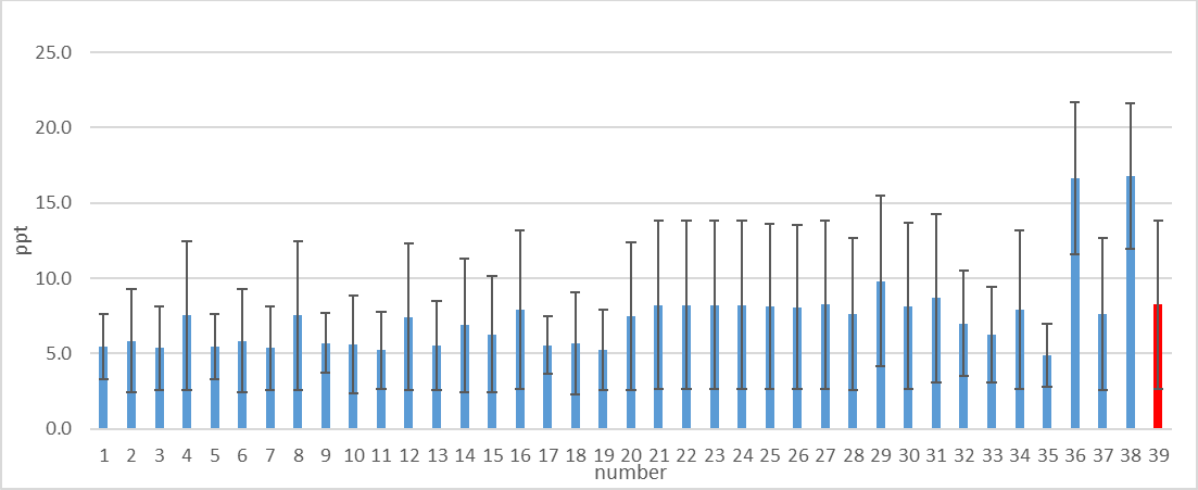

Figure 6.9: Average concentrations of RO_2 with standard deviation between 06:00-18:00 h under different scenarios based on Table 6.1. The baseline scenario is marked in red.

Deviations in the concentrations of TOTPANs are mainly related to those in OH concentrations, as NO_2 concentrations are largely invariant. The greatest deviations from the baseline TOTPANs concentration (166.4 ppt) are for the following runs:

- Runs 1 and 5: the use of Glass C, CF=1.2 and for the longest and shortest day at the equator can both cause a 92% increase in TOTPANs concentrations.
- Runs 9 and 17: the use of Glass C, CF=1.2 and for the longest day at 40˚N and 65˚N can cause 108% and 104% increases respectively in TOTPANs concentrations.
- For indoor artificial lights, adjacent to UFT (Run 36) and FT (Run 38) can cause 153% and 175% increases respectively in TOTPANs concentrations.

The deviations in concentrations of TOTPANs under the different scenarios are smaller than those in OH concentrations (Figure 6.10). Even though the production of PANs is reliant on the OH concentration, OH also reacts with other species, which vary depending on the photolysis rates as shown throughout this dissertation.

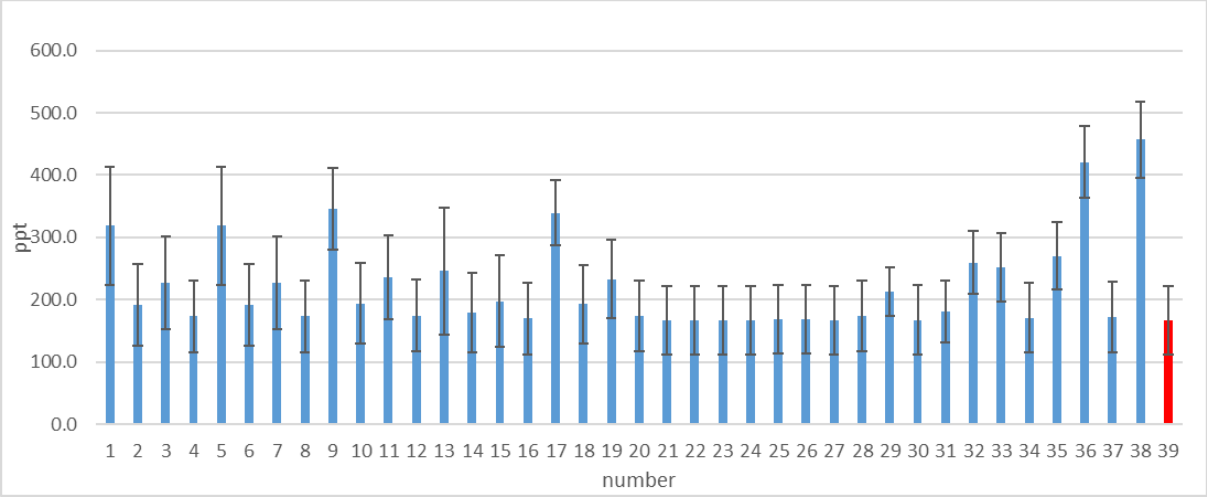

Figure 6.10: Average concentrations of total generated PANs (TOTPAN) with standard deviation between 06:00-18:00 h under different scenarios based on Table 6.1. The baseline scenario is marked in red.

In summary, the greatest deviations for many of the studied species (O_3, HONO, NO_2, HCHO, OH, $TOTORGNO_3$, NO) are seen for Runs 1, 5, 9 and 17 with the use of Glass C, CF=1.2, for both the longest and shortest day at the Equator and the longest day at 40˚N and 65˚N. Meanwhile, adjacent to UFT (Run 36) and FT (Run 38) can lead to the greatest deviations for predicted HO_2, RO_2 and TOTPAN concentrations.

Table 6.2: Average concentrations of key indoor species in the baseline scenario (dark indoors) between 06:00-18:00 h. O_3, HCHO, NO and NO_2 are in units of ppb; HONO, HO_2, RO_2, TOTPAN and $TOTORGNO_3$ in unit of ppt; OH in unit of 10^4 molecule/cm^3. Also shown are the differences (%) in concentrations for the different scenarios relative to the baseline. % difference = (chemical concentrations – baseline) / baseline × 100.

	O_3	HONO	HCHO	OH	HO_2	RO_2	NO	NO_2	TOTPAN	$TOTORGNO_3$
background	4.0	253.8	33.1	9.9	3.7	8.2	0.7	3.6	166.4	26.5
1	90.1	-33.6	0.8	657.0	22.9	-33.8	270.6	-14.6	91.7	514.6
2	7.9	-2.1	0.1	47.5	-5.3	-29.2	37.3	-2.2	14.9	45.2
3	19.6	-9.5	0.2	135.4	1.3	-34.9	76.8	-4.3	36.2	119.7
4	1.4	-0.4	0.0	8.9	0.1	-8.6	6.3	-0.5	4.1	8.4
5	90.1	-33.6	0.8	657.1	23.0	-33.8	270.6	-14.6	91.7	514.6
6	7.9	-2.1	0.1	47.5	-5.3	-29.2	37.3	-2.2	14.9	45.2
7	19.6	-9.5	0.2	135.4	1.3	-34.9	76.8	-4.3	36.2	119.7
8	1.4	-0.4	0.0	8.9	0.1	-8.6	6.3	-0.5	4.1	8.4
9	107.6	-41.4	0.9	789.4	31.2	-31.0	322.6	-17.4	107.9	608.9
10	9.5	-4.0	0.1	56.4	-6.5	-32.2	48.3	-2.7	16.7	53.2
11	23.5	-13.0	0.2	163.1	2.2	-36.7	95.4	-5.3	41.9	142.8
12	1.7	-2.0	0.0	10.8	0.0	-9.8	8.1	-0.6	4.7	10.0
13	40.9	-12.4	0.4	289.5	4.3	-33.0	133.2	-7.0	47.9	244.0

14	3.4	3.5	0.1	21.0	-1.8	-16.4	13.9	-1.0	8.1	20.1
15	8.4	0.2	0.1	58.0	-0.2	-23.8	31.6	-1.9	18.7	52.7
16	0.6	4.2	0.0	3.6	-0.1	-4.1	2.4	-0.2	1.8	3.5
17	101.5	-39.6	0.9	739.5	27.0	-32.7	318.7	-16.6	103.8	584.8
18	8.8	-3.2	0.1	52.5	-6.1	-31.0	47.2	-2.5	15.8	50.2
19	22.0	-11.7	0.2	152.0	1.5	-36.4	92.6	-4.9	40.0	135.6
20	1.6	-1.3	0.0	10.0	0.0	-9.1	7.8	-0.5	4.4	9.5
21	0.0	7.4	0.0	-0.2	-0.5	-0.2	0.1	0.0	-0.1	-0.1
22	0.0	7.4	0.0	-0.3	-0.5	-0.2	0.1	0.0	-0.1	-0.1
23	0.0	7.4	0.0	-0.3	-0.5	-0.2	0.1	0.0	-0.1	-0.1
24	0.0	7.4	0.0	-0.3	-0.5	-0.2	0.1	0.0	-0.1	-0.1
25	0.4	-1.4	0.0	3.2	1.6	-1.4	0.8	-0.1	1.6	2.7
26	0.5	-1.5	0.0	3.4	1.3	-2.0	1.3	-0.1	1.7	3.0
27	0.0	-1.3	0.0	0.2	0.1	0.0	-0.1	0.0	0.1	0.2
28	1.4	-1.9	0.0	9.6	0.8	-7.4	6.7	-0.4	4.2	9.1
29	4.8	-2.8	-0.1	49.2	69.0	18.9	-22.6	-1.2	27.8	32.5
30	0.2	-1.3	0.0	1.4	0.2	-1.2	0.9	-0.1	0.7	1.3
31	1.6	-1.8	0.0	15.9	20.6	5.2	-7.9	-0.4	8.8	11.0
32	19.5	-8.4	0.1	148.2	45.4	-15.3	38.7	-4.6	55.8	124.0
33	21.2	-9.3	0.1	153.7	28.3	-24.0	60.2	-4.9	51.1	133.4
34	0.8	-1.5	0.0	5.4	1.0	-4.2	3.5	-0.3	2.5	4.8
35	53.8	-21.4	0.6	364.0	4.6	-40.8	217.2	-10.8	62.5	318.7
36	25.2	-11.2	-0.5	268.3	391.6	101.7	-51.7	-7.6	152.6	153.4
37	1.4	-1.7	0.0	8.6	0.5	-7.3	6.7	-0.4	3.7	8.2
38	30.5	-13.1	-0.5	317.3	406.3	103.1	-47.2	-8.9	174.7	185.6

Table 6.3 shows the average impacts of the different controlling factors on all key studied species compared to baseline conditions. These values were calculated by averaging all scenarios with the same controlling factor (e.g. all scenarios with the use of Glass C were selected and the differences between concentrations of O_3 in these scenarios and the baseline condition were averaged to identify the impacts of Glass C on O_3). As shown in this table, simulations with Glass C produced the highest impacts on all of the studied species concentrations except for HO_2 and TOTPAN, whilst the simulations run 1 m away from indoor artificial lights had the lowest impacts (except for HO_2). Overall, cloudiness and the time of year had the next biggest impact, followed by latitude and distance to artificial light source. The largest deviations for HO_2 concentrations were adjacent to artificial lights, and these were approximately 10 times higher than simulations 1 m away from the artificial lights. The simulations adjacent to artificial lights also had the highest impacts on the production of TOTPANs, whilst 1m away from artificial lights had the lowest effects. For RO_2, the differences between the impacts from the different controlling factors are small,

with up to an approximately 25-28% decrease relative to the baseline conditions for changes in glass composition, cloudiness , time of year and latitude.

Table 6.3: Average percentage deviations from baseline concentrations for different factors and for each key species, as well as the overall average impact for all species of each controlling factor.

Factor		O_3	HONO	HCHO	OH	HO_2	RO_2	NO	NO_2	TOTPAN	$TOTORGNO_3$	Average
Window material	Glass C	43.6	-15.8	0.4	314.6	9.5	-27.6	140.8	-7.6	51.3	253.1	76.2
	LEWF	3.7	0.6	0.1	22.2	-2.2	-14.9	17.9	-1.1	7.4	21.1	5.5
Cloudiness factor	CF=1.2	39.0	-12.8	0.4	279.7	6.9	-25.2	125.0	-6.7	42.8	223.4	67.2
	CF=0.2	8.3	-2.4	0.1	57.1	0.4	-17.3	33.7	-1.9	16.0	50.8	14.5
Season	summer	32.9	-13.5	0.3	235.2	5.7	-27.1	111.0	-6.0	40.2	190.2	56.9
	winter	14.3	-1.7	0.1	101.7	1.6	-15.4	47.7	-2.6	18.6	84.0	24.8
Latitude	0˚	29.7	-11.4	0.3	212.2	4.8	-26.6	97.8	-5.4	36.7	172.0	51.0
	65˚	16.7	-3.3	0.2	119.1	2.5	-13.8	58.4	-3.1	20.4	97.5	29.5
Artificial lights	1m	1.3	-1.7	0.0	11.8	13.4	1.7	-3.0	-0.3	6.4	8.6	3.8
	adjacent	21.8	-9.5	0.0	180.8	125.4	16.2	32.5	-5.4	71.8	132.6	56.6

Table 6.3 also shows the impacts of different factors (latitude, season, window material, cloudiness factor and indoor artificial light) on all of the studied species on average. These percentage values were calculated by averaging the deviations from baseline values for each of the controlling factors for all of the species. In summary, glass type gives rise to 70.7% (76.2-5.5%), cloudiness to 52.7%, difference in time of year to 32.1%, difference in latitude to 21.5% and proximity of artificial light to 52.8%, when averaging the deviations for each controlling factor on all of the key species that were investigated.

6.4.2 Impact on model predicted concentrations of individual species

The box and whisker plots (Figure 6.11) show the minimum, 25th percentile, median, 75th percentile and maximum predicted concentrations for each of the key species and over the 38 model runs. This figure confirms that the greatest variations are seen in the predicted OH, $TOTORGNO_3$ and NO concentrations, with 142, 113 and 56% average differences from the baseline respectively. There were intermediate impacts on TOTPAN, HO_2 and O_3 concentrations, with 33, 28 and 19% average differences from the baseline respectively. Finally, there were very few impacts on RO_2, HONO, NO_2 and HCHO concentrations with 10, 7, 4 and approximately 0 % average differences from the baseline respectively (Table 6.2, Figure 6.11).

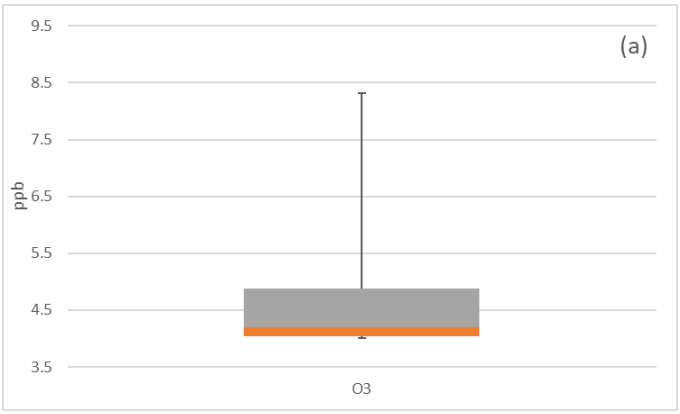
(a)
9.5
8.5
7.5
6.5
5.5
4.5
3.5
ppb
O3

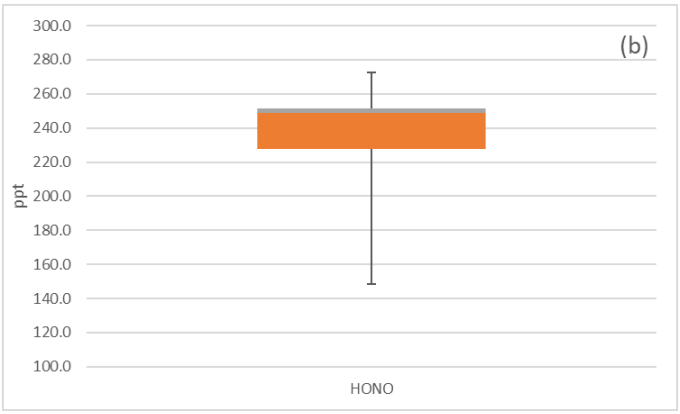
(b)
300.0
280.0
260.0
240.0
220.0
200.0
180.0
160.0
140.0
120.0
100.0
ppt
HONO

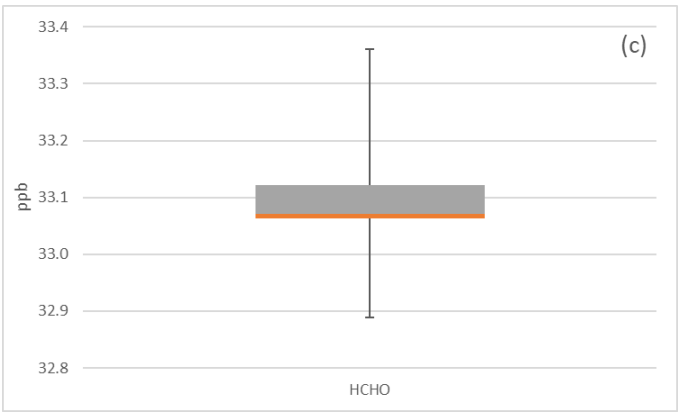
(c)
33.4
33.3
33.2
33.1
33.0
32.9
32.8
ppb
HCHO

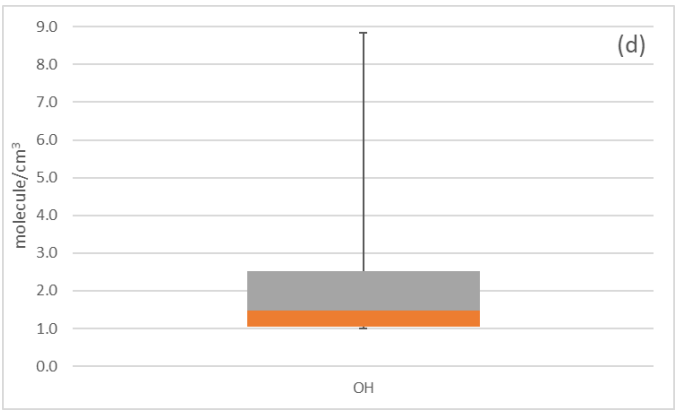
(d)
9.0
8.0
7.0
6.0
5.0
4.0
3.0
2.0
1.0
0.0
molecule/cm³
OH

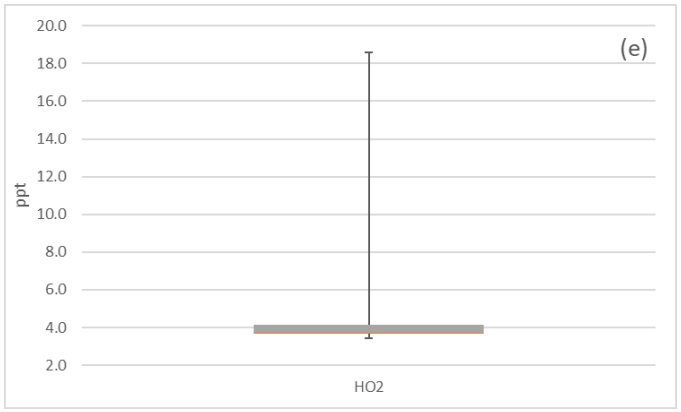
(e)
20.0
18.0
16.0
14.0
12.0
10.0
8.0
6.0
4.0
2.0
ppt
HO2

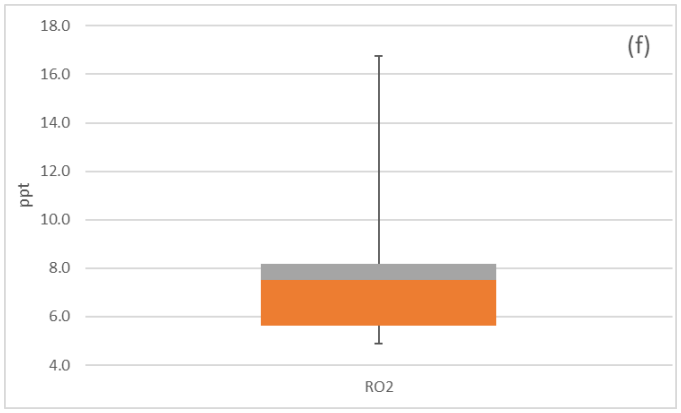
(f)
18.0
16.0
14.0
12.0
10.0
8.0
6.0
4.0
ppt
RO2

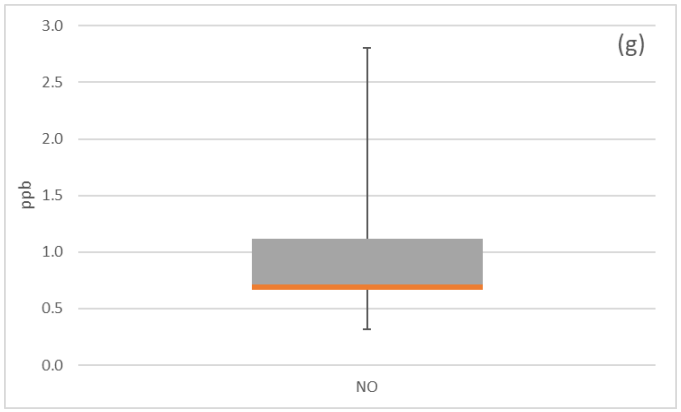
(g)
3.0
2.5
2.0
1.5
1.0
0.5
0.0
ppb
NO

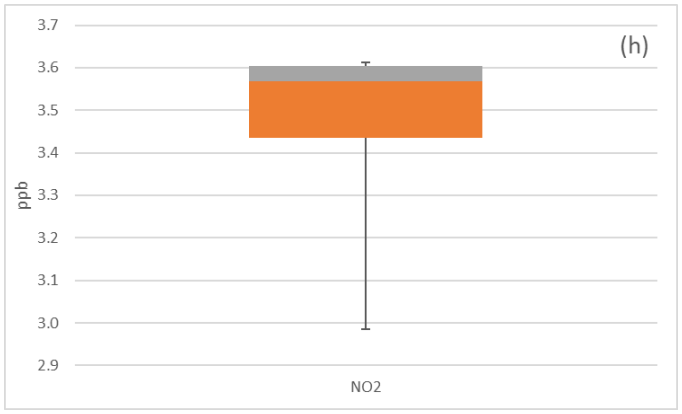
(h)
3.7
3.6
3.5
3.4
3.3
3.2
3.1
3.0
2.9
ppb
NO2

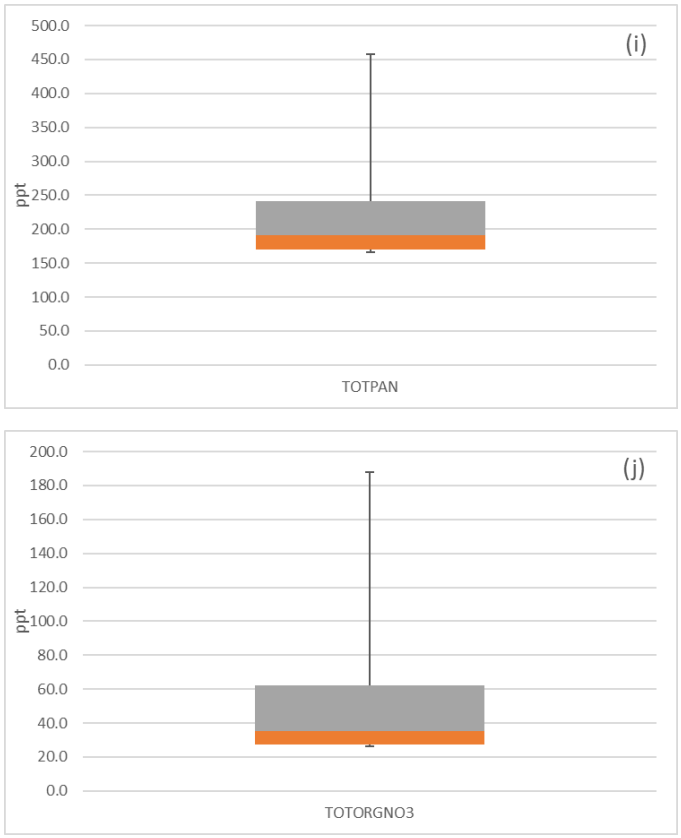

Figure 6. 11: (a) to (j) show the distribution of average concentrations of the key indoor species studied between 06:00-18:00 h. The box and whisker plot shows the minimum, 25%, median, 75% and maximum values in different units (O_3, HCHO, NO and NO_2 in unit of ppb; HONO, HO_2, RO_2 TOTPAN and $TOTORGNO_3$ in unit of ppt; OH in unit of 10^5 molecule/cm^3).

The HCHO and NO_2 concentrations are relatively invariant throughout these scenarios (and chapters 4 and 5), suggesting that indoor photolysis does not control their concentrations. Another four sensitivity tests were carried out, in which the deposition rate, air exchange rate, outdoor HCHO concentration or outdoor NO_2 concentration were doubled. For HCHO, the results show that doubling the deposition rate, air exchange rate or outdoor HCHO concentration caused the average HCHO concentration (between 06:00-18:00 h) to decrease by 45% and 13% and increase by 2% respectively compared to the baseline condition. According to Mendez et al. (2015), deposition processes and ventilation determined the loss rate of HCHO in their study of a French classroom and contributed to 25% and 75% of the HCHO loss respectively with an AER of 2 h^{-1} and 73% and 26% respectively with an AER of 0.2 h^{-1}.

For NO_2, the results show that doubling the deposition rate, air exchange rate or outdoor NO_2 concentration caused the average NO_2 concentration (between 06:00-18:00 h) to decrease by

45%, and increase by 68% and 193% respectively compared to the baseline. Therefore, both HCHO and NO_2 concentrations are clearly controlled by factors other than photolysis.

6.5. Conclusion

Glass composition leads to the highest deviations in predicted concentrations (71%) relative to baseline conditions for most of the key species, followed by cloudiness and proximity of artificial light (~53%). Meanwhile, time of year and latitude also have important impacts on the predicted indoor concentrations of key chemicals with average deviations of 32% and 22% respectively.

For all of the controlling factors studied, the greatest impacts are for OH concentrations (142% average difference), followed by $TOTORGNO_3$ (113% average difference) and then NO (56% average difference). Meanwhile, relatively small differences are predicted in TOTPAN (33% average difference), HO_2 (28% average difference) and O_3 (19% average difference) concentrations. Moreover, there are relative small impacts on predicted RO_2 (10% average difference) and HONO (7% average difference) concentrations. Variations in NO_2 (4% average difference) and HCHO (close to zero on average) concentrations are both small, with other factors such as exchange rate, deposition rate and outdoor concentrations shown to be more important in determining their indoor concentrations.

This chapter has shown that most of the indoor artificial lights have relatively small impacts on indoor air chemistry, particularly LED (see Run 27). For this reason, they could be recommended for use in areas where people spend time, as the concentrations of TOTPAN and $TOTORGNO_3$ (as proxies for harmful secondary pollutant formation) are found to be unchanged when LED lighting is used, relative to the same conditions in the dark. Note also that it is better to be at least 1m from indoor artificial lights, as the concentrations of TOTPAN and $TOTORGNO_3$ are 11 and 15 times higher respectively when adjacent to the lights). Glasses with a higher wavelength cut-off (e.g. LEWF) are also recommended to be used based on their lower impacts on indoor air chemistry (the predicted concentrations for Glass C are 7 and 12 times higher than LEWF for TOTPAN and $TOTORGNO_3$ respectively).

Using LEDs and glass with a film can effectively reduce the formation of radicals which can themselves lead to the formation of secondary pollutants (e.g. PANs, organic nitrates and particulate matter). It is also confirmed that HCHO and NO_2 concentrations are clearly controlled by factors other than photolysis. Therefore, reduced photolysis rates can

effectively reduce concentrations of O_3, PANs and organic nitrates, but not lead to an increased concentration of NO_2 and HCHO concentrations (which also have known health effects). Clearly, there is little to be gained by replacing one harmful pollutant with another.

However, there are still many uncertainties with this analysis. This chapter only focused on 10 key chemicals, however, there are many other potentially important chemicals with known health effects, which may play an important role in indoor air chemistry (e.g. acetaldehyde). Also, as stated in chapter 4, it is hard to be more definitive about differential health impacts, when toxicological data for many air pollutants are absent. Therefore, future research should focus more on the health effects of common indoor air pollutants and the different mixtures that can form for different lighting conditions.

Chapter 7: Case studies: impact of indoor photolysis on radical production following cleaning activities

7.1. Photolysis driven indoor air chemistry following cleaning of hospital wards

7.1.1. Abstract

It is essential to identify effective cleaning techniques for the sterilization of rooms in industrial settings, hospitals and also public buildings. No-touch devices (NTDs) are a relatively recent innovation for automated cleaning, which use disinfectants such as chlorine dioxide (OClO), ozone (O_3), formaldehyde (HCHO) and hydrogen peroxide (H_2O_2) at very high concentrations. A previously unconsidered potential consequence of such cleaning technologies is the photochemical formation of high concentrations of hydroxyl radicals (OH), hydroperoxy radicals (HO_2), organic peroxy radicals (RO_2), and chlorine radicals (Cl) which can form harmful reaction products when exposed to other chemicals commonly found in indoor air. Measured indoor photon fluxes and typical disinfectant concentrations were used to drive a model, that calculated radical concentrations during and after cleaning events. Photolysis of disinfectants was initiated by sunlight, fluorescent tubes without covers, and plastic-covered fluorescent tubes. Maximum radical concentrations occurred following photolysis of disinfectants, when concentrations were found to be orders of magnitude higher than background levels. Maximum predicted radical concentrations were 1.3×10^7 molecule/cm^3 for OH, 2.4 ppb for HO_2, 6.8 ppb for RO_2 and 2.2×10^8 molecule/cm^3 for Cl. These elevated concentrations may persist for several hours after the cleaning event, depending on the air composition and air exchange rate. There is the potential, therefore, for elevated radical concentrations which can in turn form potentially harmful secondary pollutants leading to adverse health effects for occupants, especially for vulnerable people (e.g. old and young people).

7.1.2. Introduction

As we spend more time indoors, it has become increasingly important to consider how we might keep the air inside clean. The preferred approach is to remove sources of pollution from a building, though such sources can often be hard to control because of occupant activities in the building. Another approach is through dilution by ventilation, but this assumes that outdoor air is clean and if using mechanical ventilation, also requires energy. The final approach is to adopt one of the numerous methods of air cleaning (Siegel, 2016).

These can include techniques such as electrostatic precipitation, ion generation, UV germicidal irradiation, filtration (of particles), adsorption and thermal-or photocatalytic oxidation (Zhang et al., 2011). However, according to Zhang et al. (2011), many air cleaning technologies can produce undesirable secondary products when used and none of the technologies they reviewed removed all pollutants effectively indoors.

Specialised indoor environments such as hospital wards require scrupulously clean air, where it is essential to eliminate harmful pathogens. Air cleaning in hospitals is used to prevent the spread of infections amongst occupants, but particularly among the patients, many of whom will have compromised immune systems. The rise of drug resistant bacteria such as vancomycin-resistant enterococci (VRE) (Martinez et al., 2003; Bhalla et al., 2004; Duckro et al., 2005; Huang et al., 2006; Drees et al., 2008; Hayden et al., 2008; White et al., 2008) and methicillin-resistant *Staphylococcus aureus* (MRSA) (Boyce et al., 1997; Martinez et al., 2003; Bhalla et al., 2004; Hardy et al., 2006; Huang et al., 2006; Sexton et al., 2006; White et al., 2008) require that rooms are cleaned effectively, in order to protect patients and prevent the spread of infections.

Wiping surfaces by hand with bleach or other liquid cleaning agents are the most traditional cleaning techniques, but are often less than 100% effective, time-consuming and labour-intensive. In addition, pathogens can reside on inaccessible surfaces and antibacterial resistance can also be an issue (French et al., 2004; Jeanes et al., 2005; Otter and French 2009; Manian et al., 2011). According to Carling et al. (2008), only 48% of high-risk surfaces in hospital rooms were adequately cleaned between different patients on average, although this number was increased to 77% by improved cleaning protocols. However, this still leaves almost 20% of high-risk surfaces with potential contamination.

Automated cleaning techniques (sometimes referred to as no-touch devices, NTDs) have been developed to clean and disinfect surfaces more effectively than traditional cleaning, not only in hospitals, but also in the food industry and laboratories (Boyce 2009; Otter et al., 2013; Loveday et al., 2014 etc.). NTDs are much more effective than traditional cleaning techniques and other automated techniques (e.g. ultraviolet light), and can eliminate harmful pathogens in areas inaccessible to human hands and UV instruments (Dancer 2013; Otter et al., 2013; Weber et al., 2016).

This technique is very convenient to use. The NTD is placed in the room to be cleaned, and the windows and doors of the room kept shut during operation (Figure 7.1.1). NTDs use very

high concentrations of disinfectant gases, typically many hundreds of ppb (parts per billion) to thousands of ppm (parts per million) (Currier et al., 2001; Rogers et al., 2007; Rogers et al., 2008; Beswick et al., 2011; Byrns and Fuller 2011; Davies et al., 2011; Fu et al., 2012; Murdoch et al., 2016).

Figure 7.1.1: No-touch devices, NTDs (STERIS, nd).

NTDs can use a number of different disinfectant gases. Hydrogen peroxide (H_2O_2) is a popular cleaning agent for NTDs, since it has relatively low effects on human health and is a very effective biocide and virucide (McDonnell and Russell 1999; French et al., 2004; Jeanes et al., 2005; Andersen et al., 2006; Otter and French 2009; Carling et al., 2008; Pottage et al., 2010; Manian et al., 2011; Passaretti et al., 2013; Zonta et al., 2016). During the operation of NTDs, the H_2O_2 vapour is released into a sealed room where it can condense onto surfaces and efficiently kill viruses and bacteria (French et al., 2004; Andersen et al., 2006; Boyce 2009; Otter and French 2009; Otter et al., 2010; Passaretti et al., 2013; Zonta et al., 2016)

Industrial, food, medical and laboratory settings commonly use formaldehyde (HCHO) as a disinfectant (Fink et al., 1988; Lach 1990; Munro et al., 1999; Mitchell et al., 2000; Rogers et al., 2007). Gaseous HCHO is formed by heating paraformaldehyde. At the end of the cleaning period, it is neutralized by using ammonia gas generated from ammonium carbonate to form hexamethylenetetramine powder, which can be easily removed (Mitchell et al., 2000). Such a technique was used for disinfection purposes during the 2001 United States anthrax attacks (Munro et al., 1999; Canter et al., 2005; Rogers et al., 2007; Rogers et al., 2008).

Chlorine dioxide (OClO) and ozone (O_3) can also be used as cleaning agents in NTD systems to combat highly infectious diseases (Rogers et al., 2008; Beswick et al., 2011). Bioclean

rooms, food products and water supplies usually use O_3 to clean (Rice 2002; Kim et al., 2003). OClO is commonly used in the food industry, in pulp mills (particleboard manufacturing) and to treat drinking water, and was also used for remediation after the 2001 anthrax attacks (Canter et al., 2005; Gordon and Rosenblatt 2005; Rogers et al., 2008; Lowe et al., 2013). OClO has also been used to deal with bed bugs in hospitals (Gibbs et al., 2012), but it must be generated on site and kept in the dark prior to use and the treated area must be sealed due to its toxic nature.

Owing to the high concentrations of disinfectant gases used in NTDs, there have been safety concerns around the toxicity of the cleaning agents (Puskar and Plese 1996; Weschler and Shields 1996; Erickson et al., 2012; Fu et al., 2012). However, the secondary pollutants formed from reactions involving these disinfectants have not been considered to date. There is the potential for secondary reactions or indoor photolysis of these gases to produce radical species, which can then further react to form potentially harmful species. Figure 7.1.2 shows some of the potential reactions that arise following use of these 4 NTD gases indoors. Photolysis of O_3 and H_2O_2 produces OH, whilst photolysis of HCHO and OClO produces HO_2 and Cl respectively. The produced radicals can then be cycled to each other and also RO_2 through various reactions (Figure 7.1.2)

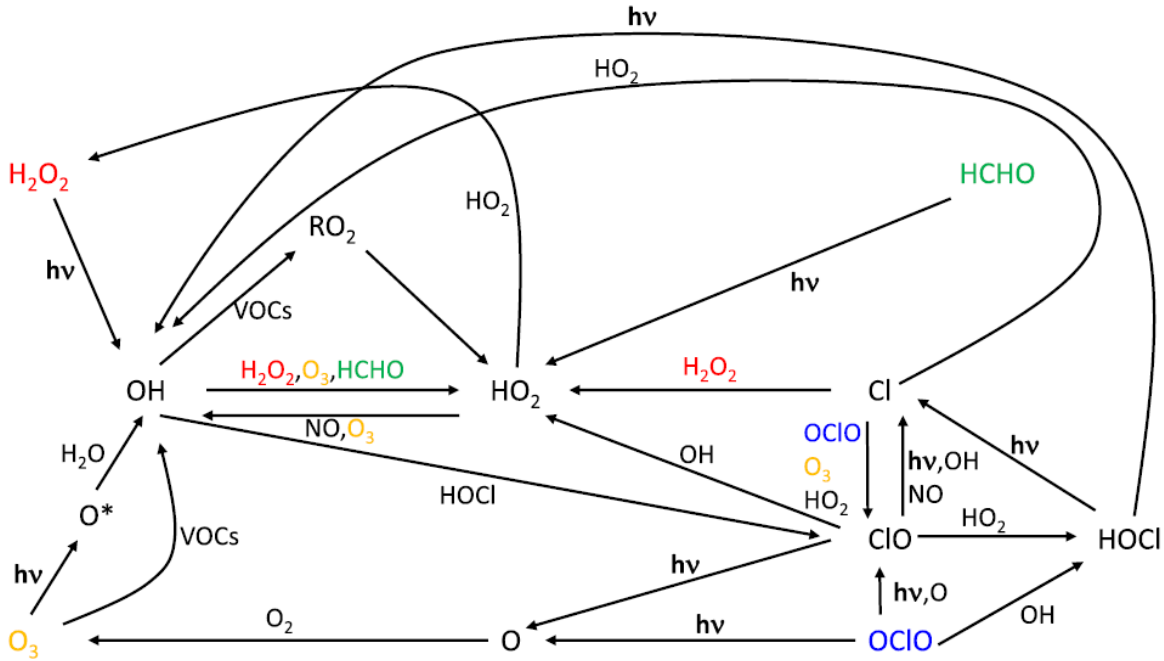

Figure 7.1.2: The formation of radicals from NTD disinfectant gases and some of the subsequent reactions. The NTD gases are shown as: O_3 (gold), H_2O_2 (red), HCHO (green) and OClO (blue). 'hν' denotes photolysis reactions.

The aim of this section is to investigate radical behaviour indoors during and after simulated NTD cleaning events using O_3, OClO, HCHO and H_2O_2. The specific objectives are to:

- Use measured photolysis rate coefficients to calculate the concentrations of OH, HO_2, and Cl indoors following NTD use.
- Investigate the concentrations of RO_2 radicals during NTD use, given they coexist with other radical species and can contribute to OH formation (Figure 7.1.2).
- To investigate radical behaviour during and following the use of these technologies and under different lighting conditions.

7.1.3. Methods

7.1.3.1. Model

The concentrations of each disinfectant gas, radical and other indoor trace gases were calculated using the INDCM (INdoor Detailed Chemical Model) (Carslaw 2007; Carslaw et al., 2012; Kruza et al., 2017) as described in chapter 3. For this work, the model was used as described in Wong et al. (2017) for chlorine cleaning, but adapted through the addition of reactions to account for additional OClO chemistry not in the MCM (Table 7.1.1), with rate coefficients from the IUPAC recommendations (IUPAC nd).

Table 7.1.1: New reactions added to the model together with their rate coefficients.

Reactions	Rate coefficients
$NO + OClO \rightarrow NO_2 + ClO$	$2.5 \times 10^{-12}\, e^{(-600/temp)}$ (cm^3 $molecule^{-1}$ s^{-1})
$Cl + OClO \rightarrow ClO + ClO$	$3.4 \times 10^{-11}\, e^{(160/temp)}$ (cm^3 $molecule^{-1}$ s^{-1})
$O + OClO \rightarrow ClO$	$2.4 \times 10^{-12}\, e^{(-960/temp)}$ (cm^3 $molecule^{-1}$ s^{-1})
$OH + OClO \rightarrow HOCl$	$1.4 \times 10^{-12}\, e^{(600/temp)}$ (cm^3 $molecule^{-1}$ s^{-1})
$ClO + hv \rightarrow O + Cl$	Dark: 0 CF: 0 BF: 7.96×10^{-6} (s^{-1}) ATT: 0

$ClOOCl + hv \rightarrow ClOO + Cl$	Dark: 0 CF: 2.91×10^{-7} (s^{-1}) BF: 2.05×10^{-5} (s^{-1}) ATT: 7.03×10^{-5} (s^{-1})
$ClO + ClO \rightarrow ClOOCl$	$K190 = 2 \times 10^{-32} \times ((temp/300)^{-4}) \times M$ $K19I = 1 \times 10^{-11}$ $KR19 = K190/K19I$ $FC19 = 0.6$ $N19 = (0.75\text{-}1.27 \times LOG_{10}(FC19))$ $F19 = 10^{(LOG10(FC19)/(1+(LOG10(KR19)/N19)^2))}$ Rate coefficient (KMT19) = (K190 × K19I) × F19/(K190+K19I) (cm^3 $molecule^{-1}$ s^{-1})
$ClOOCl \rightarrow ClO + ClO$	$K200 = 3.7 \times 10^{-7} e^{(-7690/temp)} \times M$ $K20I = 1.8 \times 10^{14} e^{(-7690/temp)}$ $KR20 = K200/K20I$ $FC20 = 0.6$ $N20 = (0.75\text{-}1.27 \times LOG_{10}(FC20))$ $F20 = 10^{(LOG10(FC20)/(1+(LOG10(KR20)/N20)^2))}$ Rate coefficient (KMT20) = (K200 × K20I) × F20/(K200+K20I) (s^{-1})
$ClOO + M \rightarrow Cl + O_2 + M$	$5.62 \times 10^{-13} \times N_2$ (cm^3 $molecule^{-1}$ s^{-1})

*temp=temperature; $M=2.51\times10^{19}$ molecule/cm^3. All information is from IUPAC website (http://iupac.pole-ether.fr/). *Dark: dark indoors. *CF: covered fluorescent tube. *BF: bare fluorescent tube. *ATT: attenuated sunlight + covered fluorescent tube.

As described in chapter 3, the INDCM includes terms that represent both indoor and attenuated outdoor lighting, which are added together to give the total photolysis rate (Carslaw 2007; Wong et al., 2017). The method described in Carslaw (2007) was used for all 37 species in the model that undergo photolysis (this work was started before the model modifications were completed), with the exception of the four disinfectant gases under investigation (see next section).

7.1.3.2. Hospital ward conditions in the model

A ward volume of 35 m^3 was assumed with an area to volume ratio of 1 m^2/m^3 (Wong et al., 2017). The internal temperature was assumed to be 293 K with 50% relative humidity. Outdoor VOC concentrations were initialized based on Sarwar et al. (2002), whilst annual mean concentrations of CO, SO_2, NO and NO_2 (250, 0.6, 2.7 and 13.5 ppb respectively) from the west Toronto/downtown were used to initialize the model (OMECC, 2016) following Wong et al. (2017). Under baseline conditions, internal O_3, NO and NO_2 concentrations were approximately 30 ppb, 80-130 ppt (higher with more light) and 8 ppb respectively averaged from 09:00 h to 17:00 h.

Typical air change rates of ~6.5 h^{-1} for regular outpatient rooms in hospitals have been reported (Knibbs et al., 2011), but this includes recirculation. The exchange rate with outdoor air was ~2 h^{-1} (Knibbs et al., 2011), so this value was used in the model. The model results were similar (<3%) even if 6.5 h^{-1} was used, given that the ventilation is assumed to be off when disinfection occurs. Ventilation was stopped in the model at 10:00 h, and the emission from the NTD was assumed to begin. The emissions were set to provide the approximate concentrations reported in the literature for NTD use: 25 ppm for ozone (Currier et al., 2001; Davies et al., 2011), 1000 ppm for formaldehyde (Rogers et al., 2007; Rogers et al., 2008; Beswick et al., 2011), 100-500 ppm for H_2O_2 (Fu et al., 2012; Murdoch et al., 2016), and 3000 and 350 ppm for OClO (to reflect two commonly used concentrations) (Rogers et al., 2008; Byrns and Fuller 2011). This required emission rates of 0.01 ppm s^{-1} to generate 25 ppm of O_3, 0.5 ppm s^{-1} for 1000 ppm of HCHO, 0.3 ppm s^{-1} for 500 ppm of H_2O_2 and 0.8 and 0.1 ppm s^{-1} to deliver 3000 and 350 ppm respectively of OClO.

The emission rates were set to achieve these concentrations in the dark and the same emission rates were then used for all lighting conditions for each individual gas. The emissions were assumed to last for one hour and then stop. After another hour (at noon), ventilation was resumed at 2 h^{-1}. There is very little information in the literature on how long the gases will be emitted for during cleaning; there is no standard practice. The little information that exists suggests that emissions could last from between 30 minutes to 24 hours (Rogers et al., 2008). Duration of cleaning and ventilation regime afterwards will obviously affect the results, but this assumption allows the impact of one hour of cleaning at typical concentrations to be assessed.

Four lighting scenarios were considered in this study: No indoor lighting (dark); light either from a covered fluorescent (CF) or bare fluorescent (BF) tube; and from a combination of CF and attenuated sunlight (ATT). Covered and bare fluorescent tubes are both common in industrial and commercial settings, due to their long life and high efficiency characteristics (Heffernan et al., 2007). Literature values of absorption cross sections (σ) and photolysis quantum yields (ϕ) of O_3, H_2O_2, HCHO, and OClO were used, with photon fluxes (F) from Kowal et al. (2017) used to calculate photolysis rate constants (J) across the wavelength (λ) range of interest using E1 Chapter 1:

$$J = \int_{\lambda_i}^{\lambda_f} \sigma(\lambda)\phi(\lambda)F_\lambda d\lambda \qquad \text{E1}$$

7.1.4. Results and Discussion

7.1.4.1. Baseline conditions

To investigate the baseline conditions, the model was run without any emissions of the disinfectant gases to quantify the impact of outdoor pollutants and the ventilation regime in isolation. Figure 7.1.3 shows the trends of HO_2, OH and RO_2 for the four lighting conditions. The abrupt concentration changes at 10:00 h and noon are caused by the ventilation system switching off and on respectively. The OH concentration is ~3×10^5 molecule/cm^3 under no lighting or lighting by covered or bare fluorescent tubes, and ~5×10^5 molecule/cm^3 with attenuated outdoor light before the emission starts. This enhancement is caused by production through R39, since NO concentrations are ~2× higher under attenuated outdoor light before ventilation is turned off than the other conditions (not shown) due to enhanced NO_2 photolysis:

$$HO_2 + NO \rightarrow OH + NO_2 \qquad \text{R39}$$

The OH concentration decreases once the ventilation is turned off under all conditions and recovers once ventilation is turned on again. With ventilation, O_3 and VOC concentrations are replenished indoors from outdoors, permitting reactive chemistry to occur and OH radicals to form. The concentrations of HO_2 are similar for the first three lighting conditions before the ventilation is turned off and after it is turned back on again. For attenuated outdoor light, the HO_2 and RO_2 concentrations are lower before the ventilation is turned off owing to suppression by NO (e.g. R39 for HO_2). The main HO_2 source under these conditions is reactions with OH, so the two radicals display similar behaviour, with the HO_2 concentration

decreasing with OH when ventilation is turned off. When ventilation is turned off, RO_2 concentrations rapidly increase then decay. This is due to OH reacting quickly with any remaining VOCs to form RO_2 radicals, which then react with any NO present. As NO concentrations are lower in the dark (not shown), peak RO_2 is highest under these conditions. After ventilation resumes, RO_2 levels return to the initial values.

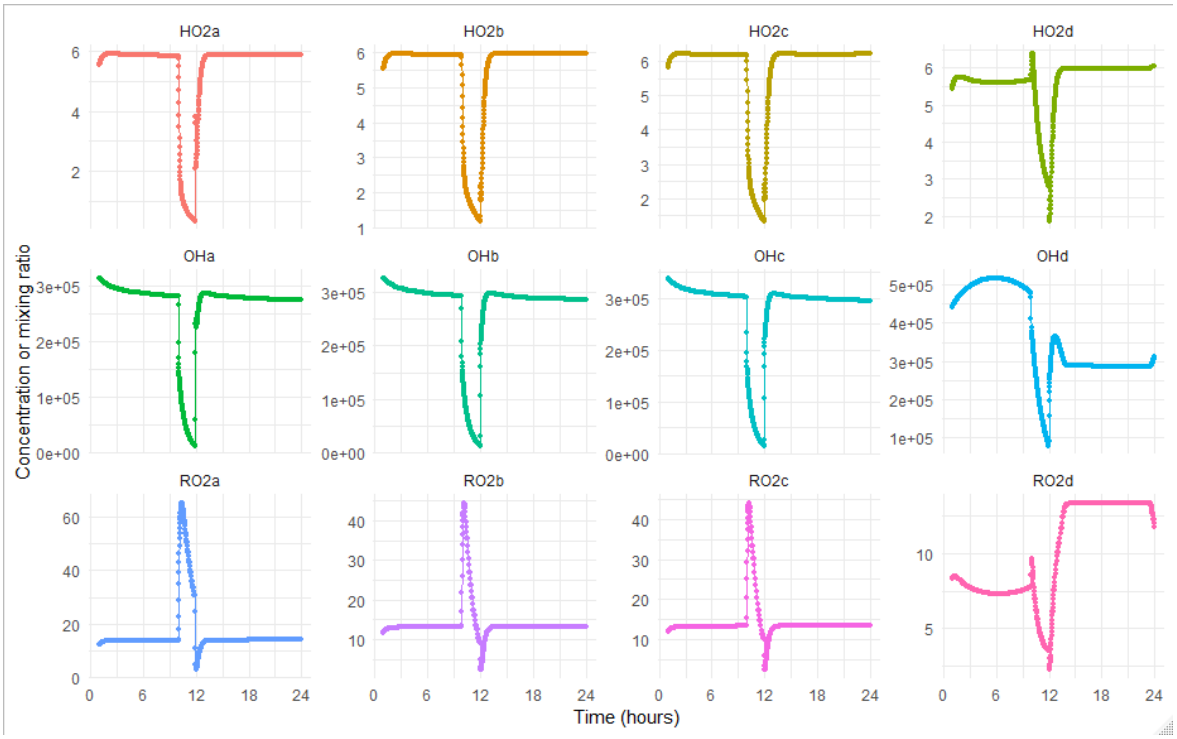

Figure 7.1.3: Profiles of baseline (without any disinfectant emission) HO_2, OH and RO_2 under different lighting conditions (a: dark; b: CF; c: BF; d: ATT) over the course of the study day. Concentrations of HO_2 and RO_2 are in ppt and concentrations of OH are in molecule/cm^3. Note that the changes at 10:00 h and noon are driven by the ventilation system being turned off and on respectively.

7.1.4.2. Disinfectant gases

Figure 7.1.4 shows the predicted temporal profiles of the four disinfectant gases under the different lighting conditions. The profiles for each disinfectant (except OClO) are very similar: A rapid increase in concentration is seen when the NTD is turned on, peaking when disinfection stops at around 11:00 h, followed by a decrease to background levels over the course of ~1.5 hours after generation ceases. Peak concentrations are similar for different lighting conditions.

As shown in Figure 1.4, OClO absorbs light much more strongly than the other disinfectant gases at typical wavelengths present indoors. The temporal profile of its concentration is therefore influenced strongly by the lighting conditions. Peak OClO concentrations are greatest in the dark; under attenuated sunlight they are only ~3% that predicted in the dark due to rapid photolysis. This extremely rapid photolysis is the reason OClO must be prepared and stored in the dark, as noted in Section 7.1.2. The temporal profile for OClO looks very different to those for the other gases, particularly in the dark and for attenuated outdoor light. OClO is only removed in the model through photolysis, or reaction with NO, Cl, O or OH (Table 7.1.1). Given the formation of these latter four species is photolysis-dependent, their reaction rates are relatively slow in the dark. The flat peak between ~11:00 – 12:00 h occurs because emission has stopped but ventilation is still turned off and there is no effective loss. Once ventilation is resumed, the OClO is gradually removed. For attenuated outdoor light, there is also a (narrower) flat-topped peak; in this instance, the flat peak is caused by the balance between emission strength and photolysis rate between 10:00-11:00 h. Once the emission ceases, the remaining OClO is rapidly photolyzed.

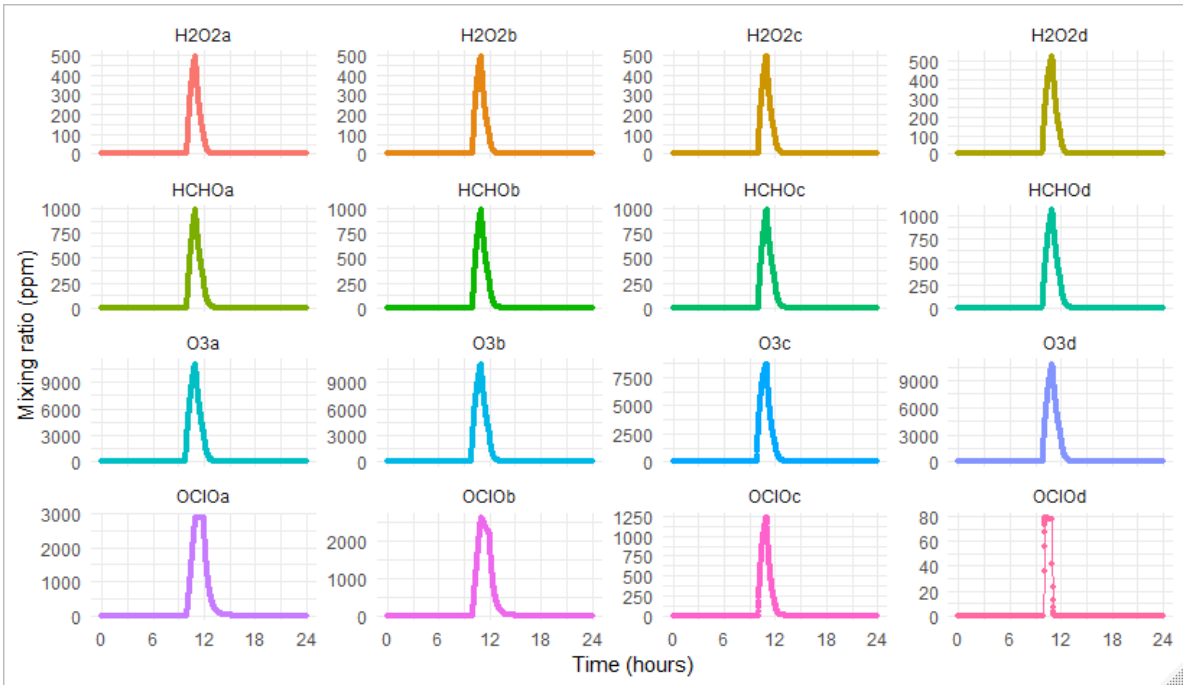

Figure 7.1.4: O_3, HCHO, H_2O_2 and OClO concentrations under different lighting conditions (a: dark; b: CF; c: BF; d: ATT) over the course of the study day.

7.1.4.3. Ozone

The primary radical generated by O_3 photolysis is OH (Figure 7.1.2). Table 7.1.2 illustrates modelled OH steady-state concentrations at ozone concentrations corresponding to baseline levels in hospitals (30 ppb), during cleaning events (~25 ppm), and at the short term and long term exposure limits (300 and 100 ppb) (OSHA, nd). Photolysis rates are low in the dark and with lighting from covered fluorescents and attenuated sunlight, owing to the small O_3 photolysis quantum yields at wavelengths longer than 320 nm (IUPAC, nd). Correspondingly, OH concentrations under lighting from covered fluorescent lighting and attenuated sunlight are similar to those in the dark. The photolysis rate from bare fluorescent tube lighting is 2 orders of magnitude higher than that from sunlight because bare fluorescent tubes emit light at ~312 nm, where the O_3 photolysis quantum yield is much higher than at longer wavelengths (Kowal et al., 2017). This photolysis results in very high peak OH steady-state concentrations (1.3×10^7 molecule/cm^3). For context, outdoor OH concentrations in unpolluted urban centres are generally a few $\times 10^6$ molecule/cm^3 (Stone et al., 2012).

***Table 7.1.2*:** INDCM predicted OH concentrations for O_3 photolysis by sunlight (ATT), covered (CF) and bare (BF) fluorescent bulbs at a distance of 1 m for peak (25 ppm), 300, 100 and 30 ppb O_3; and calculated photolysis rate constants 1 m from each light source based on data from Kowal et al. (2017).

Light Source	Peak O_3 /ppm	Photolysis rate constant /s^{-1}	[OH] in 10^5 molecule/cm^3			
			Peak O_3	300 ppb	100 ppb	30 ppb
Dark	24.9	0	13.4	3.7	3.3	2.7
CF	24.9	1.29×10^{-10}	14.1	3.7	3.3	2.8
BF	24.8	1.27×10^{-6}	127	4.3	3.7	2.9
ATT	24.8	2.06×10^{-8}	13.9	3.8	3.4	2.8

Figure 7.1.5 shows predicted time-resolved profiles of the radical species. Peak values of OH, HO_2 and RO_2 with O_3 emission are similar for the dark, covered fluorescent bulb and attenuated sunlight conditions. Both OH and HO_2 are ~2× higher for the bare fluorescent tube, whereas RO_2 concentrations are similar under all conditions. In the dark, under covered fluorescent lighting and attenuated sunlight, OH, HO_2 and RO_2 concentrations peak when the ventilation is turned off at 10:00 h, as O_3 reacts with VOCs to form OH (and HO_2 and RO_2) (Figure 7.1.2). However, given the short radical lifetime, radical concentrations decrease rapidly once the VOCs are reacted away. There is additional HO_2 loss due to reaction with O_3; OH levels are too low to regenerate HO_2 except under BF conditions, when OH is formed rapidly via O_3 photolysis (Figure 7.1.2). A second spike in OH and HO_2 concentrations

(under all conditions except BF) is observed just after noon when the ventilation is turned back on and VOCs are re-introduced indoors. Radicals are formed from VOCs reacting with O_3 at this time. This production of radicals is more sustained for RO_2 than for OH or HO_2, due to relatively high O_3 concentration under these conditions (still at ~0.8 ppm at 12:40 h). This O_3 removes the NO that would otherwise suppress RO_2 concentrations. The RO_2 only begins to decrease once the NO recovers at around 13:00 h.

For bare fluorescent bulb lighting OH and HO_2 radicals show a single peak that coincides with peak O_3 concentrations at 11:00 h. Peak concentrations are much higher than under the weaker lighting conditions, owing to the much higher O_3 photolysis rates (Table 7.1.2). The behaviour of RO_2 under BF is similar to that under the other lighting conditions. The higher HO_2 concentrations under BF conditions also suppress RO_2 through reactions such as R40:

$$HO_2 + CH_3O_2 \rightarrow CH_3OOH + O_2 \qquad \text{R40}$$

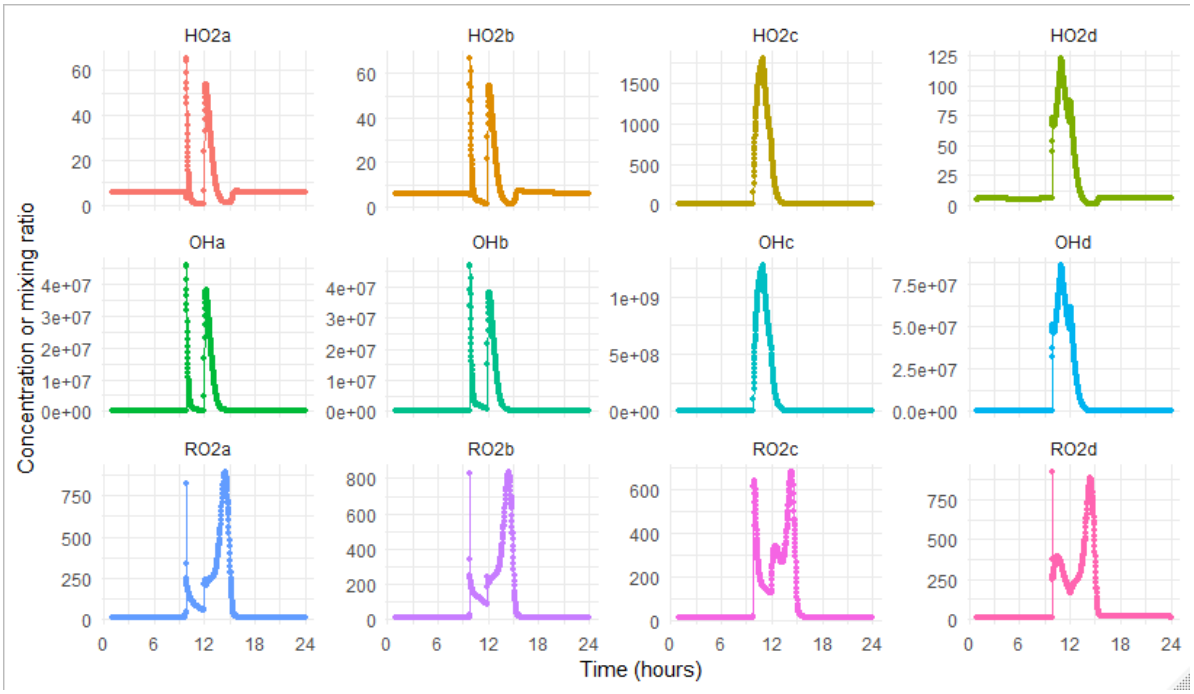

Figure 7.1.5: Profiles of HO_2, OH and RO_2 under different lighting conditions (a: dark; b: CF; c: BF; d: ATT) for O_3 emission. Concentrations of HO_2 and RO_2 are in ppt and concentrations of OH are in molecule/cm^3.

7.1.4.4. Formaldehyde

Table 7.1.3 reports predicted HO_2 steady-state concentrations for various lighting conditions for formaldehyde levels corresponding to the baseline level used in the model (2.6 ppb),

during cleaning events (~1000 ppm), and at the long-term exposure limit (1 ppm) (OSHA, nd). The HO_2 radicals are produced following HCHO photolysis (Figure 7.1.2). At peak HCHO levels generated during cleaning events, the model predicts a steady-state HO_2 concentration of ~2.4 ppb under lighting from a bare fluorescent tube. For context, typical outdoor HO_2 concentrations in unpolluted urban centres are reported to be ~0.6-40 ppt (Stone et al., 2012). Predicted concentrations remain elevated even after HCHO levels decrease below the long-term exposure limits (when people are allowed back into the room) especially under illumination by bare fluorescent bulbs, with concentrations of ~70 ppt at 1 ppm HCHO.

Table 7.1.3. INDCM predicted HO_2 concentrations for HCHO photolysis by sunlight (ATT), covered (CF) and bare (BF) fluorescent bulbs at a distance of 1 m for peak, 1 ppm and 2.6 ppb HCHO; and calculated photolysis rate constants 1m from each light source based on data from Kowal et al. (2017).

Light Source	Peak HCHO /ppm	Photolysis rate constant at 1 m /s^{-1}	[HO_2] in ppt for different HCHO concentrations		
			Peak HCHO	1 ppm	2.6 ppb
Dark	982	0	6	12.4	6.4
CF	982	0	7.2	12.8	6.4
BF	978	7.7×10^{-7}	2424	69.6	7.2
ATT	1053	5.2×10^{-9}	203	14	6.4

Figure 7.1.6 shows the time-resolved model predictions of radical concentrations following HCHO emission. Peak concentrations of HO_2 correlate with photolysis rate (Table 7.1.3) given the direct formation through HCHO photolysis. Hydroperoxy radicals produced from formaldehyde photolysis have three major fates: react with each other to form hydrogen peroxide, with RO_2 to form organic peroxides (e.g. R40), or with nitric oxide to form hydroxyl radicals (Figure 1.3). For peak HCHO concentration, the self-reaction dominates HO_2 loss for bare fluorescent or attenuated outdoor lighting, whilst for the other two conditions, reaction with RO_2 is most important. For the other HCHO concentrations shown in Table 7.1.3, reaction with NO dominates HO_2 loss under all lighting conditions. Note that HO_2 is formed directly from HCHO photolysis, but also from R41:

$$HCHO + OH\ (+O_2) \rightarrow HO_2 + CO + H_2O \qquad \text{R41}$$

This means that even when the photolysis rate of HCHO to form HO_2 is negligible (under no/low lighting conditions), it is still possible to form HO_2, though at lower concentrations than observed under lighting from fluorescent tubes or attenuated sunlight.

Although OH is formed from the reaction between HO_2 and NO, its concentration depends negatively on HCHO concentrations. This is because HCHO is an OH sink (via R41), and loss of OH to HCHO is greater than formation from HO_2 and NO. Thus, OH levels during and immediately after disinfection are lower than under background conditions for all lighting conditions. The OH and RO_2 concentrations for attenuated outdoor light are also notably higher and lower respectively before the emission than afterwards. This is because of elevated NO under these lighting conditions compared to the others (see section 7.1.4.1). RO_2 concentrations are also suppressed by the high concentrations of HO_2 when HCHO is the disinfectant gas (e.g. R40).

For all conditions, there is a brief peak in RO_2 concentrations at 10:00 h as OH reacts with the remaining VOCs to form RO_2, and then a decrease as HO_2 concentrations increase and react with RO_2 (e.g. via R40). The concentration of RO_2 then increases again after 12:00 h as ventilation resumes and oxidation reactions restart. There is a sharp increase and peak of NO at 12:00 h under dark and covered fluorescent lighting conditions (not shown) when the ventilation is turned back on which causes the RO_2 concentration to decrease sharply to a very low concentration.

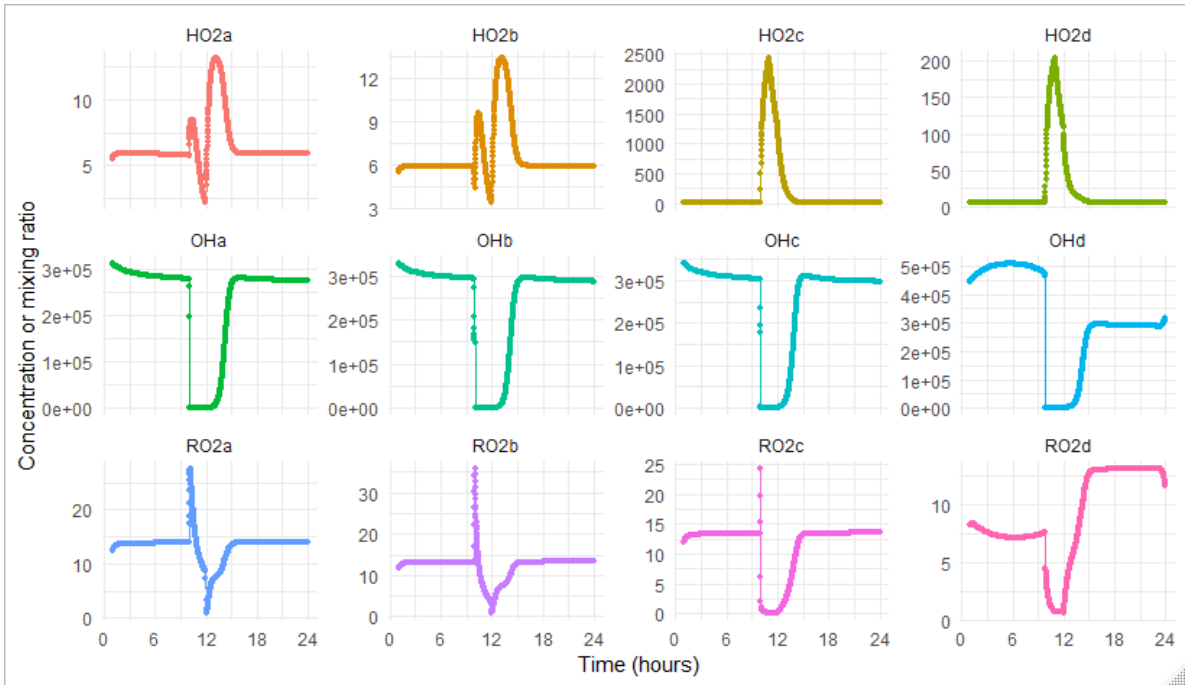

Figure 7.1.6: Profiles of HO_2, OH and RO_2 under different lighting conditions (a: dark; b: CF; c: BF; d: ATT) for HCHO emission. Concentrations of HO_2 and RO_2 are in ppt and concentrations of OH are in molecule/cm^3.

7.1.4.5. Hydrogen peroxide

Table 7.1.4 illustrates predicted OH steady-state concentrations at H_2O_2 concentrations during cleaning events (~500 and 120 ppm), at the long-term exposure limit (1 ppm) (OSHA, nd), and at background levels (1 ppb) (Li et al., 2002).

Table 7.1.4. INDCM predicted OH concentrations from H_2O_2 photolysis by sunlight (ATT), covered (CF) and bare (BF) fluorescent bulbs at a distance of 1 m for peak, 120, 1 and 0.001 ppm H_2O_2; and calculated photolysis rate constants 1 m from each light source based on data from Kowal et al. (2017).

Light Source	Peak H_2O_2 /ppm	Photolysis rate constant /s^{-1}	[OH] in 10^5 molecule/cm^3			
			Peak H_2O_2	120 ppm	1 ppm	1 ppb
Dark	495	0	0.0003	0.0004	1.4	2.8
CF	495	9.5×10^{-10}	0.01	0.01	1.5	3.0
BF	494	1.6×10^{-7}	1.9	1.9	3.5	3.0
ATT	524	1.2×10^{-7}	1.5	1.5	3.5	3.0

The temporal profiles of OH (Figure 7.1.7) resemble those under baseline conditions, although the minima last longer due to loss of OH through R42.

$$OH + H_2O_2 \rightarrow HO_2 + H_2O \qquad R42$$

In the dark and with covered fluorescent lighting, OH concentrations are well below baseline levels (of ~3×10^5 molecule/cm^3) when H_2O_2 levels are elevated and are close to baseline levels when H_2O_2 decreases to <1 ppm. Under bare fluorescent and attenuated sunlight conditions, OH concentrations increase somewhat compared to the darker conditions, for similar reasons as for the HCHO simulation. Unlike OH, the temporal profiles of HO_2 do not resemble background conditions. Small fluctuations in HO_2 concentrations are observed during disinfection in the dark, but clear increases are observed under lighting by all light sources, with much higher concentrations observed under bare fluorescent and attenuated outdoor light than covered fluorescent light. The elevated HO_2 levels are from R42, and time-dependent HO_2 concentrations under illuminated conditions correlate with H_2O_2 concentrations. The trends for RO_2 during H_2O_2 emission are similar to those for HCHO emission. Once high concentrations of HO_2 are formed via R42, reactions between HO_2 and RO_2 to form peroxides (e.g. R40) suppress RO_2.

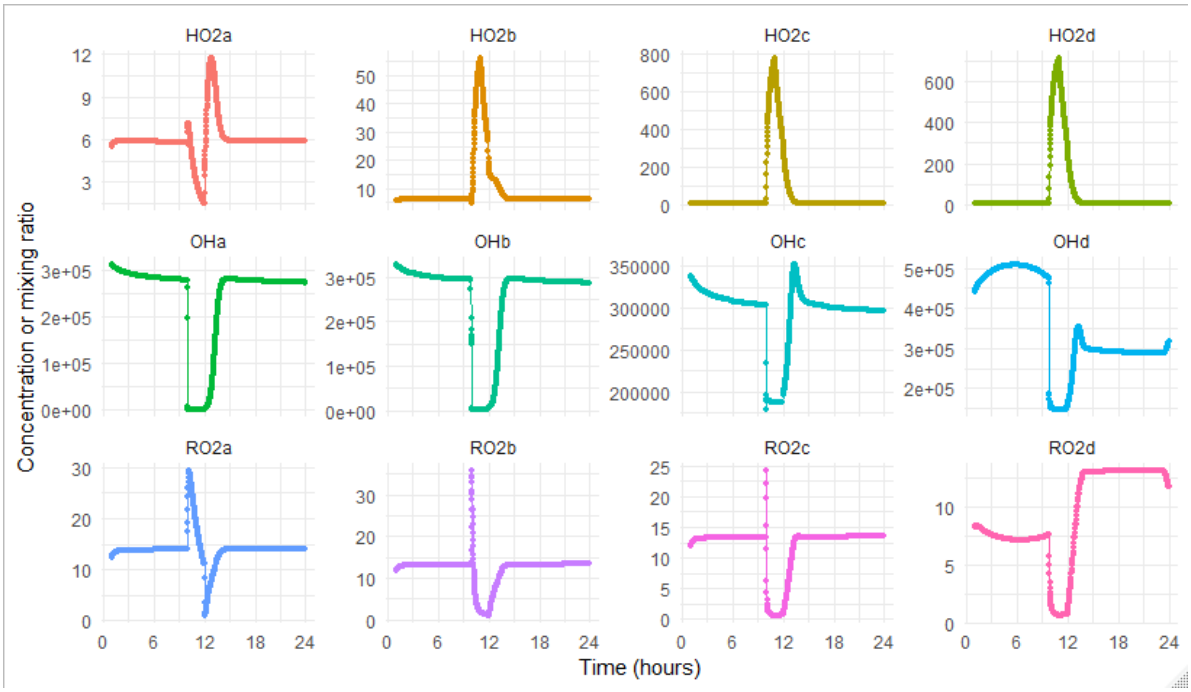

Figure 7.1.7: Profiles of HO_2, OH and RO_2 under different lighting conditions (a: dark; b: CF; c: BF; d: ATT) for H_2O_2 emission. Concentrations of HO_2 and RO_2 are in ppt and concentrations of OH are in molecule/cm^3.

7.1.4.6. Chlorine Dioxide

Chlorine dioxide photolysis forms oxygen atoms and ClO radicals (R43). The ClO radical absorption spectrum has little overlap with wavelengths present indoors, except for high-energy photons from bare fluorescent tubes that can form Cl (R44). ClO dimers can absorb at wavelengths > 500 nm. Under NTD cleaning conditions, there is likely sufficient production of ClO to form dimers, which photolyze to form chloroperoxy radicals (ClOO) and Cl (R45).

$$OClO + h\nu \rightarrow O + ClO \qquad R43$$

$$ClO + h\nu \rightarrow O + Cl \qquad R44$$

$$ClOOCl + h\nu \rightarrow ClOO + Cl \qquad R45$$

There is no ClOO absorbance at wavelengths longer than 280 nm, so there is no overlap with light indoors (IUPAC nd).

Table 7.1.5 reports predicted Cl steady-state concentrations at OClO concentrations corresponding to peak levels (~3000 ppm) during cleaning events, at the short- and long-term exposure limits (300 and 100 ppb, respectively) (OSHA, nd) and at 10 ppb. Steady-state Cl concentrations are elevated at all OClO concentrations under bare fluorescent and attenuated outdoor lighting, with little dependence on OClO concentration. This is because species involved in the reactions that lead to Cl formation, as well as Cl itself, can undergo competing reactions (Figure 7.1.2), some of which depend on light and OClO concentrations. This chemistry can be understood by examining the time-resolved concentrations of relevant species (Cl, HO_2, OH, RO_2 and O_3), shown in Figure 7.1.8.

Table 7.1.5. INDCM predicted Cl concentrations from OClO photolysis by sunlight (ATT), covered (CF) and bare (BF) fluorescent bulbs at a distance of 1 m for peak, 300, 100 and 10 ppb OClO; and calculated photolysis rate constants 1 m from each light source based on data from Kowal et al. (2017).

Light Source	Peak OClO /ppm	Photolysis rate constant /s^{-1}	[Cl] in 10^5 molecule/cm^3			
			Peak OClO	300 ppb	100 ppb	10 ppb
Dark	2879	0	0	1×10^{-5}	6×10^{-5}	6×10^{-4}
CF	2623	4.9×10^{-5}	0.003	0.6	1.1	0.02
BF	1232	5.3×10^{-4}	2.8	26.4	27.9	24.3
ATT	79	9.9×10^{-3}	27.7	75.4	76.8	79.6

Figure 7.1.4 showed that the time-dependent behaviour of OClO is very different from the other disinfectant gases studied. This is because it is extremely photolabile, even at wavelengths relevant to indoor environments. The temporal profiles of radicals and other oxidants formed during OClO disinfection are also very different than those produced from other disinfectant gases. Small amounts of Cl are formed in the dark, and very high peak levels are observed under illuminated conditions (1.5×10^5, 2.8×10^6, and 2.2×10^8 molecule/cm^3 for covered and bare fluorescent and attenuated outdoor lighting respectively). Note that peak Cl concentrations do not coincide with peak OClO concentrations. For instance, peak Cl levels are observed 167 minutes after OClO levels peak with bare fluorescent lighting, and 208 minutes after OClO levels peak in attenuated outdoor light. Peak OClO concentrations are always at around 11:00 h (except for ATT where they occur just after 10:00 h), whereas the peak in ozone gets earlier as the OClO photolysis rate increases, occurring at 11:00 h for ATT, but after 15:00 h in the dark. Given that Cl reacts rapidly with O_3, Cl concentrations only peak once O_3 concentrations have decreased.

Concentrations of OH and HO_2 decrease at around 10:00 h, returning to 'normal' with a slower recovery rate compared to OH trends for the emission of other gases. When ClO concentrations are high in the more intense light conditions, OH and HO_2 react with ClO and are depleted. In the dark, OH reacts with OClO, only returning to background concentrations when OClO is no longer present. An increase in RO_2 levels is observed under all lighting conditions, with the highest levels observed under ATT. In the dark, RO_2 is formed as the remaining VOCs react with OH when the ventilation is turned off. Under the illuminated conditions, the Cl produced by photolysis can additionally oxidize VOCs to form RO_2. The RO_2 concentration is therefore enhanced relative to the dark case, particularly for bare fluorescent and attenuated sunlight conditions. Moreover, as shown in Table 7.1.5, OClO photolysis under attenuated sunlight is ~20 times faster than under bare fluorescent lighting, resulting in an earlier (~40 minutes) and higher peak of RO_2. Once the ventilation is turned back on, the chlorine radicals are slowly depleted, which means the opportunities to form more RO_2 become limited and the RO_2 eventually decreases.

The confounding factor with using OClO as a disinfectant gas is that photolysis of OClO produces O atoms (R43), which react with O_2 to produce O_3. Depending on the light levels, this can produce high ozone levels (with peak concentrations of 1100 ppm for BF and 1440 ppm for ATT, as shown in Figure 7.1.8) that can then affect the chemistry. We note that the O_3 levels generated from OClO photolysis are much higher than those commonly attained

using O_3 as the primary disinfectant (25 ppm). The combination of high OClO and O_3 concentrations means that OH is suppressed for many hours following disinfection. Although OH radicals can be produced via O_3 photolysis, the reaction of O_3 with Cl is a more important loss route for O_3, particularly under attenuated sunlight conditions. Any OH that forms therefore rapidly reacts with the OClO that is formed through the reaction of Cl with O_3.

The model was also run assuming peak OClO concentrations of 350 ppm as explained in Section 7.1.3.2. Under these conditions, Cl concentrations peaked in the attenuated sunlight at ~2×10^7 molecule/cm^3. These values reflect the fact that the OClO emission into the room is ~10 times lower than under the conditions illustrated in Figure 7.1.8.

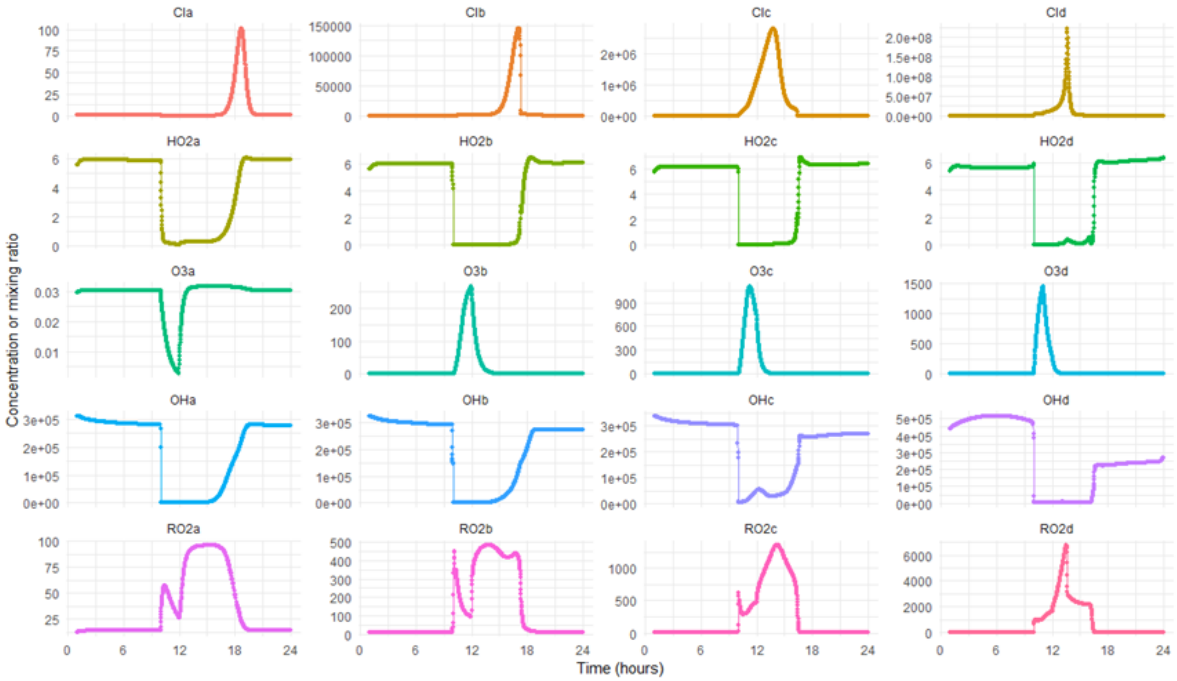

Figure 7.1.8: Profiles of Cl, HO_2, O_3, OH and RO_2 under different lighting conditions (a: dark; b: CF; c: BF; d: ATT) for OClO emission. Concentrations of HO_2 and RO_2 are in ppt, concentrations of Cl and OH are in molecule/cm^3 and concentrations of O_3 are in ppm.

The predicted concentrations of OH, HO_2, RO_2, and Cl after NTD cleaning events may be orders of magnitude higher than indoor and outdoor baseline levels, with elevated concentrations potentially persisting for several hours after NTD use. Long-term exposure limits (when rooms are deemed safe for re-entry) are reached 2-4.5 hours after disinfection ceases, depending on the disinfectant gas used and the lighting condition. Table 7.1.6 shows radical concentrations when rooms are considered safe for re-entry for each disinfectant gas

under different lighting conditions. These can remain elevated under some conditions many hours after disinfection, especially for the bare fluorescent and attenuated sunlight conditions. Note also that when OClO is used as a disinfectant gas, O_3 levels can also remain elevated after OClO concentrations reach a safe limit: under bare fluorescent lighting, O_3 concentrations are still 3.5 ppm (concentrations return to below 100 ppb at 14:52 h) and for attenuated outdoor light, 1150 ppm (concentrations return to below 100 ppb at 13:32 h), well above the safe limit for O_3 of 100 ppb.

Table 7.1.6: Concentrations of OH, HO_2, Cl (OClO only) and RO_2, clockwise from top left for the 4 disinfectant gases at the time when the disinfectant gas has returned to the long-term exposure limit value (O_3 and OClO: 100 ppb; HCHO and H_2O_2: 1 ppm). OH and Cl concentrations in 10^5 molecule/cm^3. HO_2 and RO_2 concentrations in ppt.

	O_3		HCHO		H_2O_2		OClO	
dark	3.2	1.1	0.4	12.5	1.4	10.3	0.8	1.1
	418.4	/	8.5	/	10.2	/	85.1	0.0
CF	3.3	1.2	0.5	12.8	1.5	10.5	0.7	0.1
	430.4	/	8.0	/	9.8	/	432.8	1.1
BF	3.7	1.4	1.1	69.4	3.5	24.3	0.3	0.0
	399.5	/	6.3	/	11.9	/	1259.4	27.9
ATT	3.4	1.3	0.5	13.9	3.5	21.5	0.0	0.0
	367.8	/	7.7	/	10.5	/	1192.8	76.8

Background levels of the radicals studied in this work (when ventilation is running) are: 3 - 5 × 10^5 molecules/cm^3 (OH), 6 ppt (HO_2), 0 molecule/cm^3 (Cl), and 8 - 15 ppt (RO_2). For cleaning events, after O_3 concentrations have decreased to safe levels, OH, HO_2, and Cl will be at or near baseline levels, but Table 7.1.6 shows that RO_2 will be greatly elevated (~400 ppt under all conditions). After HCHO has reached safe levels, HO_2 will be greatly elevated under lighting by bare fluorescent bulbs (~70 ppt). After H_2O_2 levels have decreased to safe levels, HO_2 will be elevated by 3 - 4 times compared to background levels under lighting from bare fluorescent tubes and attenuated sunlight. After OClO has returned to safe levels, Cl will be elevated under these same two lighting conditions (2.8 × 10^6 and 7.7 × 10^6 molecule/cm^3 respectively), and RO_2 will be elevated under all conditions, ranging from 85 ppt in the dark to ~1.2 ppb under lighting by bare fluorescent tubes and attenuated outdoor

light. These elevated concentrations could lead to the formation of harmful secondary pollutants such as chlorinated and oxygenated organics and particulate matter, resulting in a temporary but significant decrease in air quality in rooms employing NTDs.

Current safety guidelines do not account for potentially elevated radical concentrations either before or after safe levels of the respective compounds are reached. The results of this study in no way suggest that the disinfectants discussed should not be used to disinfect hospital rooms; their efficacy at deactivating bacteria makes them an extremely important tool to keep hospitals safe for staff and patients. It is possible, however, that revised operating procedures should be considered for some of these instruments to reduce exposure to photochemically-generated gas-phase species, such as running the instruments in the dark, waiting until ambient levels of the disinfectant are an order of magnitude below current safety guidelines, or increasing air change rates during NTD use.

7.1.5. Conclusions

Significant uncertainties remain regarding radical formation indoors (whether NTDs are employed or not), due primarily to a lack of measurements of indoor radicals and their sources and sinks (Young et al., 2019). This study suggests that radical levels may be extremely elevated for extended time periods after NTD use, both in the dark and under common forms of indoor lighting. This work also highlights the need for indoor measurements of species such as OH, HO_2, Cl, and RO_2 to better predict the effects of NTDs on indoor air quality. The efficacy of NTDs for reducing viral and bacterial loadings should be further studied in the dark and for different indoor lighting. Efficacy may be greatly enhanced under common lighting sources such as fluorescent lights due to the production of radicals that may inactivate bacteria more effectively than the disinfection agents, but the production of secondary pollutants and adequate ventilation afterwards must be considered.

7.2. Hydrogen Peroxide Emission and Fate Indoors during Non-bleach Cleaning: A Chamber and Modelling Study

7.2.1. Abstract

This section uses a detailed chemical model to investigate hydrogen peroxide (H_2O_2) concentrations following the use of a household non-bleach cleaning fluid for surface cleaning, in a chamber designed to simulate a residential room. The aim of this work was to investigate the sources and fates of oxidants and oxidant precursors arising from household surface cleaning. Measured concentrations before and during cleaning were used to calculate an emission rate for H_2O_2 that could be used to drive the model simulations of cleaning. A detailed chemical model was used to simulate the radical concentrations that could arise following cleaning with the peroxide solution for different lighting conditions. Four different lighting conditions were considered: dark, fluorescent lighting only (BF), attenuated sunlight only (OUT) and the sum of the latter two conditions (BFOUT). Two different forms of cleaning were used which are regular cleaning (the cleaner was wiped off the floor 1.5-2 minutes after spraying it on) and deep cleaning (the cleaner was left on the floor for more than 1 h before being rinsed off). The results show that maximum radical concentrations occurred for the BFOUT conditions (1.3×10^6 molecule/cm^3 OH, 1.2 ppt HO_2, 0.8 ppt RO_2 for regular cleaning; 1.5×10^6 molecule/cm^3 OH, 1.7 ppt HO_2, 0.8 ppt RO_2 for deep cleaning). These concentrations were elevated considerably above baseline conditions (26%, 69%, 22% increase compared to baseline conditions for OH, HO_2 and RO_2 respectively for regular cleaning; 45%, 143%, 40% increase compared to baseline conditions for OH, HO_2 and RO_2 respectively for deep cleaning). Therefore, the deep cleaning method caused a greater production rate of radicals compared to regular cleaning, as more H_2O_2 was released into the room. Elevated radical concentrations can lead to the production of many secondary pollutions (e.g. particulate matter) which can lead to the deterioration of indoor air quality.

7.2.2 Introduction

Indoor cleaning is a common activity, during which a wide variety of chemicals can be released into the indoor environment, some of which can then undergo a number of further reactions (e.g. Figure 7.1.2). The secondary produced chemicals (e.g. particulate matter) from these reactions can then potentially degrade indoor air quality and even cause adverse health

impacts (Wolkoff et al., 1998; Nazaroff and Weschler 2004; Dimitroulopoulou et al., 2015; Trantallidi et al., 2015).

A recent study observed high concentrations of OH and HO_2 radicals during desk cleaning (one-minute averaged OH and HO_2 concentrations of 4×10^6 and 4×10^8 molecule/cm^3 respectively) with a limonene-based cleaner (Carslaw et al., 2017). Moreover, nitryl chloride ($ClNO_2$), molecular chlorine (Cl_2) and hypochlorous acid (HOCl) were also observed during surface cleaning with bleach (containing sodium hypochlorite) (Wong et al., 2017, Farmer et al., 2019, Mattila et al., 2020). These reactive chlorine species are photolabile and free Cl radicals can be formed in the indoor environment as shown in Figure 7.1.2. (Young et al., 2019).

Hydrogen peroxide (H_2O_2) contaning cleaners are common cleaning products and many different formulations are commericially available (Fu et al., 2012, Murdoch et al., 2016). According to Murdoch et al. (2016), it is difficult for microbiological organisms to withstand exposure to H_2O_2 due to its nonselective characteristics. These same characteristics can lead to potentially adverse health impacts on humans, primarily through accidental exposure. Both throat and nasal irritation were found in healthy volunteers after exposure to a concentration of 2.2 ppm H_2O_2 for 2 hours (Ernstgard et al., 2012). Moreover, tightening of the chest, shortness of breath, hoarseness, inflammation of the nose and upper airway irritation can also be caused through exposure to H_2O_2 (US CDC 2016).

As mentioned in section 7.1, the photochemical formation of radicals (e.g. OH, HO_2 and RO_2) which can subsequently form harmful reaction products following reaction in indoor air, is a previously unconsidered consequence of indoor cleaing. This section continues to focus on the impact of indoor photolysis on radical production following cleaning activities, but this time focusing on surface cleaning.

The aim of this section is to investigate the impacts of indoor photolysis on indoor air chemistry following cleaning activities by traditional cleaning techniques (wiping surfaces by hand with liquid cleaning agents). The specific objectives are to:

- Use measured photolysis rate coefficients to simulate the concentrations of OH, HO_2 and RO_2 indoors following cleaning with a hydrogen peroxide solution.
- To investigate radical behaviour during and following cleaning and under different lighting conditions.

- To differentiate these impacts on indoor air chemistry for regular cleaning and deep cleaning.

7.2.3. Method

7.2.3.1. Model

The model used in this work is the INDCM (INdoor Detailed Chemical Model). According to the method developed by Nazaroff and Cass (1986), indoor light sources in the model are assumed to have constant transmission between 300-400 nm (UV) and 400-700 nm (visible). This method was used for all 37 species/groups of species in the model that undergo photolysis, with the exception of the six species listed in Table 7.2.1. For these six species, we used measured photolysis coefficients, following the method described in Section 7.1 (as this work was started before the model modifications were completed) for bare fluroescent lighting and attenuated sunlight. We considered four different conditions: dark, fluorescent lighting only (BF), attenuated sunlight only (OUT) and the combination of these two to represent internal lighting plus attenuated sunlight contributions to indoor photolysis (BFOUT).

Table 7.2.1: Measured photolysis rates of H_2O_2, NO_2, HONO, NO_3, O_3 and HCHO under indoor fluorescent lights and attenuated sunlight through windows.

J (s^{-1})	fluorescent	Sunlight
H_2O_2	8.06×10^{-8}	6.66×10^{-8}
NO_2	4.50×10^{-5}	5.82×10^{-4}
HONO	7.07×10^{-6}	6.90×10^{-5}
NO_3	8.78×10^{-3}	3.17×10^{-2}
O_3	2.94×10^{-7}	8.62×10^{-9}
HCHO	3.80×10^{-7}	6.73×10^{-10}

7.2.3.2. Experimental conditions and model assumptions

The size of the experimental chamber (laboratory space) was 3.47 m × 3.05 m × 2.75 m (29.1 m^3). A non-bleach H_2O_2 multipurpose cleaner spray which is commercially available in Canada was used for the experiments. During the cleaning experiments, two different forms

of cleaning were tested: 'regular cleaning' and 'deep cleaning'. For regular cleaning, the cleaner was wiped off the floor 1.5-2 minutes after spraying it on whilst for deep cleaning, it was left on the floor for more than 1 h before being rinsed off. Gaseous H_2O_2 was measured during the whole time for each of the experiments.

For each of the cleaning episodes, it was estimated that ~10-20 ml of cleaning spray was used, which contained 0.88% H_2O_2 by volume. Based on the volume of the room (29.1 m^3), a total emission into the room of the order of ~5.4-10.8×10^{13} molecule/cm^3/s of H_2O_2 was calculated. In order to investigate the impact of lighting on the H_2O_2 chemistry, the aim was to reproduce the H_2O_2 measurements with the model and then investigate the simulated radical concentrations. A series of model sensitivty tests were run where the total emission rate, the proportion of H_2O_2 that stuck to the surface and the off-gassing rate for H_2O_2 for both the regular and deep cleaning scenarios were run. The aim of these scenarios was to minimise the difference between measured and modelled H_2O_2 concentrations for the two different scenarios.

Table 7.2.2 shows the results of the sensitivity study to fit modelled H_2O_2 to the measurements. For regular cleaning, the best results (smallest difference between measured and modelled data) were found when the emission was assumed to last for 210s with an emission rate of 1.1×10^{12} molecules/cm^3/s (total emission of 2.2×10^{14} molecule/cm^3 corresponding to ~40 ml of cleaning fluid). Meanwhile, for deep cleaning, the best results were found when the emission lasted for 1500s with an emission rate of 7.8×10^{10} molecules/cm^3/s (total emission of 1.2×10^{14} molecule/cm^3, corresponding to about 21 ml of cleaning fluid). Also, an off-gassing rate of 7×10^{-4} s^{-1} was required to simulate the deep cleaning scenario. Off-gassing was assumed not to be important for regular cleaning, as the cleaning fluid was wiped off the floor after 1.5-2 minutes.

Table 7.2.2: Results of sensitivity study to fit modelled H_2O_2 to the measurements

deep cleaning	emission time(s)	H_2O_2 sticks (%)	emission rate (molecules/cm^3/s)	off-gassing	*[1]sum of (measurement-model)^2
1	1500	88	7.0×10^{10}	7.5×10^{-4}	293694
2	1500	88	6.6×10^{10}	7.5×10^{-4}	393617
3	1500	88	7.3×10^{10}	7.5×10^{-4}	258742
4	1500	88	7.3×10^{10}	7.0×10^{-4}	217209
5	1500	80	7.3×10^{10}	7.0×10^{-4}	397186
6	1500	90	7.3×10^{10}	7.0×10^{-4}	194998

7	1500	90	7.5×10^{10}	7.0×10^{-4}	174134
8	1500	92	7.5×10^{10}	7.0×10^{-4}	154502
9	1500	95	7.5×10^{10}	7.0×10^{-4}	144624
10	1500	99	7.8×10^{10}	7.0×10^{-4}	150045
11	**1500**	**95**	**7.8×10^{10}**	**7.0×10^{-4}**	**133036**
12	1500	95	7.8×10^{10}	7.5×10^{-4}	183068
13	1500	95	7.5×10^{10}	8.0×10^{-4}	228184
regular cleaning	emission time(s)	H_2O_2 sticks (%)	emission rate (molecules/cm^3/s)	off-gassing	*[1]sum of (measurement-model)^2
1	180	95	1.2×10^{12}	/	36204
2	180	95	1.1×10^{12}	/	39978
3	180	95	1.0×10^{12}	/	36010
4	190	95	1.2×10^{12}	/	32505
5	190	95	1.1×10^{12}	/	32007
6	200	95	1.2×10^{12}	/	37923
7	200	95	1.1×10^{12}	/	34615
8	**210**	**95**	**1.1×10^{12}**	**/**	**30897**
9	210	95	1.2×10^{12}	/	32314

*[1]: For each sensitivity test, the sum of difference between measurement and model was calculated. The lowest sum shows the lowest difference between measured and modelled H_2O_2 and hence the best fit

The model was initialised with the room volume, average temperature (25.7 ˚C) and humidity (23.7%), measured background key chemical concentrations (e.g. 2.5ppb O_3 and 26.5 ppb HCHO) and also different lighting conditions based on of the measured photolysis rates of key chemicals (Table 7.2.1).

7.2.4. results and discussion

7.2.4.1. Baseline conditions

Figures 7.2.1-7.2.3 show the baseline conditions (in the absence of cleaning) for OH, HO_2 and RO_2 and for the different lighting conditions. The average OH background concentration from the model in the dark (1.7×10^5 molecule/cm^3) is lower than typical OH concentrations outdoors in urban environments ($1.2\text{-}20 \times 10^6$ molecule/cm^3) but similar to typical OH levels outdoors at night ($1.8\text{-}2.6 \times 10^6$ molecule/cm^3) (Stone et al., 2012). The average HO_2 background concentration from the model in the dark (3.8×10^6 molecule/cm^3) is much lower than previous reported outdoor concentrations ($0.16\text{-}10 \times 10^8$ molecule/cm^3) , while the predicted average RO_2 concentration is similar to outdoors (4.0×10^6 molecule/cm^3) (Stone et al., 2012).

Under the attenuated sunlight condition, photolysis of HONO can produce more OH which leads to an average concentration of 8.8×10^5 molecule/cm^3, almost 4 times more than its background concentration in the dark. This concentration is in reasonable agreement with previous predicted concentrations under background conditions ($1.7\text{-}24 \times 10^5$ molecule/cm^3) (Carslaw 2007; Gomez Alvarez et al., 2013; Waring and Wells 2015; Won et al., 2019). In addition, photolysis of HCHO produces HO_2 while the reaction of OH with VOCs forms RO_2, which leads to the increase of HO_2 and RO_2 concentrations by 3 and 2.4 times compared to the background concentrations respectively. Concentrations of OH are highest under BFOUT, then OUT and lowest under BF and in the dark (Figure 7.2.1), even though the H_2O_2 photoylsis rate to form OH is higher for BF compared to OUT. This is because of compensation via photolysis of HONO, which is much higher for attenuated sunlight conditions compared to BF (Table 7.2.1). The distributions of HO_2 (Figure 7.2.2) and RO_2 (Figure 7.2.3) are similar to OH.

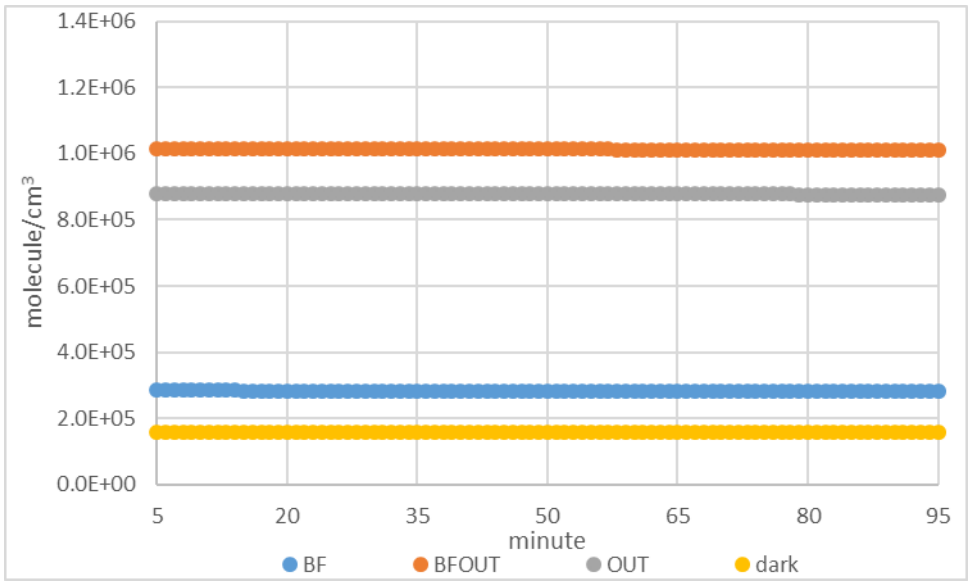

Figure 7.2.1: Profiles of baseline (without emission) OH concentration under fluorescent lamps (BF), fluorescent lamps + sunlight (BFOUT), sunlight (OUT) and dark.

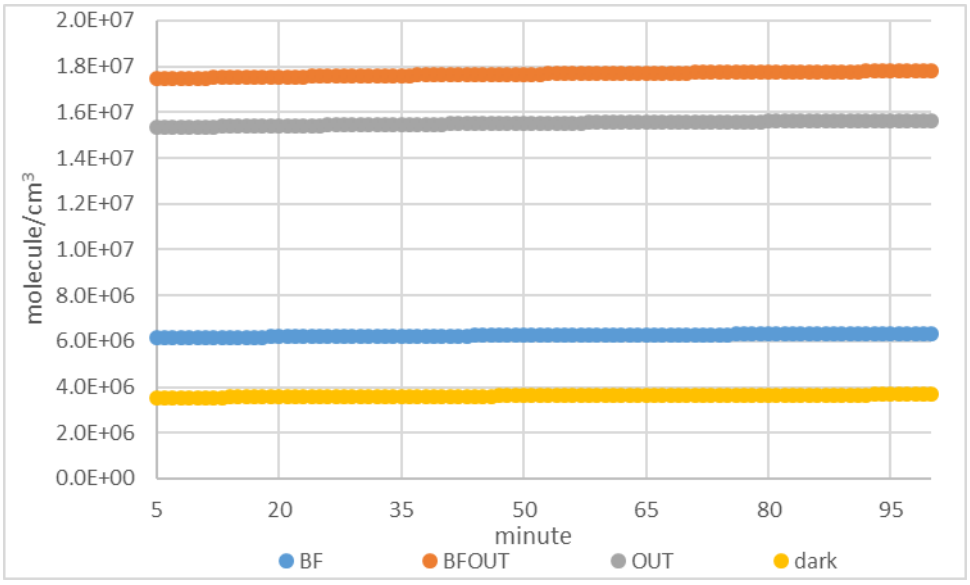

Figure 7.2.2: Profiles of baseline (without emission) HO_2 concentration under fluorescent lamps (BF), fluorescent lamps + sunlight (BFOUT), sunlight (OUT) and dark.

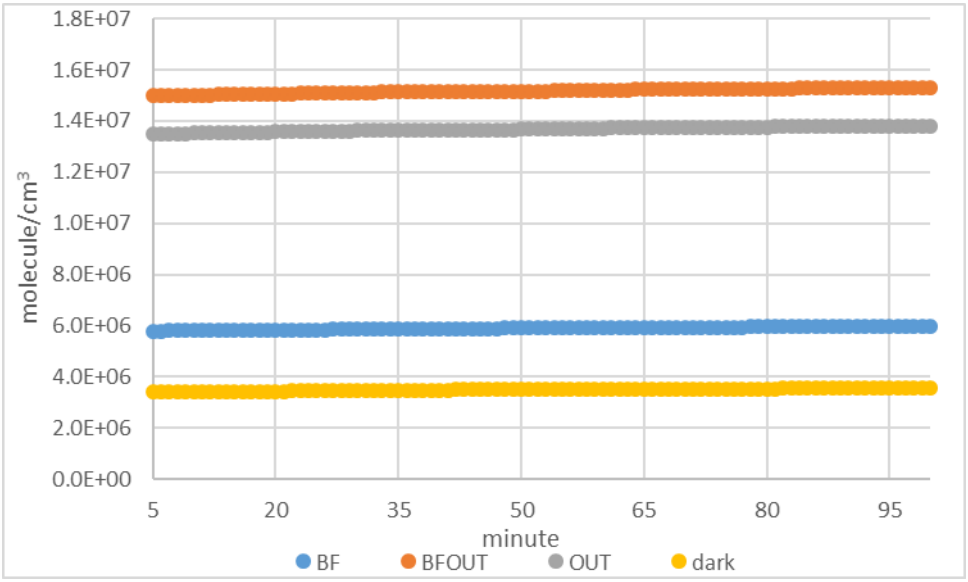

Figure 7.2.3: Profiles of baseline (without emission) RO_2 concentration under fluorescent lamps (BF), fluorescent lamps + sunlight (BFOUT), sunlight (OUT) and dark.

7.2.4.2. Regular cleaning

For regular cleaning, Figure 7.2.4 shows the predicted temporal profiles of the disinfectant gas under the different lighting conditions. The profiles for the disinfectant are very similar: a rapid increase in the concentration during cleaning, peaking when cleaning stops, followed by a decrease to background levels afterwards. It took approximately 40 minutes to return to

background levels following the start of the cleaning event. Peak H_2O_2 concentrations are similar for all of the different lighting conditions.

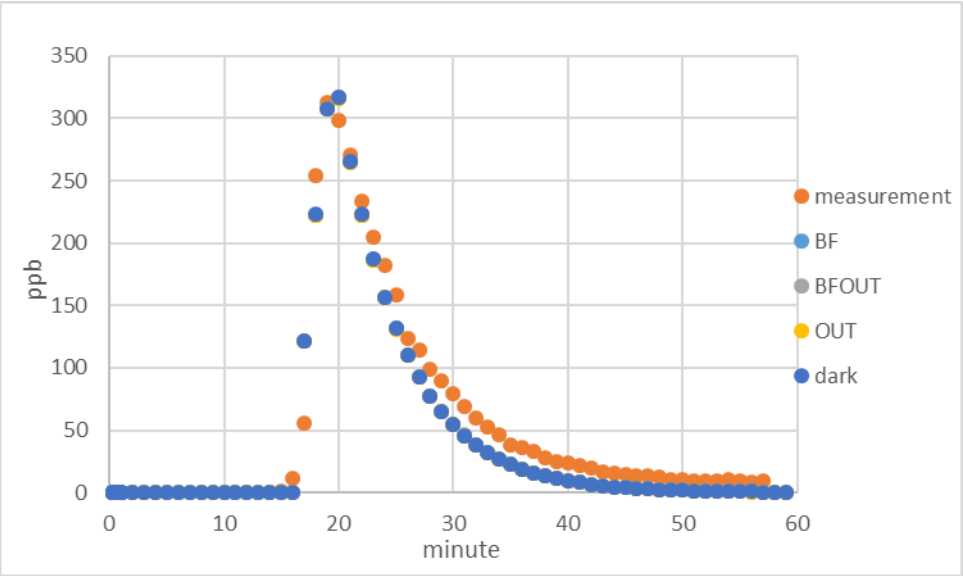

Figure 7.2.4: Profile of H_2O_2 concentration under fluorescent lamps (BF), fluorescent lamps + sunlight (BFOUT), sunlight (OUT), dark and measurement for regular cleaning. Profiles of H_2O_2 under the different lighting conditions are all overlaid on top of each other.

Under BFOUT, the concentration of OH (1.3×10^6 molecule/cm^3) is higher than for BF (4.0×10^5 molecule/cm^3) and OUT (9.7×10^5 molecule/cm^3) as shown in Figure 7.2.5. The highest OH concentration coincides with the highest photolysis rate of H_2O_2 under BFOUT conditions (1.47×10^{-8} s^{-1}). The OH concentration with attenuated sunlight is higher than that under BF, despite the photolysis coefficient of H_2O_2 for the latter being higher (Table 7.2.1). Again, this is due to a higher photolysis rate of HONO under attenuated sunlight conditions compared to BF (Table 7.2.1) which enhances OH production. The concentration of OH in the dark is quite low and fairly stable.

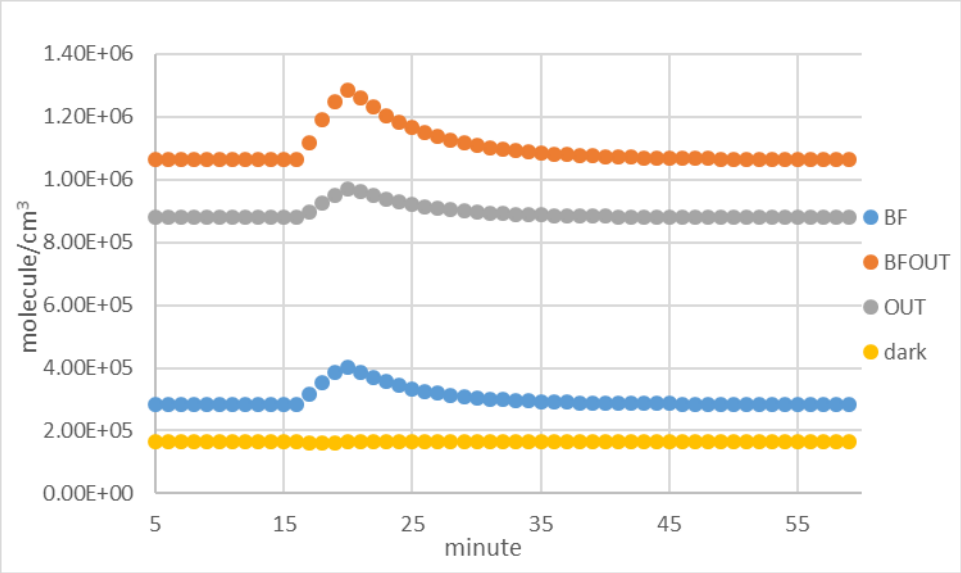

Figure 7.2.5: Profiles of OH concentrations under fluorescent lamps (BF), fluorescent lamps + sunlight (BFOUT), sunlight (OUT) and in the dark for regular cleaning.

According to Figure 7.2.6, the HO_2 concentrations under BFOUT (3.0×10^7 molecule/cm^3) and OUT (2.3×10^7 molecule/cm^3) are much higher than that under BF (1.1×10^7 molecule/cm^3) and in the dark . The distrbution of RO_2 (BFOUT: 1.9×10^7; OUT: 1.5×10^7; BF: 7.7×10^6 molecule/cm^3) is similar to HO_2 (Figure 7.2.7). Compared to the baseline conditions (no H_2O_2 emission) under the same lighting scenario, peak concentrations of HO_2 increase the most (up to 73%) followed by OH (up to 41%) and then RO_2 (up to 30%) for regular cleaning. The highest increrase in HO_2 is caused by photolysis of H_2O_2, followed by the reaction of the OH produced in this way with H_2O_2 to produce HO_2 (R42).

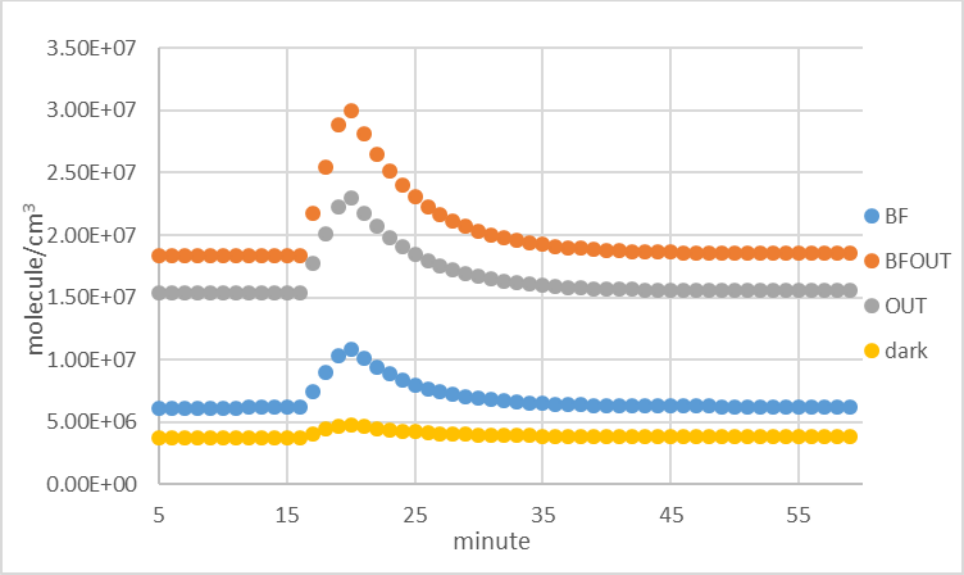

Figure 7.2.6: Profiles of HO_2 concentrations under fluorescent lamps (BF), fluorescent lamps + sunlight (BFOUT), sunlight (OUT) and in the dark for regular cleaning.

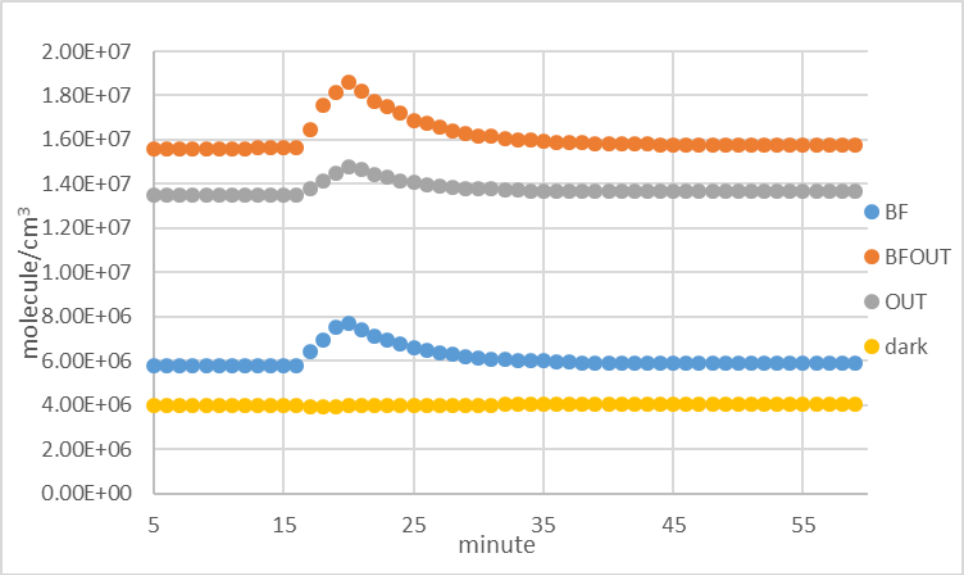

Figure 7.2.7: Profiles of RO_2 concentrations under fluorescent lamps (BF), fluorescent lamps + sunlight (BFOUT), sunlight (OUT) and in the dark for regular cleaning.

7.2.4.3. Deep cleaning

For deep cleaning, the concentrations of H_2O_2 are also very similar under the different lighting conditions (Figure 7.2.8). More H_2O_2 is released into the room under this scenario as the cleaning fluid is not rinsed off as for the regular cleaning episode. It took approximately 300 minutes for the model simulated H_2O_2 concentration to return to background levels from the beginning of cleaning event (not shown due to lack of measured data after 100 minutes).

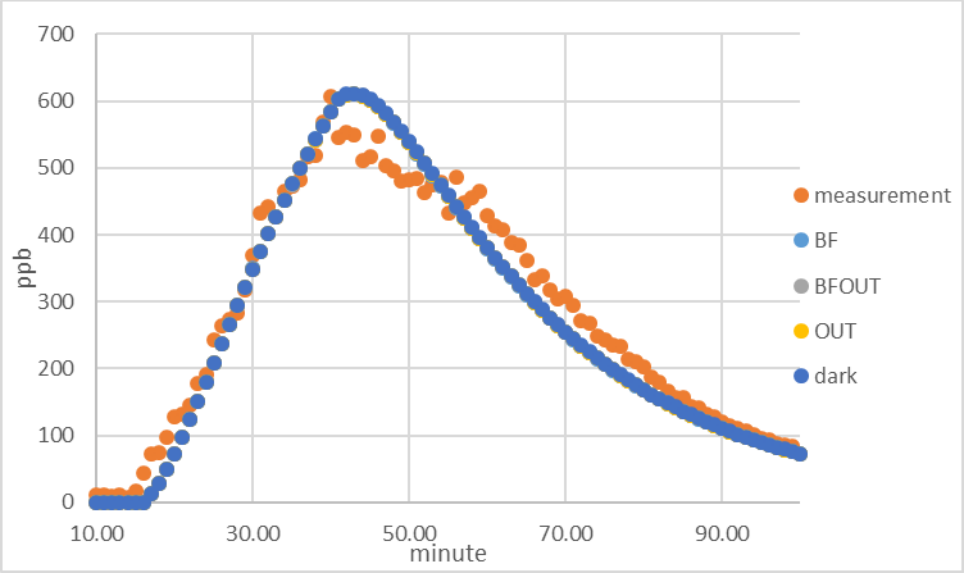

Figure 7.2.8: Profile of H_2O_2 under fluorescent lamps (BF), fluorescent lamps + sunlight (BFOUT), sunlight (OUT), dark and measurement for deep cleaning. Profiles of H_2O_2 under different lighting conditions all overlay each other.

OH concentrations are highest under BFOUT (1.5×10^6 molecule/cm^3) and then OUT (1.0×10^6 molecule/cm^3), and much lower under BF (5.0×10^5 molecule/cm^3). The concentration of OH in the dark is quite low and stable during the period of interest. Wong et al. (2017), investigated the impacts of indoor cleaning on radicals under different lighting conditions. This study investigated mopping with a chlorine-containing bleach solution and found an increase in OH concentration of up to 2×10^6 molecule/cm^3, which is similar to the results found in this study (Wong et al., 2017). Furthermore, peak concentrations of HO_2 (Figure 7.2.10) (BFOUT: 4.3×10^7; OUT: 3.1×10^7; BF: 1.6×10^7 molecule/cm^3) and RO_2 (Figure 7.2.11) (BFOUT: 2.1×10^7; OUT: 1.6×10^7; BF: 9.3×10^6 molecule/cm^3) are similar with the highest concentrations under BFOUT and lowest in the dark.

Compared to baseline conditions for the same light, peak concentrations of HO_2 increase the most (up to 159%) followed by OH (up to 76%) and then RO_2 (up to 58%) for deep cleaning. Again, concentrations of HO_2 increse the most due to photolysis of H_2O_2 (R13) and the reaction of the OH so produced with H_2O_2 to produce HO_2 (Figure 7.1.2).

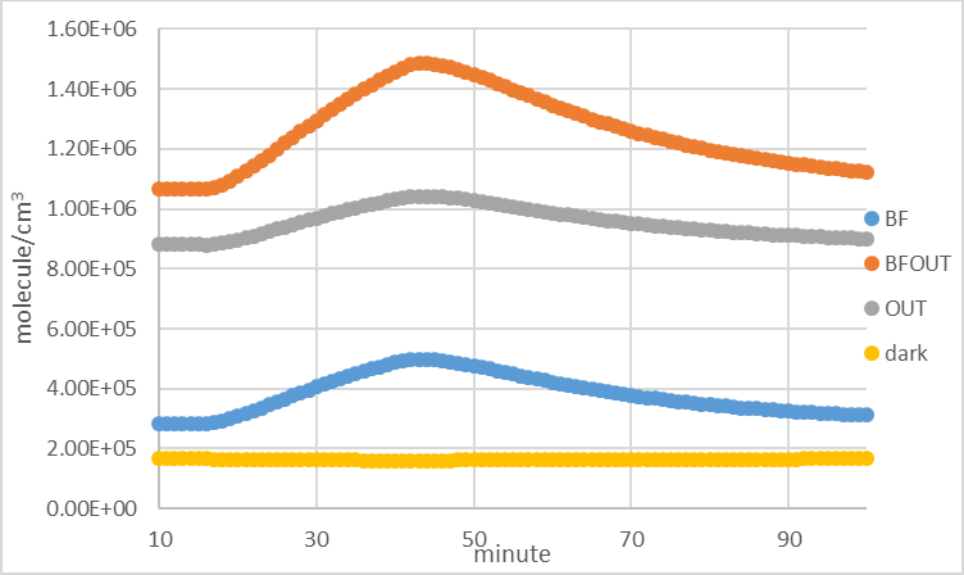

Figure 7.2.9: Profiles of OH concentrations under fluorescent lamps (BF), fluorescent lamps + sunlight (BFOUT), sunlight (OUT) and in the dark for deep cleaning.

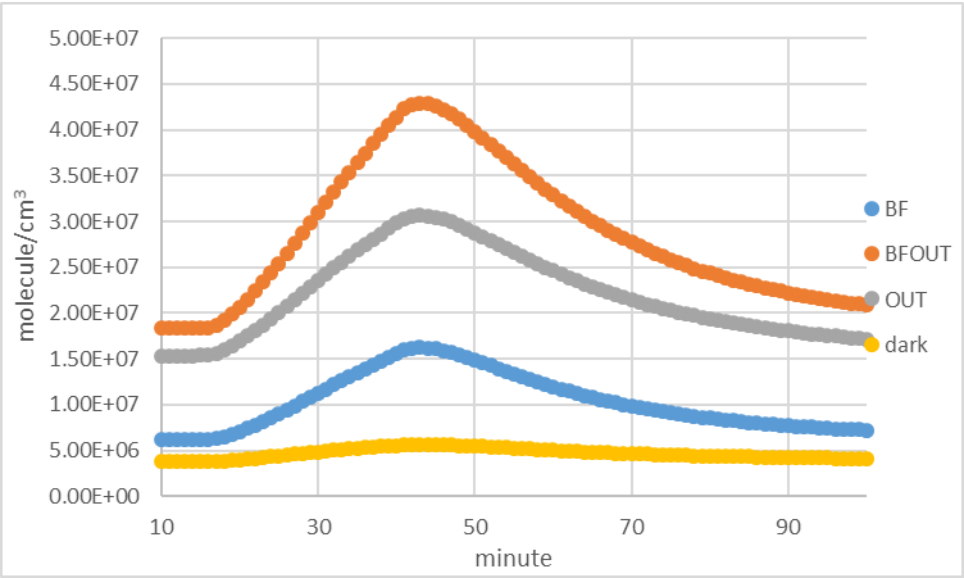

Figure 7.2.10: Profiles of HO_2 concentrations under fluorescent lamps (BF), fluorescent lamps + sunlight (BFOUT), sunlight (OUT) and in the dark for deep cleaning.

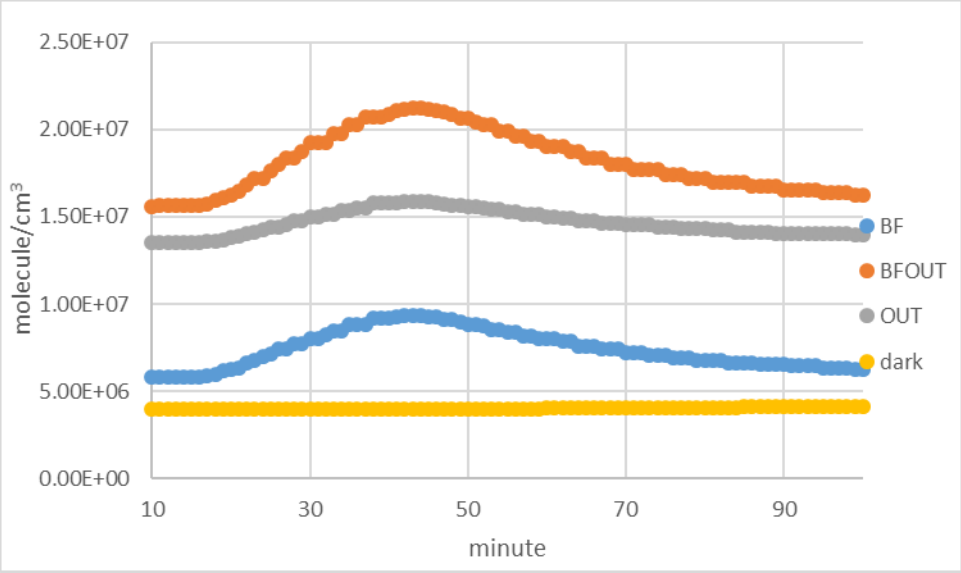

Figure 7.2.11: Profiles of RO_2 concentrations under fluorescent lamps (BF), fluorescent lamps + sunlight (BFOUT), sunlight (OUT) and in the dark for deep cleaning.

In summary, both regular and deep cleaning cause large changes in radical concentrations (OH, HO_2 and RO_2) with the highest increase in HO_2 concentrations. The different lighting conditions lead to different concentrations of radicals with highest peak concentrations under the combined attenuated sunlight and indoor artificial light. These results prove again that outdoor attenuated sunlight has greater impacts on indoor air quality than indoor artificial lights.

7.2.5. Conclusion

In summary, the results from this section show that:

- Different lighting conditions lead to different concentrations of radicals (radical concentrations are highest under sunlight + fluorescent lamps followed by sunlight only and then fluorescent lamps only).
- The use of non-bleach H_2O_2 multipurpose cleaner causes an obvious increase in radical concentrations (OH, HO_2 and RO_2).
- Deep cleaning leads to higher concentrations of radicals compared to regular cleaning.

Under the current Covid-19 pandemic, there have been increased cleaning activities as people are more concerned about hygiene. Such an increase in these activities is likely to increase human exposure to the harmful secondary products that are formed from the enhanced radical

concentrations. Considering the findings in this section, indoor cleaning is recommended to be carried out when it is dark outside, with artificial lighting only. Based on the findings in Chapter 4, LED lights, which provide the lowest indoor photolysis rates and consequent indoor air chemistry processing, could also be recommended.

It remains unclear which type of cleaning product (e.g. terpene or peroxide based) is better for indoor air quality and hence human health. For instance, it would be valuable if these different cleaning products were investigated in the same chamber, under the same background conditions, and for a range of lighting conditions. Concentrations of the main chemical species released should be measured under different lighting conditions (e.g. different cloud cover conditions, glass types with different cut-off wavelengths, different distances to different artificial lights and so on). Models can then be used to predict concentrations of radicals and key indoor species to identify the conditions that lead to the lowest concentrations of harmful indoor air pollutants.

This work highlights the need for indoor measurements of species such as OH, HO_2, and RO_2 radicals indoors to better predict the effects of indoor cleaning on indoor air quality. In addition, it highlights the need for research to focus on not only the efficiency of cleaning products but also their impacts on indoor air quality.

Chapter 8: Conclusion

Recently, increasing attention has been paid to indoor air quality. We were already aware that in developed countries, people were spending most of their time (~90%) indoors and consequently receiving most of their exposure to air pollution there. However, the ongoing COVID-19 pandemic has made us even more aware of the importance of indoor air quality and has also meant that people are spending much more time indoors. Many governments around the world have asked their citizens to work at home, students to take online courses at home, and restricted travel to prevent the spread of disease (Pragholapati 2020). Therefore, air quality in the indoor environment and especially our homes, has become even more important.

The importance of outdoor photolysis is well known, however, the role of photolysis indoors is less well studied and hence quantified. Therefore, this thesis has investigated this knowledge gap, particularly the role that photolysis plays in indoor chemical processing, through the use of a detailed chemical model (the INDCM). This thesis focused on a previously unconsidered potential consequence of indoor photolysis: that under certain conditions, photochemical formation of high concentrations of radicals, such as OH, HO_2 and RO_2 can happen indoors, and that these radicals can go on to form harmful reaction products when exposed to other chemicals commonly found in indoor air.

The INDCM is a near explicit box model that enables the user to study indoor air chemistry in detail. It considers many of the controlling factors of indoor air chemistry, such as chemical reactions, internal emissions, photolysis, deposition, and exchange with outdoors. Two recent studies found that different artificial lights have unique spectral characteristics (Kowal et al., 2017) and that transmission of outdoor light will vary depending on the window type, namely the composition of the glass (Blocquet et al., 2018). These two papers permitted the indoor photolysis parametrisation in the model to be updated as explained in Chapter 4.

Chapters 4-6 then used the updated model to investigate the impacts of indoor artificial light and glass composition (building factors) and cloudiness, time of year and latitude (external factors), in order to identify the most important controls on indoor air chemistry with respect to indoor photolysis. The results show that all five controlling factors play an important role on indoor photolysis rates and hence indoor air chemistry. The highest impacts on the

concentrations of most of the key species were found to be caused by glass type (71% on average) followed by cloudiness and proximity of artificial light (~53% on average). Moreover, the time of year and latitude also have important impacts on the predicted indoor concentrations of key indoor species with average impacts of 32% and 22% respectively.

The greatest impacts of these controlling factors on predicted indoor concentrations were found for OH, TOTORGNO$_3$ and NO, which varied by 142, 113 and 56% respectively depending on the input values used. For predicted TOTPAN, HO$_2$, O$_3$, RO$_2$ and HONO concentrations, these controlling factors led to smaller variations in predicted concentrations at 33%, 27.9%, 19.2%, 10.1% and 6.9% respectively. Differences in predicted NO$_2$ (3.8% average difference) and HCHO concentrations (close to zero on average) were much smaller when these controlling factors were varied, as these two concentrations were controlled by factors other than photolysis (including the deposition rate, air exchange rate and outdoor concentrations).

Although the impacts on predicted indoor concentrations were smaller for artificial lights compared to glass type, there were still some noticeable effects for predicted OH concentrations. Compared to the baseline scenario where it was dark inside, OH concentrations increased by 49% when 1m away from a UFT light and by 16% when 1m from an FT light. However, there were only 0.2 and 1.4 % increases respectively when 1m away from LED and CFT lighting, so these two have the lowest impacts on indoor air chemistry. Therefore, LED and CFT are recommended for daily use, to reduce the effect of indoor lighting on indoor air chemistry. Moreover, being 1 m away from indoor lighting reduced OH concentrations by 169% on average, compared to being adjacent to the light.

The results also showed that the transmission factors for sunlight through windows strongly depend on the wavelength cut-off of the glass. Glass types with a relatively low cut-off wavelength (e.g. glass-C at 315 nm) can impact predicted indoor concentrations by 76% compared to the baseline scenario, those with higher cut-off wavelengths (e.g. LEWF at 380 nm) only perturb concentrations by 5.5% relative to the baseline. Therefore, glass types with higher cut-off wavelengths will reduce radical concentrations indoors.

The degree of cloudiness was found to play an important role on indoor air chemistry, especially for an unoccluded sun with slightly cloudy conditions (67% on average compared to 15% for an occluded solar disk and more overcast conditions). Moreover, differences in the average concentrations of key species during the year were found to be small for lower

latitudes (especially at the Equator), but much larger at higher latitudes, particularly for the non-summer months. In addition, average concentrations of all the studied key indoor species were highest (O_3, HCHO, OH, HO_2, RO_2 and NO) or lowest (HONO and NO_2) in mid-latitudes (between 30˚N and 40˚N) in summer, owing to the balance between the intensity of sunlight and length of daytime as explained in Chapter 5. For the non-summer months, their concentrations were correlated with the change of latitude.

Chapter 7 included two case studies describing the impacts of indoor photolysis on radical production following two very different ways of indoor cleaning (automated and traditional cleaning techniques). Both studies found that the use of cleaning agents can lead to concentrations of predicted radicals that are orders of magnitude higher than background levels during and immediately following cleaning events. In addition, the elevated concentrations of radicals may persist for several hours after the cleaning event, depending on the air composition and air exchange rate. Therefore, indoor cleaning activities can cause an increase of radical concentrations which have ability to produce potentially harmful secondary pollutants. Consequently, indoor cleaning can lead to adverse health effects to occupants. Based on these results, exposure to indoor air pollution will be lower if cleaning is carried out with indoor artificial lights only (e.g. LED) or dark indoors (for automated cleaning techniques).

Indoor photolysis has been found to play an important role in indoor air chemistry and hence indoor air quality. This thesis has shown that many factors influence the role of indoor photolysis on indoor air chemistry, including indoor artificial light type, glass composition, degree of cloudiness, time of year and location. For future studies, more measurements of the key species focused on in this study, as well as other indoor species such as acetaldehyde and PM are needed under different indoor lighting conditions. This could be achieved through an advanced sensor network (as explained in Chapter 4) to measure different chemical species and photon intensities under different conditions (e.g. different places in a room and different times of day). To better understand the impacts of cloud cover on indoor photolysis and hence indoor air chemistry, actinic flux should be measured indoors and outdoors for a range of cloud cover and types and at different times of year.

It is worth considering how lighting and glazing has changed in recent years, how it might change in the future and what the impacts have been/will be on indoor photolysis rates. The long lifetimes and high efficiency characteristics of fluorescent tubes (used mainly in office

blocks and industrial settings) led to their being a dominant indoor lighting source for many years in such locations (Heffernan et al., 2007). However, LED lights are becoming more popular, owing to much higher efficiency. For instance, they are estimated to provide 56-62% energy savings and an increase in lifetime of a factor of 9 compared to the use of fluorescent tubes (Jenkins and Newborough 2007; Ahn et al., 2014). In residential settings, incandescent lighting was a dominant lighting source for many years (Lim et al., 2013). However, this type of lighting is also being replaced by LED lights. Relative to incandescent lights, LEDs use ~85% less energy and have 50 times longer lifetimes (Mottier 2009). Therefore, LEDs are likely to remain as the dominant source of illumination in the future (Pandharipande and Caicedo 2011). The replacement of fluorescent tubes and incandescent lighting by LEDs will reduce the impacts of light on indoor air chemistry based on the findings in this thesis.

Nowadays, numerous kinds of glass types are available with different characteristics, such as multipane glazing (Liu et al., 2017), tinted (Li et al., 2015), low-emissivity coatings (Mempouo et al., 2010), anti-reflective coatings (Rosencrantz et al., 2005) and vacuum glazing (Fang and Arya 2019), compared to the single pane and compositionally simple glass types that used to be more common (Aguilar-Santana et al., 2020).

A final model test was run which aimed to bring together all of the elements of this thesis by investigating the formation of $PM_{2.5}$ following cleaning under different indoor lighting conditions and glass types. For Run 1, it was assumed that there were incandescent bulbs indoors, combined with a glass type with a low cut-off wavelength (glass-C). These could be broadly considered to represent a typical UK home in the 1970-80s. For Run 2, it was assumed that LEDs were used with a high cut-off wavelength glass type (LEWF), more typical of modern housing. For both runs, it was assumed there was a cleaning event (the emissions were assumed to last for one hour) with the use of a limonene-containing cleaning product, based on the conditions described in Carslaw et al. (2012). Peak concentrations of limonene were ~170 ppb for both runs and figure 8.1 shows the predicted $PM_{2.5}$ concentrations for both lighting conditions.

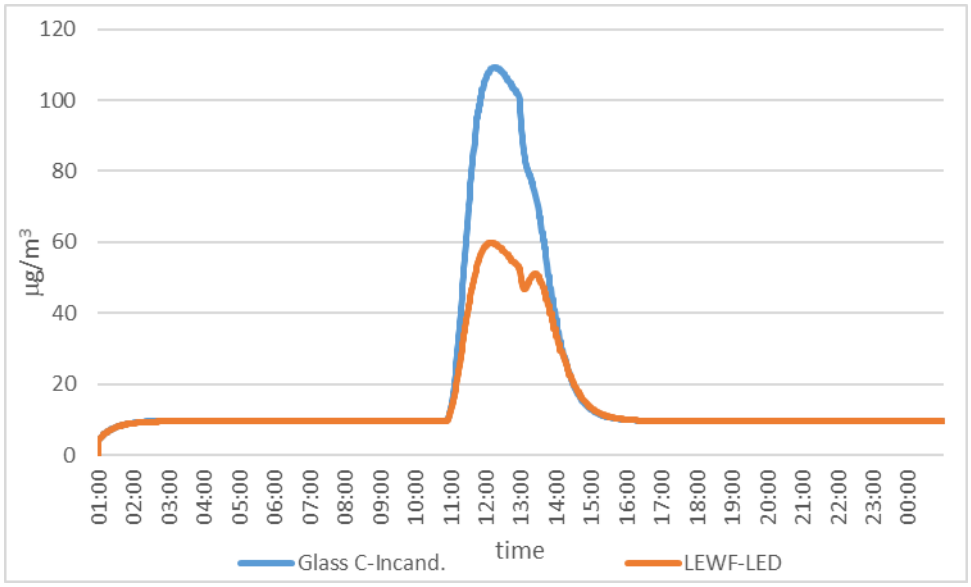

Figure 8.1: Concentrations of $PM_{2.5}$ under two conditions (1: Incandescent with glass-C; 2: LEDs with LEWF).

The peak $PM_{2.5}$ concentration for Run 1 was 109.2 µg/m^3, approximately two times the peak concentration for Run 2 (59.8 µg/m^3). Therefore, it is likely that more modern lighting and window conditions have reduced indoor photolysis rates and hence the production of secondary pollutants such as $PM_{2.5}$, all other things being equal.

Finally, it is worth reiterating that health data for indoor (and outdoor) air pollutants is currently only available for relatively few species. This limits the ability to fully quantify the impacts of reducing indoor photolysis on human health. Future studies should focus on assessing which type of lighting indoors (combination of glass type and artificial lighting) is most beneficial for human health, through testing the health effects of the different air pollutant mixtures formed under the different lighting conditions that are typically experienced in residences.

References

Aguilar-Santana JL, Jarimi H, Velasco-Carrasco M, Riffat S, Review on window-glazing technologies and future prospects, International Journal of Low-Carbon Technologies. 2020;15(1):112-120.

Ahn BL, Jang CY, Leigh SB, Yoo S, Jeong H. Effect of LED lighting on the cooling and heating loads in office buildings. Appl. Energy. 2014;113:1484-1489.

Alicke B, Geyer A, Hofzumahaus A, Holland F, Konrad S, Patz HW, Schafer J, Stutz J, Volz-Thomas A, Platt U. OH formation by HONO photolysis during the BERLIOZ experiment. Journal of Geophysical Research. 2003;108:8247.

Altshuller A. Review: natural volatile organic substances and their effect on air quality in the United States. Atmos. Environ. 1983;17(11):2131-2165.

Alvarez EG, Amedro D, Afif C, Gligorovski S, Schoemaecker C, Fittschen C, Doussin JF, Wortham H. Unexpectedly high indoor hydroxyl radical concentrations associated with nitrous acid. Proceedings of the National Academy of Sciences. 2013;110(33):13294-13299.

Andersen BM, Rasch M, Hochlin K, Jensen FH, Wismar P, Fredriksen JE. Decontamination of rooms, medical equipment and ambulances using an aerosol of hydrogen peroxide disinfectant. J Hosp Infect. 2006;62(2):149-155.

Asdrubali F, Baldinelli G. Theoretical modelling and experimental evaluation of the optical properties of glazing systems with selective films. Building Simulation. 2009; 2:75-84.

Assaf E, Sheps L, Whalley L, Heard D, Tomas A, Schoemaecker C, Fittschen C. The Reaction between CH_3O_2 and OH Radicals: Product Yields and Atmospheric Implications. Environ Sci Technol. 2017;51(4):2170-2177.

Atkinson R, Aschmann SM, Arey J, Shorees BJ. Formation of OH radicals in gas phase reactions of O_3 with a series of terpenes, J. Geophys. Res. 1992; 97:6065-6073.

Atkinson R. Gas-phase tropospheric chemistry of volatile organic compounds: 1. Alkanes and alkenes. J. Phys. Chem. Ref. Data. 1997;26(2):215-290.

Atkinson R, Arey J. Gas-phase tropospheric chemistry of biogenic volatile organic compounds: a review. Atmos. Environ. 2003;37:197-219.

Bartolomei V, Gomez AE, Wittmer J, Tlili S, Strekowski R, Temime-Roussel B, Quivet E, Wortham H, Zetzsch C, Kleffmann J, Gligorovski S. Combustion processes as a source of high levels of indoor hydroxyl radicals through the photolysis of nitrous acid. Environ. Sci. Technol. 2015;49(11):6599-6607.

Bentayeb M, Simoni M, Norback D, Baldacci S, Maio S, Viegi G, Annesi-Maesano I. Indoor air pollution and respiratory health in the elderly. Journal of Environmental Science and Health, Part A, Toxic/Hazardous Substances and Environmental Engineering. 2013;48:1783–1789.

Beswick AJ, Farrant J, Makison C, et al. Comparison of multiple systems for laboratory whole room fumigation. Appl Biosaf. 2011;16(3):139-157.

Bhalla A, Pultz NJ, Gries DM, et al. Acquisition of nosocomial pathogens on hands after contact with environmental surfaces near hospitalized patients. Infect Cont Hosp Epidemiol. 2004;25(2):164-167.

Blitz MA, Heard DE, Pilling MJ. Pressure and temperature-dependent quantum yields for the photodissociation of acetone between 279 and 327.5 nm. Geophys. Res. Lett. 2004;31:L06111.

Blocquet M, Guo F, Mendez M, Ward M, Coudert S, Batut S, Hecquet C, Blond N, Fittschen C, Schoemaecker C. Impact of the spectral and spatial properties of natural light on indoor gas-phase chemistry: Experimental and modeling study. Indoor Air. 2018;28(3):426-440.

Blondeau P, Iordache V, Poupard O, Genin D, Allard F. Relationship between outdoor and indoor air quality in eight French schools. Indoor Air. 2005;15:2-12.

Bloss C, Wagner V, Jenkin ME, Volkamer R, Bloss WJ, Lee JD, Heard DE, Wirtz K, Martin-Reviejo M, Rea G, Wenger JC, Pilling MJ. Development of a detailed chemical mechanism (MCMv3.1) for the atmospheric oxidation of aromatic hydrocarbons. Atmospheric Chemistry and Physics. 2005;5:641−664.

Boyce JM, Potter-Bynoe G, Chenevert C, King T. Environmental contamination due to methicillin-resistant Staphylococcus aureus: Possible infection control implications. Infect Cont Hosp Epidemiol. 1997;18(9):622-627.

Boyce JM. New approaches to decontamination of rooms after patients are discharged. Infect Cont Hosp Epidemiol. 2009;30(6):515-517.

Brown SK, Sim MR, Abramson MJ, Gray CN. Concentrations of Volatile Organic Compounds in Indoor Air – A Review. Indoor Air. 1994;4:123-134.

Buchanan ISH, Mendell MJ, Mirer AG, Apte MG. Air filter materials, outdoor ozone and building-related symptoms in the BASE study. Indoor Air. 2008;18:144-155.

Byrns G, Fuller TP. The risks and benefits of chemical fumigation in the health care environment. J Occup Environ Hyg. 2011;8(2):104-112.

Calvert JG, Yarwood G, Dunker AM. An evaluation of the mechanism of nitrous acid formation in the urban atmosphere. Res. Chem. Intermed. 1994;20(3-5):463-502.

Canter DA, Gunning D, Rodgers P, O'Connor L, Traunero C, Kempter CJ. Remediation of Bacillus anthracis contamination in the US department of justice mail facility. Biosecur Bioterror. 2005;3(2):119-127.

Carling PC, Parry MM, Rupp ME, Po JL, Dick B, Von Beheren S. Improving cleaning of the environment surrounding patients in 36 acute care hospitals. Infect Cont Hosp Epidemiol. 2008;29(11):1035-1041.

Carslaw N. A new detailed chemical model for indoor air pollution. Atmospheric Environment. 2007;41(6):1164−1179.

Carslaw N, Mota T, Jenkin ME, Barley M, McFiggans G. New evidence for the importance of nitrate and peroxide groups in indoor secondary organic aerosol: results from a model investigation. Environmental Science and Technology. 2012;46:9290−9298.

Carslaw N. A mechanistic study of limonene oxidation products and pathways following cleaning activities. Atmospheric Environment. 2013;80:507-513.

Carslaw N, Ashmore M, Terry AC, Carslaw DC. Crucial Role for Outdoor Chemistry in Ultrafine Particle Formation in Modern Office Buildings. Environmental Science and Technology. 2015;49:11011-11018.

Carslaw N, Fletcher L, Heard D, Ingham T, Walker H. Significant OH production under surface cleaning and air cleaning conditions: impact on indoor air quality. Indoor Air. 2017;27:1091-1100.

Carter WPL. (2000). Documentation of the SAPRC-99 chemical mechanism for VOC reactivity assessment. Available online: https://intra.engr.ucr.edu/~carter/pubs/s99doc.pdf

Carter WPL. (2000). Implementation of the SAPRC-99 chemical mechanism into the models-3 framework. Available online: https://intra.cert.ucr.edu/~carter/pubs/s99mod3.pdf

Carter WPL. The SAPRC-99 Chemical Mechanism and Updated VOC Reactivity Scales. California Air Resources Board. 2003.

Carter WPL. Development of the SAPRC-07 chemical mechanism. Atmos. Environ. 2010;44:5324-5335.

Cheng YH, Lin CC, Hsu SC. Comparison of conventional and green building materials in respect of VOC emissions and ozone impact on secondary carbonyl emissions. Build. and Environ. 2015;87:274-282.

Coley DA, Beisteiner A. Carbon dioxide levels and ventilation rates in schools. Int. J. Vent. 2002;1(1):45-52.

Crawford J, Shetter RE, Lefer B, Cantrell C, Junkermann W, Madronich S, Calvert J. Cloud impacts on UV spectral actinic flux observed during the International Photolysis Frequency Measurement and Model Intercomparison (IPMMI). Journal of Geophysical Research. 2003;108:8545.

Criegee R. Mechanism of ozonolysis. Angewandte Chemie Int. Ed. 1975;14(11):745-752.

Cui SQ, Cohen M, Stabat P, Marchio D. CO_2 tracer gas concentration decay method for measuring air change rate. Building and Environment. 2015;84:162-169.

Currier RP, Torraco DJ, Cross JB, Wagner GL, Gladden PD, Vanderberg LA. Deactivation of clumped and dirty spores of Bacillus globigii. Ozone-Sci Eng. 2001;23(4):285-294.

Dancer SJ. Floor wars: The battle for 'clean' surfaces. J Hosp Infect. 2013;84(4):339-340.

Davies A, Pottage T, Bennett A, Walker J. Gaseous and air decontamination technologies for Clostridium difficile in the healthcare environment. J Hosp Infect. 2011;77(3):199-203.

De Paor DG, Dordevic MM, Karabinos P, Burgin S, Coba F, Whitmeyer SJ. Exploring the reasons for the seasons using Google Earth, 3D models, and plots. International Journal of Digital Earth. 2017;10(6):582–603.

Destaillats H, Maddalena RL, Singer BC, Hodgson AT, McKone TE. Indoor pollutants emitted by office equipment: A review of reported data and information needs. Atmospheric Environment. 2008;42:1371-1388.

Dimitroulopoulou C, Ashmore MR, Byrne MA, Kinnersley RP. Modelling of indoor exposure to nitrogen dioxide in the UK. Atmos. Environ. 2001;35(2):269-279.

Dimitroulopoulou C, Ashmore MR, Hill MTR, Byrne MA, Kinnersley R. INDAIR: a probabilistic model of indoor air pollution in UK homes. Atmos. Environ. 2006;40(33):6362-6379.

Dimitroulopoulou C. Ventilation in European dwellings: A review. Build. And Environ. 2012;47:109-125.

Dimitroulopoulou C, Trantallidi M, Carrer P, Efthimiou GC, Bartzis JG. EPHECT II: exposure assessment to household consumer products. Sci. Total Environ. 2015;536:890-902.

Domingo JL, Rovira J. Effects of air pollutants on the transmission and severity of respiratory viral infections. Environmental Research. 2020;187:109650.

Drakou G, Zerefos C, Ziomas I, Voyatzaki M. Measurements and numerical simulations of indoor O_3 and NO_X in two different cases, Atmospheric Environment. 1998;32:595-610.

Drees M, Snydman DR, Schmid CH, et al. Prior environmental contamination increases the risk of acquisition of vancomycin-resistant enterococci. Clin Infect Dis. 2008;46(5):678-685.

Duckro AN, Blom DW, Lyle EA, Weinstein RA, Hayden MK. Transfer of vancomycin-resistant enterococci via health care worker hands. Arch Intern Med. 2005;165(3):302-307.

Ebi KL, McGregor G. Climate Change, Tropospheric Ozone and Particulate Matter, and Health Impacts. Environmental Health Perspectives. 2008;116(11):1449-1455.

Englert N. Fine particles and human health—a review of epidemiological studies. Toxicology Letters. 2004;149(1-3):235.

Emmerson KM, Carslaw N, Pilling MJ. Urban atmospheric chemistry during the PUMA campaign. 2. Radical budgets for OH, HO_2 and RO_2. Journal of Atmospheric Chemistry. 2005;52:165–183.

Erickson PR, Grandbois M, Arnold WA, McNeill K. Photochemical formation of brominated dioxins and other products of concern from hydroxylated polybrominated diphenyl ethers (OH-PBDEs). Environmental Science & Technology. 2012;46(15):8174-8180.

Ernstgard L, Sjogren B, Johanson G. Acute effects of exposure to vapors of hydrogen peroxide in humans. Toxicol Lett. 2012;212:222-227.

Fang Y, Arya F. Evacuated glazing with tempered glass. Sol Energ. 2019;183:240-247.

Farmer DK, Vance ME, Abbatt JPD, Abeleira A, Alves MR, Arata C, Boedicker E, Bourne S, Cardoso-Saldana F, Corsi R, DeCarlo PF, Goldstein AH, Grassian VH, Hildebrandt Ruiz L, Jimenez JL, Kahan TF, Katz EF, Mattila, JM, Nazaroff WW, Novoselac A, O'Brien RE Or VW, Patel S, Sankhyan S, Stevens PS, Tian Y, Wade M, Wang C, Zhou S, Zhou Y. Overview of HOMEChem: House Observations of Microbial and Environmental Chemistry. Environ. Sci.: Processes Impacts. 2019;21:1280−1300.

Fiadzomor P. Industrial placement report, Gas standards for indoor and in-car air, VAM 1.8 project, DTI ITT Number GBBK/C/14/26. 2002.

Fink R, Liberman DF, Murphy KIM, Lupo D, Israeli E. Biological safety cabinets, decontamination or sterilization with paraformaldehyde. Am Indust Hygiene Assoc J. 1988;49(6):277-279.

Finlayson-Pitts BJ, Pitts JN. Chemistry of the upper and lower atmosphere: theory, experiments, and applications. Academic Press, San Diego. 2000:43-81. DOI: https://doi.org/10.1016/B978-0-12-257060-5.X5000-X.

Folberth GA, Hauglustaine DA, Lathiere J, Brocheton F. Interactive chemistry in the Laboratoire de Météorologie Dynamique general circulation model: model description and impact analysis of biogenic hydrocarbons on tropospheric chemistry. Atmos. Chem. Phys. 2006;6:2319.

French GL, Otter JA, Shannon KP, Adams NMT, Watling D, Parks MJ. Tackling contamination of the hospital environment by methicillin-resistant Staphylococcus aureus (MRSA): a comparison between conventional terminal cleaning and hydrogen peroxide vapour decontamination. J Hosp Infect. 2004;57(1):31-37.

Fu TY, Gent P, Kumar V. Efficacy, efficiency and safety aspects of hydrogen peroxide vapour and aerosolized hydrogen peroxide room disinfection systems. J. Hosp. Infect. 2012;80:199-205.

Gandolfo A, Gligorovski V, Bartolomei V, Tlili S, Gómez Alvarez E, Wortham H, Kleffmann J, Gligorovski S. Spectrally resolved actinic flux and photolysis frequencies of key species within an indoor environment. Build. Environ. 2016;109:50-57.

Gao NP, Niu JL, Perino M, Heiselberg P. The airborne transmission of infection between flats in high-rise residential buildings: Tracer gas simulation. Building and Environment. 2008;43(11):1805-1817.

Gibbs SG, Lowe JJ, Smith PW, Hewlett AL. Gaseous chlorine dioxide as an alternative for bedbug control. Infect Cont Hosp Epidemiol. 2012;33(5):495-499.

Gligorovski S, Weschler CJ. The oxidative capacity of indoor atmospheres. Environ. Sci. Technol. 2013;47:13905-13906.

Gomez Alvarez E, Amedro D, Afif C, Gligorovski S, Schoemaecker C, Fittschen C, Doussin JF, Wortham H. Unexpectedly high indoor hydroxyl radical concentrations associated with nitrous acid. Proceedings of the National Academy of Sciences. 2013;110:13294-13299.

Gordon G, Rosenblatt AA. Chlorine dioxide: The current state of the art. Ozone-Sci Eng. 2005;27(3):203-207.

Gori T, Daiber A. Non-Hemodynamic Effects of Organic Nitrates and the Distinctive Characteristics of Pentaerithrityl Tetranitrate. American Journal of Cardiovascular Drugs. 2009;9:7–15.

Grontoft T, Raychaudhuri MR. Compilation of tables of surface deposition velocities for O_3, NO_2 and SO_2 to a range of indoor surfaces. Atmos. Environ. 2004;38(4):533-544.

Han KH, Zhang JS, Wargocki P, Knudsen HN, Guo B. Determination of material emission signatures by PTR-MS and their correlations with odor assessments by human subjects. Indoor Air. 2010;20:341-354.

Hansen JS, Norgaard AW, Koponen IK, Sorli JB, Paidi MD, Hansen SWK, Clausen PA, Nielsen GD, Wolkoff P, Larsen ST. Limonene and its ozone-initiated reaction products attenuate allergic lung inflammation in mice. Journal of Immunotoxicology. 2016;13(6):793-803.

Hardy KJ, Oppenheim BA, Gossain S, Gao F, Hawkey PM. Study of the relationship between environmental contamination with methicillin-resistant Staphylococcus aureus (MRSA) and patients' acquisition of MRSA. Infect Cont Hosp Epidemiol. 2006;27(2):127-132.

Hauglustaine DA, Hourdin F, Jourdain L, Filiberti MA,Walters S, Lamarque JF, Holland EA. Interactive chemistry in the Laboratoire de Meteorologie Dynamique general circulation

model: description and background tropospheric chemistry evaluation. J. Geophys. Res. Atmos. 2004:109.

Hayden MK, Blom DW, Lyle EA, Moore CG, Weinstein RA. Risk of hand or glove contamination after contact with patients colonized with vancomycin-resistant Enterococcus or the colonized patients' environment. Infect Control Hosp Epidemiol. 2008;29(2):149-154.

Heffernan WJB, Frater LP, Watson NR. LED replacement for fluorescent tube lighting. 2007 Australasian Universities Power Engineering Conference, Perth, WA, Australia. 2007:1-6.

Hough AM. The calculation of photolysis rates for use in global tropospheric modelling studies, AERE Rep. R-13259, Her Majesty's Stn. Off., Norwich, England. 1988.

Huang SS, Datta R, Platt R. Risk of acquiring antibiotic-resistant bacteria from prior room occupants. Arch Intern Med. 2006;166(18):1945-1951.

IARC. Diesel engine exhaust carcinogenic. Press release, No. 213. Available online at: http://www.iarc.fr/en/media-centre/pr/2012/pdfs/pr213_E.pdf.

IUPAC (nd). Available online: http://iupac.pole-ether.fr/

Jeanes A, Rao G, Osman M, Merrick P. Eradication of persistent environmental MRSA. J Hosp Infect. 2005;61(1):85-86.

Jenkin ME, Saunders SM, Pilling MJ. The tropospheric degradation of volatile organic compounds: a protocol for mechanism development. Atmospheric Environment. 1997;31:81-104.

Jenkin ME, Saunders SM, Wagner V, Pilling MJ. Protocol for the development of the Master Chemical Mechanism, MCM v3 (Part B): tropospheric degradation of aromatic volatile organic compounds. Atmospheric Chemistry and Physics. 2003;3:181-193.

Jenkins D, Newborough M. An approach for estimating the carbon emissions associated with office lighting with a daylight contribution. Applied Energy. 2007;84(6):608-622.

Jenkin ME, Wyche KP, Evans CJ, Carr T, Monks PS, Alfarra MR, Barley MH, McFiggans GB, Young JC, Rickard AR. Development and chamber evaluation of the MCM v3.2 degradation scheme for β-caryophyllene, Atmos. Chem. Phys. 2012;12:5275-5308.

Jenkin ME, Young JC, Rickard AR. The MCM v3.3.1 degradation scheme for isoprene, Atmos. Chem. Phys. 2015;15:11433-11459.

Jones AP. Indoor air quality and health. Atmospheric Environment. 1999;33:4535-4564.

Kahan TF, Washenfelder RA, Vaida V, Brown SS. Cavity-enhanced measurements of hydrogen peroxide absorption cross sections from 353 to 410 nm. J Phys Chem A. 2012;116(24):5941-5947.

Kazanasmaz T, Grobe LO, Bauer C, Krehel M, Wittkopf S.Three approaches to optimize optical properties and size of a South-facing window for spatial Daylight Autonomy. Building and Environment. 2016;102:243-256.

Kim J-G, Yousef AE, Khadre MA. Ozone and Its Current and Future Application in the Food Industry. Advances in food and nutrition research. 2003;45:167-218.

Kim Y, Choi YH, Kim MK, Paik HJ, Kim DH. Different adverse effects of air pollutants on dry eye disease: Ozone, $PM_{2.5}$, and PM_{10}. Environmental Pollution. 2020;265(Part B):115039.

Knibbs LD, Morawska L, Bell SC, Grzybowski P. Room ventilation and the risk of airborne infection transmission in 3 health care settings within a large teaching hospital. Am J Infect Control. 2011;39(10):866-872.

Kowal SF, Allen SR, Kahan TF. Wavelength-Resolved Photon Fluxes of Indoor Light Sources: Implications for HO_x Production. Environmental Science and Technology. 2017;51:10423-10430.

Kraus A, Hofzumahaus A. Field measurements of atmospheric photolysis frequencies for O_3, NO_2, HCHO, CH_3CHO, H_2O_2, and HONO by UV spectroradiometry. J. Atmos. Chem. 1998;31(1):161-180.

Kruza M, Lewis AC, Morrison GC, Carslaw N. Impact of surface ozone interactions on indoor air chemistry: A modeling study. Indoor Air. 2017;27(5):1001-1011.

Lach VH. A study of conventional formaldehyde fumigation methods. J Appl Bacteriol. 1990;68(5):471-477.

Li TH, Turpin BJ, Shields HC, Weschler CJ. Indoor hydrogen peroxide derived from ozone/d-limonene reactions. Environ Sci Technol. 2002;36(15):3295-3302.

Li C, Tan J, Chow T, Qiu Z. Experimental and theoretical study on the effect of window films on building energy consumption. Energ Build. 2015;102:129-138.

Lim HS, Kim G. Spectral Characteristics of UV Light Existing in Indoor 775 Visual Environment. Indoor Built Environ. 2010;19:586-591.

Lim SR, Kang D, Ogunseitan OA, Schoenung JM. Potential Environmental Impacts from the Metals in Incandescent, Compact Fluorescent Lamp (CFL), and Light-Emitting Diode (LED) Bulbs. Environ. Sci. Technol. 2013;47(2):1040–1047.

Lippmann M, Frampton M, Schwartz J, Dockery D, Schlesinger R, Koutrakis P, Froines J, Nel A, Finkelstein J, Godleski J, Kaufman J, Koenig J, Larson T, Luchtel D, Liu L-JS, Oberdorster G, Peters A, Sarnat J, Sioutas C, Suh H, Sullivan J, Utell M, Wichmann E, Zelikoff J. The US environmental protection agency particulate matter health effects research centers program: a mid-course report of status, progress, and plans. Environ. Health Perspect. 2003;111(8):1074-1092.

Liu C, Wu Y, Li D, Zhou Y, Wang Z, Liu X. Effect of PCM thickness and melting temperature on thermal performance of double glazing units. J Build Eng. 2017;11:87-95.

Loveday HP, Wilson JA, Pratt RJ, et al. EPIC3: National evidence-based guidelines for preventing healthcare-associated infections in NHS hospitals in England. J Hosp Infect. 2014;86:S1-S70.

Lovelock JE. PAN in the natural environment; its possible significance in the epidemiology of skin cancer. Ambio. 1977;131-133.

Lowe JJ, Gibbs SG, Iwen PC, Smith PW, Hewlett AL. Decontamination of a hospital room using gaseous chlorine dioxide: Bacillus anthracis, Francisella tularensis, and Yersinia pestis. J Occup Environ Hyg. 2013;10(10):533-539.

Malig BJ, Pearson DL, Chang YB, Broadwin R, Basu R, Green RS, et al. A time-stratified case-crossover study of ambient ozone exposure and emergency de-partment visits for specific respiratory diagnoses in California (2005-2008). Environ. Health Perspect. 2016;124(6):745-753.

Manian FA, Griesenauer S, Senkel D, et al. Isolation of Acinetobacter baumannii complex and methicillin-resistant Staphylococcus aureus from hospital rooms following terminal cleaning and disinfection: Can we do better? Infect Cont Hosp Epidemiol. 2011;32(7):667-672.

Martinez JA, Ruthazer R, Hansjosten K, Barefoot L, Snydman DR. Role of environmental contamination as a risk factor for acquisition of vancomycin-resistant enterococci in patients treated in a medical intensive care unit. Arch Intern Med. 2003;163(16):1905-1912.

Matsumi Y, Comes FJ, Hancock G, Hofzumahaus A, Hynes AJ, Kawasaki M, Ravishankara AR. Quantum yields for production of $O(^1D)$ in the ultraviolet photolysis of ozone: Recommendation based on evaluation of laboratory data. J. Geophys. Res. 2002;107:ACH1/1-ACH1/12.

Matsumi Y, Kawasaki M. Photolysis of Atmospheric Ozone in the Ultraviolet Region. Chem. Rev. 2003;103(12):4767-4782.

Mattila JM, Lakey PSJ, Shiraiwa M, Wang C, Abbatt JPD, Arata C, Goldstein AH, Ampollini L, Katz EF, DeCarlo PF, Zhou S, Kahan TF, Cardoso-Saldana FJ, Ruiz LH, Abeleira A, Boedicker EK, Vance ME, Farmer DK. Multiphase Chemistry Controls Inorganic Chlorinated and Nitrogenated Compounds in Indoor Air during Bleach Cleaning. Environ. Sci. Technol. 2020;54:1730-1739.

McDonnell G, Russell AD. Antiseptics and disinfectants: Activity, action, and resistance. Clin Microbiol Rev. 1999;12(1):147-179.

MCM (nd). Available online: http://mcm.leeds.ac.uk/MCM/parameters/photolysis.htt

Mempouo B, Cooper E, Riffat SB. Novel window technologies and the code for sustainable homes in the UK. Int J Low-Carbon Tec. 2010;5:167-174.

Mendell MJ. Indoor residential chemical emissions as risk factors for respiratory and allergic effects in children: a review. Indoor Air. 2007;17:259-277.

Mendez M, Blond N, Blondeau P, Schoemaecker C, Hauglustaine DA. Assessment of the impact of oxidation processes on indoor air pollution using the new time-resolved INCA-Indoor model. Atmos. Environ. 2015;122:521-530.

Mendez M, Amedro D, Blond N, Hauglustaine DA, Blondeau P, Afif C, Fittschen C, Schoemaecker C. Identification of the major HO_x radical pathways in an indoor air environment. Indoor Air. 2016;27:434-442.

Met Office. UK Climate Averages. 1981 - 2010 Averages. Available Online: https://www.currentresults.com/Weather/United-Kingdom/annual-sunshine.php

Mitchell BW, Witcher GC, Hammond J. Automated fumigation and neutralization systems for formaldehyde gas. J Appl Poult Res. 2000;9(3):359-363.

Mottier P. LEDs for Lighting Applications; ISTE Ltd and John Wiley & Sons, Inc.: London, UK and Hoboken, NJ, 2009.

Mukesh K. (2015). How does remote sensing utilize electromagnetic radiation? [WWW Document]. Quora. URL https://www.quora.com/How-useful-is-the-electromagnetic-spectrum-toremote-sensing

Munro K, Lanser J, Flower R. A comparative study of methods to validate formaldehyde decontamination of biological safety cabinets. Appl Environ Microbiol. 1999;65(2):873-876.

Murdoch LE, Bailey L, Banham E, Watson F, Adams NM, Chewins J. Evaluating different concentrations of hydrogen peroxide in an automated room disinfection system. Lett. Appl. Microbiol. 2016;63:178-182.

Murray RW. Mechanism of ozonolysis. Acc. Chem. Res. 1968;1(10):313-320.

Murray DM, Burmaster DE. Residential air exchange rates in the United States: empirical and estimated parametric distributions by season and climatic region. Risk Analys. 1995;15(4):459-465.

Nazaroff WW, Cass GR. Mathematical modelling of chemically reactive pollutants in indoor air. Environmental Science and Technology. 1986;20:924-934.

Nazaroff WW, Weschler CJ. Cleaning products and air fresheners: Exposure to primary and secondary air pollutants. Atmospheric Environment. 2004;38:2841-2865.

NCAS. (2018). Available online: https://www.ncas.ac.uk/en/282-amf-main-category/amf-spectral-radiometer/1389-spectral-radiometer

Nuvolone D, Petri D, Voller F. The effects of ozone on human health. Environ. Sci. Pollut. Res. Int. 2018;25(9):8074-8088.

OMECC. Ontario Ministry of the Environment and Climate Change, Air Quality in Ontario 2013 Report. Accessed September 12, 2016.

OSHA, Hydrogen peroxide in workplace atmospheres, method ID-126-SG. Occupational Safety and Health Administration. Available online:

https://www.osha.gov/dts/sltc/methods/partial/t-id126sg-pv-01-0201-m/t-id126sg-pv-01-0201-m.html. Accessed June 18, 2014.

OSHA, OSHA Instruction CPL 02-02-052/ CPL 2-2.52 (REVISED). Occupational Safety and Health Administration. Available online: https://www.osha.gov/OshDoc/Directive_pdf/CPL_02-02-052.pdf. Accessed June 18, 2014.

OSHA, Permissible exposure limits for chemical contaminants. Occupational Safety and Health Administration. Available online: https://www.dir.ca.gov/title8/5155table_ac1.html. Accessed June 18, 2014.

Otter JA, French GL. Survival of nosocomial bacteria and spores on surfaces and inactivation by hydrogen peroxide vapor. J Clin Microbiol. 2009;47(1):205-207.

Otter JA, Havill NL, Boyce JM. Hydrogen peroxide vapor is not the same as aerosolized hydrogen peroxide. Infect Cont Hosp Epidemiol. 2010;31(11):1201-1202.

Otter JA, Yezli S, Perl TM, Barbut F, French GL. The role of 'notouch' automated room disinfection systems in infection prevention and control. J Hosp Infect. 2013;83(1):1-13.

Pandharipande A, Caicedo D. Daylight integrated illumination control of LED systems based on enhanced presence sensing. Energy and BuildingS. 2011;43(4):944-950.

Parrish DD, Xu J, Croes B, Shao M. Air quality improvement in Los Angeles—Perspectives for developing cities. Frontiers of Environmental Science & Engineering. 2016:10(5):11.

Passaretti CL, Otter JA, Reich NG, et al. An evaluation of environmental decontamination with hydrogen peroxide vapor for reducing the risk of patient acquisition of multidrug-resistant organisms. Clin Infect Dis. 2013;56(1):27-35.

Paulson SE, Flagan RC, Seinfeld JH. Atmospheric photo-oxidation of isoprene part I: The hydroxyl radical and ground state atomic oxygen reactions. Int. J. Chem. Kinet. 1992;24:103-125.

Paulson SE, Seinfeld J. Atmospheric Photochemical Oxidation of 1-Octene: OH, O_3 and $O(^3P)$ Reactions. J. H. Environ. Sci. Technol. 1992;26:1165-1173.

Paulson SE, Fenske JD, Sen AD, Callahan TW. A Novel Small-Ratio Relative-Rate Technique for Measuring OH Formation Yields from the Reactions of O_3 with Alkenes in the

Gas Phase, and Its Application to the Reactions of Ethene and Propene. J. Phys. Chem. A 1999;103:2050-2059.

Peak MJ, Belser WL. Some effects of the air pollutant, peroxyacetyl nitrate, upon deoxyribonucleic acid and upon nucleic acid bases. Atmos. Environ. 1969;3(4):385-397.

Persily A. What we think we know about ventilation. Int. J. Vent. 2006;5(3):275-290.

Petry T, Vitale D, Joachim FJ, Smith B, Cruse L, Mascarenhas R, Schneider S, Singal M. Human health risk evaluation of selected VOC, SVOC and particulate emissions from scented candles. Regulatory Toxicology and Pharmacology. 2014;69(1):55-70.

Platt U, Perner D, Winer AM, Harris GW, Pitts Jr JN. Detection of NO_3 in the polluted troposphere by differential optical absorption. Geophysical Research Letters. 1980;7(1):89-92.

Platt U, Alicke B, Dubois R, Geyer A, Hofzumahaus A, Holland F, Martinez M, Mihelcic D, Klupfel T, Lohrmann B, Patz W, Perner D, Rohrer F, Schafer J, Stutz J. Free radicals and fast photochemistry during BERLIOZ. Journal of Atmospheric Chemistry. 2002;42:359-394.

Pope CA, Dockery DW, Schwartz J. Review of epidemiological evidence of health effects of particulate air pollution. Inhalation Toxicology. 1995;7:1-18.

Pottage T, Richardson C, Parks S, Walker JT, Bennett AM. Evaluation of hydrogen peroxide gaseous disinfection systems to decontaminate viruses. J Hosp Infect. 2010;74(1):55-61.

Pragholapati, A. Covid-19 Impact On Students. 2020.

Public Health England. 2013. Available online: https://www.gov.uk/government/publications/diesel-particulate-filters-guidance-note/diesel-particulate-filters.

Puskar MA, Plese MR. Evaluation of real time techniques to measure hydrogen peroxide in air at the permissible exposure limit. Amer Indust Hygiene Assoc J. 1996;57(9):843-848.

Quirce S, Barranco P. Cleaning agents and asthma. Journal of Investigational Allergology and Clinical Immunology. 2010;20:542-550.

Raunemaa T, Kulmala M, Saari H, Olin M, Kulmala MH. Indoor Air Aerosol Model: Transport Indoors and Deposition of Fine and Coarse Particles. Aerosol Sci. Technol. 1989;11(1):11-25.

Rebbert RE. Primary processes in the photolysis of ethyl nitrate. J. Phys. Chem. 1963;67(9):1923-1925.

Rice RG. Ozone and anthrax - knowns and unknowns. Ozone-Sci Eng. 2002;24(3):151-158.

Rogers JV, Choi YW, Richter WR, et al. Formaldehyde gas inactivation of Bacillus anthracis, Bacillus subtilis, and Geobacillus stearothermophilus spores on indoor surface materials. J Appl Microbiol. 2007;103(4):1104-1112.

Rogers J, Choi W, Richter W, Stone H, Taylor M. Bacillus Anthracis spore inactivation by fumigant decontamination. Appl Biosaf. 2008;13:89-98.

Rosencrantz T, Bulow-Hube H, Karlsson B, Roos A. Increased solar energy and daylight utilisation using anti-reflective coatings in energy-efficient windows. Sol.Energy Mater. Sol. Cells. 2005;89:249-260.

Roulet CA, Foradini F. Simple and cheap air change rate measuring using CO_2 concentration decays. Int. J. Vent. 2002;1(1):39-44.

Rubin M, Von Rottkay K, Powles R. Window optics. Solar Energy. 1998;62(3):149-161.

Sarwar G, Corsi R, Kimura Y, Allen D, Weschler C. Hydroxyl radicals in indoor environments. Atmospheric Environment. 2002;36:3973-3988.

Sarwar G, Olson DA, Corsi RL, Weschler CJ. Indoor fine particles: the role of terpene emissions from consumer products. J. Air Waste Manag. Assoc. 2004;54(3):367-377.

Saunders SM, Jenkin ME, Derwent RG, Pilling MJ. Protocol for the development of the Master Chemical Mechanism, MCM v3 (Part A): tropospheric degradation of non-aromatic volatile organic compounds. Atmospheric Chemistry and Physics. 2003;3:161-180.

Schoemaecker C, Verriele M, Hanoune B, Petitprez D, Leclerc N, Dusanter S, Le Calve S, Millet M, Bernhardt P, Mendez M, Blond N, Hauglustaine D, Clappier A, Blondeau P, Abadie M, Locoge N. Characterization of the IAQ in low energy public buildings in France through a dual experiment and modelling approach. In: Proceedings of the 13th International Conference on Indoor Air Quality and Climate. Hong-Kong; 000-008. 2014.

Schripp T, Etienne S, Fauck C, Fuhrmann F, Mark L, Salthammer T. Application of proton-transfer-reaction-mass-spectrometry for Indoor Air Quality research. Indoor Air. 2014;24:178-189.

Sexton T, Clarke P, O'Neill E, Dillane T, Humphreys H. Environmental reservoirs of methicillin-resistant Staphylococcus aureus in isolation rooms: correlation with patient isolates and implications for hospital hygiene. J Hosp Infect. 2006;62(2):187-194.

Shallcross DE, Taatjes CA, Percival CJ. Criegee intermediates in the indoor environment: new insights. Indoor Air. 2014;24:495-502.

Shepson PB, Kleindienst TE, Edney EO, Nero CM, Cupitt LT, Claxton LD. Acetaldehyde: the mutagenic activity of its photooxidation products. Environ. Sci. Technol. 1986;20(10):1008-1013.

Siegel JA. Primary and secondary consequences of indoor air cleaners. Indoor Air. 2016;26:88-96.

Singh HB, Hanst PL. Peroxyacetyl nitrate (PAN) in the unpolluted atmosphere: An important reservoir for nitrogen oxides. Geophysical Research Letters. 1981;8(8):941-944.

Steinemann AC, MacGregor IC, Gordon SM, Gallagher LG, Davis AL, Ribeiro DS, Wallace LA. Fragranced consumer products: chemicals emitted, ingredients unlisted. Environmental Impact Assessment Review. 2011;31(3):328-333.

Stephens ER, Darley EF, Taylor OC, Scott WE. Photochemical reaction products in air pollution. International Journal of Air and Water Pollution. 1961;4:79-100.

Stone D, Whalley LK, Heard DE. Tropospheric OH and HO_2 radicals: field measurements and model comparisons. Chem Soc Rev. 2012;41(19):6348-6404.

Strickland MJ, Darrow LA, Klein M, Flanders WD, Sarnat JA, Waller LA, et al. Short-term associations between ambient air pollutants and pediatric asthma emergency department visits. Am. J. Respir. Crit. Care Med. 2010;182(3):307-316.

Sun Y, Hou J, Sheng Y, Zhang X, Sundell J. Indoor air quality, ventilation and their associations with sick building syndrome in Chinese homes, Energy and Buildings. 2019;197:112-119.

STERIS (nd). Reduce the risk of contamination after routine shutdowns, repairs, or emergency responses of your cleanrooms, controlled environments, equipment, and spaces. Available online: https://www.sterislifesciences.com/services/decontamination-services

Taatjes CA, Meloni G, Selby TM, Tre-vitt AJ, Osborn DL, Percival CJ, Shallcross DE. Direct obser-vation of the gas-phase Criegee interme-diate (CH_2OO) in dimethyl sulphoxide oxidation, J. Am. Chem. Soc. 2008;130:11883-11885.

Taatjes CA, Welz O, Eskola AJ, Savee JD, Osborn DL, Lee EPF, Dyke JM, Mok DWK, Shallcross DE, Percival CJ. Direct measure-ment of Criegee intermediate (CH_2OO)reactions with acetone, acetaldehyde, andhexafluoroacetone, Phys. Chem. Chem.Phys. 2012;14:10391-10400.

Taatjes CA, Welz O, Eskola AJ, Savee JD, Scheer AM, Shallcross DE, Ro-tavera B, Lee EPF, Dyke JM, Os-born DL, Mok DMK, Percival CJ. Direct measurements of con-former-dependent reactivity of the Crie-gee intermediate CH_3CHOO, Science. 2013;340:177-180.

Taylor O. Importance of peroxyacetyl nitrate (PAN) as a phytotoxic air pollutant. J. Air Pollut. Contr. Assoc. 1969;19(5):347-351.

Temple P, Taylor O. World-wide ambient measurements of peroxyacetyl nitrate (PAN) and implications for plant injury. Atmos. Environ. 1983;17(8):1583-1587.

Trantallidi M, Dimitroulopoulou C, Wolkoff P, Kephalopoulos S, Carrer P. EPHECT III: health risk assessment of exposure to household consumer products. Sci. Total Environ. 2015;536:903-913.

Urman R, McConnell R, Islam T, Avol EL, Lurmann FW, Vora H, et al. Associations of children's lung function with ambient air pollution: joint effects of regional and near-roadway pollutants. Thorax. 2014;69(6):540-547.

US CDC (Centres for Disease Control & Prevention) (2016) http://www.atsdr.cdc.gov/MMG/MMG.asp?id=304&tid=84 accessed 17th May 2016.

Valavanidis A, Fiotakis K, Vlachogianni T. Airborne particulate matter and human health. Toxicological assessment and importance of size and composition of particles for oxidative damage and carcinogenic mechanisms. J Env Sci Health. 2008;26:339-362.

Verriele M, Schoemaecker C, Hanoune B, Leclerc N, Germain S, Gaudion V, Locoge N. The MERMAID study: indoor and outdoor average pollutant concentrations in 10 low-energy school buildings in France. Indoor Air. 2016;26(5):702-713.

Volkamer R, Platt U, Wirtz K. Primary and secondary glyoxal formation from aromatics: Experimental evidence for the bicycloalkyl-radical pathway from benzene, toluene, and pxylene. J. Phys. Chem. A, 2001;105(33):7865-7874.

Volkamer R, Klotz B, Barnes I, Imamura T, Wirtz K, Washida N, Becker KH, Platt U. OH-initiated oxidation of benzene – Part I. Phenol formation under atmospheric conditions. Phys. Chem. Chem. Phys. 2002;4(9):1598-1610.

Vyskocil A, Viau C, Lamy S. Peroxyacetyl nitrate: review of toxicity. Human & Experimental Toxicology. 1998;17(4):212–220.

Wallace L. Indoor Particles: A Review. Journal of the Air & Waste Management Association. 1996;46(2):98-126.

Wang H, Morrison GC. Ozone-Initiated Secondary Emission Rates of Aldehydes from Indoor Surfaces in Four Homes. Environ. Sci. Technol. 2006;40(17):5263-5268.

Wang ZX, Kowal SF, Carslaw N and Kahan TF. Photolysis-driven indoor air chemistry following cleaning of hospital wards. Indoor Air. 2020;30:1241–1255.

Waring MS, Wells JR. Volatile organic compound conversion by ozone, hydroxyl radicals, and nitrate radicals in residential indoor air: magnitudes and impacts of oxidant sources. Atmos. Environ. 2015;106:382-391.

Weber DJ, Rutala WA, Anderson DJ, Chen LF, Sickbert-Bennett EE, Boyce JM. Effectiveness of ultraviolet devices and hydrogen peroxide systems for terminal room decontamination: Focus on clinical trials. Am J Infect Control. 2016;44(5):E77-E84.

Weschler CJ, Shields HC. Production of the Hydroxyl Radical in Indoor Air. Environ. Sci. Technol. 1996;30:3250-3258.

Weschler CJ, Shields HC. Indoor ozone/terpene reactions as a source of indoor particles. Atmospheric Environment. 1999;33:2301-2312.

Weschler CJ. Ozone in Indoor Environments: Concentration and Chemistry. Indoor Air. 2000;10:269-288.

Weschler CJ. Ozone-initiated reaction products indoors may be more harmful than ozone itself. Atmospheric Environment. 2004;38:5715-5716.

Weschler CJ, Wells R. Guest editorial. Indoor Air. 2004;14:373-375.

White LF, Dancer SJ, Robertson C, McDonald J. Are hygiene standards useful in assessing infection risk? Am J Infect Control. 2008;36(5):381-384.

World Health Organization (WHO). (2016). Ambient air pollution: a global assessment of exposure and burden of disease. World Health Organization. https://apps.who.int/iris/handle/10665/250141.

WHO Expert Consultation: Available evidence for the future update of the WHO Global Air Quality Guidelines (AQGs). (2016). Available online: https://www.euro.who.int/en/health-topics/environment-and-health/air-quality/publications/2016/who-expert-consultation-available-evidence-for-the-future-update-of-the-who-global-air-quality-guidelines-aqgs-2016

Wolkoff P, Schneider T, Kildesø J, Degerth R, Jaroszewski M, Schunk H. Risk in cleaning: chemical and physical exposure. The Science of the Total Environment. 1998;215:135-156.

Wolkoff P, Clausen PA, Wilkins CK, Nielsen GD. Formation of strong airway irritants in terpene/ozone mixtures. Indoor Air. 2000;10:82-91.

Wolkoff P, Wilkins CK, Clausen PA, Nielsen GD. Organic compounds in office environments—sensory irritation, odor, measurements and the role of reactive chemistry. Indoor Air. 2005;16:7-19.

Wolkoff P, Larsen ST, Hammer M, Kofoed-Sørensen V, Clausen PA, Nielsen GD. Human reference values for acute airway effects of five common ozone-initiated terpene reaction products in indoor air. Toxicology Letters. 2013;216(1):54-64.

Won Y, Waring M, Rim D. Understanding the Spatial Heterogeneity of Indoor OH and HO_2 due to Photolysis of HONO Using Computational Fluid Dynamics Simulation. Environ. Sci. Technol. 2019;53:14470-14478.

Wong JPS, Carslaw N, Zhao R, Zhou S, Abbatt JPD. Observations and impacts of bleach washing on indoor chlorine chemistry. Indoor Air. 2017;27:1082-1090.

Young CJ, Zhou S, Siegel JA, Kahan TF. Illuminating the dark side of indoor oxidants. Environ. Sci.: Processes Impacts. 2019;21:1229-1239.

Zhang L, Moran MD, Makar PA, Brook JR, Gong S. Modelling gaseous dry deposition in AURAMS: A unified regional air quality modelling system. Atmos. Environ. 2002;36(3):537-560.

Zhang YP, Mo JH, Li YG, et al. Can commonly-used fan-driven air cleaning technologies improve indoor air quality? A literature review Atmos Environ. 2011;45:4329-4343.

Zhu L, Ding CF. Temperature dependence of the near UV absorption spectra and photolysis products of ethyl nitrate. Chem. Phys. Lett. 1997;265:177-184.

Zhou S, Kowal SF, Cregan AR, Kahan TF. Factors affecting wavelength-resolved ultraviolet irradiance indoors and their impacts on indoor photochemistry. Indoor Air. 2020;00:1–12.

Zonta W, Mauroy A, Farnir F, Thiry E. Virucidal efficacy of a hydrogen peroxide nebulization against murine norovirus and feline calicivirus, two surrogates of human norovirus. Food Environ Virol. 2016;8(4):275-282.